

2010

Hydrogen Storage in Metal Fragments grafted Silicas and Chromium Hydrazide Gels

Ahmad Hamaed
University of Windsor

Follow this and additional works at: <http://scholar.uwindsor.ca/etd>

Recommended Citation

Hamaed, Ahmad, "Hydrogen Storage in Metal Fragments grafted Silicas and Chromium Hydrazide Gels" (2010). *Electronic Theses and Dissertations*. Paper 392.

This online database contains the full-text of PhD dissertations and Masters' theses of University of Windsor students from 1954 forward. These documents are made available for personal study and research purposes only, in accordance with the Canadian Copyright Act and the Creative Commons license—CC BY-NC-ND (Attribution, Non-Commercial, No Derivative Works). Under this license, works must always be attributed to the copyright holder (original author), cannot be used for any commercial purposes, and may not be altered. Any other use would require the permission of the copyright holder. Students may inquire about withdrawing their dissertation and/or thesis from this database. For additional inquiries, please contact the repository administrator via email (scholarship@uwindsor.ca) or by telephone at 519-253-3000ext. 3208.

**Hydrogen Storage in Metal-fragments Grafted Silicas
and Chromium Hydrazide Gels**

by

Ahmad Hamaed

A Dissertation

Submitted to the Faculty of Graduate Studies and Research

Through Chemistry and Biochemistry

in Partial Fulfillment of the Requirements for

the Degree of Doctor of Philosophy at the

University of Windsor

Windsor, Ontario, Canada

2010

© 2010, Ahmad Hamaed

**Hydrogen Storage in Metal-fragments Grafted Silicas and Chromium
Hydrazide Gels**

by

Ahmad Hamaed

APPROVED BY

Dr. R. H. Morris, External Examiner
University of Toronto

Dr. D. O. Northwood
Department of Mechanical & Materials Engineering

Dr. T. Carmichael
Department of Chemistry & Biochemistry

Dr. R. F. Aroca
Department of Chemistry & Biochemistry

Dr. D. M. Antonelli, Advisor
Department of Chemistry & Biochemistry

Dr., L. Porter, Chair of Defense
Department of Biology

27 July 2010

Declaration of Co-Authorship / Previous Publication

I. Co-Authorship Declaration

I hereby declare that this thesis incorporates material that is result of joint research, as follows:

This thesis incorporates the outcome of a joint research undertaken in collaboration with Claire Skipper and professor Nicholas Kaltsoyannis at University College London (UCL), related to computational studies in Chapter 5. This thesis also incorporates the work undertaken in collaboration with Dr. Michel Trudeau at Hydro-Quebec Research Institute related to X-ray photo-electron spectroscopy. The collaboration with Tuan K. A. Hoang under the supervision of Dr. Antonelli in Chapter 3 and 4 and with Hung Van Mai in Chapter 4 of this thesis. In all cases, the key ideas, primary contributions, experimental designs, data analysis and interpretation, were performed by the author.

I am aware of the University of Windsor Senate Policy on Authorship and I certify that I have properly acknowledged the contribution of other researchers to my thesis, and have obtained written permission from each of the co-authors to include the above materials in my thesis.

I certify that, with the above qualification, this thesis, and the research to which it refers, is the product of my own work.

II. Declaration of Previous Publication

This thesis includes five original papers that have been previously published/submitted for publication in peer reviewed journals, as follows:

Thesis Chapter	Publication title/full citation	Publication status
Chapter 2	Hamaed, A., Trudeau, M., Antonelli, D., H ₂ Storage Materials (22 kJ/mol) Using Organometallic Ti Fragment as σ -H ₂ Binding Sites, <i>J. Am. Chem. Soc.</i> , 2008 , 130, 6992-6999	Published
Chapter 3	Hamaed, A., Hoang, T.K.A., Trudeau, M., Antonelli, D., Optimization of Hydrogen Storage Capacity in Silica-supported Low Valent Ti Systems Exploiting Kubas Binding of Hydrogen, <i>J. Organomet. Chem.</i> , 2009 , 694, 2793-2800	Published
Chapter 4	Hamaed, A., Mai, H.V., Hoang, T.K.A., Trudeau, M., Antonelli, D., Functionalized Porous Silicas with Unsaturated Early Transition Metal Moieties as Hydrogen Storage Materials: Comparison of Metal and Oxidation State, <i>J. Phys. Chem. C</i> , 2010 , 114 (18), 8651-8660.	Published
Chapter 5	Skipper, C., Hamaed, A., Kaltsoyannis, N., Antonelli, D., Computational Studies on Silica Supported Transition Metal Fragments for Kubas-Type Hydrogen Storage, <i>J. Am. Chem. Soc.</i> (Manuscript in Preparation)	In Preparation
Chapter 6	Hamaed, A., Hoang, T.K.A., Trudeau, M., Antonelli, D., Hydride-induced Amplification of Performance and Binding Enthalpies in Alkylchromium (II) Hydrazide Gels for Kubas- type Hydrogen Storage, <i>Nature Materials</i> , (Manuscript in Preparation)	In Preparation

I certify that I have obtained a written permission from the copyright owner(s) to include the above published material(s) in my thesis. I certify that the above material

describes work completed during my registration as graduate student at the University of Windsor.

I declare that, to the best of my knowledge, my thesis does not infringe upon anyone's copyright nor violate any proprietary rights and that any ideas, techniques, quotations, or any other material from the work of other people included in my thesis, published or otherwise, are fully acknowledged in accordance with the standard referencing practices. Furthermore, to the extent that I have included copyrighted material that surpasses the bounds of fair dealing within the meaning of the Canada Copyright Act, I certify that I have obtained a written permission from the copyright owner(s) to include such material(s) in my thesis.

I declare that this is a true copy of my thesis, including any final revisions, as approved by my thesis committee and the Graduate Studies office, and that this thesis has not been submitted for a higher degree to any other University or Institution.

Abstract

Hexagonally-packed mesoporous silicas (HMS) grafted with low-valent titanium, vanadium, and chromium organometallic fragments possessing oxidation states between (II) and (IV) were synthesized, tested for their hydrogen storage capacities, and characterized by XRD, nitrogen adsorption, XPS, and EA. The effects of the variation in the surface area, pore size, transition metal type, and metal oxidation state, the organometallic loading levels, as well as the ligand environment on the H₂ adsorption capacity and the binding enthalpies of these systems were investigated.

This study demonstrated that titanium is more effective at hydrogen binding than vanadium and chromium. HMS silica grafted with benzyl titanium (III) fragments can accommodate up to 4.85 H₂ per Ti center. This compares to 2.74 H₂ per vanadium center as for the HMS grafted with tris(mesityl) vanadium, and to 1.82 and 2.20 H₂ per chromium as for the HMS treated with the tris[bis(trimethylsilyl)methyl] chromium and bis[(trimethylsilyl)methyl]chromium respectively. The hydrogenation of the metal centers had a pronounced effect on the adsorption capacity of the Cr-grafted HMS. This capacity increased from 1.82 to 3.20 H₂ per chromium in the case of HMS treated with tris[bis(trimethylsilyl)methyl] chromium, and from 2.20 H₂ to 3.50 H₂ per chromium in the case of HMS treated with tris[(trimethylsilyl)methyl] chromium.

The investigated systems in the first part were used as modules in the design of novel chromium hydrazide gels that use low valent chromium centers as H₂ binding sites. These materials were synthesized at various Cr to hydrazine molar ratios and have room temperature excess hydrogen storage of up to 1.01 wt%, and binding enthalpy of up to

22.9 kJ/mol. However, the hydrogenation of these materials induced an amplification of the performance and binding enthalpies. The excess room temperature hydrogen storage of the hydrogenated samples goes up to 1.65 wt%, with the room absolute volumetric density goes up to 29.92 Kg/m³, and with binding enthalpy goes up to 51.59 kJ/mol. These materials would use pressure instead of temperature as a toggle and can thus be used in compressed gas tanks, to increase the amount of hydrogen stored, and therefore the driving range of any vehicle.

For my parents, my wife & my little Ali

Acknowledgements

First of all, I would like to thank my advisor professor David Antonelli for introducing me to the magic world of hydrogen storage, without his encouragement, help and entrustment this piece of work would never come to light. Dr. Antonelli was only “one click” away when not physically present at the University of Windsor, I really appreciate his reply to my messages in a matter of minutes, and sometimes seconds!!! Also without the “road map” he devised for my last project I would get lost among the various molar ratios, heating conditions, and hydrogenation protocols.

I would like to thank my committee members Dr. Ricardo Aroca, Dr. Tricia Breen-Carmichael, and Dr. Derek Northwood. Also, I wish to thank Dr. Robert Morris for agreeing to be my External Examiner.

Thank you to Dr. Holger Eichhorn for his help with the XRD data collection as well as with the translation of many synthetic protocols from German to English. Dr James Green is also thanked for his help with the NMR “diagnosis” during the titanium organic precursor’s synthesis. Dr. Michel Trudeau at Hydro-Quebec is thanked for his help with the XPS analysis for all of my samples. Dr. Philip Dutton and Mrs. Elizabeth Kickham and Mr. Horst Schmidt are thanked for managing our group account and helping out with the funding during the last year of this work. The present and former members of Dr. Antonelli group Mr. Tuan Hoang, Mr. Van Hung Mai, Dr. Xin Hu, Dr. Yuxiang Rao, Dr. Junjie Kang, Dr. Sun Jing, and Dr. Longhui Qiu are thanked for their help and advice and making working in the lab a fun, enjoyable and memorable experience.

Saving the best for the last, my deep gratitude goes to my parents for their support during my undergraduate and graduate studies, to my wife for her love, patience, encouragement and for her caring for our beautiful baby during my long-hour stay in the lab, to my little Ali for providing the meaning to all of this.

Table of Contents

Declaration of Co-Authorship/Previous Publication.....	iv
Abstract.....	vii
Dedication	ix
Acknowledgments	x
List of Tables.....	xvii
Lists of Figures.....	xix
Lists of Schemes.....	xix
Lists of Appendices.....	xxiv
Lists of Abbreviations, Symbols, Nomenclatures.....	xxv
CHAPTER 1 – INTRODUCTION.....	1
1.1 Hydrogen the Ultimate Fuel.....	1
1.2 Hydrogen Storage Methods.....	4
1.2.1 Pressurized tank gaseous Hydrogen Storage.....	4
1.2.2 Cryogenic Liquid Hydrogen Storage.....	5
1.2.3 Hydrogen Storage by Chemical Adsorption.....	6
1.2.4 Hydrogen Storage by Physical Adsorption.....	7
1.3 System Requirements and Department of Energy Targets for Hydrogen Adsorption in Solid State Materials.....	8
1.4 Enhancing the H ₂ -adsorbent Binding Through Kubas-interaction.....	10
1.5 Mesoporous Silica Gel as Hydrogen Storage Materials.....	12
1.5.1 Silica Surface Properties.....	13
1.5.2 Surface Functionalization of Mesoporous Silica by Metal-fragments Grafting.....	14
1.6 Characterization of Solid-state Hydrogen Storage Materials.....	15
1.6.1 Infra-red Spectroscopy.....	16
1.6.2 Raman Spectroscopy.....	17
1.6.3 Inelastic Neutron Scattering.....	18

1.6.4	<i>Solid-state Nuclear Magnetic Resonance (NMR) Spectroscopy</i>	20
1.6.5	<i>X-ray Diffraction</i>	21
1.6.6	<i>Computational Modeling</i>	21
1.6.7	<i>Elemental Analysis</i>	23
1.6.8	<i>Nitrogen Adsorption</i>	24
1.6.9	<i>Helium Pycnometry</i>	25
1.7	Dissertation Overview.....	25
1.8	References.....	27
CHAPTER 2 – H₂ STORAGE MATERIALS (22kJ/mol) USING		
ORGANOMETALLIC Ti FRAGMENTS AS σ-H₂ BINDING SITES		
2.1	Introduction.....	36
2.2	Experimental.....	38
2.2.1	<i>Synthesis of Tetrabenzyl Titanium</i>	38
2.2.2	<i>Synthesis of Tribenzyl Titanium</i>	38
2.2.3	<i>Synthesis of Hexagonally-packed Mesoporous Silica (HMS)</i>	38
2.2.4	<i>Synthesis of Ti-Grafted Mesoporous Silica</i>	39
2.2.5	<i>Concentration of Exposed Ti Metal sites</i>	39
2.2.6	<i>Measurements</i>	39
2.3	Results and Discussion.....	41
2.4	Conclusions.....	59
2.5	References.....	60
CHAPTER 3 – OPTIMIZATION OF HYDROGEN STORAGE CAPACITY IN		
SILICA-SUPPORTED LOW VALENT Ti SYSTEMS EXPLOITING KUBAS		
BINDING OF HYDROGEN		
3.1	Introduction.....	63
3.2	Experimental.....	65
3.2.1	<i>Synthesis of Hexagonally-packed Mesoporous Silica (HMS)</i>	65
3.2.2	<i>Synthesis of Ti-Grafted Mesoporous Silica</i>	66
3.2.3	<i>Synthesis of Trimethyl Ti-Grafted Mesoporous Silica</i>	66
3.2.4	<i>Synthesis of (Allyl)₃Ti Grafted Mesoporous Silica</i>	67

3.2.5 XPS Spectroscopy.....	67
3.3 Results and Discussion.....	67
3.3.1 Variation of Silica to Surfactant Molar Ratio.....	67
3.3.2 Variation of Pore Size.....	69
3.3.3 Variation of Metal-fragment Precursor and Precursor Loading Levels.....	71
3.3.4 $Ti(CH_3)_3$ Grafted on HMS.....	75
3.3.5 $Ti(Allyl)_3$ Grafted on HMS.....	77
3.3.6 XPS Studies and Enthalpies.....	79
3.4 Conclusions.....	82
3.5 References.....	83

**CHAPTER 4 – FUNCTIONALIZED POROUS SILICA WITH UNSATURATED
EARLY TRANSITION METAL MOIETIES AS HYDROGEN STORAGE
MATERIALS: COMPARISON OF METAL AND OXIDATION STATE.....** 85

4.1 Introduction.....	85
4.2 Experimental.....	87
4.2.1 Synthesis of Hexagonally Packed Mesoporous Silica (HMS) ...	87
4.2.2 Synthesis of Doped HMS Materials.....	88
4.2.3 Preparation of Bis(Naphthalene) Titanium.....	88
4.2.4 Preparation of Tris(Mesityl) Vanadium.....	88
4.2.5 Hydrogenation of Metal-fragment Grafted HMS Materials.....	89
4.2.6 Preparation of Tris[bis(trimethylsilyl)methyl] Chromium (III)...	89
4.2.7 Preparation of Bis[(trimethylsilyl)methyl] Chromium (II).....	89
4.2.8 Calculation of the Number of Hydrogen Molecules per Transition Metal Center.....	90

4.2.9 Measurements.....	90
4.3 Results and Discussion.....	91
4.4 Conclusions.....	116
4.5 References.....	118
CHAPTER 5 – COMPUTATIONAL STUDIES ON SILICA SUPPORTED TRANSITION METAL FRAGMENTS FOR KUBAS-TYPE HYDROGEN STORAGE.....	122
5.1 Introduction.....	122
5.2 Computational Details.....	124
5.3 Results and Discussion.....	127
5.3.1 Comparison to the Experimental Study.....	127
5.3.2 The Effect of the Ancillary Ligand.....	130
5.3.3 The Effect of the Metal Center.....	136
5.4 Conclusions.....	141
5.5 References.....	143
Chapter 6 – HYDRIDE-INDUCED AMPLIFICATION OF PERFORMANCE AND BINDING ENTHALPIES IN ALKYLCHROMIUM (II) HYDRAZIDE GELS FOR KUBAS- TYPE HYDROGEN STORAGE.....	149
6.1 Introduction.....	149
6.2 Experimental.....	151
6.2.1 Preparation of Bis[(trimethylsilyl) methyl]chromium(II).....	151
6.2.2 Preparation of Anhydrous Hydrazine.....	152
6.2.3 Preparation of 1:1 Chromium Hydrazide Gel (Cr-MHZ (1.0)).....	152
6.2.4 Preparation of Cr-MHZ (0.5), Cr-MHZ (1.5), Cr-MHZ (2.0).....	153
6.2.5 Hydrogenation of Cr-MHZ.....	153
6.2.6 Infra-red Spectroscopy.....	153
6.2.7 Hydrogen Adsorption Measurements.....	153
6.3 Results and Discussion.....	156
6.4 Conclusions.....	170
6.5 References.....	171

CHAPTER 7 – DISSERTATION SUMMARY AND FUTURE OUTLOOK	174
7.1 Summary.....	174
7.2 Future Outlook.....	177
7.3 References.....	178
Appendices	181
A Supplementary Tables for Chapter 6.....	182
B Supplementary Figures for Chapter 4.....	184
C Copyright Release Forms.....	189
Vita Auctoris.....	195

List of Tables

Table 1.1	Properties of hydrogen (H ₂).....	3
Table 1.2	Summary of the DOE hydrogen storage system targets.....	9
Table 2.1	Hydrogen storage capacities of mesoporous silicas at 77K with different surface areas synthesized using various molar ratios of tribenzyl and tetrabenzyl titanium.....	56
Table 2.2	Hydrogen storage capacities of pristine and Ti-grafted mesoporous silica at different temperatures.....	57
Table 3.1	A summary of the apparent density, skeletal density, gravimetric storage, gravimetric adsorption, and surface area of all HMS pristine synthesized using different molar ratios of tetraethyl orthosilicate to dodecylamine.....	68
Table 3.2	Hydrogen sorption capacity of micro- and mesoporous silica at 77K with different surface areas and pore sizes synthesized using amine templating agents of various chain lengths.....	70
Table 3.3	Summarizing the storage and adsorption capacities of C ₁₂ -HMS treated with different molar equivalents of tetrabenzyl Ti.....	72
Table 3.4	Summarizing the storage and adsorption capacities of C ₁₂ -HMS treated with different molar equivalents of tribenzyl Ti.....	73
Table 3.5	Summarizing the adsorption capacities of plain and treated 380-Aerosil with different molar ratios of tetrabenzyl Ti.....	75
Table 3.6	Summarizing the adsorption capacities of C ₁₂ -HMS treated with different molar equivalents of TiMe ₃	77
Table 3.7	Summarizing the adsorption capacities of C ₁₂ HMS treated with different molar ratios of triallyl Ti.....	78
Table 4.1	Summary of the skeletal densities, gravimetric adsorptions, surface areas, and number of H ₂ per transition metal of all samples tested.....	94
Table 4.2	Elemental analysis of C, H, Si, and TM for HMS silica treated with various TM precursors.....	95
Table 5.1	The HOMO and LUMO levels of molecule 1 with 1 H ₂ unit bound and titanium as the metal center with various ligands, which are subsequently involved in bonding to the 2 nd H ₂ . When more than 1 LUMO interacted with	

	the H ₂ an average was taken and the ± value shows the range of the LUMO energies.....	133
Table 5.2	The HOMO and LUMO energy levels for molecule 1 with no H ₂ units bound and with hydride as the ancillary ligand with various metal centers, which are subsequently involved in bonding to the 1 st H ₂	139
Table 5.3	The energies of the HOMOs and LUMOs of molecule 1 with 1 H ₂ unit bound and a hydride ancillary ligand with various metal centers, which are subsequently involved in bonding to the 2 nd H ₂ . When more than 1 LUMO interacted with the H ₂ an average was taken and the ± value shows the range of the LUMO energies.....	140
Table 5.4	The energies of the HOMOs and LUMOs of molecule 1 with 2 H ₂ units bound and hydride as the ancillary ligand with various metal centers, which are/would be subsequently involved in bonding to the 3 rd H ₂ . When more than 1 LUMO interacted with the H ₂ an average was taken and the ± value shows the range of the LUMO energies.....	141
Table 6.1	Summary of excess storage results of chromium hydrazide materials before and after hydrogenation (data are taken at 85 bar, and the samples were dried at the optimal drying temperature of 100 °C).....	161

List of Figures

Figure 1.1	Hydrogen phase diagram.....	4
Figure 1.2	Orbitals representation of the H ₂ -M donation through σ , and M-H ₂ backdonation through π in a Kubas complex.....	11
Figure 1.3	The structure of the three types of silanol groups on silica surface as well as that of siloxane.....	13
Figure 1.4	Raman spectra of hydrogen as a free gas and in the presence of MOF-5 at room temperature and 30.3 bar.....	17
Figure 1.5	INS spectra of H ₂ in HKUST-1 at 0.2, 0.5, 1.0, 1.5, 2.0 H ₂ :Cu.....	20
Figure 2.1	Representative X-ray diffraction pattern of mesoporous silica treated with 0.2 equiv. of tetrabenzyl titanium.....	43
Figure 2.2	Representative nitrogen adsorption/desorption isotherm of material from Fig.2.1.....	44
Figure 2.3	Hydrogen storage and adsorption isotherms at 77 K for mesoporous silica treated with various molar equivalents of tribenzyl titanium: (a) Gravimetric storage density; (b) Volumetric storage density; (c) Gravimetric adsorption density; (d) Volumetric adsorption density.....	44
Figure 2.4	Hydrogen storage and adsorption isotherms at 77 K for mesoporous silica treated with various molar equivalents of tetrabenzyl titanium: (a) Volumetric storage density; (b) Volumetric adsorption density.....	48
Figure 2.5	Hydrogen storage isotherms at 77 K for mesoporous silica treated with various molar equivalent of tetrabenzyl titanium: (a) Gravimetric storage density; (b) Gravimetric adsorption (excess storage) density. Slight fluctuations at higher pressure in some adsorption isotherms were not related to temperature fluctuations, as this parameter was strictly controlled.....	49
Figure 2.6	Hydrogen storage capacity in a 20 cycle test of mesoporous silica treated with 0.2 molar equivalent of tetrabenzyl titanium.....	54
Figure 2.7	Adsorption and desorption isotherms for the material from Fig. 2.6.....	54
Figure 2.8	Hydrogen binding enthalpies of mesoporous silicas from Table 1: Pristine silica (black), the 0.2 molar equiv. tetrabenzyltitanium material after heating at 180°C (red), the 0.3 molar equiv. tetrabenzyltitanium material after heating at 180°C (brown) and the 0.2 molar equiv. tetrabenzyltitanium material before heating (pink).....	55

Figure 2.9	Adsorption isotherms for the materials from Figure 2 recorded at liquid argon and liquid nitrogen temperatures: (a) Pristine mesoporous silica; (b) Silica treated with 0.2 molar equivalents tetrabenzyl titanium after heating; (c) Silica treated with 0.3 molar equivalents tetrabenzyl titanium after heating; (d) Silica treated with 0.2 molar equivalents tetrabenzyl titanium before heating.....	58
Figure 3.1	Hydrogen adsorption isotherms at 77 K for mesoporous silica synthesized using different molar ratios of tetraethyl-orthosilicate:dodecyl-amine.....	69
Figure 3.2	Hydrogen adsorption isotherms at 77 K of C ₆ , C ₈ , C ₁₀ and C ₁₂ -HMS.....	71
Figure 3.3	Hydrogen adsorption isotherms at 77 K of C ₁₂ -HMS grafted with various molar equivalents of tetrabenzyl Ti.....	73
Figure 3.4	Hydrogen adsorption isotherms at 77 K of C ₁₂ -HMS grafted with various molar equivalents of (benzyl) ₃ Ti.....	74
Figure 3.5	Excess hydrogen adsorption (filled symbols) and desorption (unfilled symbols) isotherms at 77 K and 60 atm of HMS treated with 0.2, 0.3, and 0.5 molar equivalents of TiMe ₃	77
Figure 3.6	Excess hydrogen adsorption (filled symbols) and desorption (unfilled symbols) isotherms at 77 K and 60 atm of HMS treated with 0.2, 0.3, and 0.5 molar equivalents of (Allyl) ₃ Ti.....	79
Figure 3.7	Ti 2p XPS spectra of HMS treated with 0.2 equivalents of (a) trimethyl Ti, (b) triallyl Ti, (c) Tetrabenzyl Ti.....	80
Figure 3.8	Hydrogen binding enthalpies of pristine HMS (×), 0.2Me ₃ Ti-HMS (◆), 0.2(Allyl) ₃ Ti-HMS (■), 0.2Bz ₄ Ti-HMS (▲), 0.3Bz ₃ Ti-HMS (*)......	81
Figure 4.1	Adsorption isotherms at 77K of plain HMS silica and HMS silica treated with bis (naphthalene) titanium and tetrabenzyl titanium. Desorption isotherms omitted for clarity.....	96
Figure 4.2	Hydrogen binding enthalpies of HMS silica compared to those of HMS silica grafted with bis (naphthalene) titanium and with tetrabenzyl titanium.....	96
Figure 4.3	XPS spectrum with simulations for HMS silica treated with tetra benzyl titanium showing the Ti 2p _{1/2} , 3/2 emissions.....	97
Figure 4.4	XPS spectrum with simulations for HMS silica treated with bis(naphthalene) titanium showing the Ti 2p _{1/2} , 3/2 emissions.....	97

Figure 4.5	Adsorption isotherms at 77 K of HMS silica treated with tris(mesityl) vanadium before and after hydrogenation compared to that of plain HMS silica. Desorption isotherms omitted for clarity.....	100
Figure 4.6	Hydrogen binding enthalpies of HMS silica treated with tris(mesityl) vanadium before and after hydrogenation compared to that of HMS silica.....	101
Figure 4.7	XPS spectrum with simulations for HMS silica treated with tris(mesityl) vanadium before hydrogenation showing the V 2p _{1/2} , 3/2 emissions.....	101
Figure 4.8	XPS spectrum with simulations for HMS silica treated with tris(mesityl) vanadium after hydrogenation showing the V 2p _{1/2} , 3/2 emissions.....	102
Figure 4.9	Adsorption isotherms of HMS silica treated with tris[bis(trimethylsilyl)methyl] chromium before and after hydrogenation compared to that of HMS silica. Desorption isotherms omitted for clarity.....	105
Figure 4.10	Hydrogen binding enthalpies of HMS silica treated with tris[bis(trimethylsilyl)methyl] chromium before and after hydrogenation compared to that of HMS silica.....	106
Figure 4.11	XPS spectrum with simulation for HMS silica treated with tris[bis(trimethylsilyl)methyl] chromium showing the Cr 2p _{1/2} , and 3/2 emissions.....	109
Figure 4.12	XPS spectrum with simulations for HMS silica treated with tris[bis(trimethylsilyl)methyl]chromium after hydrogenation showing the Cr 2p _{1/2} , and 3/2 emissions.....	109
Figure 4.13	Adsorption isotherms of HMS silica treated with bis[(trimethylsilyl)methyl]chromium before and after hydrogenation as compared to that of plain silica. Desorption isotherms omitted for clarity.....	111
Figure 4.14	Hydrogen binding enthalpies of HMS silica treated with bis[(trimethylsilyl)methyl] chromium before and after hydrogenation compared to that of plain HMS silica.....	111
Figure 4.15	XPS spectrum of HMS silica treated with bis[(trimethylsilyl)methyl]Cr before hydrogenation showing the Cr 2p _{1/2} , and 3/2 emissions.....	112

Figure 4.16	XPS spectrum of HMS silica treated with bis[(trimethylsilyl)methyl]Cr after hydrogenation showing the Cr 2p _{1/2} , and 3/2 emissions.....	113
Figure 5.1	Schematic representations of the molecular modules employed a) benzyl disiloxy Ti (III) (molecule 1) and b) dibenzyl siloxy Ti (III) (molecule 2).....	125
Figure 5.2	A) molecule 1 with 3 H ₂ units bound, B) molecule 2 with 4 H ₂ units bound.....	127
Figure 5.3	Orbital representations for molecule 1 with 1 H ₂ unit bound. A) The HOMO showing σ -bonding from the H ₂ unit to the metal. In B) and C) the HOMO and HOMO-1 respectively shows π -back-bonding from the metal to the H ₂ unit.....	128
Figure 5.4	The partial charge on the titanium metal center of molecule 1 with a benzyl ligand, as a function of the number of H ₂ units bound.....	128
Figure 5.5	Comparison of the experimental hydrogen binding enthalpies calculated by Hamaed et al. ^[14] the computed enthalpies, and Ti-H ₂ bond energies of the experimental model. The computational values are a 50:50 average of molecules 1 and 2 and the error bars show the range of these values.....	129
Figure 5.6	The average Ti-H ₂ bond energy calculated for molecule 2 with various ancillary ligands.....	130
Figure 5.7	The average Ti-H ₂ bond energy calculated for molecule 1 with various ancillary ligands. The high average bond energy when 2 H ₂ units are bound to the titanium with an allyl ancillary ligand has been circled....	131
Figure 5.8	Molecule 1 with titanium as the metal and with 1 or 2 H ₂ units bound with A allyl, B benzyl, C methyl and D hydride ancillary ligand.....	134
Figure 5.9	The average V-H ₂ bond energy for molecule 1 with vanadium as the metal center and with various ancillary ligands.....	135
Figure 5.10	The average M-H ₂ bond energy as a function of the number of H ₂ units bound for molecule 1 with a hydride ancillary ligand and various metal centers.....	136
Figure 5.11	The graph of the average M-H ₂ bond energy against the number of H ₂ units bound for molecule 1 with methyl ancillary ligands and various metal centers.....	137
Figure 5.12	Molecular orbital diagram of molecule 1 with a Ti metal atom and a	

	hydride ancillary ligand with 0, 1 and 2 H ₂ units bound.....	138
Figure 6.1	Nitrogen adsorption/desorption isotherms of the as-synthesized Cr-MHZ materials.....	158
Figure 6.2	Nitrogen adsorption/desorption isotherms of the as-synthesized Cr-MHZ materials.....	159
Figure 6.3	Excess storage isotherms at 298K for the as-synthesized Cr-hydrazide samples prepared with various ratios (samples were dried at 100 °C)...	160
Figure 6.4	Excess storage isotherms at 77K for the as-synthesized Cr-hydrazide samples prepared with various ratios.....	162
Figure 6.5	Infra-red spectra of Cr-MHZ (1.5) before (BLUE) and after (PINK) hydrogenation at 180 °C and 85 atm for 4 hours.....	163
Figure 6.6	Infra-red spectra of Cr-MHZ (1.0) before (BLUE) and after (PINK) hydrogenation at 180 °C and 85 atm for 4 hours.....	164
Figure 6.7	Figure 6.7: Infra-red spectra of Cr-MHZ (2.0) before (BLUE) and after (PINK) hydrogenation at 180 °C and 85 atm for 4 hours.....	164
Figure 6.8	Infra-red spectra of Cr-MHZ (0.5) before (BLUE) and after (PINK) hydrogenation at 180 °C and 85 atm for 4 hours.....	165
Figure 6.9	Room temperature excess storage isotherms of Cr-hydrazides prepared with various ratios after hydrogenation at 180 °C and 85 atm for 4 hours.....	166
Figure 6.10	Excess storage isotherms of Cr-hydrazides prepared with various ratios at 77K after hydrogenation.....	168
Figure 6.11	Binding enthalpies for the as-synthesized chromium hydrazide samples prepared in various ratios.....	169
Figure 6.12	Binding enthalpies of chromium hydrazides prepared in various ratios after hydrogenation.....	170
Figure 6.13	Hydrogen excess storage at 298 K in a 20 cycle test of H ₂ -Cr-MHZ (1.5).....	170

List of Schemes

- Scheme 2.1** Schematic representation of the grafting of benzyl Ti species onto the surface of mesoporous silica and the subsequent formation of tunable low-coordinate H₂ binding sites with enthalpies over 20 kJ/mol.....42
- Scheme 3.1** Material prepared by coating HMS surface with trimethyl Ti precursor..77
- Scheme 3.2** Material prepared by grafting HMS surface with triallyl Ti precursor....79
- Scheme 4.1** Schematic representation of the grafting of Ti onto the surface of HMS silica treated with bis(naphthalene)Ti, and the formation of Ti(II) species on the surface, favourable for H₂ binding.....98
- Scheme 4.2** HMS silica treated with tris(mesityl)vanadium.....100
- Scheme 4.3** Schematic representation of the grafting of mesoporous silica by treatment with bis(trimethylsilyl)methyl chromium leading to the formation of Cr(II) sites favorable for H₂ binding, Si'= Si(CH₃).....108
- Scheme 6.1** Proposed structure of Cr-MHZ (before hydrogenation).....158
- Scheme 6.2** Proposed structure of Cr-MHZ (after hydrogenation).....165

List of Appendices

Appendix A – Supplementary Tables for Chapter 6

Table A.6.1	Summary of excess storage results on the as-synthesized chromium hydrazide materials for the samples dried at room T (data are taken at 85bar).....	182
Table A.6.2	Summary of excess storage results on the as-synthesized chromium hydrazide materials for the samples dried at 150 °C (data are taken at 85bar).....	183

Appendix B – Supplementary Figures for Chapter 4

Figure B.4.1	Hydrogen adsorption and desorption isotherms at 77K and at 298K for plain silica (HMS).....	184
Figure B.4.2	Hydrogen adsorption and desorption isotherms at 77K and at 298K for tetra(benzyl)Ti-HMS.....	184
Figure B.4.3	Hydrogen adsorption and desorption isotherms at 77K and at 298K for bis(naphthalene)Ti-HMS.....	185
Figure B.4.4	Hydrogen adsorption and desorption isotherms at 77K and at 298K for tris(mesityl)V-HMS before hydrogenation.....	185
Figure B.4.5	Hydrogen adsorption and desorption isotherms at 77K and at 298K for tris(mesityl)V-HMS after hydrogenation.....	186
Figure B.4.6	Hydrogen adsorption and desorption isotherms at 77K and at 298K for tris[bis(trimethylsilyl)methyl]Cr-HMS before hydrogenation.....	186
Figure B.4.7	Figure S 4.7 - Hydrogen adsorption and desorption isotherms at 77K and at 298K for tris[bis(trimethylsilyl)methyl]Cr-HMS after hydrogenation.....	187
Figure B.4.8	Hydrogen adsorption and desorption isotherms at 77K and at 298K for bis[(trimethylsilyl)methyl]Cr-HMS before hydrogenation.....	187
Figure B.4.9	Hydrogen adsorption and desorption isotherms at 77K and at 298K for bis[(trimethylsilyl)methyl]Cr-HMS after hydrogenation.....	188

Appendix C – Copyright Permission Forms

C.1	Permission to include my Journal of the American Chemical Society paper in this thesis.....	189
C.2	Permission to include my Journal of the Organometallic Chemistry paper in this thesis (Chapter 3).....	190
C.3	Permission to include the Figure 1.1 in this thesis.....	191
C.4	Permission to include Figure 1.4 in this thesis.....	192
C.5	Permission to include Figure 1.5 in this thesis.....	193
C.6	Permission to include the computational calculations in this thesis.....	194

List of Abbreviations, Symbols, Nomenclature

ADF	Amsterdam density functional
App. d	apparent density
Å	angstrom
atm	atmosphere (= 101.325 kPa)
BET	Brunauer-Emmet-Teller
°C	degree Celsius
DFT	density functional theory
DOE	US-department of energy
EA	elemental analysis
ESR	electron spin resonance
h	hour
HMS	hexagonally-packed mesoporous silica
ICP-AAS	inductively coupled plasma-atomic absorption spectroscopy
INS	inelastic neutron scattering
IR	infrared spectroscopy
kJ	kilojoules
L	liter
M	mol L ⁻¹
MAS	magic angle spinning
Me	methyl CH ₃
MOF	metal organic frameworks

NMR	nuclear magnetic resonance
Ph	phenyl, C ₆ H ₅
R	gas constant
Sk. d	skeletal density
T	absolute temperature
THF	tetrahydrofuran
wt %	weight percent
XPS	X-ray photoelectron spectroscopy
XRD	X-ray diffraction

Chapter 1 – Introduction

1.1 Hydrogen: The Ultimate Fuel

Hydrogen, which is Greek for water forming, is a colorless, odorless, tasteless, non-toxic flammable gas.^[1] It is the simplest, lightest and most abundant element in the universe and it is estimated to make up about three quarters of the mass of the universe.^[2] However, on earth less than 1 % of hydrogen is present as molecular hydrogen gas. It mainly occurs in combination with oxygen as in water, or bound with carbon as in hydrocarbon fuels (petroleum).^[3] Hydrogen is often called an energy carrier or energy vector, instead of an energy source. This is because energy must be used to extract hydrogen from water, natural gas, or other compounds that contain hydrogen. Hydrogen gas was first produced in the early 16th century, but was not recognized as a new substance till 1776 by the British scientist Henry Cavendish. He called it an “inflammable air” rising from a zinc-sulfuric acid mixture, but later Antoine Lavoisier succeeded in reproducing Cavendish's experiment and gave the element its name.^[4] Hydrogen exhibits the highest heating value per mass of all chemical fuels (142 MJ/kg), which equivalent to three times that of gasoline (47 MJ/kg).^[5] It represents the ultimate solution for converting to less and less carbon-containing fuel. Throughout history, humanity has been moving towards carbon-free fuel, considering that our ancestors relied mainly on wood and charcoal for their energy needs, which was later replaced by coal at the outbreak of the industrial revolution. Coal, which has higher energy density per mass than woods and charcoal, was used to power steamships and railroad engines and it is considered as the energy symbol of the industrial revolution

era. Later, at the beginning of the 20th century, coal was replaced by oil. If one follows this trajectory, as time progresses subsequent fuel sources will contain less carbon and more hydrogen by unit mass.^[6] Therefore, fuel evolution must eventually reach the ultimate destination of pure hydrogen.

Hydrogen is a renewable and environmentally friendly fuel, and it is the ideal energy carrier for mobile application; but the problem of adequate and safe storage is still unsolved. Storage implies the reduction of the enormous volume that hydrogen gas occupies at standard temperature and pressure. At room temperature and atmospheric pressure, 4 kg of hydrogen occupies a volume of 45 m³.^[5] The problem of poor hydrogen energy content per volume (0.01 kJ/L at STP and 8.4 MJ/ L for liquid hydrogen vs. 32 MJ/L for petroleum) can be overcome by compressing the gas, or by cooling it below its critical temperature (Fig. 1.1) or by reducing the repulsion forces by the interaction of hydrogen with the surface of another material.^[7]

The hydrogen atom (H) consists of an electron circling a proton. It has an atomic weight of 1.00797. This element is a major constituent of water and all organic matter. There are three isotopes of hydrogen: protium, which makes up to 99.98% of the natural element; deuterium, which makes up about 0.02%; and tritium, which occurs in extremely small amounts in nature.^[8] The physical properties of hydrogen are summarized in Table 1.1.

As it is the nature's lightest element, when gaseous hydrogen escapes it quickly rises in the Earth's atmosphere because of its extreme buoyancy; it also diffuses through air much more rapidly than any other gaseous fuel. Since hydrogen gas rises so quickly, it is difficult to accumulate a large hydrogen-air mixture to sustain a substantial fire. This

fact makes hydrogen perhaps the safest fuel for transportation application.^[9] However, if hydrogen were to leak into an enclosed space, i.e., a car garage, then hydrogen sensors must be installed at some locations in the garage to provide leak warning. Also adequate ventilation would help reduce the possible formation of hydrogen-air flammable mixtures in the event of a hydrogen leak.

Table 1.1 - Properties of hydrogen (H₂).^[8]

Property	Value
Molecular weight	2.01594 g/mol
Density of gas at 0°C and 1 atm.	0.08987 kg/m ³
Density of solid at -259°C	85.8 kg/m ³
Density of liquid at -253°C	70.8 kg/m ³
Melting temperature	-259 °C
Boiling temperature at 1 atm.	-253 °C
Critical temperature	-240 °C
Critical pressure	12.8 atm.
Critical density	31.2 kg/m ³
Lower heat value	119.9 MJ/kg
Higher heat value	141.6 MJ/kg
Flame temperature	2207 °C

Molecular hydrogen (H₂) exists in two different energy states or spin isomers. The ortho hydrogen form, in which the nuclei have parallel spins with a molecular spin number of 1($\frac{1}{2} + \frac{1}{2}$), and the para hydrogen in which the nuclei have antiparallel spins and the molecule has a spin number of 0 ($\frac{1}{2} - \frac{1}{2}$). At ambient temperature and pressure about 25% of the hydrogen gas is of the para form and 75% of the ortho form.^[10]

The hydrogen molecule is a very weak acid, with a pKa value of 49 in THF.^[11] The diameter of the hydrogen molecule is 0.41 nm.^[5]

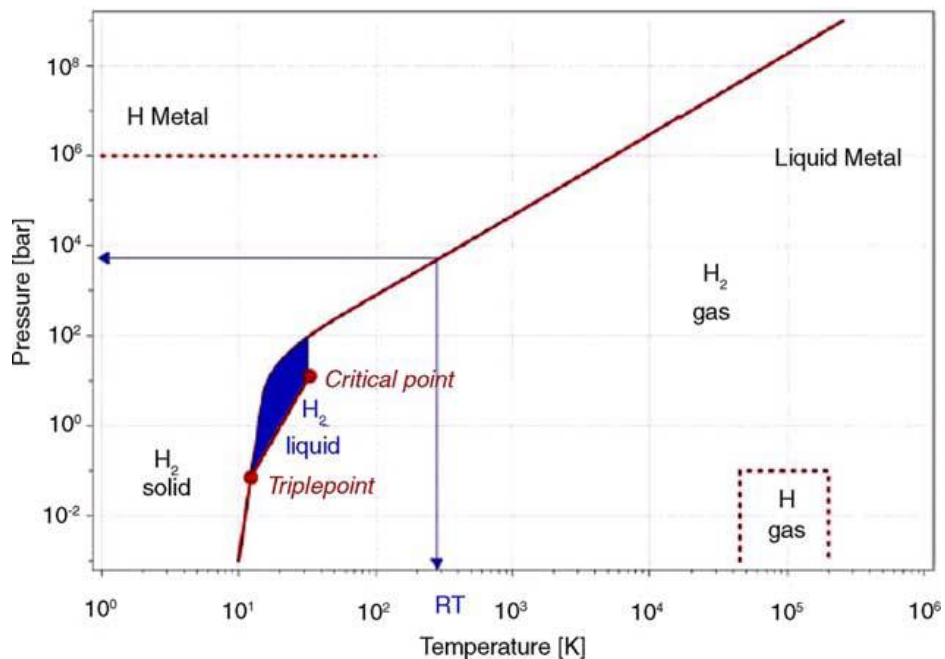


Figure 1.1 – Hydrogen phase diagram^[12] (reproduced with permission from Elsevier).

1.2 Hydrogen Storage Methods

Effective, efficient, and safe hydrogen storage technique is a key for the transition to carbon-free fuel. However, more challenges must be overcome for on-board hydrogen storage transportation applications. The currently available hydrogen storage methods with their advantages and drawbacks are reviewed in this section.

1.2.1 Pressurized Tank Gaseous Hydrogen Storage

Storing hydrogen as a compressed gas is a currently available method, with storage tanks that withstand pressure up to 350 bars. This storage technique is about five times less energy-dense than gasoline, i.e., storing hydrogen, employing this technique, requires a volume 5 times that of the gasoline tank.^[13] Therefore, there is a need for

further compression, with the current aim for a pressure increase up to 700 bars in special tanks which would provide a gravimetric hydrogen storage capacity of 4.5 wt%, equivalent to the DOE 2010 target; however the volumetric capacity in this case is only $0.025 \text{ kgH}_2\text{L}^{-1}$.^[14] The energy loss in compressing H_2 gas to 700 bar of about 15% of the total energy value of the H_2 gas, and the safety issues in the event of an accident, are major drawbacks that prevent the implementation of this hydrogen storage method for mobile application.

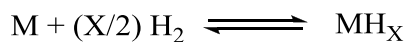
1.2.2 Cryogenic Liquid Hydrogen Storage

Liquid hydrogen (LH_2) is already in use as a fuel for space rockets. Hydrogen gas can be liquefied at temperatures below 33 K as shown in Fig. 1.1.^[15] At atmospheric pressure, hydrogen has a boiling point of 20 K and the liquid H_2 density (1atm, 20K) is 70.8 kg/ m^3 .^[16] This translates into 2.35 kWhL^{-1} system volumetric capacity, which exceeds the DOE new target for 2015 (1.3 kWhL^{-1}). However, the large-scale applications of LH_2 for on-board vehicular use are difficult, due to the energy penalties associated with cooling and liquefying, which are equivalent to about 30% of the total energy value of H_2 , and also the problem of hydrogen boil-off on standing and the energy loss and safety concerns associated with it, especially for a vehicle left in an enclosed space.^[17]

LH_2 storage method, with all of its drawbacks, has lots of advantages over gaseous storage in pressurized tanks. The LH_2 storage tank is of lower mass and smaller volume than that used for hydrogen gas at very high pressure; this translates into a higher energy capacity per tank and therefore longer driving range. However, it is still not an appropriate storage method for mobile application.

1.2.3 Hydrogen Storage by Chemical Adsorption

The conventional storage methods of compressed gas and LH₂ fail to meet the strict requirements for the implementation of hydrogen as a transportation fuel as a result of low volumetric capacity, problematic energy efficiency, and safety concerns. Therefore, it is desirable to explore alternative solutions to these storage techniques, such as using a chemical substance as a carrier. Hydrogen can be stored in solids by chemical binding to a metallic substrate by forming a metal hydride in noble metals and alloys. In this process the molecular hydrogen dissociates at the metal surface to form a hydride phase. The reaction of H₂ with a metal (M) is represented as follows: ^[17]

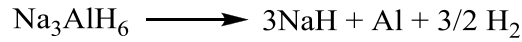
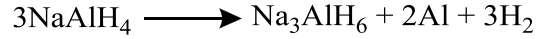


This reaction is normally very exothermic. For example, MgH₂ with its high gravimetric capacity of 7.6 wt% possesses an H₂ binding enthalpy of about 70 kJ/mol H₂ and requires a heating temperature of about 300 °C to desorb hydrogen at normal pressure. On the other hand, metal hydrides such as VH₂ and LaNi₅H_x have more a moderate binding energy (of about 40 kJ/mol H₂), but the presence of relatively heavy metals limits their gravimetric capacity. In summary, metal hydrides are effective in achieving high volumetric densities of hydrogen, but the problems associated with the high heating temperature needed for H₂ release, and their low gravimetric hydrogen content when heavy metals are incorporated into the structure limits their use as hydrogen storage materials for mobile application.

Another class of hydrides that shows promise for hydrogen storage is complex hydrides. They are inorganic compounds of hydride anions such as [AlH₄]⁻, [BH₄]⁻, combined with alkali metal cations to form soluble salts e.g., NaAlH₄, LiBH₄. These

materials have a higher gravimetric capacity than most metal hydrides and they release hydrogen under more moderate conditions than those of metal hydrides.

The thermal decomposition of the alanate NaAlH_4 is shown below:^[18]



The first step occurs over the temperature range 50-100 °C, and corresponds to the release of 3.7 wt. % hydrogen. The second step occurs at a higher temperature in the range 130-180 °C with the release of a further 1.9 wt. % H_2 . These reactions are only reversible at temperature above 183 °C.

LiBH_4 and NaBH_4 contain more hydrogen than the alanates, 18.5 and 10.6 wt. % respectively, but they start to decompose at much higher temperatures (300 °C for LiBH_4 , and 375 °C for NaBH_4). Incorporating Ti into the alanate lattice can make the decomposition reaction of the alanate easier. Titanium metal located on or near the surface, catalyzes the dissociation reaction by lowering the activation barrier.^[19]

Therefore, these complex hydrides are not suitable as hydrogen storage materials for on-board application as they release H_2 at undesirable temperature and pressure conditions for vehicular application.^[20]

1.2.4 Hydrogen Storage by Physical Adsorption

Maintaining the molecular identity of adsorbed H_2 is proposed as a fast and efficient way for H_2 charge and release.^[21] The non-dissociative H_2 adsorption on high surface area porous materials is of great importance for the development of storage systems displaying good reversibility, fast kinetics and high storage capacities. Thus materials with large surface areas such as activated carbon,^[22] carbon nanotubes,^[23, 24]

fullerenes,^[25-27] zeolites,^[28] molecular clathrates,^[29] metal-organic frameworks,^[30-34] and mesoporous metal oxides,^[35-40] are great candidates for hydrogen adsorption in a non-dissociative manner. However the type of interactions that hold the H₂ molecules to the surface are generally weak dispersive forces. Therefore the system requires cooling at cryogenic temperatures (usually at 77 K) to guarantee an acceptable storage capacity. This condition is not suitable for vehicular application, which requires H₂ uptake at ambient temperature. Thus, it is highly desirable to devise a way to strengthen the H₂-adsorbent interactions without breaking the H-H bond. This can be achieved by the inclusion of other types of interactions such as electrostatic (charge-induced dipole interaction) and orbital interactions (Kubas binding) through the incorporation of new functionalities on the surface. Many attempts were made to increase the H₂ adsorption enthalpy in metal organic frameworks. This was accomplished through various methods. However the most effect means to increase hydrogen binding enthalpies in MOFs was accomplished by the introduction of open metal sites, by catenations/ interpenetration, or by spillover.^[41]

1.6 System Requirements and Department of Energy targets for Hydrogen Adsorption in Solid-state Materials

To be considered as practical for onboard applications, the hydrogen storage materials must display high gravimetric and volumetric capacities, i.e., materials must be light in weight and conservative in space, and must have fast adsorption/desorption kinetics, i.e., quick hydrogen uptake and release, appropriate thermodynamics, i.e. favorable enthalpies of H₂ adsorption and desorption, high robustness, mechanical strength and durability, and a long cycle life time for H₂ adsorption and desorption, and

a high tolerance for recycling, safety under normal use and acceptable risk under abnormal conditions.^[42]

The United States department of energy (DOE) has set system targets for the year 2015 that must be met by the material to be considered ideal for hydrogen storage. A summary of the DOE old (2003)^[43] and the newly revised (2009)^[44] hydrogen storage targets are displayed in the table 1.2 below.

Table 1.2 – Summary of the DOE hydrogen storage system targets.

Storage Property	Old targets (2003)		Newly revised targets (2009)		
	For 2010	For 2015	For 2010	For 2015	Ultimate
Gravimetric capacity in wt.%	6	9	4.5	5.5	7.5
Volumetric capacity in Kg/m ³	45	81	28	40	70
Operating pressure in Mpa	0.4-10	0.3-10	0.5-1.2	0.5-1.2	0.3-1.2
Kinetics in (g H ₂ /s)/kW	0.02	0.02	0.02	0.02	0.02

Computational studies and theoretical investigations have shown that for optimal storage at room temperature, the hydrogen-adsorbent binding enthalpy should be between 20-40 kJ/mol,^[21, 45] 15-20 kJ/mol,^[46] 20-30 kJ/mol,^[47] or 15 kJ/mol^[48] depending on the study. For the two main classes of solid-state hydrogen storage materials currently under investigation: the materials that uptake hydrogen through

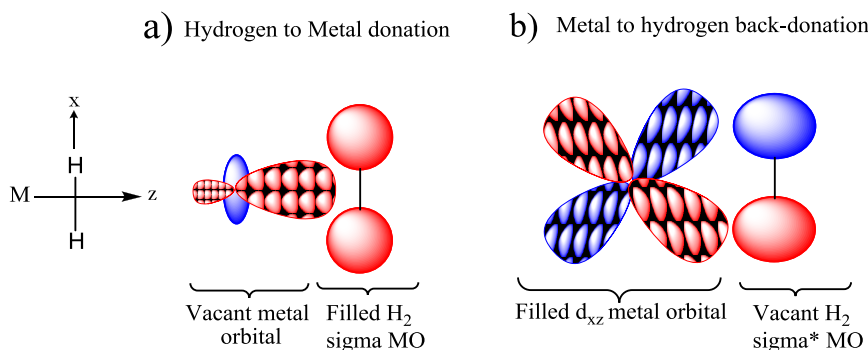
chemical adsorption have binding energies in the range of 40-80 kJ/mol and require heating for H₂ adsorption and release,^[49] and those that uptake hydrogen by weak physical adsorption require cooling to cryogenic temperature in order to hold the H₂ molecule into the binding sites and their binding energies are typically in the range 4-7 kJ/mol.^[50] Therefore, in order to arrive at materials with H₂-adsorbent binding energy in the optimal range for practical applications, it is required to reduce the magnitude of the binding enthalpy when chemisorption is taking place and to increase the strength of the binding interactions when physisorption is under consideration. In other words, it is highly desired to find adsorption sites with hydrogen binding enthalpy in the mid-way between those of physisorption and chemisorption materials.

1.4 Enhancing the H₂-adsorbent binding through Kubas-interaction

The year 1984 brought a great breakthrough in the field of the coordination chemistry of dihydrogen when Kubas and his co-workers discovered a new type of H₂-complex in which the H₂ molecule acts as a ligand without losing its molecular identity.^[51] The side-on binding of H₂ to a metal center in an η^2 -manner through the donation of the hydrogen two electrons to an empty d orbital through σ bonding was thus delineated. This interaction is augmented by back-bonding from filled metal d orbitals to a vacant H₂ σ^* antibonding orbital through π bonding as shown in Fig. 1.2 below. The finding of a side-on bonded H₂ was first observed in the complex [W(CO)₃(P-i-Pr₃)₂(H₂)].^[52, 53] The H-H bond length of the tungsten complex was 0.89 Å, or about 20% longer than that of the free H₂. The Kubas-interaction represents a middle class between physical adsorption and chemical adsorption, with a binding

enthalpy falling in the optimal range of 20-30 kJ/mol required for H₂ storage at ambient temperature.

Figure 1.2 – Orbital representation of the H₂-M bonding through σ , and M-H₂ back-bonding through π in a Kubas complex.

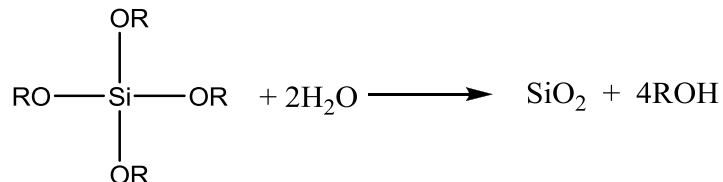


The stability of the H₂ complexes depends on the nature of the metal, ligands, and charge, i.e. first-row metal, electron withdrawing ligand, and positive charge shorten d_{HH} and favor molecular H₂ binding.^[54] As we go from left to the right in the transition series or down a group to third row metals, back-donation ability increases and the σ bond cleaves to form a dihydride because of the overpopulation of H₂ σ^* .^[55] Also the ligand trans to H₂ has a powerful influence: strong π -acceptors such as CO greatly reduce back-donation and keeps $d_{\text{HH}} < 0.9 \text{ \AA}$. If the trans ligand is a strong σ -donor such as hydride, there is a powerful trans influence that reduces σ electron donation from H₂ to keep the orbital electron population in balance because the orbitals are shared.^[55] A weak σ -donor ligand trans to H₂ elongates the H₂ and therefore disfavors an H₂ complex. A mild π -donor such as Cl trans to H₂ elongates the d_{HH} (0.96-1.34 \AA) and therefore disfavors H₂ complexes.^[55] The influence of cis ligands is

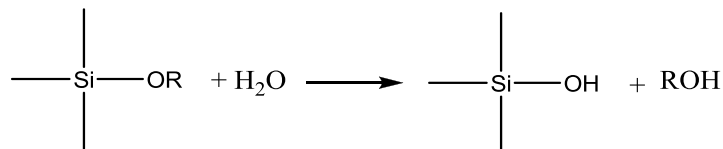
less consequential because the orbitals are independent of each other. Positive charges on M favor η^2 -H₂ binding while negative charges promote oxidative addition to dihydride.^[52]

1.5 Mesoporous Silica Gel as Hydrogen Storage Materials

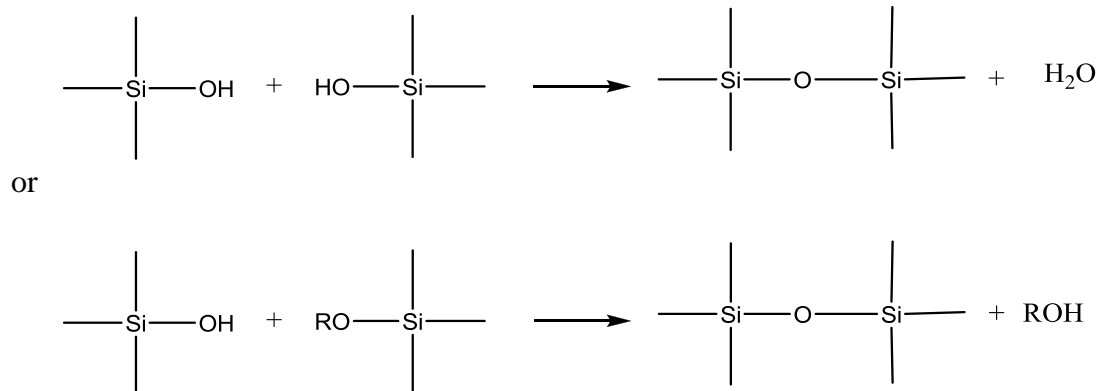
Hexagonally-packed mesoporous silicas (HMS) are very light in weight with an apparent density of 0.16 g/cc and with a surface area up to 1800 m²/g.^[56] They are made from cheap materials (silicon alkoxides, water, ethanol, and amine template) and can be synthesized in large scale.^[57] Silica gel preparation involves reactions of silicon alkoxides with water; by this route a variety of materials can be produced. The silica gel obtained is amorphous and composed of small globular particles having sizes of 10 to 20 Å.^[58] This procedure is usually referred to as a “sol-gel” route, and can be represented by the following reactions:^[59, 60]



Silicic acids are also formed by hydrolysis:



The silicic acids can then polymerize via the reaction:

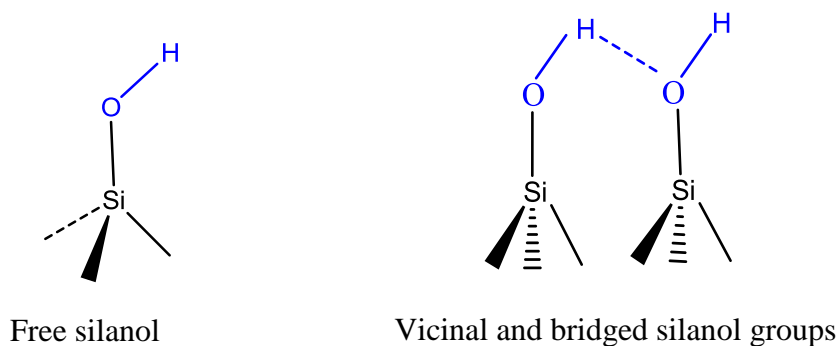


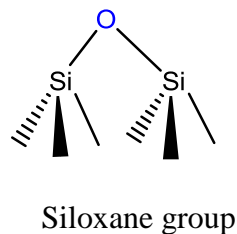
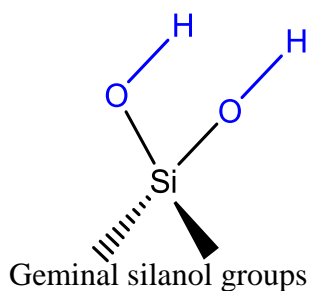
The pore size and structure can be tuned by using ligand assisted templating procedure employing different chain length amines. The pH value is also a major factor in tailoring the pore dimensions. An acidic pH will lead to microporosity, whereas a basic pH results in mesoporosity.^[60]

1.5.1 Silica Surface Properties

The silanol groups (Si-O-H) on the surface of the HMS silica are the main functional groups that play a significant role in determining the application properties of HMS silica.^[61, 62] These groups participate in adsorption (physisorption) as well as in the chemical modification and functionalization of the silica surface. There are three types of silanol groups on the silicas, as shown in the figure below.^[63]

Figure 1.3 – The structures of the three types of silanol groups on silica surface as well as that of siloxane.





The most important factor in play here is the surface silanol group density (i.e. SiOH/nm^2), also called the silanol number, so that the framework silica to be used as a hydrogen gas adsorbent must be optimized in order to maximize the silanol density on surface. The silanol number can be determined by different methods:

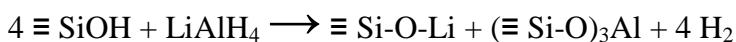
1- Deuterium exchange method:^[64]

The H atoms of the surface silanol are exchanged with D in D_2O . Infrared spectroscopy permits the monitoring of the reaction process, and the analysis of the H_2O , HDO and D_2O mixture provides a quantitative determination of the silanol groups.

2- The lithium aluminum hydride method:^[65]

It is regarded as the simplest and most accurate method for determining the silanol number on silica surface. In this method, the amount of hydrogen produced by the reaction of the silanol groups with lithium aluminum hydride is found by a pressure measurement. The hydride ion is small enough and highly reactive, so that all silanol groups on the surface are detected.

The reaction between the surface silanols and LiAlH_4 is represented as follows:



1.5.2 Surface Functionalization of Mesoporous Silica by Metal-fragments Grafting.

HMS has a robust, mesoporous structure, and is highly rich in surface hydroxyl groups. These characteristics make HMS an ideal candidate for chemical grafting. The surface hydroxyl (-OH) group can stably bind a transition metal atom and form TM-functional group complexes. It has been calculated that a single site TM atom adsorbs several H₂ molecules with the binding energy of about 0.3eV/H₂ (29 kJ/mole).^[66] The strong tendency of impregnated surfaces with low-valent metal centers to interact with H₂ through a Kubas interaction makes HMS very attractive as a support in hydrogen storage materials. In a recent study by Basset et al.,^[66] aerosol silica was dehydrogenated at different temperature (800, 500, 200 °C) to give homogeneous surface species after grafting it with hafnium neopentyl. The as-synthesized and hafnium neopentyl grafted materials were characterized by IR and solid-state NMR. The obtained hafnium neopentyl grafted silica was then hydrogenated at 150 °C for 17 hours under 500 mbar H₂. The direct environment around the grafted metal has a great impact on the catalytic activity of these materials. The unique property of the surface oxidation state in porous oxides can be varied as a mean of tuning H₂ binding enthalpies and storage capacity.

1.6 Characterizations of Solid-state Hydrogen Storage Materials

The understanding of the type of the intermolecular interactions responsible for hydrogen storage as well as the binding strength and the location of the adsorption sites is very crucial for the design and the development of new storage materials that can function at ambient temperature and pressure.^[50] Among the techniques employed for the investigation of the H₂-interaction within solid-state hydrogen storage materials and

the other properties of these materials are infra-red spectroscopy, Raman spectroscopy, inelastic-neutron scattering, X-ray diffraction, as well as computational modeling. These are reviewed in the following sections.

1.6.1 Infra-red Spectroscopy

In infra-red spectroscopy, the vibrational motions of the atoms are considered. The change in the molecular dipole moment when the atoms vibrate determines whether the vibration is IR active or inactive. The dipole moment is determined by the magnitude of the charge difference and the distance between the two centers of charge.^[67]

The free H₂ molecule vibrates without any change to its dipole moment, i.e. its vibration does not produce an oscillating dipole; therefore it is IR inactive.^[68] However, the interaction of the H₂ molecules with the surface of any framework polarizes the H-H bond, therefore leading to an oscillating dipole when vibrating and making the H₂ molecule IR active by the polarization effect of the surface.^[50] IR spectroscopy has been employed as a tool to investigate the H₂ binding sites as in the article by Presitino et al^[69] in which the IR-spectrum of hydrogen adsorbed to Cu-BTC was reported. The spectrum exhibits two groups of bands centered at 4160 and 4100 cm⁻¹ which were assigned to H₂ adsorbed in different sites. The latter band undergoes a red shift to 4090 cm⁻¹ at higher H₂ pressures. The first band was assigned to H₂ molecules weakly perturbed by unspecific binding sites, by considering previous data collected on MOF-5 and other microporous materials.^[70-74] The infra-red spectrum collected on H₂ adsorbed on Cu(I)-exchanged zeolites shows a $\nu(\text{HH})$ band as low as 3090 cm⁻¹. It is believed that

the $\Delta\nu(\text{HH})$ of the order of -1000 cm^{-1} is due to hydrogen binding in a Kubas-type fashion.^[75]

IR spectroscopy also enables us to get insight into the strength of the interaction between the hydrogen molecules and the binding sites by measuring the bathochromic shift of the IR bands as compared to those of the unperturbed system. The magnitude of the bathochromic shift gets larger as the interaction gets stronger. Also, the binding energy of any specific site can be measured from the isobaric temperature dependence of the intensity of the corresponding absorption band.

1.6.2 Raman Spectroscopy

The inelastic light scattering phenomena, which is called Raman Effect, was discovered in 1928 by Chandrasekhara Venkata Raman.^[76] This effect is due to the interaction of electromagnetic radiation with the electron cloud of the molecule. Molecular vibrations are called Raman active if the polarizability tensor for the molecule changes. The oscillation of the polarizability of the molecule due to vibration and rotation is responsible for the inelastic scattering of light.

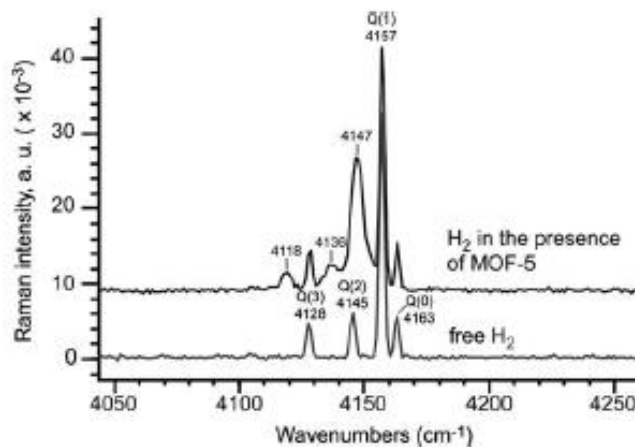


Figure 1.4: Raman spectra of hydrogen as a free gas and in the presence of MOF-5 at room temperature and 30.3 bar (adopted from ref # 78 with permission from Elsevier).

Raman spectroscopy may provide a great technique to gain insight into the interactions between the adsorbent and the adsorbate by analyzing the changes in the vibrational and rotational transition energies of the adsorbed hydrogen as compared to those of the free molecule.^[77] A. Centrone et al.^[78] have recorded the Raman spectra of H₂ adsorbed to MOF-5 and compared it to that of unperturbed H₂. They observed down-shifted lines in the case of adsorbed H₂ as compared to those of the free gas. Figure 1.4 above shows the Q-branch of the unperturbed H₂ and those of the H₂ adsorbed on MOF-5. The spectrum of the unperturbed H₂ has a peak at 4163 cm⁻¹ which is attributed to the Q(0) transition, whereas those at 4157, 4145 and 4128 cm⁻¹ are attributed to Q(1), Q(2), and Q(3), respectively. The spectrum of the H₂ adsorbed to MOF-5 shows a 10 cm⁻¹ red-shift for the Q(1) frequency. The same shift was also observed for the Q(2) and Q(3) frequencies. As with IR, the magnitude of the shift is an indication of the interaction strength. Therefore, it should be noted that the weakly shifted peaks in the case of H₂ adsorbed onto the surface of MOF-5 indicate that H₂ is weakly physisorbed on the surface, and it does not undergo chemisorption.

1.6.3 Inelastic Neutron Scattering

The neutron is an uncharged nucleon with the same mass as that of a proton, a spin of ½ and a magnetic moment of -1.913 nuclear Bohr magnetons.^[17] The neutron-nucleus interaction, rather than the magnetic interaction, is of special interest for the characterization of hydrogen storage materials and the study of the behavior of hydrogen. As the neutrons collide with atomic nuclei of a sample, they either gain or lose kinetic energy. This energy change is due to energy transfer to and from the sample.

The magnitude of this interaction is dependant on the particular nuclei involved. For instance, hydrogen atoms scatter more strongly than deuterium atoms.^[79]

Inelastic neutron scattering (INS) is therefore a valuable technique that provides information which cannot be attained by other techniques, and it is a widely used to study the structures and dynamics of liquids and solids.^[80] Neutron scattering possesses many advantages over IR spectroscopy as it does not depend on the weak transition dipole moment induced in H₂ by the adsorbent's surface.^[81]

INS is a very expensive technique and requires a nuclear reaction in order to get an intense beam of neutrons. Therefore it is available only at very few laboratories worldwide, for example at the Chalk River Laboratories (CRL) in Ontario, Canada or at ILL, Grenoble, France or at the Argonne and National Institute of Standards and Technology (NIST) in USA. The advantage of neutron scattering over X-ray scattering is that in the neutron scattering, the scattering power is not a function of the atomic number. In neutrons, the atomic nuclei, rather than the electron clouds, are responsible for the scattering and therefore hydrogen is considered as a strong scatterer of neutrons.^[82]

In spite of the large number of articles in the field of hydrogen storage, there is still no consensus as to where and how the H₂ molecule is being adsorbed. Neutrons with wavelengths in the range 0.1-2 Å have the ability to penetrate deeply through matter, as the neutron size is comparable or less than the spacing between atoms and therefore to provide information about adsorbent-adsorbate interactions.^[17] The use of inelastic neutron scattering can provide the answer about the location of the binding sites and the strength of the binding interactions. The INS measurement is aimed at

probing the structure of the rotational energy spectrum of the adsorbed molecules at different adsorption sites by measuring the spectra as a function of the H₂ loading level.

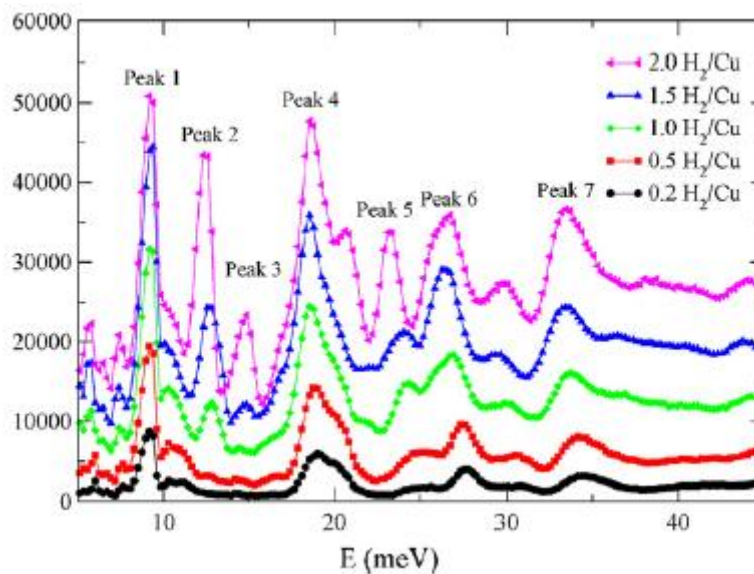


Figure 1.5 – INS spectra of H₂ in HKUST-1 at 0.2, 0.5, 1.0, 1.5, 2.0 H₂: Cu (adopted from ref # 80 with permission from Elsevier)

Y. Liu et al.^[80] have measured the INS spectra of H₂ adsorbed in HKUST-1 [Cu₃(1,3,5-benzentricarboxylate)₂] as shown in Fig. 1.5. By measuring the INS spectra at different H₂ loading levels, they were able to distinguish three binding sites for H₂ on the HKUST-1. Also by measuring the INS spectra at different temperatures, they were able to estimate the relative binding strength of H₂ adsorbed on the three available sites. It is also important to mention that in the INS studies of the hydrogen coordination to Kubas-complexes the H₂ ligand undergoes rotation about the M-H₂ axis. This phenomenon is extensively studied by Eckert^[83-86] because it distinguishes molecular H₂ binding from that of classical hydride binding.

1.6.4 Solid-state NMR spectroscopy

NMR spectroscopy employs the magnetic spin energy of atomic nuclei and its interaction with electric and/or magnetic fields to create interesting effects that can be utilized to interpret molecular structures.^[87] For non-zero nuclear spin elements, such as ^1H , ^2H , ^6Li , and ^{13}C , an applied magnetic field influences the energy of the nuclei. In the magic angle spinning (MAS) technique, the sample is rotated at a high velocity at an angle of 54.74° to the applied magnetic field to yield spectra with sharp peaks with much structural information. These sharp peaks arise from averaging of the large anisotropic NMR interactions by rapid molecular tumbling.^[88-91]

The solid-state ^1H NMR technique, through the measurement of the dipolar coupling between the two protons, allows the identification of stable transition metal dihydrogen complexes as well as the determination of the H-H bond distance. This technique usually provides very accurate measurement, and it was applied to study the H_2 bonding in the original Kubas-complex $\text{W}(\text{CO})_3(\text{Pcy}_3)_2(\text{H}_2)$. As the H-H is lengthened by stronger interactions with the metal centre, the coupling between the nuclei should be reduced. Therefore, it is reasonable to have an inverse relationship between the H-H distance in a hydrogen complex and the $J_{\text{H-D}}$ observed for the H-D complex.

The correlation between $J_{\text{H-D}}$ and $d_{\text{H-H}}$ is usually determined through the Morris and the Heinekey equations:^[92]

$$d_{\text{H-H}} = 1.42 - 0.0167J_{\text{H-D}} \text{ \AA} \text{ [Morris]}$$

$$d_{\text{H-H}} = 1.44 - 0.0168J_{\text{H-D}} \text{ \AA} \text{ [Heinekey]}$$

1.6.5 X-Ray Diffraction

The X-Ray diffraction technique has been applied for the purpose of direct observation of hydrogen molecules in pores. Takamizawa and his co-worker^[93] were able to locate dense aggregates of H₂ molecules in the [Rh(II)₂(bza)₄(pyz)]_n (bza = benzoate, pzy = pyrazine) MOF material at 90 K. They also found that the crystal unit cell volume of the material loaded with H₂ has expanded significantly by 0.43% in comparison with that of the empty crystal unit cell.

1.6.6 Computational Modeling

Computational chemists have played a great role in the search for promising materials for hydrogen storage. They provided ideas for designing materials for experimental realization.^[94] To accomplish a computational study one must first choose an electronic structure calculation method and basis set.^[95, 96] Currently the most dominant first principal calculation method is the density functional theory (DFT), in its two most popular realizations: the local density approximation (LDA) and the generalized gradient approximations (GGA) of Perdew et al.^[97], which is believed to be more accurate in describing gas adsorption than the (LDA).^[17] Then an appropriate atomic orbital basis set within which the calculation will be performed must be selected. A basis set is a set of functions that are used to describe atomic orbitals.^[96] The larger the basis set, the more accurate is the description of the molecular orbitals, however the calculation becomes computationally demanding. DFT along with the best functionals available can take into account all the interactions available for the hydrogen molecules, i.e., dispersion (van der Waals), electrostatic, and orbital interactions except long range dispersion interactions. A second order Moller-Plesset perturbation theory (MP2) has

the capability of describing dispersion, therefore this wave-function based method may be employed when dispersion forces are the dominant interactions in hydrogen storage materials, but the MP2 method has been widely known to overestimate the binding affinity. On the other hand, the use of a limited and incomplete basis set leads to a systematic error in the calculations of intermolecular interaction energies.^[45] This error is called the basis set superposition error (BSSE),^[98] and it is due to the fact that electrons from one fragment of the structure borrow basis functions from other fragment of the structure to compensate for the limitations of their own basis functions. To minimize this error, one must first employ an appropriate basis set, and rely either on a cancellation of these effects or a correction for them. It has become popular to correct for this effect by applying the counterpoise correction of Boys^[99] to all binding affinities.

Transition metal hydrides have been considered for their capacity to bind hydrogen in a Kubas fashion. A theoretical study by Schaefer III and co-workers investigated the H₂ molecular binding of the three simplest possible hydrogen complexes TiH₂.H₂, VH₂.H₂, and CrH₂.H₂. The energetics comparisons of these complexes along with their isomers are of great importance to understand the dihydrogen/dihydride interconversion. Another theoretical study by Gagliardi et al. found that up to 6 H₂ molecules can be bound to one metal atom, with up to 4 H₂ units binding in a Kubas-type fashion and can be detached more easily than the 4 classical M-H hydrides.^[100]

1.6.7 Elemental Analysis^[67]

The analysis of elements present in a sample is essential for chemical characterization in materials sciences as well as in other fields. Elemental analysis is an analytical technique that determines the amount of an element in a compound as a weight percent. This method is based upon high-temperature oxidation of the compound in order to convert the elements of interest to gaseous molecules. The sample to be analyzed is weighed accurately inside a small tin capsule. The capsule is introduced into the analyzer's furnace and oxidized at 950 °C, and combusts at high oxygen environment to form tin oxide. This combustion causes a temperature increase to above 1800 °C, at which the sample undergoes complete combustion to form CO₂, N₂, and H₂O and other by-products. Undesirable products such as sulphur, phosphorus, and halogens are removed. Then, the gases flow through a reduction tube in order to remove any unused O₂, and to convert N_xO_y to N₂. Then the gases are brought to a stable temperature in a mixing chamber. The mixture is analyzed by passing it through a series of thermal conductivity detectors, where the quantity of each gas is measured. From the gas quantities measurements and the original sample weight, it is possible to find the %C, %H, and %N. The analysis of other elements and metals is also possible, but different methods are employed.

1.6.8 Nitrogen Adsorption

Nitrogen adsorption is a widely used technique to characterize the internal structures of mesoporous and microporous materials. The amount of nitrogen adsorbed and desorbed on a sample is measured as a function of the partial pressure of the nitrogen gas. Nitrogen adsorption allows the determination of the surface area, pore volume, pore size distribution as well as the study of the surface properties.^[101] The nitrogen adsorption

experiment is done at 77K, the boiling point of liquid nitrogen under normal pressure, and the molecular area of the adsorbate is equal to 16.2\AA^2 , estimated through the average distance of molecules in liquid nitrogen.

1.6.9 Helium Pycnometry

Helium pycnometry is used to determine the skeletal density of porous solids.^[102] Helium, which can enter the smallest pores, is used to measure the volume per unit weight of a porous material; the result is reported as the skeletal density of the material. Therefore the skeletal density of a solid is defined as the mass of the unit of the solid skeleton inaccessible to helium. Helium, with its small dimensions, assures penetration into pores approaching 1 Å in dimension.^[103] Also its ideal gas behavior is desirable as the pycnometer uses the ideal gas equation $PV = n.R.T$ to measure the volume occupied by the sample.

1.7 Dissertation Overview

This dissertation contains 6 additional chapters that explore the effects of grafting a silica surface with various organometallics on the hydrogen storage capacities and binding enthalpies of the obtained materials. It also describes the synthesis and the hydrogen storage capacity of a new class of materials, metal-hydrazide gels. Chapter 2 describes the synthesis of hexagonally-packed mesoporous silica and the grafting of low-coordinate Ti(III) fragments on the surface, and the effects of these Ti-fragments on the hydrogen capacity as well as on the H₂ binding enthalpies into these materials.

In Chapter 3 we try to further optimize the storage capacities of the materials in chapter 2 by tuning the pore size and surface area of the silica support as well as by

changing the ancillary ligand of the grafted Ti-fragment, and investigate the effects of the steric and electronic factors on the storage capacity of these single sites.

Chapter 4 is a systematic study of the effects of metal type, metal oxidation state and coordination environment on the storage capacities of the silica functionalized with unsaturated early transition metal moieties in order to establish which transition metal fragments and oxidation states can function as the most effective binding sites for hydrogen.

In Chapter 5, density functional theory calculations are employed in order to gain insight into effects of metal type and ancillary ligand on the hydrogen capacity and binding enthalpy of organometallic fragments grafted on silica.

The results obtained in Chapter 6 which show amplification on the hydrogen capacity of silica grafted with (trimethylsilyl)methylCr fragments as a result of hydrogenation was employed in the synthesis of a new class of materials consisting of Cr(II) centers linked together by hydrazine bridges. The materials show lots of promise as hydrogen storage materials for practical applications.

Finally Chapter 7 provides a summary of the whole thesis as well as an explanation of the importance of the results obtained on the silica-supported metals fragments on designing extended solid with binding sites similar of those of silica single sites but with higher metal concentration in order to maximize the hydrogen uptake at room temperature.

1.8 References

1. Jones, R.H., Thomas, G.J., (Eds) *Materials for the Hydrogen Economy*, CRC Press, **2008**.
2. Sorensen, B., *Hydrogen and Fuel Cells: Emerging Technologies and Applications*, Elsevier, **2005**.
3. Hordeski, M.F., *Alternative Fuels: The Future of Hydrogen*, 2nd Edition, The Fairmont Press, Inc., Lilburn, GA, **2008**.
4. Züttel, A., Borgschutle, A., Schlapbach, L. (Eds.), *Hydrogen as a Future Energy Carrier*, Wiley-VCH, Weinheim, 2008, pp 9.
5. Schlapbach, L., Züttel, A., *Nature*, **2001**, 414, 353-358.
6. Hamilton, C.W., Baker, R.T., Staubiltz, A., Manners, I., *Chem. Soc. Rev.*, **2009**, 38, 279-293.
7. Busby, R.L., *Hydrogen and Fuel Cells: A Comprehensive Guide*, Penwell Corp., 1ST American Ed., Tulsa, Oklahoma, **2005**, pp. 6.
8. Gupta, R.B. (Ed.), *Hydrogen Fuel: Production, Transport, and Storage*, CRC Press, **2009**, pp. 6.
9. Hordeski, M.F., *Alternative Fuels: The Future of Hydrogen*, 2nd Ed., The Fairmont Press, **2008**, pp. 27.
10. Rand, D.A.J., Dell, R.M., *Hydrogen Energy Challenges and Prospects*, RSC Publishing, Cambridge, UK, **2008**.
11. Heinekey, D.M., Odham, W. J., *Chem. Rev.*, **1993**, 93, 913-926.

11. Abdur-Rashid, K., Fong, T. P., Greaves, B., Gusev, D. G., Hinman, J. G., Landau, S. E., Lough, A. J., Morris, R. H., *J. Am. Chem. Soc.*, **2000**, 122, 9155-9171
12. Leug, W.B., March, N.H., Motz, H., *Phys. Lett. A*, **1976**, 56, 425-426.
13. Züttel, A., *Naturwissenschaften*, **2004**, 91, 157-172.
14. Takeichi, N., Senoh, H., Yokota, T., Tsuruta, H., Hamada, K., Takeshita, H. T., Tanaka, H., Kiyobayashi, T., Takano, T., Kuriyama, N., *Int. J. Hydrog. Energy*, **2003**, 28, 1121-1129.
15. Zhou, L., *Renew. Sustain. Energy Rev.*, **2005**, 9, 395-408.
16. Fichtner, M., *Adv. Eng. Mater.*, **2005**, 7, 6, 443-455.
17. Walker, G., (Ed.), *Solid State Hydrogen Storage: Materials and Chemistry*, Woodhead Publishing Ltd., **2008**, pp. 7.
18. Seayad, A.M., Antonelli, D.M., *Adv. Mater.*, **2004**, 16, 765-777.
19. Chaudhuri, S., Graetz, J., Ignatov, A., Reilly, J. J., Muckerman, J. T., *J. Am. Chem. Soc.*, **2006**, 128, 11404-11415.
20. Yang, J., Sudik, A., Wolverton, C., Siegel, D. J., *Chem. Soc. Rev.*, **2010**, 39, 656- 675.
21. Rowsell, J.L.C., Yaghi, O., *Angew. Chem. Int. Ed.*, **2005**, 44, 4670-4679.
22. Chahine, R., Bose, T., *Int. J. Hydrogen Energy*, **1994**, 19, 161.
23. Shelvin, S. A., Guo, Z. X., *J. Phys. Chem. C*, **2008**, 112, 17456.

24. Lee, S., Lee, Y., *Appl. Phys. Lett.*, **2000**, 76, 2877.
25. Wu, G., Wang, J., Zhang, X., Zhu, L., *J. Phys. Chem. C*, **2009**, 113, 7052.
26. Zhao, Y., Kim, Y., Dillon, A.C., Heben, M.J., Zhang, S.B., *Phys. Rev. Lett.*, **2005**, 94, 155504.
27. Sun, Q., Wang, Q., Jena, P., Kawazoe, Y., *J. Am. Chem. Soc.*, **2005**, 127, 14582.
28. Weitkamp, J., Fritz, M., Ernst, S., *Int. J. Hydrogen Energy*, **1995**, 20, 967.
29. Hu, Y., Ruckenstein, E., *Angew. Chem. Int. Ed.*, **2006**, 45, 2011.
30. Dincă, M., Long, J., *J. Am. Chem. Soc.*, **2005**, 127, 9376.
31. Rosi, N., Ecket, J., Eddoudi, M., Vodak, D., Kim, J., O’Keeffe, M., Yaghi, O., *Science*, **2003**, 300, 1127.
32. Rowsell, J., Milward, A., Park, K., Yaghi, O., *J. Am. Chem. Soc.*, **2004**, 126, 5666.
33. Panella, B., Hirscher, M., *Adv. Mater.* **2005**, 17, 538.
34. Wong-Foy, A., Matzger, A., Yaghi, O., *J. Am. Chem. Soc.*, **2006**, 128, 3494.
35. Hu, X., Skadtchenko, B., Trudeau, M., Antonelli, D., *J. Am. Chem. Soc.*, **2006**, 128, 11740.
36. Hu, X., Trudeau, M., Antonelli, D., *Chem. Mater.*, **2007**, 19, 1388.

37. Hamaed, A., Trudeau, M., Antonelli, D., *J. Am. Chem. Soc.*, **2008**, 130, 6992-6999.
38. Hamaed, A., Hoang, T.K.A., Trudeau, M., Antonelli, D.M., *J. Organomet. Chem.*, **2009**, 694, 2793-2800.
39. Hoang, T.K.A.; Hamaed, A., Trudeau, M., Antonelli, D., *J. Phys.Chem C*, **2009**, 113, 17240-17246.
40. Hamaed, A., Van Mai, H., Hoang, T.K.A., Trudeau, M., Antonelli, D., *J. Phys. Chem.C*, **2010**, 114, 8651-8660.
41. Li, Y., Yang, R. T., *J. Am. Chem. Soc.*, **2005**, 128, 726-727.
42. *The Hydrogen Economy: Opportunities, Costs, Barriers, and R&D Needs*, Committee on Alternatives and Strategies for Future Hydrogen Production and Use, The National Academies Press, Washington, DC, **2006**.
43. Satyapal, S., Petrovic, J., Read, C., Thomas, G., Ordaz, G., *Catal. Today*, **2007**, 120, 246.
44. http://www1.eere.energy.gov/hydrogenandfuelcells/storage/pdfs/targets_onboard_hydro_storage.pdf.
45. Lochan, R.C., Head-Gordon, M., *PhysChemChemPhys*, **2006**, 8, 1357.
46. Van den Berg, A.W.C., Arean, C.O., *Chem. Commun.*, **2008**, 668.
47. Hoang, T.K.A., Antonelli, A.M., *Adv. Mater.*, **2009**, 21, 1787-1800.
48. Bhatia, S.K., Myers, A.L., *Langmuir*, **2006**, 22, 1688-1700.

49. Orimo, S., Nakamori, Y., Eliseo, J.R., Züttel, A., Jensen, C.M., *Chem. Rev.*, **2007**, 107, 4111-4132.
50. Murray, L.J., Dincă, M., Long, J.R., *Chem. Soc. Rev.*, **2009**, 38, 1294-1314.
51. Kubas, G.J., Ryan, R.R., Swanson, B.I., Vergamini, P.J., Wasserman, H.J., *J. Am. Chem. Soc.*, **1984**, 106, 451.
52. Kubas, G.J., *J. Organomet. Chem.*, **2001**, 635, 37-68.
53. Heinekey, D.M., Lledos, A., Lluch, J.M., *Chem. Soc., Rev.*, **2004**, 33, 175-182.
54. Kubas, G.J., *PNAS*, **2007**, 104 (17), 6901-6907.
55. Kubas, G.J., *Chem. Rev.*, **2007**, 107, 4152-4205.
56. Tanev, P.T., Pinnavaia, T.J., *Science*, **1995**, 267, 865.
57. Yang, R.T., *Adsorbents: Fundamentals and Applications*, Wiley, Hoboken, N.J, **2003**.
58. Rouquerol, F., Rouquerol, J., Sing, K., *Adsorption by Powder and porous Solids*, Academic Press, San Diego, **1999**.
59. Jones, R.W., *Fundamental Principles of Sol-Gel Technology. The Institute of Metals*, London, UK, **1989**.
60. Brinker, C.J., Sherer, G.W., *Sol-Gel Science*. Academic Press, New York, NY, **1990**.
61. Zhuravlev, L.T., *Colloids and Surfaces A: Physicoch. Eng. Aspects*, **2000**, 173, 1-38.

62. Bergna, H.E., *The Colloid Chemistry of Silica*, American Chemical Society, Washington, DC, Chapter 8, **1994**.
63. Zhuravlev, L.T., *Colloids and Surfaces A*, **1993**, 74, 71.
64. Kiselev, A.V., Lygin, V.I., *Infrared Spectra of Surface Compounds* (translated by Kaner), John Wiley and Sons, New York, NY, **1975**.
65. Mathias, J., Wannemacher, G., *J. Coll. Interf. Sci.*, **1988**, 125, 61.
66. a) Durgun, E., Ciraci, S., Zhou, W., Yildirim, T., *Phys. Rev. Lett.*, **2006**, 97, 226102. b) Tosin, G., Delgado, M., Baudouin, A., Santini, C. C., Bayard, F., Basset, J. M., *Organometallics*, **2010**, 29, 1312-1322.
67. Skoog, D.A., Holler, F.J., Nieman, T.A., *Principles of Instrumental Analysis*, 5th Ed., Thomson Learning Inc., **1997**.
68. Thomas, K.M., *Dalton Trans.*, **2009**, 1487-1505.
69. Prestipino, C., Regli, L., Vitillo, J.G., Bonino, F., Damin, A., Lamberti, C., Zecchina, A., Solari, P.L., Kongshaug, K.O., Bordiga, S., *Chem. Mater.*, **2006**, 18, 1337-1346.
70. Bordiga, S., Vitillo, J.G., Ricchiardi, G., Regli, L., Cocina, D., Zecchina, A., Arstad, B., Bjorgen, M., Hafizovic, J., Lillerud, K.P., *J. Phys. Chem. B*, **2005**, 109, 18237-18242.
71. Spoto, G., Gribov, E., Bordiga, S., Lamberti, C., Ricchiardi, G., Scarano, D., Zecchina, A., *Chem. Commun.*, **2004**, 2768-2769.
72. Bordiga, S., Garrone, E., Lamberti, C., Zecchina, A., Otero Arean, C., Kazansky, V. B., Kustov, L.M., *J. Chem. Soc., Faraday Trans.* **1994**, 90, 3367-

- 3372.
73. Kazansky, V.B., Borovkov, V.Y., Serich, A., Karge, H.G., *Microporous Mesoporous Mater.*, **1998**, 22, 251-259.
74. Stephanie-Victoire, F., de Lara, E.C., *J. Chem. Phys.*, **1998**, 109, 6469-6475.
75. Solans-Monfort, X., Branchadell, V., Sodupe, M., Zicovich-Wilson, C. M., Gribov, E., Spoto, G., Busco, C., Ugliengo, P., *J. Phys. Chem. B*, **2004**, 108, 8278-8286.
76. Raman, C.V., Krishnan, K.S., *Nature*, **1928**, 121, 501-502.
77. Siberio-Perez, D.Y., Wong-Foy, A.G., Yaghi, O.M., Millward, A.R., Matzger, *Chem. Mater.*, **2007**, 19, 3681-3685.
78. Centrone, A., Siberio-Perez, D.Y., Millward, A.R., Yaghi, O.M., Matzger, A.J., Zerbi, G., *Chem. Phys. Lett.*, **2009**, 411, 516-519.
79. Hudson, B.S., *J. Phys. Chem. A*, **2001**, 105, 3949-3960.
80. Liu, Y., Brown, C.M., Neumann, D. A., Peterson, V.K., Kepert, C. J., *J. Alloys Comp.*, **2007**, 446-447, 385-388.
81. Larese, J.Z., Arnold, T., Frazier, L., Hinde, R.J., Ramirez-Cuesta, A. *J. Phys. Rev. Lett.*, **2008**, 101, 165302.
82. West, A.R., *Basic Solid State Chemistry*, John Wiler & Sons, Ltd., 2nd Ed., **1999**.
83. Eckert, J., Kubas, G.J., *J. Chem. Phys.* **1993**, 97, 2378.

84. Eckert, J., Kubas, G.J., Dianoux, A. J., *J. Chem. Phys.* **1988**, 88, 466.
85. Eckert, J., Blank, H., Bautista, M.T., Morris, R.H., *Inorg. Chem.* **1990**, 29,747.
86. Eckert, J., *Spectrochim. Acta*, **1992**, 48A, 363.
87. Slichter, C.P., *Principles of Magnetic Resonance*, Harper & Row: New York, **1963**.
88. Levitt, M., *Spin Dynamic: Basic Principle of NMR Spectroscopy*, **2001**.
89. Duer, M.J., *Introduction to Solid-State NMR Spectroscopy*, Blackwell Science Ltd., Oxford, **2004**.
90. Nelson, J.H., *Nuclear Magnetic Resonance Spectroscopy*, Prentice Hall, Upper Saddle River, **2003**.
91. Abragam, A., *Principles of Nuclear Magnetism*, Oxford University Press, Ely House, London W.1, **1961**.
92. Morris, R.H., *Coord. Chem. Rev.*, **2008**, 252, 2381-2394.
93. Takamizawa, S., Nakata, E., *CrystEngComm*, **2005**, 7, 476-479.
94. Zhang, C-G., Zhang, R., Wang, Z-H., Zhou, Z., Zhang, S.B., Chen, Z., *Chem. Eur. J.*, **2009**, 15, 5910-5919.
95. Young, D., *Computational Chemistry: A practical Guide for Applying Techniques to Real World Problems*, John Wiley & Sons, Toronto, **2001**.

96. Cramer, C.J., *Essential of Computational Chemistry*, John Wiley & Sons, West Sussex, **2002**.
97. Perdew, J.P., Burke, K., Ernzerhof, M., *Phys. Rev. Lett.*, **1996**, 77, 3865.
98. Scwenke, D.W., Truhlar, D.G., *J. Chem. Phys.*, **1985**, 82(5), 24182426.
99. Boys, S.F., Bernardi, F., *Mol. Phys.*, **1970**, 19, 553.
100. a) Ma, B., Collins, C. L., Schaefer III, H. F., *J. Am. Chem. Soc.*, **1996**, 118, 870-879. b) Gagliardi, L., Pyykkö, P., *J. Am. Chem. Soc.*, **2004**, 126, 15014-15015.
101. Kruk, M., Jaroniec, M., *Chem. Mater.*, **2001**, 13, 3169-3183.
102. Semel, F.J., Lados, D.A., *Powder Metallurgy*, **2006**, 49, 173-182.
103. Matějčíček, J., Kolman, B., Dubský, J., Neufuss, K., Hopkins, N., Zwick, J., *Materials Characterization*, **2006**, 57, 17–29

Chapter 2 - H₂ Storage Materials (22 KJ/mol) using Organometallic Ti Fragments as σ -H₂ Binding Sites

2.1 Introduction

An ideal hydrogen storage material must display fast adsorption/desorption kinetics,^[1] function near ambient temperature, and possess low density, high gravimetric/volumetric capacity, and high tolerance for recycling. Metals^[2] and various metal hydride alloys^[3] have been studied which can adsorb between 2 and 7 wt% of hydrogen between 100-200°C.^[4] Although many of these materials have high volumetric capacities close to the 2015 DOE system goal of 80 kg/m³, they fall well short of the 9 wt % gravimetric storage goal. Another major drawback is the high activation barriers of the ca. 80 kJ/mol M-H bonds that must be broken to liberate H₂. This creates problems with release kinetics and performance temperatures, and often necessitates elaborate heat exchange systems in a practical design. For this reason, many researchers are turning to high surface area porous materials as hosts for H₂ storage. Such materials adsorb H₂ on the surface through a 5-10 kJ/mol physisorption mechanism under cryogenic conditions. The leading materials in this technology are carbon based structures^[5-9] and microporous metal-organic frameworks (MOFs).^[10-12] This method of storage is of increasing interest because the technology needed for transportation of large quantities of liquid hydrogen already exist in the rocket industry and many of these materials have shown promising hydrogen uptake.^[7, 10] However, the energy lost in cooling and from boil-off is a serious challenge and no material comes close to meeting the DOE 2015 system targets for temperature or volumetric capacity. In order to surmount the problems associated with heat exchangers and cooling, materials with binding enthalpies between those of cryogenic materials and metal

hydrides must be developed. Calculations by Zhao et al^[13] have predicted high storage capacities and ideal enthalpies for room temperature performance of 20-30 kJ/mol for hypothetical Sc and Ti modified C60 moieties based on Kubas binding of the H-H σ -bond to the metal center.^[14] Yildirim has predicted similar performance benefits in Ti-decorated carbon nanotubes.^[15] Recent advances within our group^[4, 16, 17] indicate that mesoporous transition metal oxides^[18-20] may serve as hosts for hydrogen storage. Reduction of the Ti oxide based mesoporous framework with Li, Na, or bis(toluene) titanium leads to enhanced H₂ binding to the surface to a high of 4.94 wt% gravimetric storage and 40.46 kg/m³ volumetric storage capacity. The proposed mechanism for enhancement involves Kubas binding of H₂ to Ti, because this interaction is strongly dependent on the reduction level of the metal center and its ability to back-bond through σ -interaction into the antibonding H-H orbital.^[14] This enhancement effect in our system was more important than the surface area, and the binding enthalpies showed an unprecedented increase with surface coverage from 2.5 kJ/mol to 8.08 kJ/mol. However, these enthalpies fall short of those necessary for room temperature performance, and the presence of multiple Ti sites of oxidation states between II and IV suggests that only a fraction of the Ti centers act as binding sites while the rest only add excess weight and decrease the storage capacity. In order to overcome this problem we developed a new system which uses very light and inexpensive mesoporous silica as a host for single site Ti centers tailored specifically to bind a maximum number of H₂ molecules through a Kubas interaction. Here we present a study of the cryogenic and room temperature hydrogen storage properties of these materials, and show how this

new method of hydrogen storage may be valuable in increasing the capacity of compressed hydrogen tanks at room temperature.

2.2 Experimental

2.2.1 Synthesis of Tetrabenzyl titanium:^[21] to a solution of $C_6H_5CH_2MgCl$ (100 ml, 1M in diethyl ether) in diethyl ether (100ml) at $-15^\circ C$ was added a solution of $TiCl_4$ (2.5 ml, 22.8 mmol) in pentane (100ml) dropwise over 2 hours. The mixture was stirred for 3 hours at $-15^\circ C$ and filtered. The solid residue was washed with diethyl ether (2×50 ml) and the combined filtrate and washings were reduced *in vacuum*. The residue was dissolved in pentane (50 ml) and filtered followed by further washing of the residue with pentane (2×50 ml). The filtrate and pentane washings were concentrated to approximately 70 ml and cooled to $-30^\circ C$ overnight to yield a dark brown red crystalline product, with a reaction yield of 83%.

2.2.2 Synthesis of Tribenzyl titanium: tribenzyl titanium was obtained at $0^\circ C$ in a toluene solution by the reaction of tetrabenzyltitanium with ethyllithium for 2 hours. The resulting benzyllithium was precipitated by carboxylation at $-78^\circ C$. A tribenzyl titanium solution was obtained after filtration. Crystallization gave a 65% yield with respect to the initial quantity of tetrabenzyl titanium.

2.2.3 Synthesis of Hexagonally-packed Mesoporous Silica (HMS): in a typical preparation, tetraethyl orthosilicate (1.0 mol) was added with vigorous stirring to a solution of dodecylamine (0.27 mol) in ethanol (9.09 mol). The reaction mixture was aged at ambient temperature for 18 hours, and the resulting mesoporous silica was air-dried on a glass plate. The template was removed by mixing 1 g of the air-dried HMS with 150 ml of hot ethanol for 1 hour. The product was then filtered and washed with a

second 100 ml portion of ethanol. This extraction procedure was repeated twice, and the crystalline product air-dried at 80°C.

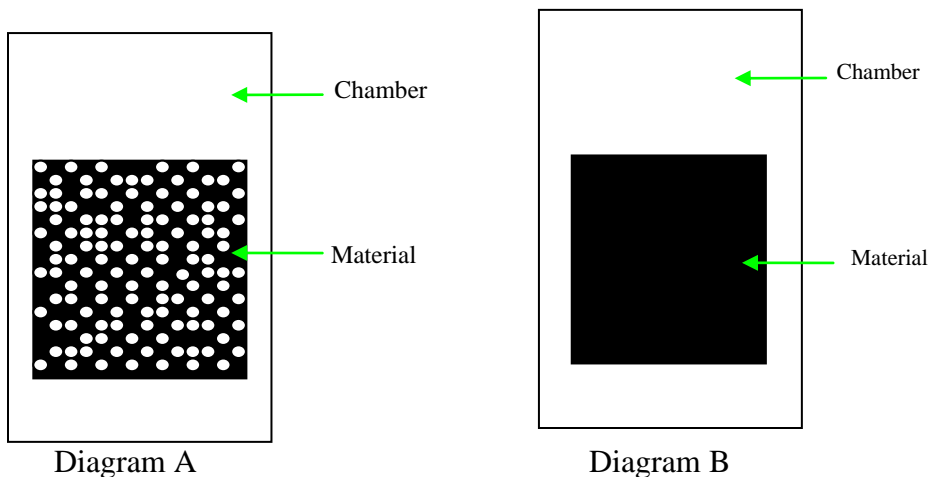
2.2.4 Synthesis of Ti-grafted mesoporous silicas: 0.2 equiv. of tetrabenzyl titanium (or tribenzyl titanium), as calculated on the basis of 33% Si in the porous oxide,^[22] was added to a suspension of hexagonally mesoporous silica in dry toluene under nitrogen. After 1 day of stirring to ensure complete absorption of the organometallic, the reduced material was collected by suction filtration under nitrogen. The resulting material was then heated in toluene at 180°C for 8 hours and washed several times with toluene and finally dried *in vacuo* at 10^{-3} Torr on a Schlenk line until all volatiles had been removed. This material was used as either a powder or a 1.3 cm diameter pellet compressed in a commercial pellet press at 4 metric tones.

2.2.5 Concentration of exposed Ti metal sites: assuming 1 g of 0.2TiBz₄-HMS, with a surface area of 1200m²/g (1.2×10^{21} nm²). 0.2TiBz₄-HMS has 4.5 wt.% Ti, therefore in 1g of 0.2TiBz₄-HMS there is 40.8 mg Ti (8.52×10^{-4} moles Ti).
Ti coverage = $(8.52 \times 10^{-4} \text{ moles Ti} \times 6.02 \times 10^{23} \text{ Ti /mole}) / (1.2 \times 10^{21} \text{ nm}^2) = 0.4275$ Ti/nm².

2.2.6 Measurements: Nitrogen adsorption and desorption data were collected on a Micromeritics ASAP 2010. Hydrogen uptake is measured with a commercial pressure-composition isotherm (PCI) unit provided by Advanced Materials. Highly purified hydrogen (99.9995% purity) was used as the adsorbent. Before all measurements the materials were activated *in vacuo* at 573K in order to remove any physisorbed water or volatile impurities. Leak testing, by running a standard AX-21 sample and by bubbles, was done prior to and during each adsorption measurement

experiment. In the H₂ adsorption-desorption experiments complete reversibility was observed for all samples across the whole range of pressures. Samples were run at liquid nitrogen temperature (77K) and liquid argon temperature (87K) to 60 atm and extrapolated to 100 atm.

The skeletal density was measured using a Quantachrome Ultra-pycnometer. When the skeletal density was used for the hydrogen uptake measurement, the compressed hydrogen within the pores is treated as part of the sample chamber volume. Therefore only the hydrogen physisorbed to the walls of the structure will be recorded by the PCI instrument as the adsorption capacity of the material (see Diagram A and B below).



In diagram A, H₂ adsorption is measured. The pycnometer skeletal density of the porous materials was employed to measure the adsorbed amount of hydrogen. The skeletal density does not ignore the presence of pores inside these materials, and therefore the void space was subtracted out (the colorless area inside and outside the sample). In diagram B, the total storage was measured, the apparent density was adopted,

and this apparent density ignores the presence of pores inside the material, and therefore the void space (the colorless area) was not subtracted out.

Taking both the 77K and 87K hydrogen adsorption data, Enthalpies of Adsorption were calculated using a variant of the Clausius-Clapeyron equation: ^[23]

$$\ln\left(\frac{P_1}{P_2}\right) = \Delta H_{ads} \frac{T_2 - T_1}{RT_1 T_2} \quad (1)$$

Where P_n = pressure for isotherm n, T_n = temperature for the isotherm n, and R = gas constant.

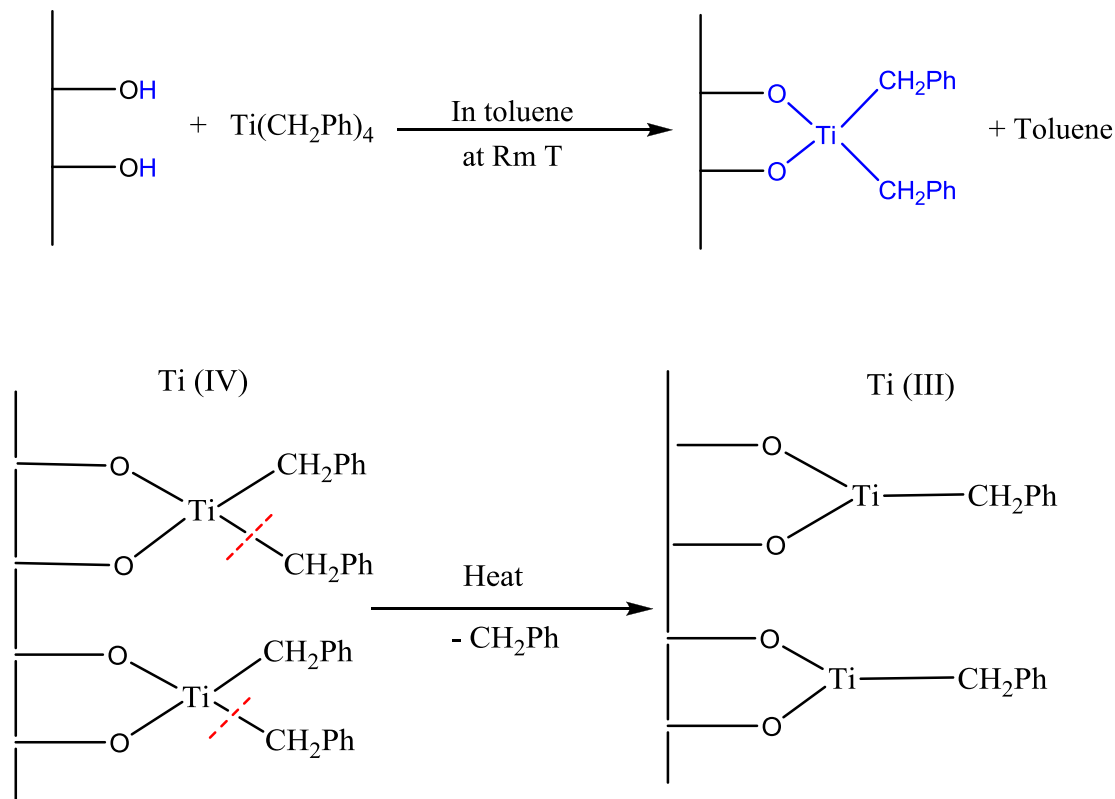
Pressure as a function of the amount adsorbed was determined by using exponential fit for each isotherm; the first 10 points of the isotherms were picked up and fit to the exponential equation. This exponential equation gives an accurate fit over the pressure up to 10 atm with the goodness of fit (R^2) above 0.99. The corresponding P_1 and P_2 values at a certain amount of H_2 adsorbed at both temperatures can be obtained by the simulated exponential equation. Inputting these numbers into the eq 1, we then calculate the enthalpies of the adsorption. The upper enthalpy range corresponds to the maximum H_2 loading level reached at 87 K.

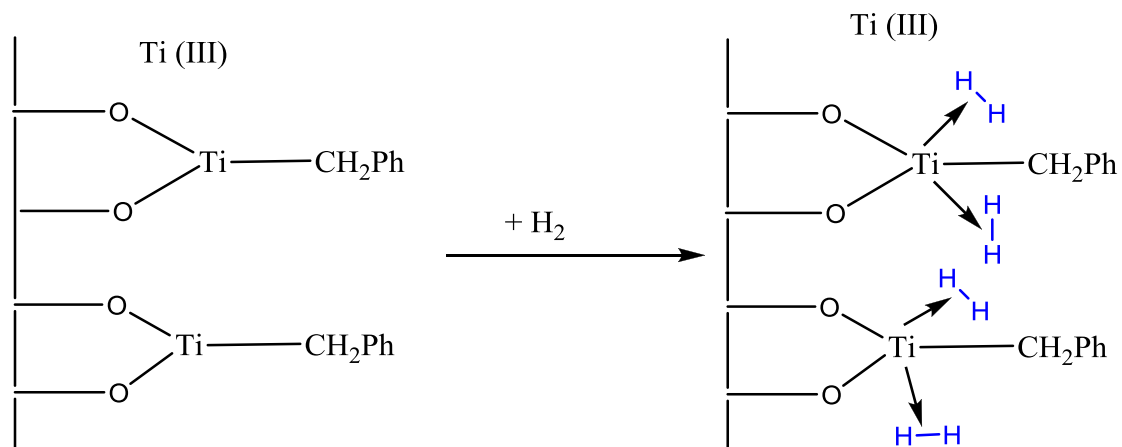
2.3 Results and Discussion

Mesoporous silica possessing a pore size of 23 Å and a B.E.T. (Brunauer, Emmett, Teller) surface area of 1219 m²/g was synthesized using a dodecylamine template according to the neutral templating method.^[24] Tris- and tetrabenzyl titanium was grafted onto the surface of the mesoporous oxide as described previously for this compound on amorphous silica.^[24] When tris- or tetrabenzyl Ti reacts with the OH groups on the surface of the silica, one or two toluene molecules, depending on the

proximity of surface OH groups, are eliminated resulting in the formation of a 4-coordinate Ti (IV) benzyl siloxy species anchored to the surface. Heating the material at 180 °C results in reductive cleavage of one of the remaining Ti-C bonds and elimination of benzyl radicals, which then couple and are subsequently removed in vacuo. Previous studies confirmed complete conversion to three coordinate Ti (III) units on the surface.^[24] According to the 18-electron rule, these Ti moieties can bind as many as five H₂ ligands via a Kubas interaction. Our synthetic strategy is shown in Scheme 2.1.

Scheme 2.1 - Schematic representation of the grafting of benzyl Ti species onto the surface of mesoporous silica and the subsequent formation of tunable low coordinate H₂ binding sites with enthalpies over 20 kJ/mol.





The X-ray diffraction pattern (Fig. 2.1) for all treated materials after heating showed complete retention of the mesostructure as evidenced by a single broad reflection at $d = 23 \text{ \AA}$. The nitrogen adsorption/desorption isotherms (Fig. 2.2) for these samples revealed a type IV isotherm consistent with a mesoporous system and surface areas ranging from 720-1294 m^2/g . The pore volume for these materials ranged from 0.7819 ml/g to 1.4201 ml/g, while the pore sizes were all in the 20-23 \AA range.

Figure 2.1 - Representative X-ray diffraction pattern of mesoporous silica treated with 0.2 equiv. of tetrabenzyl titanium.

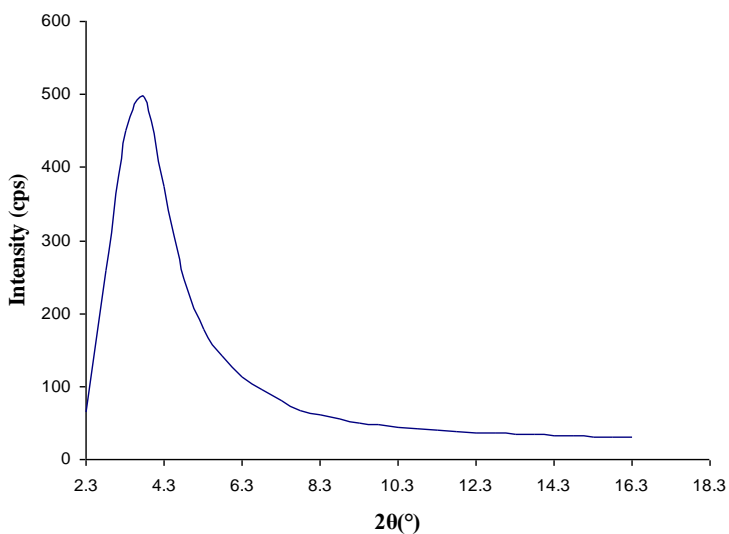


Figure 2.2 - Representative nitrogen adsorption/desorption isotherm of material from Fig. 1.1

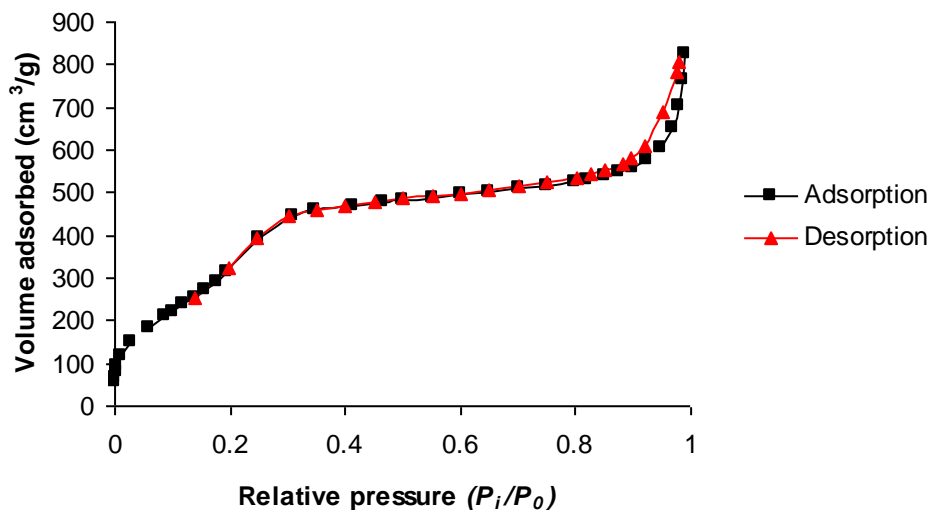
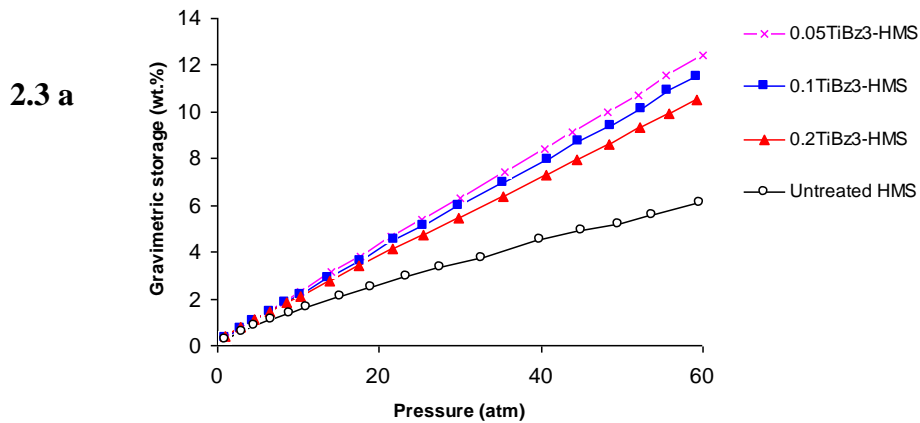
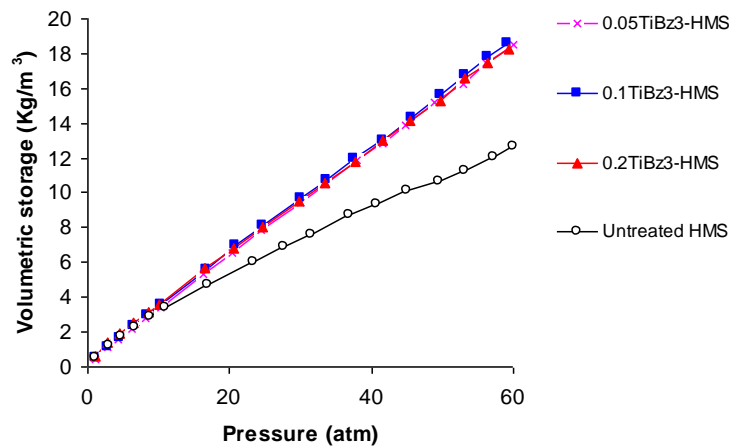


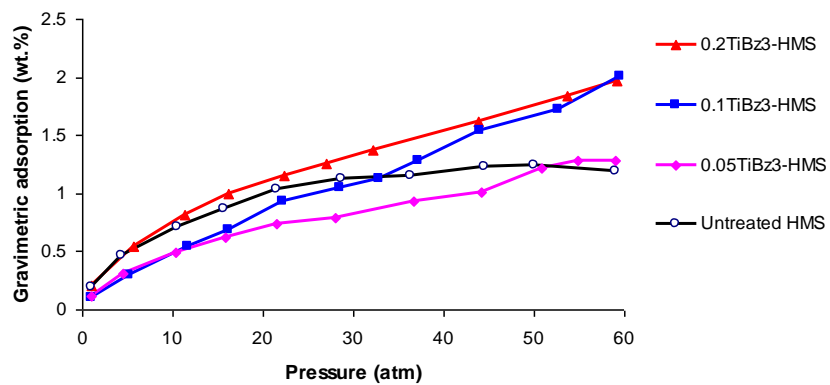
Figure 2.3 - Hydrogen storage and adsorption isotherms at 77 K for mesoporous silica treated with various molar equivalents of tribenzyl titanium. a) Gravimetric storage density. b) Volumetric storage density. c) Gravimetric adsorption density. d) Volumetric adsorption density.



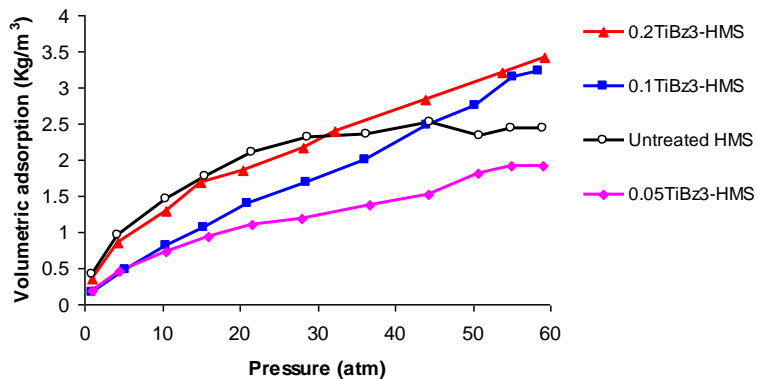
2.3 b



2.3 c



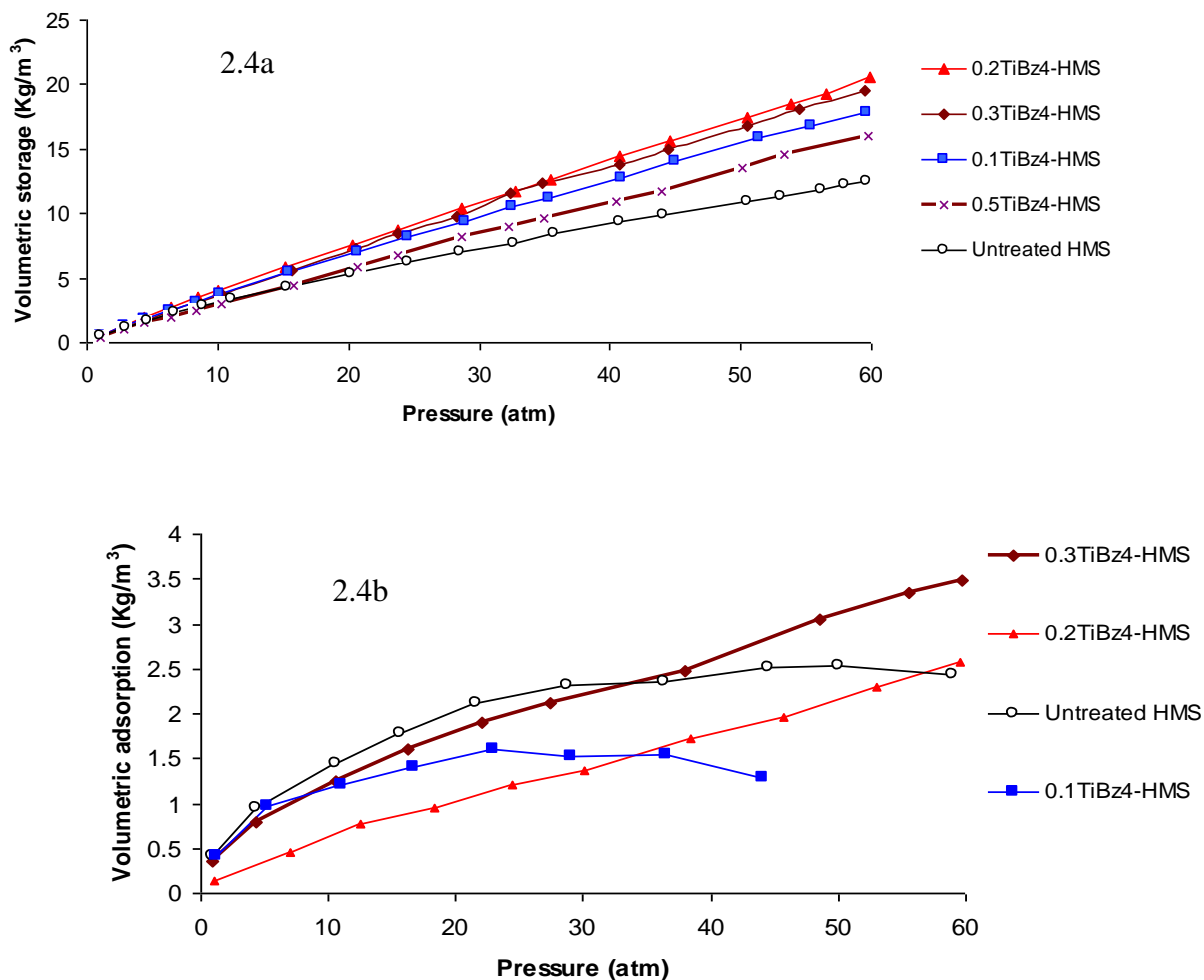
2.3 d



Hydrogen storage (including compressed gas) and adsorption (excess storage) measurements were conducted at $-196\text{ }^{\circ}\text{C}$ to determine the optimal loading level and precursor. The results are summarized in Table 2.1 with adsorption and storage isotherms shown in Fig. 2.3 and Fig. 2.4. The storage isotherms (Figure 2.5a) for all materials rose at low pressure and continued to rise in a linear fashion from 10 atm onwards to 60 atm. Extrapolation to 100 atm, a feasible pressure for cryogenic storage tanks, yields values as high as 21.45 wt% and 34.10 kg/m^3 for the sample synthesized with 0.2 molar equivalents of tetrabenzyl Ti with respect to Si. This compares to a value of 9.84 wt% and 20.34 kg/m^3 for pure mesoporous silica and 11.96 wt% and 39.23 kg/m^3 for carbon AX-21 recorded under the same conditions. While much of this 21.45 wt% consists of compressed gas, this is the highest gravimetric storage value recorded under these conditions and compressed gas in the void space of a material is usable as fuel. The adsorption for this material was 1.66 wt% as compared to 1.21 wt% in the untreated silica. On the basis of 4.08% Ti determined by inductively coupled plasma / atomic absorption spectroscopy (ICP-AAS), the difference between these values translates into 2.7 H_2 per Ti, short of the maximum of 5 H_2 allowed by the 18 electron rule, assuming 3-coordinate Ti (III). Elemental analysis revealed 11.28 % C, corresponding to an average of 1.45 benzyl ligands remaining per Ti, indicating a mix between disiloxy benzyl and dibenzyl siloxy Ti(III) species. The adsorption isotherms for treated materials did not saturate at 60 atm (Figure 2.5b). This behavior is unusual, given that physisorption materials generally saturate at low pressure and increase very little or even decrease at higher pressures. A possible explanation is that a complex pressure-dependent equilibrium exists in which the Ti units can have zero, one, two,

three, four, or five H₂ ligands bound to the surface in a Kubas type fashion. Increasing the pressure leads to a higher predominance of Ti units with more H₂ ligands, according to Le Chatelier's principle, and higher pressures than 60 atm are required to force the extra H₂ ligands into the Ti coordination sphere. A 20 run cycle of adsorption and desorption at -196 °C and 60 atm showed no change in the maximum gravimetric uptake (Fig. 2.6). The isotherms returned on desorption to zero without any hysteresis (Fig. 2.7). While hysteresis might be expected on the basis of the high binding enthalpies, such a prediction is overly simplistic and does not take into account equilibration times for each point or the entropy changes in the system and surrounding on gas expansion or compression. Storage measurements of a compressed pellet of this material showed gravimetric and volumetric densities of 3.15 wt% and 54.49 kg/m³ at 77 K and 100 atm, demonstrating that densification of this material gives a large increase in volumetric density with a corresponding penalty in gravimetric density. BET measurements were performed on the pellet, which yield a surface area of 720 m²/g and shows the porous character of the material was fully retained after compression. The slight decrease on surface area indicated that only external surfaces and pores with thin walls were lost during the compression, and that further compression will expand the hydrogen volumetric capacity to this material.

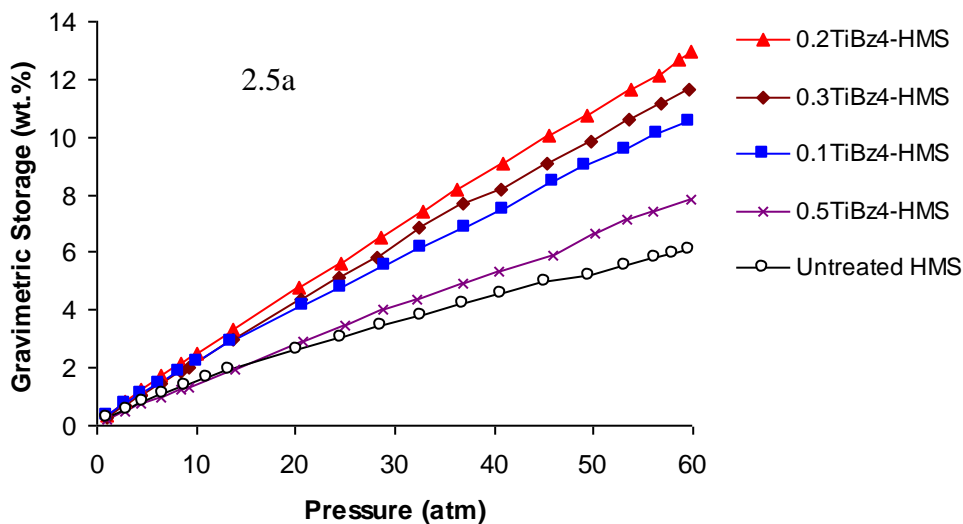
Figure 2.4 - Hydrogen storage and adsorption isotherms at 77 K for mesoporous silica treated with various molar equivalents of tetrabenzyl titanium. a) Volumetric storage density. b) Volumetric adsorption density



Materials prepared with 0.1, 0.2, 0.3 and 0.5 mol equivalent of tetrabenzyl Ti were also studied (Table 2.1). In general, the gravimetric and volumetric capacities drop from the optimal loading level of 0.2 mol equivalents, however there are some anomalies. For example, the 0.3 tetrabenzyl titanium material has a higher gravimetric adsorption (2.04 wt%) but lower volumetric storage (33.07 kg/m³) than its 0.2 tetrabenzyl titanium analogue. Also, the skeletal densities of the treated materials fall in the range of 0.94 to 1.99, but there are no clear trends with Ti-loading across the range

of materials, suggesting that both the skeletal weight and the skeletal volume are affected on anchoring various organometallic fragments to the surface in ways that are difficult to predict at this stage. Since hydrogen storage in this system relies heavily on the oxidation state and coordination sphere of the Ti units, it is crucial that there be maximum surface coverage without any disruption of the structural integrity of the anchored sites. In the case of the 0.1 mol equivalent sample, it is likely that there are not enough Ti moieties on the surface to affect the capacities to the same extent as the 0.2 mol equivalent sample, but for the higher loading levels the explanation is not so clear. Perhaps the available surface OH groups are already used at a loading level of 0.2 mol equivalents, and the addition of more tetrabenzyl titanium begins to form dimeric species on the surface, which are less able to bind H₂ due to steric or electronic factors.^[23]

Figure 2.5 - Hydrogen storage isotherms at 77 K for mesoporous silica treated with various molar equivalent of tetrabenzyl titanium. a) Gravimetric storage density. b) Gravimetric adsorption (excess storage) density. Slight fluctuations at higher pressure in some adsorption isotherms were not related to temperature fluctuations, as this parameter was strictly controlled.



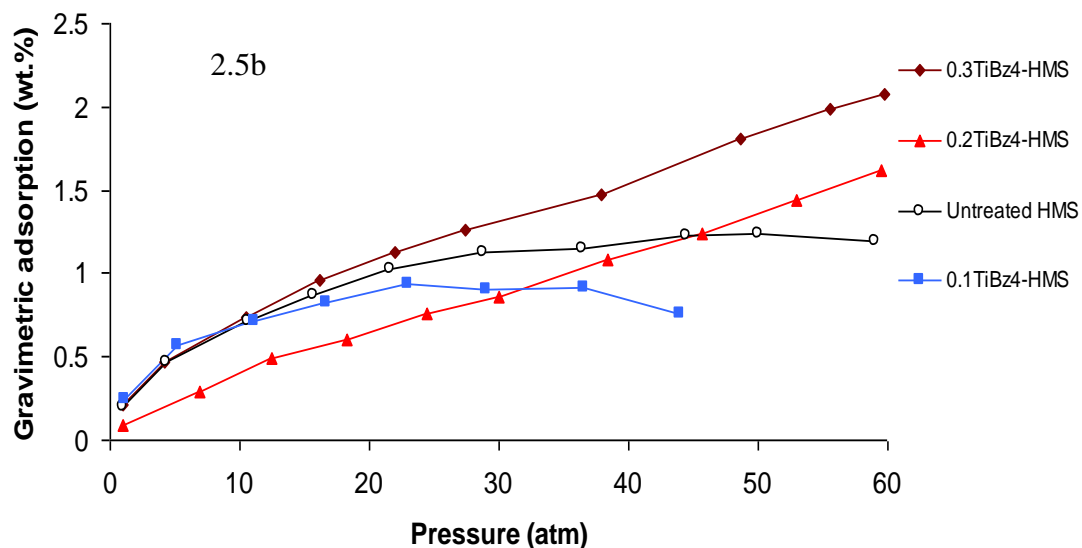


Table 2.1 also shows results from using a tribenzyl titanium precursor. The gravimetric and volumetric storage capacities are uniformly lower at a given loading level than those prepared with tetrabenzyl titanium, however the adsorption levels are higher for the tribenzyl material (2.02 wt% vs. 1.66 wt% at 0.2 equivalents).

In MOF materials it has been proposed that H_2 can bind to the metal linker and that this feature is just as important as the surface area and pore size in determining storage capacity.^[25] For some of these materials the Kubas interaction was proposed to be operative at the metal center. The maximum enthalpy observed for any MOF is 10.1 kJ/mol,^[26] recorded for a manganese benzenetristetrazolate MOF. For comparison, the ΔH values for amorphous carbon are normally in the range of 5-8 kJ/mol.^[27] In previous work we found that reduction of the surface of mesoporous Ti oxide with bis(toluene) titanium led to an increase in binding enthalpies from 2.5 kJ/mol to 8.08 kJ/mol. The enthalpy data also showed an unprecedented rise with surface coverage, suggesting a different mechanism than simple physisorption, but the values fell far short

of the predicted 20 kJ/mol for room temperature binding. In physisorption systems operating at 77K, higher binding enthalpies are undesirable because this means heat is released by the system on cycling and this creates an energy penalty in term of the coolant required to maintain 77K. However, higher binding enthalpies also mean stronger H-H bonds to the surface, which may translate into retention of storage capacities at higher temperatures. Figure 2.8 shows the binding enthalpies of untreated HMS silica, and silica treated with 0.2 mol equivalents of tetrabenzyl titanium before and after heating as calculated by a variant of the Clausius-Clapeyron equation^[21] from hydrogen adsorption data at 77 K and 87 K (Fig. 2.9). The pristine silica material shows a linear progression from 3.5 kJ/mol with decreasing slope on increasing coverage. The material treated with tetrabenzyl titanium before heating starts at 0.15 kJ/mol and increases sharply to 13.15 kJ/mol. This rising slope behavior suggests that the Ti (IV) units, which have no special affinity for H₂, have already been partially reduced to Ti(III). This is not unexpected given that tetrabenzyl titanium is both heat and light sensitive and must be stored in the dark at -78 °C to prevent reductive cleavage of the C-Ti benzyl bond.^[24] The same material after heating shows a gradual progression from 2.65 kJ/mol to 22.15 kJ/mol. This is the highest value ever recorded for a porous material under cryogenic conditions, more than double that of any previous material, and suggests that this material should retain hydrogen at room temperature. The difference between the heated and unheated materials illustrates that it is the Ti (III) centers and not the benzyl groups that provide the high enthalpy binding sites. The rising slope can be rationalized by either adsorption at multiple sites of different enthalpies and activation barriers, or a progressive change in adsorption enthalpy on H₂

ligand binding to the Ti centers. The latter was predicted by Zhao^[13] and Yildirim^[15] and can be viewed as a result of cis and trans ligand effects on the electronic environment of the Ti centers. With an increasing number of H₂ ligands on the Ti centers, the metal becomes more electron rich due to σ -donation from the H-H bond, thus facilitating π -back bonding from the metal into the H-H antibonding orbital. The enthalpy of the 0.3 tetrabenzyl titanium material was also calculated by this method and rises with coverage to 22.04 kJ/mol, demonstrating that high enthalpies are general in these materials and not specific to one set of samples or a particular composition.

Table 2.2 shows a comparison in storage capacities at $-196\text{ }^{\circ}\text{C}$, $-78\text{ }^{\circ}\text{C}$, and $25\text{ }^{\circ}\text{C}$ at 100 atm between pristine mesoporous silica and mesoporous silica treated with 0.2 equivalents of tetrabenzyl titanium after heating. The values for the compressed pellet from Table 2.1 are also shown. There is a decrease in total storage from 21.45 wt % to 8.39 wt%, and 5.05 wt% with increasing temperature in the treated material. This is accompanied by a drop in volumetric capacity from 34.10 kg/m^3 , to 14.84 kg/m^3 , and 8.93 kg/m^3 , respectively with increasing temperature. These numbers compare to 32 kg/m^3 , 12.5 kg/m^3 , and 8 kg/m^3 , calculated for compressed hydrogen at 100 atm for these temperatures. The most intriguing numbers are the adsorption values, which drop from 1.21 wt% to 0.58 wt.%, and 0.44 wt.% with increasing temperature for pure HMS silica, and 1.66 wt.%, to 0.99 wt.%, and 0.69 wt.% for the treated material. Taking into account the 4.08% Ti from ICP-AAS and the densities of the materials, this corresponds to 2.4 H₂ per Ti at $-78\text{ }^{\circ}\text{C}$ and 1.1 H₂ at ambient temperature. There is thus very little loss of H₂ binding capacity at the Ti centers at $-78\text{ }^{\circ}\text{C}$, and only 59% loss at room temperature. This confirms predictions that materials possessing binding enthalpies in

the 20 kJ/mol range may find application in room temperature hydrogen storage. While the storage capacities of the powder fall short of practical value at ambient temperature, extrapolation of the capacities to 350 atm, a pressure used in some current model hydrogen vehicle compressed gas tanks, gives 17.82 wt.% and 31.52 kg/m³ for the powder and 3.51 wt.% and 60.75 kg/m³ for the compressed pellet. These compressed pellet numbers are roughly double that of compressed hydrogen under the same conditions and resemble that of many hydrides (i.e. high volumetric with only moderate gravimetric), with volumetric densities approaching the 80 kg/m³ 2015 DOE goal, yet these materials do not require any heating or heat exchangers for hydrogen release, and thus are more advantageous from an automotive design standpoint. The extrapolated capacities for the compressed pellet at 350 atm and ambient temperature are very similar to those at -196 °C and 100 atm, demonstrating that excess pressure can be used in this system to compensate for increased temperature. This gives an obvious advantage in design as well as overcoming problems with boil off encountered under cryogenic conditions. While these capacities fall short of DOE goals, it is anticipated that by tuning the Ti coordination sphere and oxidation state, as well as optimizing surface coverage and the nature of the support material, further gains can be realized.

Figure 2.6 - Hydrogen storage capacity in a 20 cycle test of mesoporous silica treated with 0.2 molar equivalent of tetrabenzyl titanium.

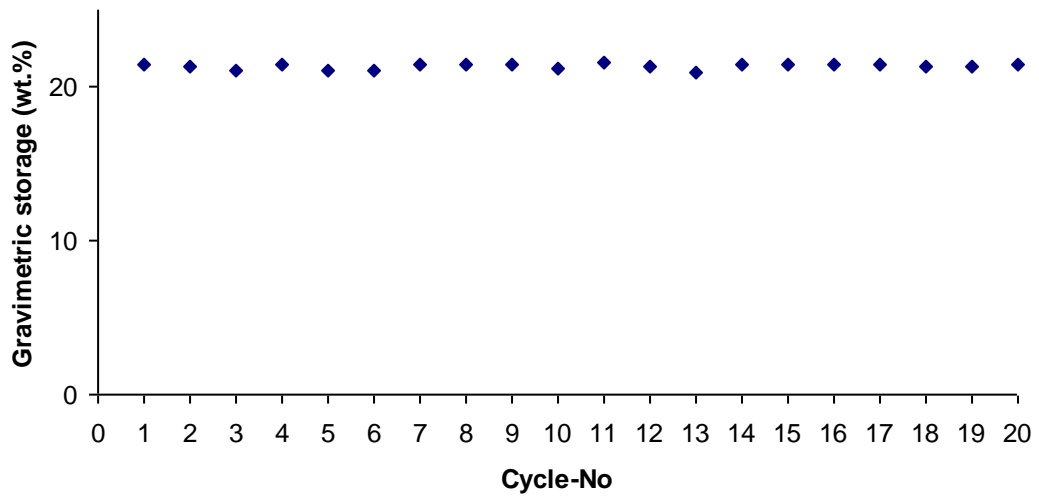


Fig. 2.7 - Adsorption and desorption isotherms for the material from Fig. 2.6.

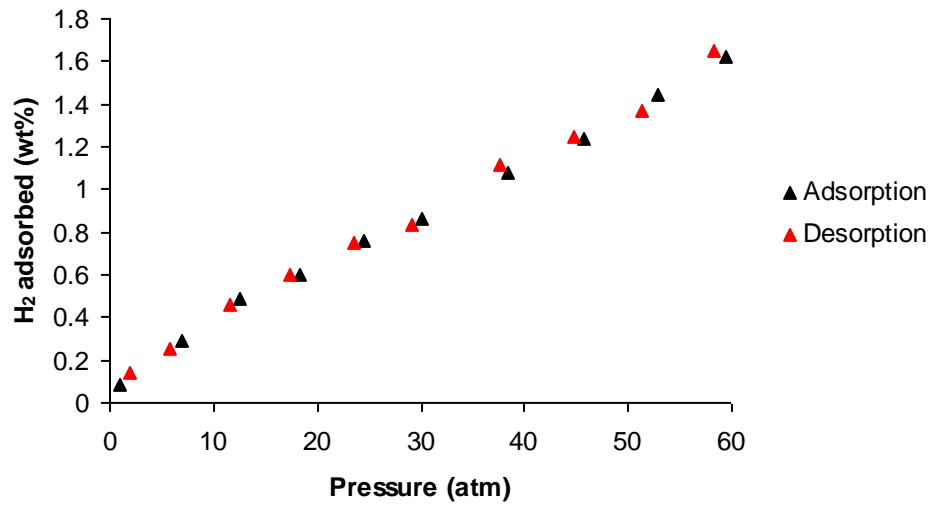


Figure 2.8 - Hydrogen binding enthalpies of mesoporous silicas from Table 1: Pristine silica (black), the 0.2 molar equiv. tetrabenzyltitanium material after heating at 180 °C (red), the 0.3 molar equiv. tetrabenzyltitanium material after heating at 180 °C (brown) and the 0.2 molar equiv. tetrabenzyltitanium material before heating (pink)

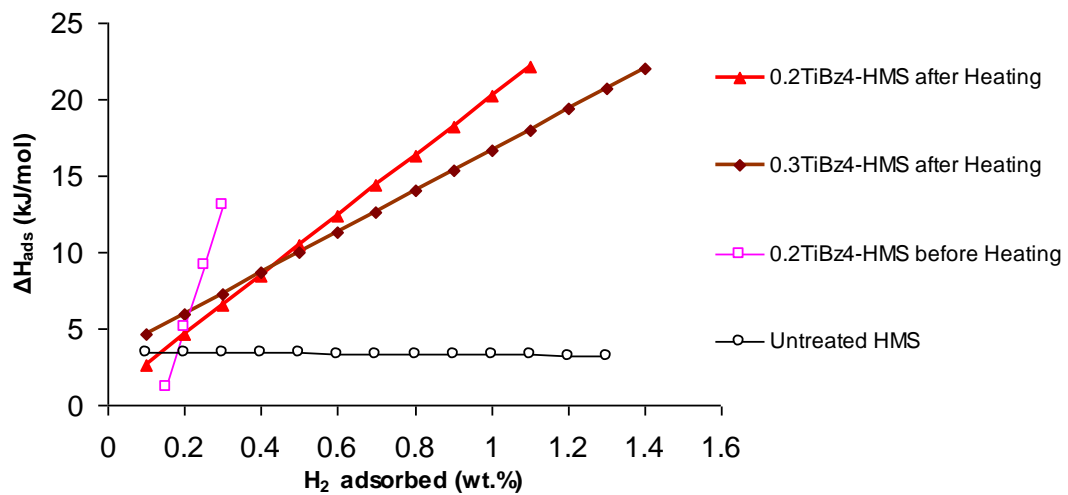


Table 2.1 - Hydrogen storage capacities of mesoporous silicas at 77 K with different surface areas synthesized using various molar ratios of tribenzyl and tetrabenzyl titanium.

Sample name	Surface area (m ² /g)	Skeletal Density (g/ml)	Apparent Density (g/ml)	Gravimetric H ₂ adsorption at 77 K (wt.%) ^a	Gravimetric H ₂ storage at 100 atm (wt.%) ^b	Volumetric H ₂ storage at 100 atm (kg/m ³) ^b
Plain HMS	1219	1.60	0.206	1.21	9.84	20.34
0.05TiBz ₃ -HMS	799	1.38	0.15	1.38	20.56	30.67
0.1TiBz ₃ -HMS	889	0.94	0.16	1.99	19.26	31.14
0.2TiBz ₃ -HMS	895	0.93	0.17	2.02	17.48	30.37
0.1TiBz ₄ -HMS	1140	1.96	0.17	0.95	17.68	30.02
0.2TiBz ₄ -HMS	1294	1.45	0.16	1.66	21.45	34.10
0.3TiBz ₄ -HMS	913	1.99	0.17	2.04	19.67	33.07
0.5TiBz ₄ -HMS	746	1.86	0.20	0.26	13.04	26.59
0.2TiBz ₄ -HMS Pellet	720	1.82	1.73	1.55	3.15	54.49
AX-21	3225	2.10	0.33	4.19	11.96	39.23

^aSaturation was not reached at 60 atm except for that of plain silica, 0.1TiBz₄-HMS, and 0.5TiBz₄-HMS .

^b Hydrogen measurement is at the temperature of 77 K and 60 atm extrapolated to 100atm with goodness of fit (R²)= 0.9966~0.9995

Table 2.2 - Hydrogen storage capacities of pristine and Ti-grafted mesoporous silica at different temperatures.

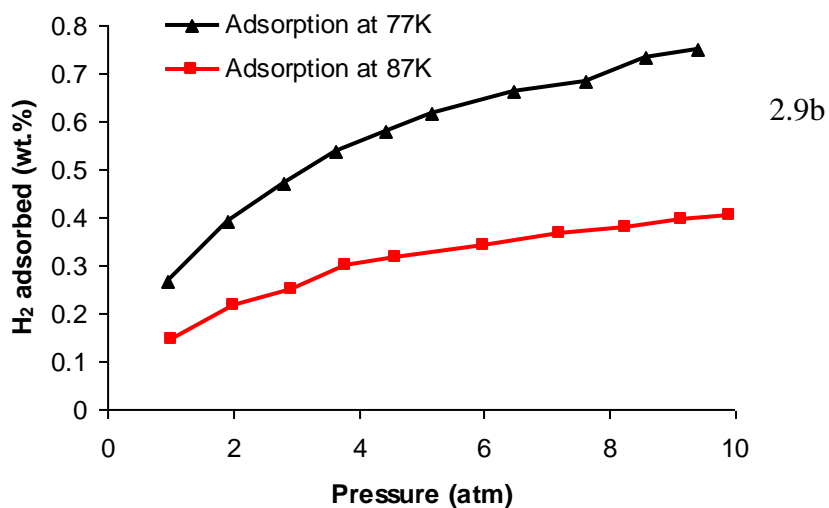
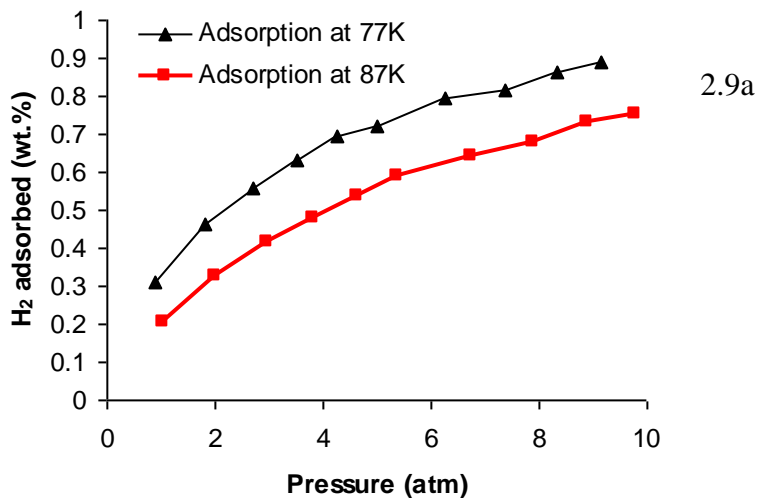
Sample name	Apparent Density (g/ml)	Skeletal Density (g/ml)	Gravimetric H ₂ adsorption (wt.%) ^a	Gravimetric H ₂ storage at 100 atm (wt.%)	Volumetric H ₂ storage at 100atm (kg/m ³) ^c
Plain HMS at -196°C	0.206	1.60	1.21 ^a	9.84	20.34
Plain HMS at -78°C	0.206	1.60	0.58 ^b	7.37	11.79
Plain HMS at 25°C	0.206	1.60	0.44 ^b	5.55	8.88
0.2TiBz ₄ -HMS at -196°C	0.17	1.45	1.67 ^b	21.45	34.10
0.2TiBz ₄ -HMS at -78°C	0.17	1.45	0.99 ^b	8.39	14.84
0.2TiBz ₄ -HMS at 25°C	0.17	1.45	0.69 ^b	5.05	8.93
0.2TiBz ₄ -HMS Pellet at -196°C	1.73	1.82	1.55	3.15	54.49
0.2TiBz ₄ -HMS Pellet at -78°C	1.73	1.82	0.82	1.28	22.14
0.2TiBz ₄ -HMS Pellet at 25°C	1.73	1.82	0.59	0.86	14.88

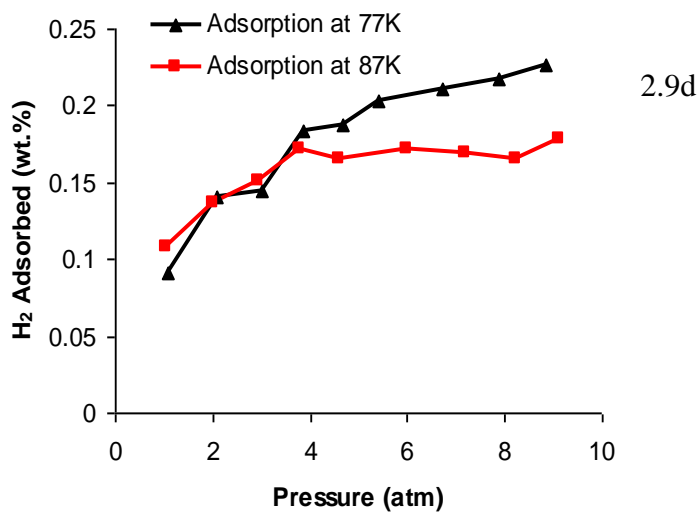
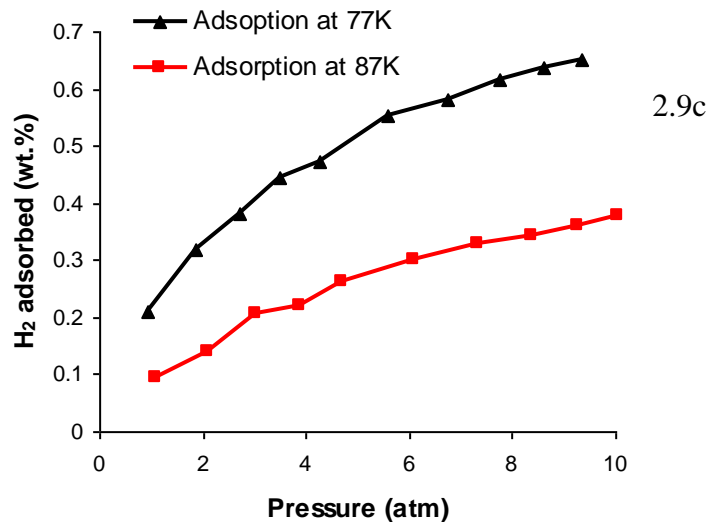
^a Hydrogen adsorption isotherm reached saturation below 60 atm .

^b Hydrogen adsorption isotherms did not reach saturation at 60 atm.

^c Hydrogen storage measurement is at 60 atm extrapolated to 100 atm with goodness of fit (R²)= 0.9966-0.9995.

Figure 2.9 - Adsorption isotherms for the materials from Figure 2 recorded at liquid argon and liquid nitrogen temperatures. a) Pristine mesoporous silica. b) Silica treated with 0.2 molar equivalents tetrabenzyl titanium after heating. c) Silica treated with 0.3 molar equivalents tetrabenzyl titanium after heating. d) Silica treated with 0.2 molar equivalents tetrabenzyl titanium before heating.





2.4 Conclusions

In summary, mesoporous silica was used as scaffolding for well-defined single site 3-coordinate Ti (III) centers capable of binding up to 5 H₂ per Ti through a Kubas interaction. These materials display binding enthalpies of up to 22.15 kJ/mol and retain 89% of their enhancement at -78 °C and 41% at room temperature. Under selected conditions volumetric densities as high as 60.75 kg/m³ were extrapolated at room

temperature and elevated pressure, suggesting that these materials may find use for increasing storage capacities of compressed gas cylinders at ambient temperature.

2.5 References

1. Schlapbach, L., Züttel, A. *Nature*, **2001**, 414, 353-358
2. Yartys, V.A., Harris, I.R., Panasyuk, V.V. *Mater. Sci.*, **2001** 37, 219.
3. Sandrock, G. *J. Alloys Comp.*, **1999**, 877, 293-295,
4. Seayad, A.M., Antonelli, D.M., *Adv. Mater.*, **2004**, 16, 765
5. Dillon, A.C., Jones, K.M., Bekkedahl, T.A., Kiang, C.H., Bethune, D.S., Heben, M.J., *Nature*, **1997**, 386, 377.
6. Chen, P. Wu, X. Lin, J. Tan, K.L. *Science*, **1999**, 285, 91.
7. Ye, Y., Ahn, C.C., Witham, C., Fultz, B., Liu, J., Rinzler, A.G., Colbert, D., Smith, K.A., Smalley, R.E., *Appl. Phys. Lett.*, **1999**, 74, 2307.
8. Liu, C., Fan, Y.Y., Liu, M., Cong, H.T., Cheng, H.M., and Dresselhaus, M.S. *Science*, **1999**, 286, 1127.
9. Poirier, E., Chahine, R., Benard, P., Cossement, D., Lafi, L., Melancon, E., Bose, T.K., Desilets, S. *Appl. Phys. A*, **2004**, 78, 961.
10. Rosi, N.L., Eckert, J., Eddaoudi, M., Vodak, D.T., Kim, J., O'keeffle, M., Yaghi, O.M. *Science*, **2003**, 300, 1127.
11. Rowsell, J.L.C., Milward, A. R. Park, K.S. Yaghi, O.M. *J. Am. Chem. Soc.*, **2004**, 126, 5666.
12. Panella, B., Hirscher, M., *Adv. Mater.*, **2005**, 17, 538.
13. Zhao, Y., Kim, Y.H., Dillon, A.C., Heben, M.J., Zhang, S.B., *Phys. Rev.*

Lett., **2005**, 94, 155504.

14. Kubas, G.J., *J. Organomet. Chem.*, **2001**, 635, 37.
15. Yildirim, T., Ciraci, S., *Phys. Rev. Lett.*, **2005**, 94, 175501.
16. Hu, X., Skadtchenko, B., Trudeau, M., Antonelli, D.M., *J. Am. Chem. Soc.*, **2006**, 128, 11740.
17. Hu, X. Trudeau, M., Antonelli, D.M., *Chem. Mater.*, **2007**, 19, 1388.
18. Sun, T. Ying, J.Y., *Nature*, **1997**, 389, 704.
19. He, X. Antonelli, D.M., *Chem. Int. Ed.*, **2002**, 41, 214.
20. Antonelli, D.M., *Micropor. and Mesopor. Mater.*, **1999**, 30, 315.
21. Roquerol, F., Rouquerol, J., Sing, K., *Adsorption by Powder and Porous Solids*, Academic Press, London, **1999**.
22. Tanev, P.T. Pinnavaia, T.J., *Science*, **1995**, 267, 865.
23. Nesterov, G.A., Zakharov, V.A., Paukshitis, E.A., Yurchenko, E. N., and Ermakov, Y.I., *Kinetika i Kataliz*, **1977**, 20, 429.
24. Maksimov, N.G., Nesterov, G.A., Zakharov, V.A., Stchastnev, P.V., Anufrienko, V. F., Yermakov, Y. I. *J. Mol. Catal.*, **1977**, 4, 167.
25. Kaye, S. S., Long, J. R., *J. Am. Chem. Soc.*, **2005**, 127, 6506.
26. Dincă, M., Dailly, A., Liu, Y., Brown, C. M., Neumann, D. A., Long, J.R., *J. Am. Chem. Soc.*, **2006**, 128, 16876.
27. Benard, P., Chahine, R., *Langmuir*, **2001**, 17, 1950.

28. Zuchni, U., Albizzati, E., Gianni, U., *J. Organomet. Chem.*, **1971**, 26, 377.

Chapter 3 – Optimization of Hydrogen Storage Capacity in Silica-Supported Low-valent Ti Systems Exploiting Kubas Binding of Hydrogen

3.1 Introduction

Research into hydrogen storage has become increasingly important due to the increased demands placed on world oil reserves as well as the various environmental issues related to global warming and the consumption of fossil fuels.^[1] Hydrogen is an ideal fuel because it has the highest energy per gram of any substance and only emits water as a combustion product, therefore avoiding green house gas emissions. The DOE has set system targets of 9.0 wt% and 81 Kg/m³ for 2015,^[2] and while some materials meet or surpass one of these values, there is no material that is close to meeting both of them. In addition to this, there are many often overlooked factors such as kinetics of release, thermal conductivity, and binding enthalpy that must be considered before a hydrogen storage material can become practical. Isothermic heats of adsorption are of special importance because they govern the strength of binding of the hydrogen to the chemical carrier and also determine the amount of heat released or required on charge/discharge respectively. Materials such as hydrides, which possess enthalpies of 70 kJ/mol and higher, release enormous amounts of heat on filling and require equally large amounts of heat to liberate the hydrogen when it is required as fuel. This creates problems with heat management and also drastically lowers the effective energy storage capacity of the system. Poor reversibility and slow kinetics are also problems with many metal hydride^[3] systems including MgH₂, NaAlH₄, and NH₃BH₃. As an alternative to hydrides, materials such as MOFs^[4,5,6] and porous carbons^[7,8,9] absorb hydrogen on their vast internal network of surface area, and offer great kinetic

advantages over hydrides. However their low binding enthalpies of generally less than 10 kJ/mol, while facilitating heat management on refueling, necessitate cooling to 77 K for optimal performance, again diminishing the energy storage capacity of the system. For these reason, it has been proposed that materials possessing 20-30 kJ/mol binding enthalpies may be ideal for on board hydrogen storage applications.^[10, 11] These moderate isosteric heats of adsorption do not cause as much difficulty in terms of heat management, but provide enough thermal stability to the interaction between the hydrogen and the material to perform at temperatures higher than 77 K. The Kubas interaction,^[12, 13] effectively a σ - π ligand interaction between a hydrogen molecule and a metal center, affords these ideal enthalpies in conjunction with predicted high storage capacities in many hypothetical systems, most involving early transition metals.^[9-11] There is also strong evidence for such an interaction at apical metal centers in many MOF and Prussian Blue^[14] framework materials. In 2008 we reported the first example of a material that possessed an enthalpy in the target 20-30 kJ/mol range.^[15] This system was comprised of Ti (III) benzyl units on mesoporous silica which increased the performance of the system from 1.2 wt% to 1.65 wt% at 77 K. The tailored Ti fragments held 3 H₂ per unit under these conditions while also retaining 41% of their capacity at room temperature. These materials constituted a substantial leap forward by demonstrating that Kubas binding may represent a potential answer to many hydrogen storage problems. In this paper we optimize the performance of this Ti (III) system by adjusting several synthetic parameters and exploring other Ti precursors. We show that after fine tuning of the surface area, pore size, and synthetic protocol that HMS silica grafted with 0.2 equivalents of TiBz₄ reaches 2.45 wt% adsorption at 77k and 60 atm

after activation to the Ti (III) form, which equates to 3.98 H₂ on average per Ti center. This is close to the theoretical maximum of 5 H₂ per Ti predicted by the 18 electron rule and demonstrates that organometallic fragments can carry more hydrogen ligands per metal at high pressure and low temperature than the maximum observed in an isolated organometallic compound at room temperature and pressure.

3.2 Experimental

All chemicals, unless otherwise stated, were obtained from Aldrich. H₂, CO₂ and N₂ gases were obtained from Praxair Canada Inc.

3.2.1 Synthesis of Hexagonally-packed Mesoporous Silica (HMS):^[16] in a typical preparation, tetraethyl orthosilicate (1.0 mol) was added with vigorous stirring to a solution of dodecylamine (DDA) (0.27 mol) (in 4:1 molar ratio of tetraethyl orthosilicate to DDA) in ethanol (9.09 mol). The reaction mixture was aged at ambient temperature for 18 hours, and the resulting mesoporous silica was air dried on a glass plate. The template was removed by mixing 1 g of the air-dried HMS with 150 ml of hot ethanol for 1 hour. The product was then filtered and washed with a second 100ml portion of ethanol. This extraction procedure was repeated twice, and the crystalline product air-dried at 80°C. Another 3 batches of HMS silica were prepared according to the procedure above, but using different molar ratios of tetraethyl orthosilicate to dodecylamine (3:1, 2:1, 1:0.75). Also C₆-HMS, C₈-HMS and C₁₀-HMS were prepared as per the same procedure, but employing hexylamine, octylamine and decylamine template, respectively.

3.2.2 Synthesis of Ti-grafted mesoporous silicas: 0.2 equiv. of tetrabenzyl titanium (or tribenzyl titanium), as calculated on the basis of 33% Si in the porous oxide was added to a suspension of HMS mesoporous silica in dry toluene under nitrogen. After 1 day of stirring to ensure complete absorption of the organometallic, the reduced material was collected by suction filtration under nitrogen and washed several times with toluene. In the case of tetrabenzyl titanium only, the reduced material was activated by heating at 120°C for 6 hours under vacuum at 10^{-3} Torr on a Schlenk line until all volatiles had been removed. This material was used as either a powder or a 1.3 cm diameter pellet compressed in a commercial pellet press at 4 metric tones. Assuming 1 g of 0.2TiBz₄-HMS, with a surface area of 1165 m²/g (1.165×10^{21} nm²) and 4.12 wt. % Ti for 0.2TiBz₄-HMS by elemental analysis, 1g of 0.2TiBz₄-HMS contains 41.2 mg Ti (8.60×10^{-4} moles Ti). The Ti coverage can then be calculated as follows: Ti coverage = (8.60×10^{-4} moles Ti x 6.02×10^{23} Ti /mole) / (1.16×10^{21} nm²) = 0.4443 Ti/nm²

3.2.3 Synthesis of Trimethyl Ti Grafted Silica:^[17]

TiMe₃ was prepared by adding TiCl₃.3THF in THF to MeMgCl in THF at -40 °C drop-wise over 3 hours, followed by stirring for another 3 hours. A deep green solution was obtained. The TiMe₃ solution was treated immediately with mesoporous silica placed into a side adaptor connected to the 3-neck flask reaction compartment. The temperature was then allowed to warm to ambient over several hours followed by further stirring at room temperature for 4 hrs. At this stage the solution was colorless and the silica had taken on a green color, suggesting complete absorption of the Ti. The

solution was then filtered under inert atmosphere in the glove box and washed 3 times with THF in order to purge the sample of MgCl_2 . The solid was then dried *in vacuo* and stored under nitrogen before use.

3.2.4 Synthesis of $(\text{Allyl})_3\text{Ti}$ Grafted Silica:^[18,19]

The preparation procedure for Allyl_3Ti was similar to that of TiMe_3 , but AllylMgCl was used instead of MeMgCl . Complete absorption of the Ti was confirmed by the colorless solution after filtration and isolation of the blue-gray solid.

3.2.5 XPS Spectroscopy: All X-ray Photoelectron Spectroscopy (XPS) peaks were referenced to the carbon C-(C, H) peak at 284.8 eV, and the data were obtained using a Physical Electronics PHI-5500 spectrometer using charge neutralization.

3.3 Results and discussion

3.3.1 Variation of Silica-to-Surfactant Molar Ratio

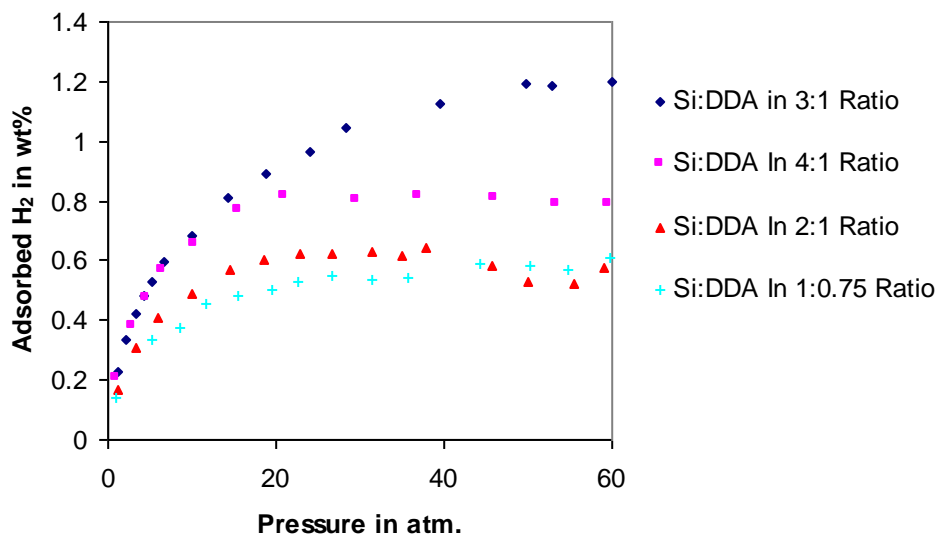
Since hydrogen adsorption in Ti-grafted mesoporous silicas contains a large component of physisorption due to the huge internal surface area, we maximized the surface area of the hexagonally-packed mesoporous silica by varying the silica-to-surfactant ratio (Table 3.1). The highest surface area of $1448 \text{ m}^2/\text{g}$ was obtained when the Si to dodecylamine ratio was 4:1. Three other HMS silica samples were prepared with silica-to-surfactant ratios of 3:1, 2:1, and 1:0.75 and possessed BET surface areas of 1165, 1117, and $822 \text{ m}^2/\text{g}$, respectively. The surprising fact was that the hydrogen adsorption capacity (excess storage) of the 4:1 sample of HMS at 77K was lower (0.75 wt.%, and a surface area of $1448 \text{ m}^2/\text{g}$) than that prepared with a Si:DDA ratio of 3:1 (1.2 wt.% and a surface area of $1165 \text{ m}^2/\text{g}$). The higher adsorption capacity of the 3:1 silica may be due to differences in micropore volume of the two samples, which may be

beyond the accuracy of nitrogen adsorption measurement. The 2:1, and 1:0.75 samples possessed H₂ adsorption values of 0.75 wt% and 0.90 wt%, respectively, at 77 K, lower than that prepared with 3:1 ratio (Fig. 3.1). The skeletal densities of the silicas ranged from 1.62-2.33 g/cc. The total storage was also measured from the apparent densities shown in Table 3.1. This is a measurement of the total hydrogen present on the surface and as compressed gas in the pores in a given volume of material normalized to the sample weight. This number is highly dependent on the compression of the sample, but is the only way of determining how much hydrogen is present in a sample of a porous solid under pressure. Again, the material synthesized at a Si:DDA ratio of 3:1 showed the highest performance, with a total gravimetric storage of 19.06 wt%.

Table 3.1 - A summary of the apparent density, skeletal density, gravimetric storage, gravimetric adsorption, and surface area of all HMS pristine synthesized using different molar ratios of tetraethyl orthosilicate to dodecylamine.

Sample	App. Density (g/ml)	Sk. Density (g/ml)	Grav. Storage at 100atm (wt%)	Grav. Adsorption at saturation (wt.%)	Surface Area (m ² /g)
C12-HMS Si:DDA 4:1	0.18	2.33	17.82	0.75	1448
C12-HMS Si:DDA 3:1	0.17	2.13	19.06	1.20	1165
C12-HMS Si:DDA 2:1	0.19	2.04	16.10	0.75	1117
C12-HMS Si:DDA 1:0.75	0.17	2.16	18.10	0.90	922

Figure 3.1 - Hydrogen adsorption isotherms at 77 K for mesoporous silica synthesized using different molar ratios of tetraethyl-orthosilicate: dodecyl-amine.



3.3.2 Variation of Pore Size

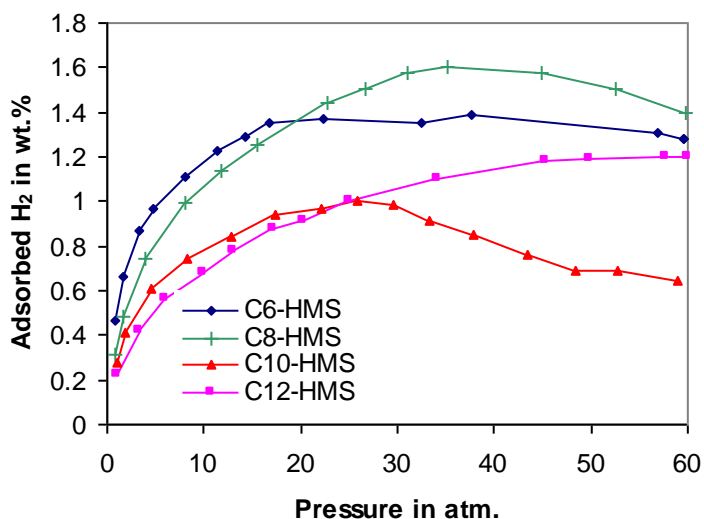
Since microporous materials are believed to absorb more hydrogen due to capillary action, HMS silica with smaller pore sizes were synthesized by shortening the surfactant chain length. The hexylamine, octylamine, decylamine, and dodecylamine templates, possessing 6, 8, 10, and 12-carbon chain lengths were thus independently employed in the synthesis procedure of HMS. The corresponding template free materials had BJH pore sizes of 12, 18, 22, and 25 Å, respectively. The pristine C₆-HMS and C₈-HMS silicas had higher hydrogen adsorption capacity (1.38 and 1.60wt%, respectively) than that synthesized by using the dodecylamine template (1.20 wt%) (Table 3.2, and Fig. 3.2). But after grafting the surface of the C₆-HMS or C₈-HMS with tetrabenzyl titanium at a 0.2 molar equivalents loading level, the adsorption capacities of these silicas decreased dramatically, from 1.38wt% to 0.70 wt% and from 1.6 to 0.95,

not the case with the C₁₂ material where the H₂ adsorption increases from 1.20 wt% for the pristine to 2.45wt% after grafting with 0.2 molar equivalents of TiBz₄. This value of 2.45 wt% is much higher than the 1.6 wt% previously reported for tetrabenzyl titanium grafted to C₁₂ HMS, likely because of the higher surface area of the sample employed in this study leading to a greater number of silanol anchoring points for the Ti fragments in the material. The smaller pores of the C₆ and C₈-HMS yield materials of higher surface areas which allows a larger quantity of hydrogen gas to physisorb on the surface, but at the same time the pore size of these microporous silicas are too small to allow the unencumbered incorporation of the large tetrabenzyl Ti fragments onto the surface, thus restricting the Ti loading level and/or effectiveness of the Ti centers for hydrogen binding. This finding is consistent with a previous study in our group, which explored the H₂ storage of microporous and mesoporous titanium oxide treated with bis (toluene) Ti.^[20, 21] C₁₀-Ti-TMS1 was found to have an adsorption capacity of 1.01wt.%, lower than that of C₁₂-Ti-TMS1, even though it had a higher surface area.

Table 3.2 - Hydrogen sorption capacity of micro- and mesoporous silica at 77K with different surface areas and pore sizes synthesized using amine templating agents of various chain lengths.

Sample	App. Density (g/ml)	Sk. Density (g/ml)	Pore Size (Å)	Grav. Storage at 100atm (wt%)	Grav. Adsorption at saturation (wt%)	Surface Area in m ² /g
C ₆ -HMS	0.15	1.92	12	21.15	1.38	1074
C ₈ -HMS	0.19	1.61	18	17.18	1.60	1321
C ₁₀ -HMS	0.14	1.52	22	20.61	1.01	1206
C ₁₂ -HMS	0.168	2.13	25	19.06	1.20	1165

Figure 3.2 - Hydrogen adsorption isotherms at 77 K of C₆, C₈, C₁₀ and C₁₂-HMS



From the above experiments, it appears that the C₁₂-HMS prepared by using silica to surfactant ratio of 3:1 is the best support for hydrogen storage in this study. In all subsequent experiments this same sample of silica was grafted with various Ti fragments at different loading levels, in order to optimize the hydrogen adsorption capacity of these materials.

3.3.3 Variation of Metal-fragment Precursor and Precursor Loading Levels

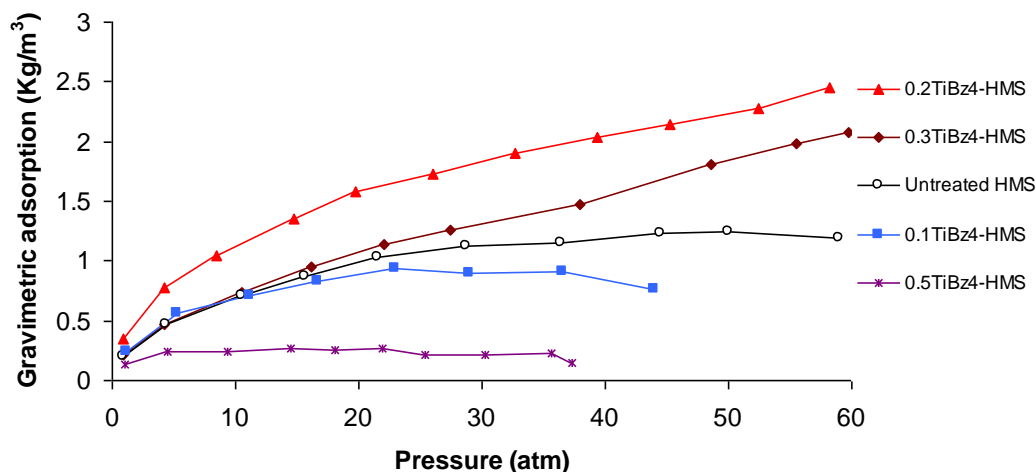
By grafting the surface of C₁₂-HMS, prepared from a 3:1 molar ratio of TEOS and dodecylamine, with 0.2 equivalents of tetrabenzyl titanium we reached 2.45 wt% adsorption, which equates to an average of 3.98 H₂ molecules per Ti metal center, only one H₂ molecule short of the saturation level predicted by the 18 electron rule. This is

the highest adsorption value reached so far for mesoporous metal oxides (Table 3.3). The room temperature adsorption of this material was 0.76 wt%, indicating that 31% of the H₂ was retained per Ti at 25 °C. This equates to 1.23 Ti per metal center, on the basis of 4.08 wt% Ti in the sample. This compares to 0.44 wt% adsorption in pure mesoporous silica under these conditions. Materials prepared at lower or higher ratios yielded lower hydrogen adsorption results. It appears that the material prepared with 0.1 equivalents of Ti does not possess enough Ti units per square nanometer to maximize the hydrogen storage performance, while samples prepared with higher levels of Ti than 0.2 equivalents, have lower performance due to clustering on the surface.

Table 3.3 – Summary of the storage and adsorption capacities of C₁₂-HMS treated with different molar equivalents of tetrabenzyl Ti.

Sample	App. Density g/cc	Sk. Density g/cc	Grav. Storage Wt%	Grav. Adsorption Wt.%
0.1TiBz ₄ -C ₁₂ -HMS	0.17	1.96	17.68	0.95
0.2TiBz ₄ -C ₁₂ -HMS	0.16	1.62	21.45	2.45
0.3TiBz ₄ -C ₁₂ -HMS	0.17	1.99	19.67	2.04
0.5TiBz ₄ -C ₁₂ -HMS	0.20	1.86	13.04	0.26

Figure 3.3 - Hydrogen adsorption isotherms at 77 K of C₁₂-HMS grafted with various molar equivalents of tetrabenzyl Ti.

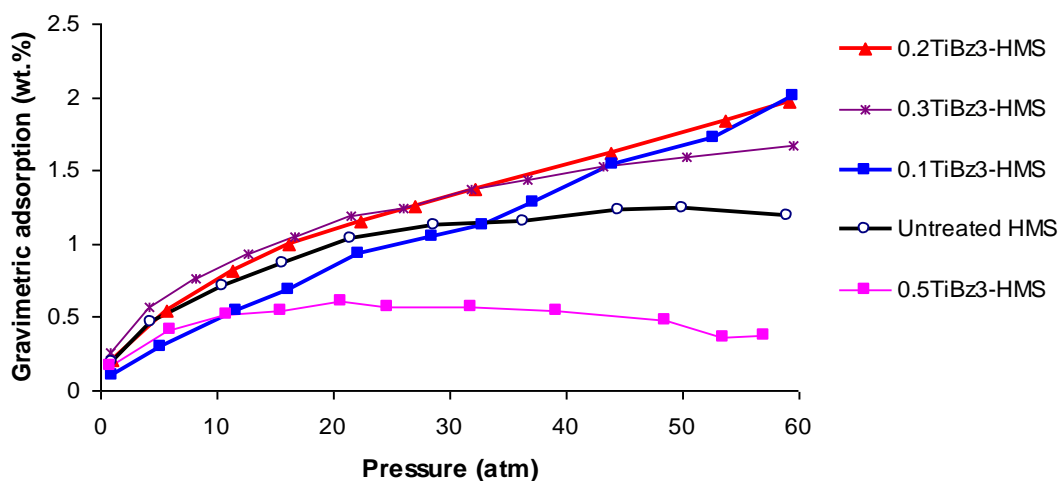


When tribenzyl titanium is anchored onto the surface of C₁₂-HMS silica, the adsorption capacities are slightly lower than those of their tetrabenzyl Ti counterparts (i.e., 2.04 wt% for the 0.2TiBz₃-HMS, compared to 2.45wt% for that of 0.2TiBz₄-HMS) (Table 3.4, and Figure 3.4). This may be due to metal clustering of low valent Ti on the surface, which disfavors H₂ binding. The Ti (III) fragments are more reactive than the Ti(IV) fragments and clustering of Ti(III) units by the creation of Ti-Ti bonds may compete with the anchoring to surface hydroxyl groups, making Ti(IV) deposition, followed by thermal cleavage of the benzyl-Ti bond yield the active Ti (III) species, more selective and effective than Ti (III) deposition.

Table 3.4 – Summary of the storage and adsorption capacities of C₁₂-HMS treated with different molar equivalents of tribenzyl Ti.

Sample	App. Density g/cc	Sk. Density g/cc	Grav. Storage Wt%	Grav. Adsorption Wt.%
0.1TiBz ₃ -C ₁₂ -HMS	0.16	0.94	19.26	1.99
0.2TiBz ₃ -C ₁₂ -HMS	0.17	0.93	17.48	2.02
0.3TiBz ₃ -C ₁₂ -HMS	0.31	1.31	10.03	1.74
0.5TiBz ₃ -C ₁₂ -HMS	0.34	1.38	7.35	0.62

Figure 3.4 - Hydrogen adsorption isotherms at 77 K of C₁₂-HMS grafted with various molar equivalents of (benzyl)₃Ti.



Finally, commercially available 380-Aerosil hydrophilic fumed silica with a surface area of 380 m²/g obtained from Evonic-Degussa Chemicals was tested for hydrogen adsorption capacity before and after grafting with tetrabenzyl Ti. The pristine Aerosil has an adsorption capacity of 1.25 wt% at 77k and 60 atm, similar to that of C₁₂-HMS (1.2 wt. %). When grafted with 0.2 molar equivalent of TiBz₄ this material shows an adsorption of only 1.15 wt%. An almost identical adsorption capacity was obtained when this material was coated with 0.3 equivalents of TiBz₄. When grafted with 0.5 equivalents of TiBz₄ the adsorption capacity increased to 1.40 wt.%. Beyond this loading level the adsorption capacity begins to decrease to levels below that of the untreated sample. The reason for this may be due to different surface diffusion properties and concentration of surface anchoring sites in the corresponding silicas affecting the surface anchoring process. The silanol group density of 380-Aerosil was approximated to an average of 1.25 SiOH/ nm² as measured by the LiAlH₄ method,^[22] compared to 4.6 SiOH/nm² for that of HMS.^[23]

Table 3.5 – Summary of the adsorption capacities of plain and treated 380-Aerosil with different molar ratios of tetrabenzyl Ti.

Sample	Sk. Density g/cc	Grav. Adsorption Wt. %
Plain 380Aerosil (compressed)	1.79	1.25
0.2TiBz4-380Aerosil	1.58	1.15
0.3TiBz4-380Aerosil	1.48	1.15
0.5TiBz4-380Aerosil	1.39	1.40

3.3.4 Ti(CH₃)₃ grafted on HMS

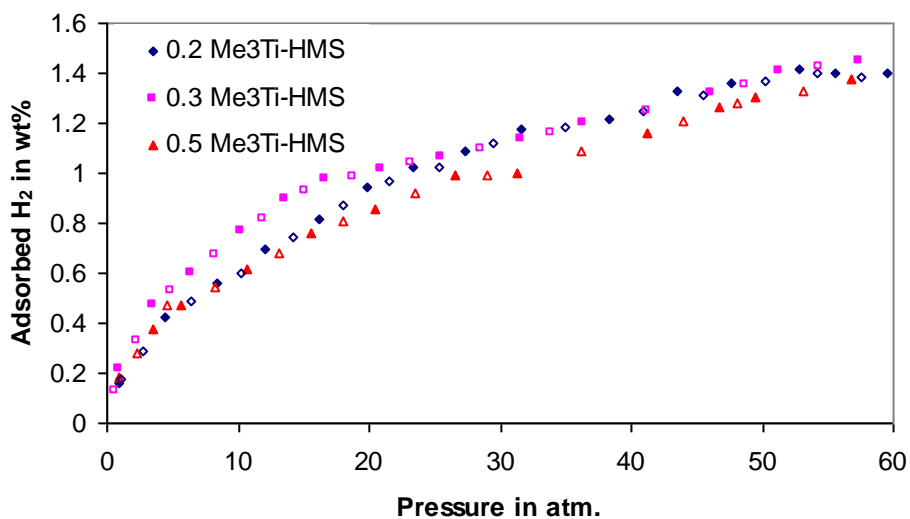
Since different ligands in the Ti (III) coordination sphere are likely to influence hydrogen binding either electronically, through their ability to donate electrons to the Ti center and thus strengthen π -back bonding to the H-H antibonding orbital, or sterically, by influencing the ease in which H₂ can access the open coordination sites on Ti, it is likely that different Ti (III) precursors will lead to grafted mesoporous silicas with different hydrogen adsorption properties. The benzyl ligand is electron withdrawing, can adopt a η^3 coordination mode thereby shutting down a coordination site, and is somewhat heavy, all factors may lead to diminished hydrogen storage performance in this system. In previous unpublished studies we attempted to remove the benzyl ligand by hydrogenation according to a literature report on benzyl Ti grafted silicas for Ziegler-Natta catalysis^[20] to leave behind a Ti (III) hydride. However the resulting material possessed a hydrogen adsorption capacity almost identical to that of the material before hydrogenation. The reason for this is not known, as a hydride ligand should provide a more facile steric environment for hydrogen binding and contributes less weight than a benzyl ligand. In order to explore the effects of different ligands and precursors, we prepared a sample of HMS silica grafted with TiMe₃. This compound is thermally

unstable and can only be synthesized in THF solution at $-78\text{ }^{\circ}\text{C}$. It exists as a THF adduct in solution, and decomposes to form methane and various carbenoid species at ambient temperature. The experimental results (Table 3.6 and Fig 3.5) showed that the adsorption capacity of TiMe_3 -HMS prepared at 0.2, 0.3 and 0.5 eq. loading levels is actually lower than that of the benzyl grafted materials (1.48, 1.44, and 1.47 wt% respectively). This may be due to the influence of coordinated THF on the Ti center, which blocks coordination sites, creates steric bulk around the Ti center, and increases the weight of the system, while also withdrawing electron density through the coordinated oxygen atom. Scheme 3.1 shows a depiction of the possible H_2 binding geometries of TiMe_3 grafted HMS on the silica surface. Decomposition of this species on the surface to methane and carbenoid species, less able to bind H_2 , may also be occurring. There is also the possibility that the η^3 coordination of the benzyl ligand is required to protect the naked low-coordinate Ti(III) center from decomposition pathways and that this ligand only adopts an η^1 coordination in the presence of excess H_2 , which can occupy the vacated orbital as an L-type ligand. In order to test this hypothesis, tris-allyl Ti grafted HMS was also prepared. The allyl ligand can also adopt η^1 or η^3 configurations and may provide a stabilizing effect, if this is indeed necessary, and is also lighter and less bulky than the benzyl ligand, both factors which should lead to improved hydrogen storage performance.

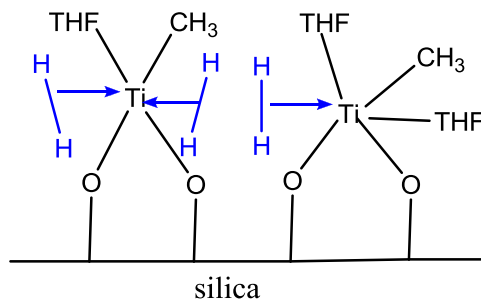
Table 3.6 – Summary of the adsorption capacities of C₁₂-HMS treated with different molar equivalents of TiMe₃.

Sample	App. Density g/cc	Sk. Density g/cc	Grav. Storage Wt.%	Grav. Adsorption Wt.%
0.2TiMe ₃ -C ₁₂ -HMS	0.18	1.55	17.84	1.48
0.3TiMe ₃ -C ₁₂ -HMS	0.18	1.49	17.11	1.44
0.5TiMe ₃ -C ₁₂ -HMS	0.30	1.73	11.04	1.47

Figure 3.5 - Excess hydrogen adsorption (filled symbols) and desorption (unfilled symbols) isotherms at 77 K and 60 atm of HMS treated with 0.2, 0.3, and 0.5 molar equivalents of TiMe₃.



Scheme 3.1- Material prepared by coating HMS surface with trimethyl Ti precursor.



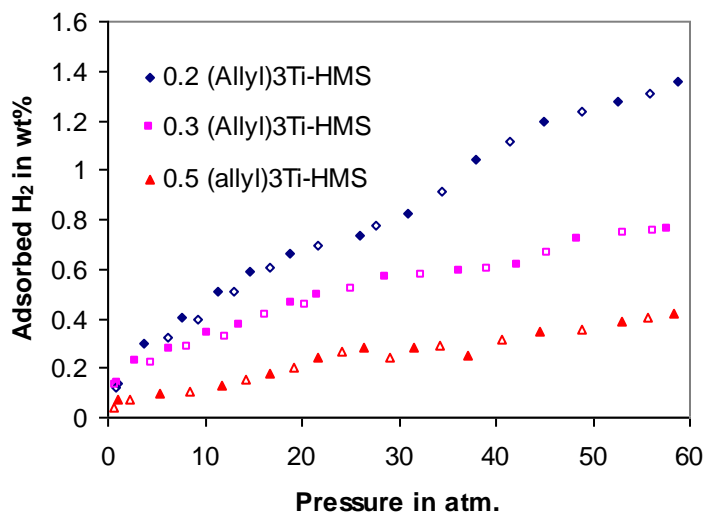
3.3.5 Ti(Allyl)₃ grafted on HMS

Ti(Allyl)₃ grafted HMS silica was prepared at loading levels of 0.2, 0.3, and 0.5 equivalents. The results are summarized in Figure 3.6 and Table 3.7. The hydrogen adsorption results were even lower than those in the trimethyl case (1.40, 0.72, and 0.51 wt% respectively). Also, while the TiMe₃ system showed little variation between the different loading levels in performance, the corresponding allyl system showed a precipitous drop off on increasing the loading to 0.3 from 0.2. This suggests that clustering may be occurring on the silica surface, essentially shutting down a large proportion of the hydrogen binding to the metal center. This demonstrates that the allyl ligand is much less efficient than the benzyl ligand in preventing surface clustering, either because of its lower steric profile, or because it is less able to adopt an η^3 binding mode due to the influence of coordinated THF, the presence of which further diminishes performance for reasons discussed above.

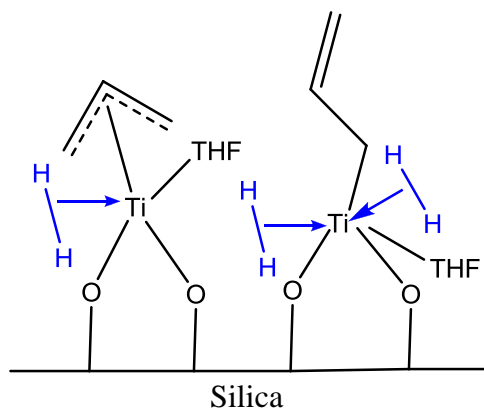
Table 3.7: summarizing the adsorption capacities of C12 HMS treated with different molar ratios of triallyl Ti.

Sample	Apparent Density g/cc	Skeletal Density g/cc	Grav. Storage Wt.%	Grav. Adsorption Wt.%
0.2Ti(Allyl) ₃ -C ₁₂ -HMS	0.33	1.67	9.36	1.40
0.3Ti(Allyl) ₃ -C ₁₂ -HMS	0.28	1.70	10.66	0.72
0.5Ti(Allyl) ₃ -C ₁₂ -HMS	0.35	1.50	5.28	0.51

Figure 3.6 - Excess hydrogen adsorption (filled symbols) and desorption (unfilled symbols) isotherms at 77 K and 60 atm of HMS treated with 0.2, 0.3, and 0.5 molar equivalents of (Allyl)₃Ti .



Scheme 3.2 - Material prepared by grafting the HMS surface with triallyl Ti precursor.

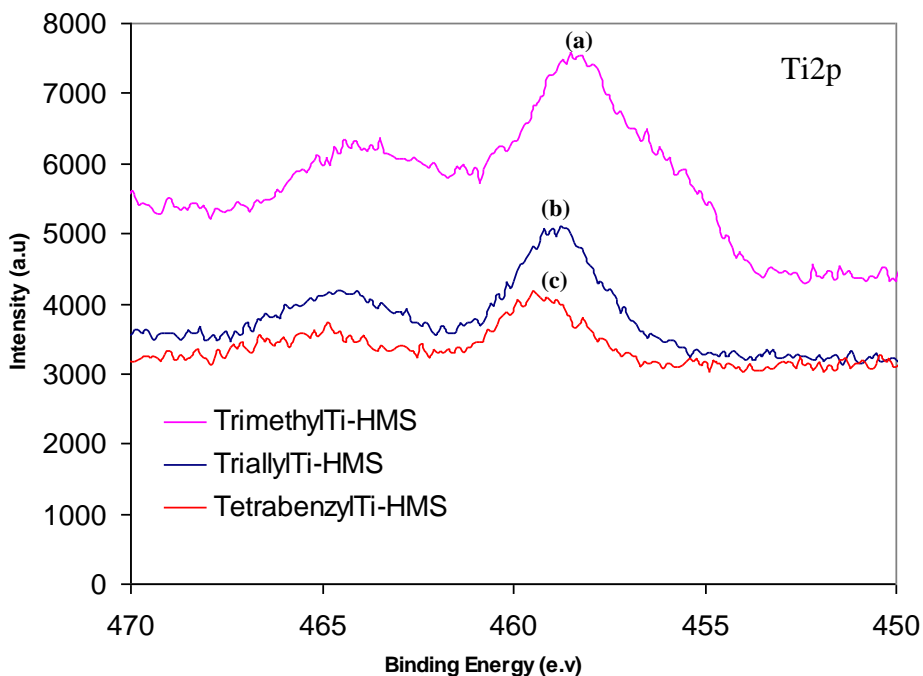


3.3.6 XPS Studies and Enthalpies

To investigate the nature of the surface species in the benzyl, methyl and allyl systems and gain further information on the trends in hydrogen adsorption performance, X-ray photoelectron spectroscopy (XPS) studies were conducted (Fig. 3.8). This is a very powerful method for revealing the electron density about a metal center and should

thus reveal which system is electronically most disposed to π back bonding to hydrogen. The spectra of the surfaces in the Ti 2p region demonstrate a trend in reduced binding energies in the Ti 2p_{3/2} emission as you go from methyl to allyl to benzyl, with binding energies at 458.5 eV, 458.8 eV, and 459.4 eV, respectively. All binding energies (BEs) were referenced to the C 1s hydrocarbon peak at 284.8 eV. In addition, the XPS spectrum of trimethyl Ti-HMS has a shoulder in the binding energy (BE) range of Ti(III) chemical state at 456.2 eV,^[24] suggesting that decomposition to a lower valent Ti species may have occurred.

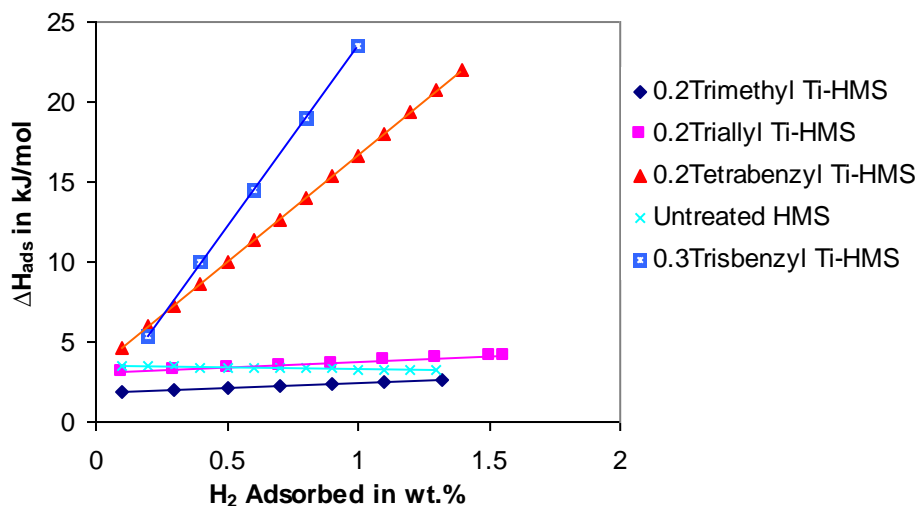
Figure 3.8 - Ti 2p XPS spectra of HMS treated with 0.2 equivalents of (a) trimethyl Ti, (b) triallyl Ti, (c) Tetrabenzyl Ti.



The binding enthalpies (Fig. 3.9) of these materials were calculated by a variant of the Clausius-Clapyron equation^[25] from hydrogen adsorption data at 77 and 87K. In all the cases, ΔH increases as H₂ capacity increases. Steep slopes were obtained for the

cases of tris and tetra benzyl Ti HMS, increasing to 23.53 and 22.15 kJ/mol respectively. But, in the case of the (methyl)₃Ti and (allyl)₃ Ti HMS the binding enthalpies increase more slowly with H₂ adsorption, and reach maxima at only 2.66 and 4.17KJ/mol, respectively. This observation is in keeping with the trend in hydrogen adsorption characteristics, the benzyl systems possessing both the higher enthalpies and the better storage performance. However both the hydrogen adsorption properties and the enthalpies of these materials are surprising in light of the XPS data which suggests that the methyl is the most electron rich, followed by the allyl, and then the benzyl. If π -back bonding were the only contributing factor to improved performance, then the methyl should be the best, followed by the allyl, and then the benzyl. This clearly suggests that many other factors such as the coordination number and geometry as well as the steric environment about the metal fragment are equally important in hydrogen storage performance in this system.

Figure 3.9 - Hydrogen binding enthalpies of pristine HMS (×), 0.2Me₃Ti-HMS (◆), 0.2(Allyl)₃Ti-HMS (■), 0.2Bz₄Ti-HMS (▲), 0.3Bz₃Ti-HMS (*).



3.4 Conclusions

In summary, we have demonstrated that by varying the Si-to-template molar ratio, the carbon chain length of surfactant, the organometallic Ti-fragment precursor on the surface, and the loading level of that precursor, we can arrive at a material with 2.45 wt% hydrogen adsorption at 77 K and 60 atm., which compares to 1.2 wt% for untreated silica under the same conditions, and 1.6 wt% under these conditions for our best benzyl Ti grafted mesoporous silica studied previously. This 2.45 wt% demonstrates that the type of silica used as a support is very crucial to obtaining the highest performance, and corresponds to almost 4 H₂ per Ti, only one less than the theoretical limit of 5 predicted by the 18-electron rule. This is much higher than that observed previously for a poly-hapto Kubas compound and suggests that at lower temperatures and higher pressures certain metal centers can be forced to adopt up to 4 H₂ per metal. Smaller methyl and allyl ligands have no advantage over benzyl, contrary to what was expected on the basis of sterics, weight, and electronic properties. The enthalpies of the benzyl Ti system were in the predicted 20-30 kJ/mol range for room temperature performance, and as expected from the inferior hydrogen adsorption abilities, but the allyl and methyl systems had enthalpies of less than 5 kJ/mol. These data all suggest that it is difficult to predict on sterics and electron donating ability alone what the hydrogen storage capacity of metal grafted fragments on silica should be.

3.5 References

1. Schlapbach, L., Züttel, A., *Nature*, **2001**, 414, 353-358.
2. http://www.hydrogen.energy.gov/annual_review06_plenary.html
3. Yartys, V.A., Harris, I.R., Panasyuk, V.V., *Mater. Sci.*, **2001**, 37, 219
4. Rowsell, J.L.C., Milward, A.R., Park, K.S., Yaghi, O.M., *J. Am. Chem. Soc.*, **2004**, 126, 5666.
5. Dincă, M., Long, J.R., *Angew. Chem. Int. Ed.*, **2008**, 47, 6766-6779.
6. Vitillo, J.G., Regli, L., Chavan, S., Ricchiardi, G., Spoto, G., Dietzel, P.D.C., Bordiga, S., and Zecchina, A., *J. Am. Chem. Soc.*, **2008**, 130, 8386-8396.
7. Dillon, A.C., et al. *Nature*, 1997, 386, 377.
8. Ye, Y., et al. *Appl. Phys. Lett.*, **1999**, 74, 2307.
9. Yildirim, T., Ciraci, S., *Phys. Rev. Lett.*, **2005**, 94, 175501.
10. Bhatia, S.K., Myers, A.L., *Langmuir*, **2006**, 22, 1688.
11. Zhao, Y., Kim, Y., Dillon, A.C., Heben, M.J., Zhang, S.B., *Phys. Rev. Lett.*, **2005**, 94, 155504.
12. Kubas, G.J., Ryan, R.R., Swanson, B.I., Vergamini, P.I., Wasserman, H.J., *J. Am. Chem. Soc.*, **1984**, 108, 7000.
13. Kubas, G.J., *Chem. Rev.*, **2007**, 107, (10), 4152-4205.
14. Kaye, S.S., Long, J.R., *J. Am. Chem. Soc.*, **2005**, 127, 6506.
15. Hamaed, A., Trudeau, M., Antonelli, D.M., *J. Am. Chem. Soc.*, **2008**, 130 (22), 6992-6999.
16. Tanev, P.T., Pinnavaia, T.J., *Science*, **1995**, 267, 865.
17. Shafer, W., Thiele, K. H., *Z. Anorg. Allg. Chem.*, **1978**, 447, 136.
18. Yakovleva, O.N., Sharev, O.K., Miesserov, K.G., Vydrina, T.K., Bondarenko,

- G.N., Tinyakova, E.I., Dolgoplosk, B.A., *Dokl. Akad.Nauk SSSR*, **1974**, 218, 593.
19. Beilin, S.I., Markevich, I.N., Gol'shtein, S.B., Bondarenko, G.N., and Dolgoplosk, B.A., *Dokl. Akad.Nauk SSSR*, **1974**, 218, 837.
 20. Hu, X., Trudeau, M., Antonelli, D.M., *Chem. Mater.*, **2007**, 19, 1388.
 21. Hu, X., Skadtchenko, B., Trudeau, M., Antonelli, D.M., *J. Am. Chem. Soc.*, **2006**, 128, 11740.
 22. Zhuravlev, L.T., *Colloids and Surfaces A: Physicochem. Eng. Aspects*, **2000**, 173, 1-38.
 23. Mathias, J., Wannemacher, G., *J. Coll. Interf. Sci.*, **1988**, 125, 61.
 24. Nesterov, G.A., Zakharov, V.A., Paukshtis, E.A., Yurchenko, E.N., and Ermakov, Y.I., *Kinetika I Kataliz*, **1979**, 20, 429-436.
 25. Langerame, F., Salvi, A.M., Silletti, M., Moretti, G., *Surf. Interface Anal.*, **2008**, 40, 695-699.

Chapter 4 – Functionalized Porous Silicas with Unsaturated Early Transition Metal Moieties as Hydrogen Storage Materials: Comparison of Metal and Oxidation State

4.1 Introduction

To meet the environmental and economic demands caused by the rapid depletion of fossil fuels, intensive research into alternative energy has become an increasing priority for industrialized nations. Hydrogen, as energy carrier, represents an ideal alternative to petroleum-based fuels because it is the most abundant element in the universe, exhibits the highest energy density of all chemical substances, and poses no threat to the environment because water is the only byproduct of its combustion.^[1] However, to implement its use as an energy carrier of the future, a storage medium that meets or surpasses all the targets set by the U.S. Department of Energy (DOE) is needed^[2] (5.5 wt% and 40 kg/m³ for the year 2015). A hydrogen storage medium capable of combining high volumetric and gravimetric densities with optimal kinetics is crucial for effective storage of hydrogen under ambient conditions for both stationary and mobile applications. While compressed and liquid hydrogen storage technologies meet some of the DOE requirements, these methods are not practical for automobile applications due to safety concerns and the energy loss during the compression and liquefaction processes. Many metal hydrides and complex hydrides surpass various DOE targets for gravimetric and volumetric densities but possess unfavorable thermodynamics and fall short of meeting the optimal kinetics or thermodynamics for adsorption and release under ambient conditions.^[3-5] Metal-organic frameworks,^[6-9]

carbon nanotubes,^[10-13] activated carbons, and zeolites^[14-15] have also been tested for hydrogen storage based on physisorption, but these materials are only effective under cryogenic conditions because of the low binding enthalpies, which fall short of the 20-30 kJ/mol predicted to be the optimal H₂ binding energy for reversible adsorption at room temperature.^[16, 17] In 2008,^[18] we reported a new model system based on benzyl titanium (III) grafted to hexagonally-packed mesoporous silicas (HMS). The purpose of this system was to explore the feasibility of using unusually low-coordinate low-valent transition metal fragments, that are too reactive to exist in molecular form and thus must be stabilized on a surface, as H₂ binding sites functioning within the ideal enthalpy range for room temperature storage. The results of this study revealed that HMS silica doped with 0.2 molar equivalents of benzyl titanium (III) absorbs up to 2.7 H₂ per Ti center in what appears to be a Kubas-type binding fashion.^[19,20] In 2009,^[21] we optimized the performance of the Ti(III) system by tuning the surface area, pore size, ligand environment around the metal, and synthetic protocol to arrive at materials which adsorb up to 3.98 H₂ per Ti center at 77K and 60 atm, demonstrating that unsaturated metals can absorb far more H₂ per metal at elevated pressure than the maximum of two that has been observed for a molecular system.^[20] While the small amounts absorbed at ambient temperature and pressure have precluded routine spectroscopic investigations, these systems operate through a mixture of physisorption on the silica surface and what is most likely the Kubas interaction, a type of weak hydrogen chemisorption that depends largely on the amount of back donation from filled metal d-orbitals into the H-H antibonding orbital. Herein, we report a systematic study on HMS treated with titanium, vanadium, and chromium transition metal fragments, in order to investigate

the effect of metal type and metal oxidation state on the H₂ binding to the metal center. Since it is not possible to keep the coordination sphere consistent for all metals and all oxidation states due to the varied availabilities and stabilities of low-valent early transition metal alkyl and aryl precursors, this study assumed that the effect of the oxidation state of the metal and type of metal was more pronounced than the different steric and electronic effects of the various alkyl ligands used because hydrogen has a low steric profile and the metal fragments studied featured only hydrocarbon ligands with C in the α -coordination sphere. The effect of hydrogenation on the binding abilities of these metal fragments was also investigated because metal hydrides generally form stronger Kubas interactions than the corresponding alkyl. While these systems are only models for investigating hydrogen binding to low-valent low-coordinate metal fragments, they demonstrate that such fragments avoid some of the kinetic and thermodynamic drawbacks of metal hydrides, MOFs and other reactive methods of storing hydrogen and show promise in the downstream development of materials based exclusively on weak chemisorption to low-valent low-coordinate transition metal centers with negligible contributions from physisorption.

4.2 Experimental

All chemicals, unless otherwise stated, were obtained from Aldrich. H₂, N₂ and Ar gases were obtained from Praxair Canada Inc.

4.2.1 Synthesis of Hexagonally-packed Mesoporous Silica (HMS):^[22] in a typical preparation, tetraethyl orthosilicate (1.0 mol) was added with vigorous stirring to a solution of dodecylamine (DDA) (0.27 mol) (in 4:1 molar ratio of tetraethyl

orthosilicate to DDA) in ethanol (9.09 mol). The reaction mixture was aged at ambient temperature for 18 hours, and the resulting mesoporous silica was air dried on a glass plate. The template was removed by mixing 1 g of the air-dried HMS with 150 ml of hot ethanol for 1 hour. The product was then filtered and washed with a second 100 ml portion of ethanol. This extraction procedure was repeated twice. Finally the HMS was washed with 150 ml of hot toluene in order to remove the final trace of surfactant, and was dried in air at 115 °C.

4.2.2 Synthesis of doped HMS materials: 5-10 mol% of the transition metal precursor (see below) with respect to Si was dissolved in toluene under Ar and the HMS silica added in small portions. After 5 h stirring the solution became colorless and the silica was collected by filtration and dried *in vacuo*. In the case of bis(naphthalene) titanium the reaction was conducted in THF at -78 °C, followed by slow warming to room temperature over 5 h. At this stage the solution became clear and the reaction was judged complete. In the case of tetrabenzyl titanium, the Ti-doped HMS silica was heated *in vacuo* at 120 °C for 2 hours in order to obtain the active Ti (III) material.

4.2.3 Preparation of bis(naphthalene) titanium: ^[23]

Bis(naphthalene) titanium complex was prepared *in situ* by the reduction of $\text{TiCl}_4 \cdot 2\text{THF}$, THF = tetrahydrofuran, with 6 equivalents of $\text{LiC}_{10}\text{H}_8$ at -78 °C in THF, under argon. After 4 hours stirring -78 °C, the reaction mixture was filtered and the bis(naphthalene) titanium solution was obtained and used immediately to prevent thermal decomposition.

4.2.4 Preparation of tris(mesityl) vanadium: ^[24]

50 ml of (mesityl)MgBr (1M) was added dropwise to a solution of 6.22g of $\text{VCl}_3 \cdot 3\text{THF}$ in THF. The solution was stirred at room temperature for 2 hrs. Then, 22 ml of dioxane

was added and the reaction was stirred for another 2 hours. The suspension was then filtered through Celite to remove the magnesium salt. The filtrate was then collected and concentrated under vacuum. 20 ml of diethyl ether was then added and the solid precipitate was filtered and washed with diethylether:THF (3:1) and dried under vacuum.

4.2.5 Hydrogenation of metal-fragment grafted HMS materials:

The hydrogenation of all metal-fragment grafted HMS materials was conducted by treating the sample loaded onto the pressure-composition isotherm (PCI) instrument with pure hydrogen for 2 hours at 85 atmospheres and 170 °C. The samples were then removed under Ar and the densities re-measured.

4.2.6 Preparation of tris [bis(trimethylsilyl)methyl] chromium (III):^[25]

Bis(trimethylsilyl)methyl-lithium (4.5 mmol) in diethyl ether (12 cm³) was added dropwise to a suspension of chromium (III) chloride (0.235g, 1.5 mmol) in diethyl ether (40 cm³) at -78 °C. The color of the solution changed from brown to green as the mixture was allowed to warm slowly to room temperature. After stirring for 2 hours, volatiles were removed *in vacuo*, and the residue was extracted with n-hexane (60 cm³) and filtered to give a deep green solution. This was concentrated (to ca. 20 cm³) and cooled to -20 °C giving bright green crystals.

4.2.7 Preparation of bis[(trimethylsilyl) methyl]chromium(II) or Cr₄(CH₂Si(CH₃)₃)₈:^[26]

To a stirred suspension of CrCl₃(THF)₃ (4.8 mmol) in hexane, was added a solution of (CH₃)₃ Si CH₂Li (18.1 mmol) also in hexane. The color of the slurry immediately changed to dark purple. The mixture was then stirred at RT for 3 h, and then filtered, and the residue was washed with three portions of hexane (10ml each). The solution was

concentrated to 50 ml and allowed to stand at -34 °C for 12 h. The color of the solution slowly turned dark brown upon standing at that temperature. The product was isolated by cold filtration, washed twice with pre-cooled hexane and dried *in vacuo*.

4.2.8 Calculation of the number of hydrogen molecules per transition metal center:

As an example, HMS silica treated with tris [bis(trimethylsilyl)methyl] chromium adsorbs 1.81 wt% H₂ as compared to 1.35 wt% for untreated HMS silica. On the basis of 6.57 wt % Cr, determined by ICP-AAS in the metal grafted material, the difference between the H₂ adsorption capacity of the untreated silica and the grafted material translates into 1.82 H₂ per Cr center.

4.2.9 Measurements. Nitrogen adsorption and desorption data were collected on a Micromeritics ASAP 2010. Hydrogen uptake was measured with a commercial pressure-composition isotherm (PCI) unit provided by Advanced Materials. Highly purified hydrogen (99.9995% purity) was used as the adsorbent. Before all measurements, the materials were activated *in vacuo* at 573K in order to remove any physisorbed water or volatile impurities. Leak testing, performed by running a standard AX-21 sample and by bubbles, was done prior to and during each adsorption measurement experiment. In the H₂ adsorption-desorption experiments complete reversibility was observed for all samples across the whole range of pressures, with small hysteresis observed at low pressures for some materials. Samples were run at liquid nitrogen temperature (77K) and liquid argon temperature (87K) to 65 atm.

The skeletal density was measured using a Quantachrome Ultra-pycnometer. When the skeletal density is used for the hydrogen uptake measurement, the compressed hydrogen within the pores is treated as part of the sample chamber volume. Therefore only the

hydrogen physisorbed to the walls of the structure is recorded by the PCI instrument as the adsorption capacity of the material. Thus, when H₂ adsorption is measured, the skeletal density of the porous materials derived from the pycnometer is employed to determine the adsorbed amount of hydrogen.

Taking both the 77K and 87K hydrogen adsorption data, enthalpies of adsorption were calculated using a variant of the Clausius-Clapeyron equation:^[27]

$$\ln\left(\frac{P_1}{P_2}\right) = \Delta H_{ads} \frac{T_2 - T_1}{RT_1 T_2} \quad (1)$$

Where P_n = pressure for isotherm n, T_n = temperature for the isotherm n, and R = gas constant.

Pressure as a function of the amount adsorbed was determined by using an exponential fit for each isotherm; the first 10 points of the isotherms were picked up and fit to the exponential equation. This exponential equation gives an accurate fit over the pressure up to 10 atm with the goodness of fit (R²) above 0.99. The corresponding P₁ and P₂ values at a certain amount of H₂ adsorbed at both temperatures can be obtained by the simulated exponential equation. Inputting these numbers into the eq 1, we then calculate the enthalpies of the adsorption.

4.3 Results and Discussion

Pristine HMS silica was prepared by the neutral templating method of Pinnavaia and co-workers,^[22] using a dodecylamine template and characterized by XRD, elemental analysis, and nitrogen adsorption. Tetrabenzyl titanium, bis(naphthalene) titanium, tris(mesityl) vanadium, tris[bis(trimethylsilyl)methyl] chromium, and bis(trimethylsilylmethyl) chromium were synthesized and grafted onto the surface by prolonged stirring at the previously confirmed optimal molar ratio of 0.2 (TM/Si) mol.^[18]

The anchoring of the transition metal fragments was achieved by the replacement of M-R groups with M-O linkages through a protonolysis reaction involving the hydroxy species on the silica surface. This creates accessible low-valent low-coordinate alkyl-alkoxide fragments on the silica surface, which can function as H₂ binding sites. All routine characterization and hydrogen storage data for these materials are summarized in Table 4.1 and Table 4.2.

In previous work we investigated the hydrogen storage capacity of Ti(III) benzyl fragments on a silica surface and found that this moiety could absorb 3.98 H₂ per Ti at 77 K and 60 bar at a binding enthalpy that rises with surface coverage to 22 kJ/mol.^[21] In the current study we repeated the synthesis of this material using the same sample of HMS silica as a support material in order to maintain consistency for the sake of comparison to the other materials. Thus, HMS grafted with tetrabenzyl Ti and then thermally activated to convert the Ti(IV) into Ti(III), retained its XRD pattern while the BET surface area dropped from 1284 m²/g to 1120 m²/g. This sample reversibly adsorbs 3.05 wt% hydrogen at 77K and 85 atm (**Fig. 4.1**), which equates to 4.85 H₂ per Ti center, based on 8.39 wt% Ti as determined by ICP-AAS (Table 2), with a binding energy in the optimal range for room temperature hydrogen storage (**Fig. 4.2**) that rises from 15-20 kJ/mol. This increasing trend has been commented on previously by our group and corroborates previous calculations which predicted such a trend for the subsequent addition of Kubas-type H₂ ligands to an unsaturated metal center.^[12,16] So, while physisorption is present in all metal-grafted samples in this study, the Kubas contribution is strong enough to influence the slope and magnitude of the isosteric enthalpy plots. At 298 K and 85 atm this material reversibly absorbs 0.82 wt%, which

equates to 1.30 H₂ per Ti center, or 27% of that adsorbed at 77 K, on the basis of the room temperature adsorption of pristine HMS of 0.44 wt%. The slightly higher value of adsorption at 77 K for this material sample relative to that originally quoted by our group^[18] of 1.65 wt% at 65 atm can be attributed to improved synthesis and handling techniques, as the Ti(III) centers are unstable to decomposition once they have been generated.

The elemental analysis revealed that the Ti:C molar ratio was 1:7.94 (**Table 4.2**), which equates to an average of 1.13 benzyl ligands per Ti center. This indicates a mixture of bis(benzyl) siloxy and bis(siloxy) benzyl species in a ratio favoring the latter. The XPS spectrum of the tetrabenzyl Ti-HMS sample after thermal activation to generate Ti (III) (**Fig. 4.3**) reveals 3 pairs of peaks in the 2p 3/2,1/2 region. The emissions at 460.1 eV and 466.4 eV can be attributed to Ti(IV), by direct comparison with the emissions of other Ti(IV) species.^[28,29] A second pair of peaks at 459.1 eV and 464.7 eV correspond to the 2p 3/2,1/2 emission of a Ti(III) species by comparison with the XPS of Ti₂O₃.^[30] The third emission at, 457.7 eV and 462.9 eV can be attributed to Ti (II) by direct comparison with the emissions of TiO.^[31] The presence of almost equal proportions of Ti(IV) and Ti(II) in this material can be attributed to the well-documented disproportionation of Ti(III) alkyls into Ti(II) and Ti(IV).^[32] This is consistent with observations in our group that this material decomposes on standing at room temperature under Ar over several weeks. In previous work we found that hydrogenation of the activated benzyl Ti HMS at 170 °C and 85 atm led to a slight decrease in the storage performance.^[21] This was attributed to the thermal decomposition of the Ti benzyl fragments which are unstable to disproportionation.

Table 4.1 - Summary of the skeletal densities, gravimetric adsorptions, surface areas, and number of H₂ per transition metal of all samples tested.

Sample	Sk. Density g/cc	Grav. Adsorption (8.6 MPa = 85 atm) Wt%	Surface Area in m ² /g	Number of H ₂ /TM
C12-HMS	2.13	1.35	1284	0
tetrabenzyl Ti-HMS (77K)	1.65	3.05	1120	4.85
tetrabenzyl Ti-HMS (298 K)	1.65	0.82	1120	1.30
bis(naphthalene) Ti-HMS(77K)	1.02	2.99	989	4.74
bis(naphthalene) Ti-HMS (298 K)	1.02	0.78	989	1.24
tris(mesityl)V(77k)	1.24	2.33	1258	2.68
tris(mesityl)V(298 K)	1.24	0.32	1258	0.37
H ₂ -tris(mesityl)V (77 K)	1.22	2.43	1218	2.74
H ₂ -tris(mesityl) V (298 K)	1.20	0.45	1218	0.51
tris[bis(trimethylsilyl)methyl] Cr HMS (77K)	1.88	1.81	946	1.82
tris[bis(trimethylsilyl)methyl] CrHMS(298 K)	1.88	0.22	946	0.22
H ₂ -tris[bis(trimethylsilyl)methyl] Cr-HMS (77K)	1.86	2.17	915	3.2
H ₂ -tris[bis(trimethylsilyl)methyl] Cr-HMS (298)	1.86	0.35	915	0.52
bis[(trimethylsilyl)methyl]Cr-HMS (77K)	1.87	2.12	1294	2.20
bis[(trimethylsilyl)methyl]Cr HMS (298 K)	1.87	0.36	1294	0.37
H ₂ -bis[(trimethylsilyl)methyl]Cr-HMS (77 K)	1.85	2.26	1018	3.5
H ₂ -bis[(trimethylsilyl)methyl]Cr HMS (298 K)	1.85	0.55	1018	0.85

Table 4.2 - Elemental analysis of C, H, Si, and TM for HMS silica treated with various TM precursors.

Sample	TM (%)	Carbon (%)	Hydrogen (%)	Silicon (%)	TM:C Molar ratio
Plain Silica	0	0.24	1.83	37.70	NA
tetrabenzyl Ti-HMS	8.39	16.96	2.97	31.5	1:7.94
bis (naphthalene) Ti-HMS	8.28	0.29	2.33	31.40	NA
tris(mesityl) V-HMS	9.31	21.17	2.09	29.00	1:9.54
hydrogenated tris(mesityl) V-HMS	10.04	20.42	2.00	28.70	1:8.52
tris[bis(trimethylsilyl)methyl]Cr-HMS	6.57	11.01	2.72	28.00	1:7.10
Hydrogenated tris[bis(trimethylsilyl)methyl]Cr-HMS	6.66	10.39	2.67	26.57	1:6.56
bis[(trimethylsilyl)methyl]Cr-HMS	6.43	4.30	2.24	31.80	1:2.60
Hydrogenated bis[(trimethylsilyl)methyl]Cr-HMS	6.75	1.54	2.93	27.20	1:0.83

Bis(naphthalene) titanium was used as a Ti precursor to represent oxidation states lower than Ti (III) because no monohapto Ti alkyls are known for Ti oxidation states lower than (III). This reagent possesses π -bonded arene rings and decomposes at -60 °C to form Ti metal and is thus considered a Ti(0) donor. Because of this, it can therefore form either Ti clusters on the surface of the HMS silica or Ti(II) species by insertion of Ti into O-H bonds as shown in **Scheme 4.1**. In this regard it can be considered a direct analogue of bis (toluene) titanium, which has been used previously by our group to deposit an amorphous low-valent Ti phase on the inner surface of mesoporous Ti oxide, dramatically increasing the hydrogen storage capacity of the material.^[33]

Figure 4.1 - Adsorption isotherms at 77K of plain HMS silica and HMS silica treated with bis (naphthalene) titanium and tetrabenzyl titanium. Desorption isotherms omitted for clarity.

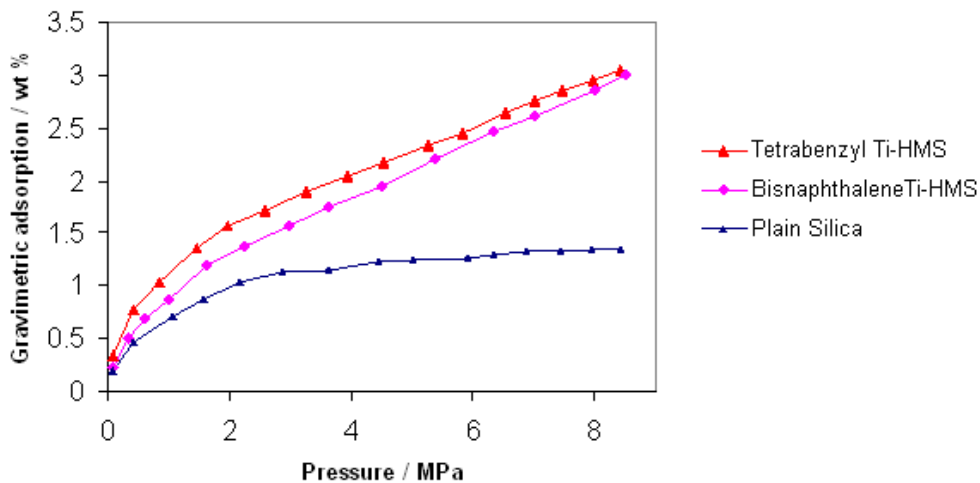


Figure 4.2 - Hydrogen binding enthalpies of HMS silica compared to those of HMS silica grafted with bis (naphthalene) titanium and with tetrabenzyl titanium.

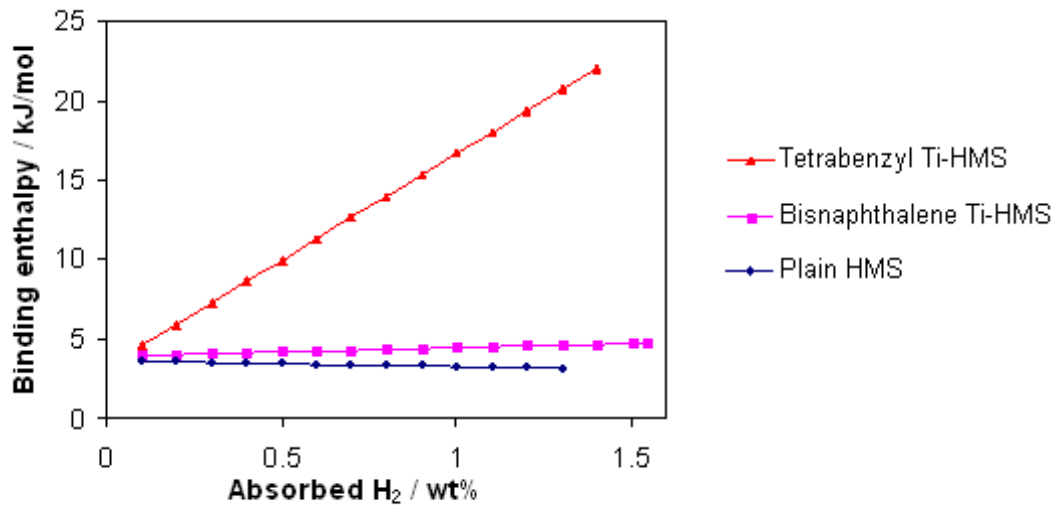


Figure 4.3 - XPS spectrum with simulations for HMS silica treated with tetra benzyl titanium showing the Ti 2p_{1/2,3/2} emissions.

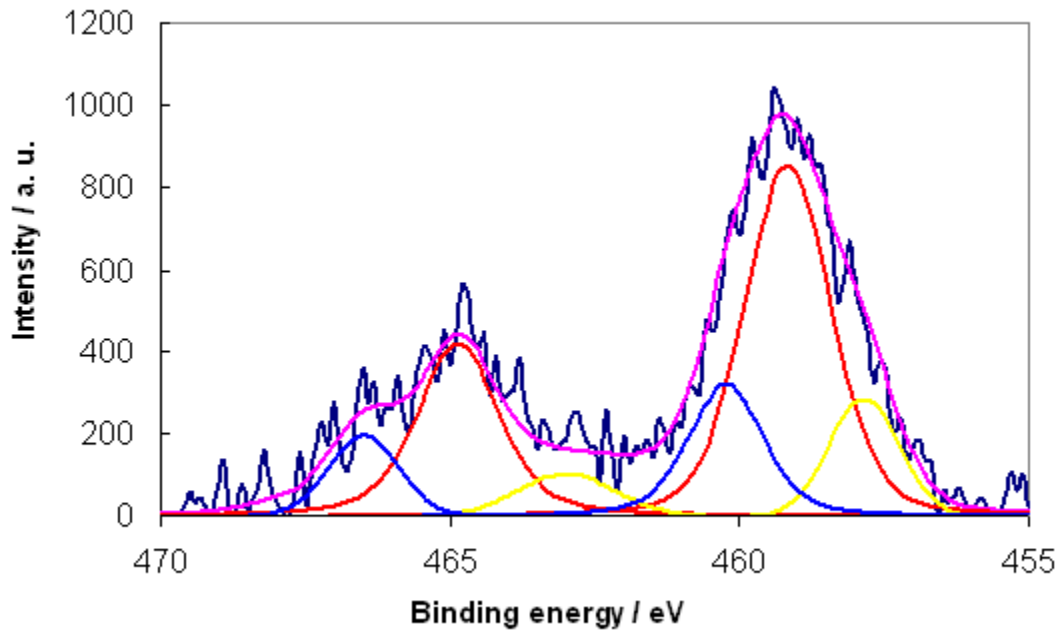
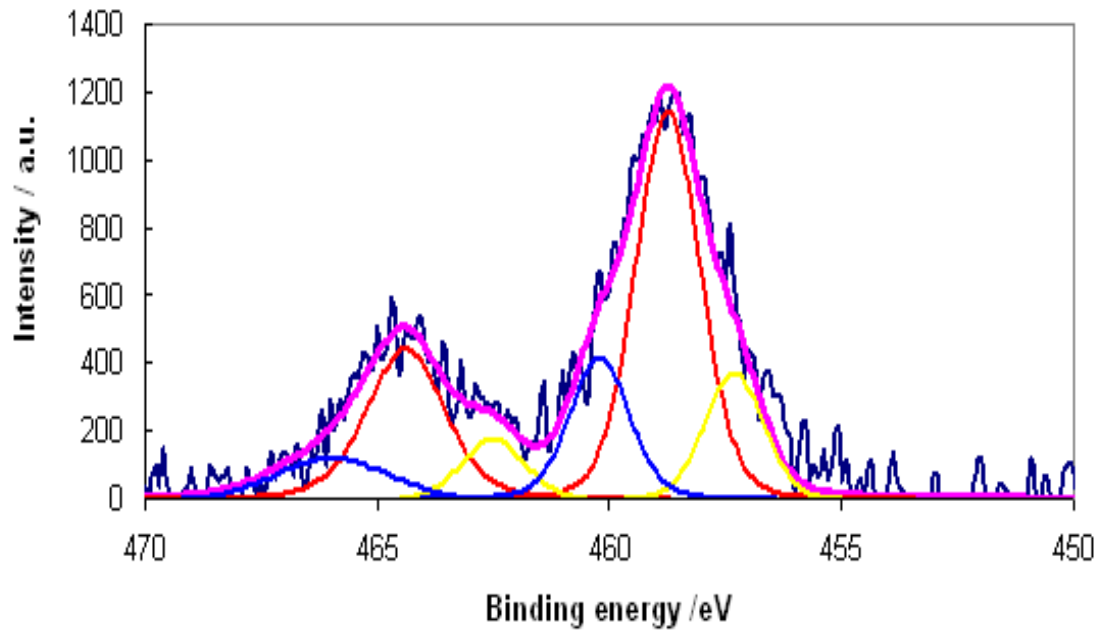
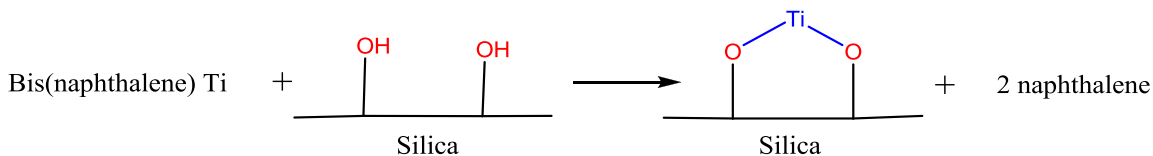


Figure 4.4 - XPS spectrum with simulations for HMS silica treated with bis(naphthalene) titanium showing the Ti 2p_{1/2,3/2} emissions.



Scheme 4.1 - Schematic representation of the grafting of Ti onto the surface of HMS silica by treatment with bis(naphthalene)Ti, and the formation of Ti (II) species on surface, favorable for H₂ binding. Ti clusters may also be formed.



After treatment of HMS with bis (naphthalene) titanium the XRD pattern of the material is retained and the surface area drops from 1284 m²/g to 989 m²/g. The elemental analysis shows a %C of 0.29 as compared to 0.24 % in the starting HMS silica, indicating complete loss of the naphthalene ligands in the doping process. The excess storage isotherms of this material are shown in **Fig. 4.1** and show 2.99 wt.% H₂ reversible adsorption at 77K and 85 atm, as compared to 1.35 wt% in the pristine HMS. This equates to 4.74 H₂ molecules per Ti center (**Table 4.1**), on the basis of 8.28% Ti (**Table 4.2**) as determined by ICP-AAS. At 298 K the system reversibly adsorbs 0.78 wt% H₂ at 298K compared to 0.44 wt% for the pristine silica, or 26% of that adsorbed at 77K, which equates to 1.24 H₂ molecules per Ti center. The binding enthalpy of these materials increases with the H₂ loading level from 4 to 4.9 kJ/mol as shown in **Fig. 4.2**. This binding enthalpy is slightly higher than that of the pristine silica (around 3 kJ/mol),^[18] but falls dramatically short of that required for room temperature hydrogen storage and is much lower than that recorded for many of the other materials in this study. The XPS spectrum with accompanying simulations is displayed in **Fig. 4.4** and shows three pairs of peaks in the Ti 2p region, each corresponding to 2p_{1/2} and 2p_{3/2}

emissions of the metal species. The emissions at 460.1 eV and 465.9 eV are attributed to the $2p_{3/2}$ and $2p_{1/2}$ of a Ti (IV) species^[28,29] which likely formed after a reaction of the original Ti (0) species with two surface hydroxy groups through an oxidative addition process. The high intensity emission at 458.7 eV and 464.2 eV can be attributed to a Ti (III) species, by direct comparison with the XPS spectrum of Ti_2O_3 .^[30] The third emission at 457.2 eV and 462.3 eV and can be attributed to a Ti (II) species by direct comparison with that of TiO .^[31] This material therefore consists of a mixture of Ti(II), Ti(III) and Ti(IV), with the Ti(III) species constituting the major proportion of the sample. Since Ti(IV) is a d^0 species it is inactive in Kubas binding and thus the large increase in hydrogen adsorption stems from the Ti(III) and Ti(II) species only. This indicates an even larger number than 4.74 H_2 per Ti when only the active Ti(III) and Ti(II) species are considered and suggests that many of the Ti centers exist in a coordination number of 3-4 if the 18 electron rule is strictly adhered to. This may be expected on the basis of the complete loss of the naphthalene on reaction with the surface, leaving behind coordinatively unsaturated Ti species on the surface. In light of these XPS studies, the low enthalpy of adsorption is still surprising based on other studies in our group (up to 23 kJ/mol for benzyl Ti(III))^[18] and the preponderance of Ti centers in low oxidation states. However mesoporous Ti oxide treated with bis(toluene) titanium is predominantly Ti(II) and possesses enthalpies that only rise from 4-8 kJ/mol, despite achieving volumetric performance of 41 kg/m^3 at 77 K and 65 atm.^[33] These results together indicate that at 77 K low enthalpy sites are still capable of binding multiple H_2 ligands per metal at higher pressures, however the room temperature

performance of such a system may still be compromised by the weaker binding interactions.

In order to explore the effect on hydrogen binding of moving from Ti(III) to V(III) we explored the hydrogen storage behavior of V(III)-doped HMS. Thus, when HMS is treated with 0.2 mol equivalents of tris(mesityl) vanadium (**Scheme 4.2**), the XRD pattern is retained and the surface area drops from 1284 m²/g to 1258 m²/g.

Scheme 4.2 - HMS silica treated with tris(mesityl) vanadium.

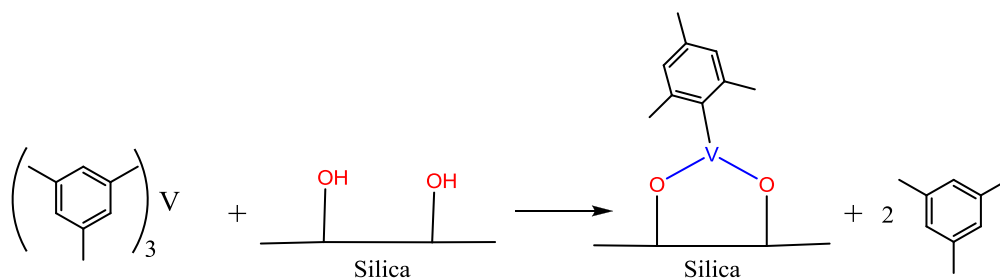


Figure 4.5 - Adsorption isotherms at 77 K of HMS silica treated with tris(mesityl) vanadium before and after hydrogenation compared to that of plain HMS silica. Desorption isotherms omitted for clarity.

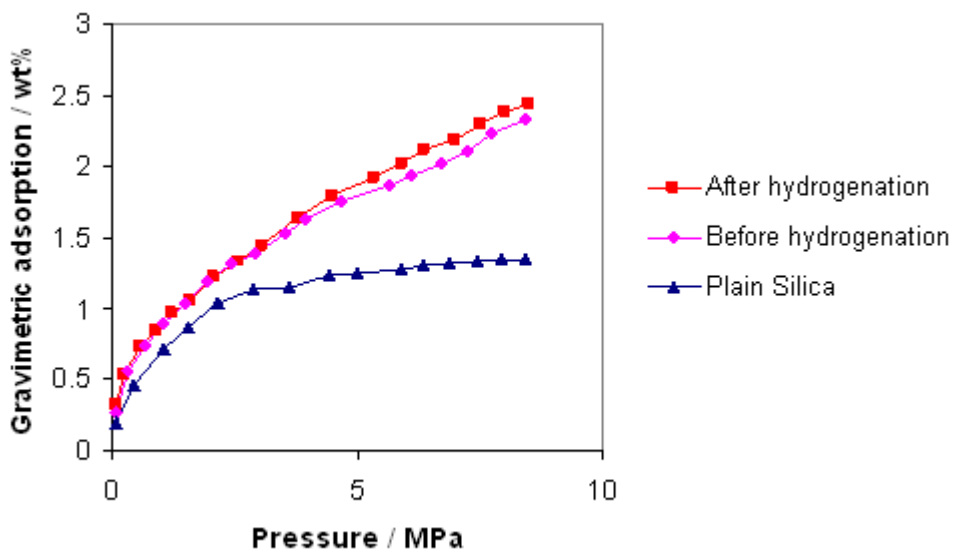


Figure 4.6 - Hydrogen binding enthalpies of HMS silica treated with tris(mesityl) vanadium before and after hydrogenation compared to that of HMS silica.

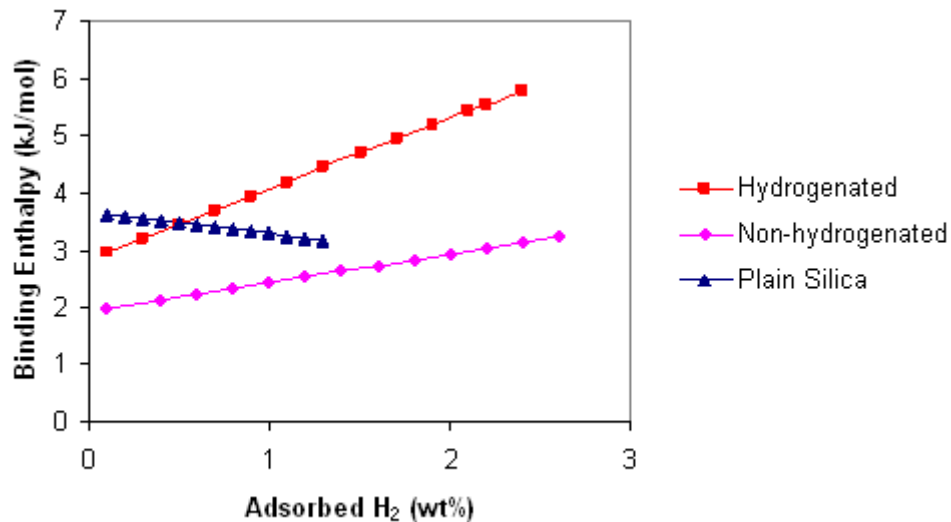


Figure 4.7- XPS spectrum with simulations for HMS silica treated with tris(mesityl) vanadium before hydrogenation showing the V 2p_{1/2,3/2} emissions.

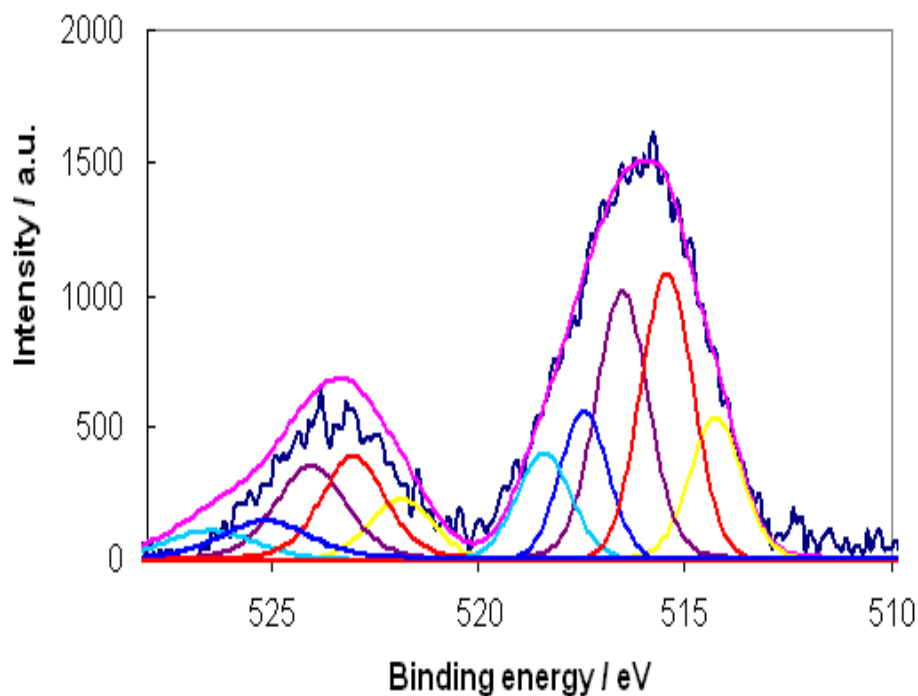
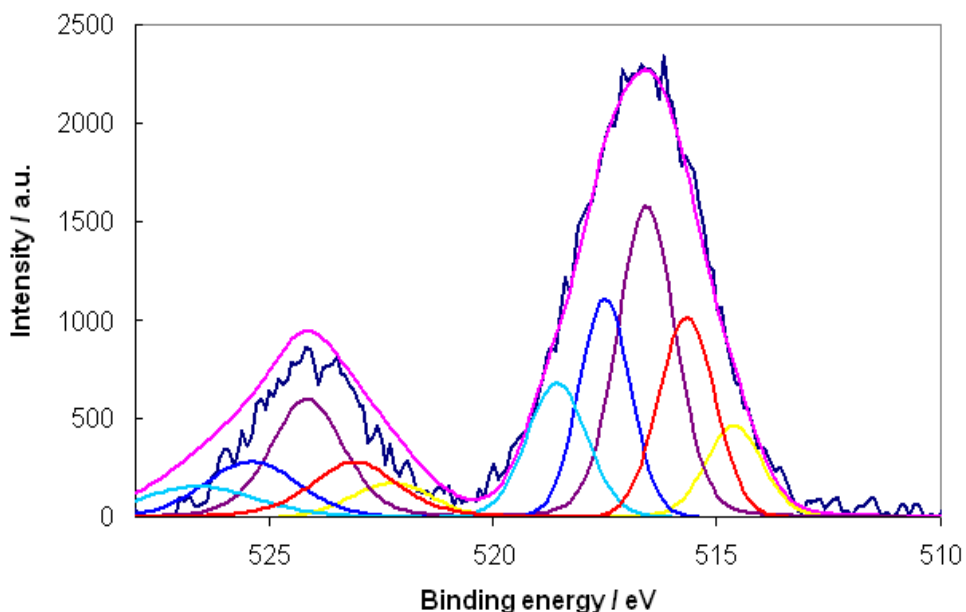


Figure 4.8 - XPS spectrum with simulations for HMS silica treated with tris(mesityl) vanadium after hydrogenation showing the V 2p_{1/2,3/2} emissions.



The hydrogen adsorption capacity of this material reaches 2.33 wt% at 77k and 85 atm, which equates to 2.68 H₂ per vanadium center on the basis of 9.31 % V determined by ICP-AAS (Table 4.1). After hydrogenation at 170 °C and 85 atm for 2 hours in an attempt to convert the vanadium mesityl moieties into V-H units predicted to be more effective at Kubas binding,^[34] the material reversibly absorbs up to 2.43 wt% hydrogen (**Fig. 4.5**) at 77 K and 85 atm, equivalent to 2.74 H₂ per vanadium center, slightly higher than the non-hydrogenated sample. As a result of hydrogenation the %C decreases from 21.17% to only 20.42%, indicating that very little hydrogenolysis has occurred, likely due to the kinetic barrier associated with hydrogenating the secondary M-C mesityl bond. This reduction in carbon composition led to an increase from 9.31% V for the non-hydrogenated sample to 10.04% V in the hydrogenated sample. This small change may be responsible for a portion of the improvement in hydrogen

adsorption of the hydrogenated sample. The V:C molar ratio for the non-hydrogenated sample was 1: 9.56 corresponding to an average of 1.06 ligands per V center and a mixture of bis(mesityl) siloxy and bis(siloxy) mesityl species on the surface. For the hydrogenated sample the V:C molar ratio was 1: 8.52, which equates to 0.95 ligands per V center, consistent with a small loss of mesitylene through σ -bond metathesis on hydrogenation. The room temperature isotherms (**Table 4.1**) demonstrated 13.8% and 18.6% retention of adsorption at 85 atm relative to the isotherms at 77 K temperature for the non-hydrogenated and the hydrogenated samples, respectively. This is lower than the 27% observed for the terabenzyl titanium system and may be due to the lower binding enthalpies for the non-hydrogenated and hydrogenated materials, which rise to 3 kJ/mol and 6 kJ/mol, respectively, as shown in **Fig. 4.6**. While this lower enthalpy may be the cause of the lower relative performance at room temperature, it is also clear that similar low enthalpies did not affect the performance of the bis(naphthalene) titanium system, suggesting that the unligated Ti centers or clusters in the bis(naphthalene) case cannot be compared directly to the ligated transition metal fragments in this study in their interaction with H₂. Also, while only a small proportion of the V centers were hydrogenated, this still led to an observable increase in the binding enthalpy recorded for this material, suggesting that replacement of alkyl with hydride increases the binding enthalpy of H₂, as would be predicted from research in organometallic chemistry.^[20]

In order to gain further insight into the V species present, XPS studies were conducted on both the non-hydrogenated (**Fig. 4.7**) and the hydrogenated trimesityl V-HMS (**Fig. 4.8**). Both spectra show 5 pairs of peaks, each corresponding to emissions in the V 2p 1/2 and 2p 3/2 region. For the non-hydrogenated HMS treated with tris(mesityl)

vanadium, the first emission falls at 514.2 eV and 521.8 eV. This can be attributed to a V^{+1} species by direct comparison with the XPS spectrum of $[VCl(C_5H_5)_2]$.^[35] The emission at 515.4 eV and 523 eV is attributed to a V^{+2} species by comparison with the XPS spectrum of the V-doped mesoporous titania analogue with an emission at 515.6 eV and 523.2 eV.^[36] The emission at 516.5 eV and 524 eV is attributed to a V^{3+} species by comparison with that of V_2O_3 at 515.8 eV and 523.4 eV,^[37] and the emission at 517.4 eV and 524.9 eV is attributed to a V^{+4} species by comparison with the XPS spectrum of VO_2 at 517.4 eV and 524.5 eV.^[29] The emission at 518.4 eV and 526.4 eV can be attributed to a V^{+5} species by comparison with the XPS spectrum of V_2O_5 supported on silica, which has an emission at 518.7 eV and 526.5 eV.^[38] The number of species present in the XPS spectrum in a wide range of oxidation states (most likely due to disproportionation) suggests, along with the elemental analysis data, that the surface species are far from homogeneous and that even after the physisorption is subtracted out, the hydrogen adsorption likely involves several V species in various ligand environments and oxidation states. Still, the hydrogen storage performance is markedly lower than both titanium-based systems discussed above, suggesting that V is not as effective in hydrogen storage as Ti. This decrease in effectiveness as you cross the periodic table has been predicted by Heben and Yilidrim in calculations,^[13, 16] and can be attributed to the higher effective nuclear charge of the later transition metal interfering with back-donation to the H-H antibonding orbital through less effective screening of the d-electrons.

For the tris[bis(trimethylsilyl)methyl] chromium (III) HMS sample the surface area drops to 915 m^2/g from 1284 m^2/g and the XRD pattern is fully retained. The

adsorption capacity of this material reaches 1.81 wt% at 85 atm at 77 K as shown in **Fig. 4.9**. This equates to 1.82 H₂ molecules per chromium center on the basis of 6.57% Cr determined by ICP-AAS. This is lower than the corresponding values for V(III) and Ti(III) presented in this study, and is consistent with the increase in Z_{eff} leading to less effective Kubas binding. Hydrogenation at 170 °C for two hours increases the hydrogen adsorption capacity of this sample to 2.17 wt% as shown in **Fig. 4.9**. This equates to 3.2 H₂ per Cr center according to the 6.66% Cr established by ICP-AAS. As in the case of the tris(mesityl) vanadium material, hydrogenation was not very effective in replacing the hydrocarbon with hydride, as the hydrogenated sample showed 10.39% C as compared to 11.01% in the non-hydrogenated sample. From these values a Cr:C molar ratio of 1: 7.10 can be

Figure 4.9 - Adsorption isotherms of HMS silica treated with tris[bis(trimethylsilyl)methyl] chromium before and after hydrogenation compared to that of HMS silica. Desorption isotherms omitted for clarity.

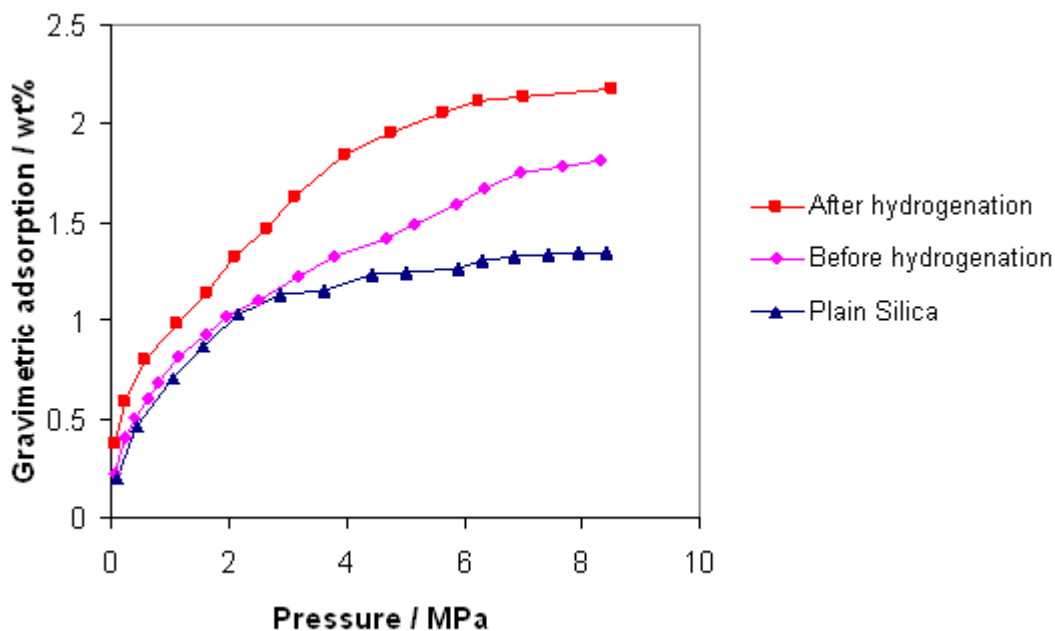
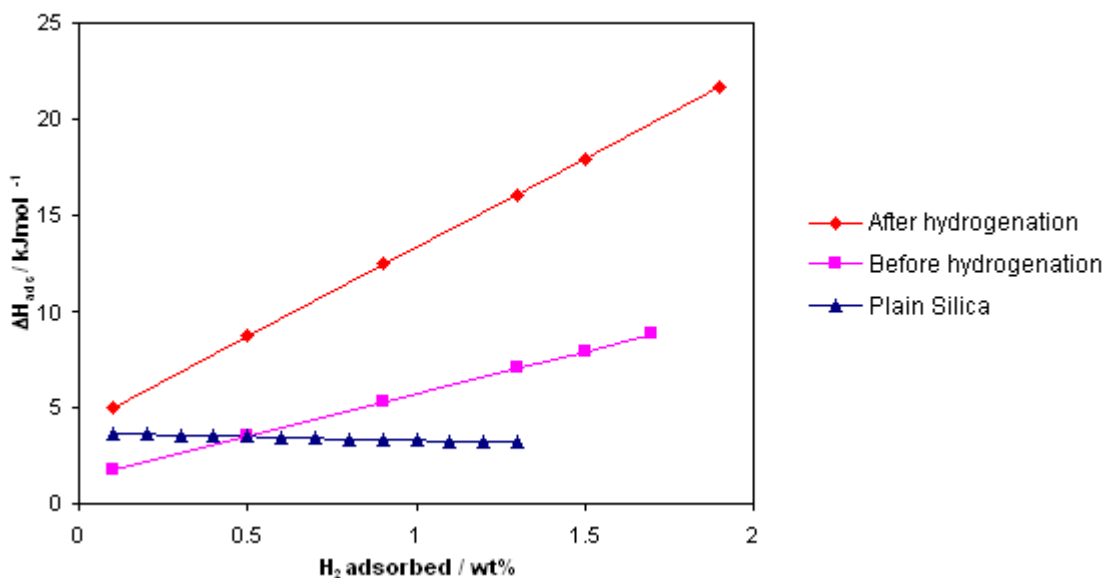


Figure 4.10 - Hydrogen binding enthalpies of HMS silica treated with tris[bis(trimethylsilyl)methyl chromium before and after hydrogenation compared to that of HMS silica.



calculated for the nonhydrogenated sample, corresponding to an average of 1.01 ligand per Cr center, and a Cr:C molar ratio of 1: 6.56 can be calculated for the hydrogenated sample, corresponding to an average of 0.94 ligand per Cr center. Surprisingly, this small decrease in hydrocarbon leads to a substantial increase in hydrogen storage capacity. This increase in performance is likely related to the high enthalpy of the hydrogenated tris[bis(trimethylsilyl)methyl]chromium-HMS material which increases with H_2 loading level up to 21.70 kJ/mol compared to 8.80 kJ/mol for the non-hydrogenated sample (**Fig. 4.10**). This increase in enthalpy is reflected in the differences in room temperature performance of 0.22 wt% and 0.52 wt% at 85 atm for the non-hydrogenated and hydrogenated samples, respectively. While loss of ligand may account for some of the changes in hydrogen adsorption properties, it is also possible that some reduction of Cr (III) to Cr (II) occurred on hydrogenation, making hydrogen

binding more facile to the lower valent metal center. In order to verify this hypothesis, the XPS of this material before and after hydrogenation was investigated.

The XPS spectrum with simulations of the non-hydrogenated tris[bis(trimethylsilyl)methyl] chromium-HMS sample (**Fig. 4.11**) features six pairs of peaks in the Cr 2p $3/2$ and 2p $1/2$ region. The first emission at 576.9 eV and 586.5 eV can be attributed to Cr (III) species on the basis of literature values.^[30] The second emission with smaller intensities appearing at 575 eV and 585.2 eV can be attributed to Cr (II) species,^[35] while the third at 578.1 eV and 587.5 eV can be attributed to a Cr (IV) species.^[39] The three other minor emissions at 579.2 eV and 588.6 eV, 581.6 eV and 589.9 eV, and 583.5 eV and 590.4 eV can be attributed to Cr species in higher oxidation states.^[40] The hydrogenated tris[bis(trimethylsilyl)methyl]Cr-HMS (**Fig. 4.12**) XPS spectrum shows three major emissions at 575.7 eV and 585.1 eV, 576.9 eV and 586.5 eV, and 578.1 eV and 587.5 eV which can be attributed to Cr(II), Cr(III), and Cr(IV) species, respectively, on the basis of the assignments above. The Cr(III) emissions have the highest relative intensity compared to the other two emissions. The other three minor emissions at 579.2 eV and 588.3 eV, 580.9 eV and 589.4, and 582.8 eV and 590.3 eV can be attributed to higher oxidation states chromium.^[41] Upon comparison of these spectra it is clear that hydrogenation leads to a decrease in the intensity of Cr species in a higher oxidation state than (IV) with an increase in intensity of Cr species in oxidation states of (III) and (II). This corroborates what was expected on the basis of the improved hydrogen adsorption capacity and higher enthalpies of the hydrogenated sample over the non hydrogenated sample: i.e. that reduction of Cr species and not just replacement of an alkyl ligand by a hydride were responsible for this increase.

In order to compare the relative effectiveness for hydrogen binding of Cr(III) and Cr(II), we doped HMS with a Cr(II) alkyl precursor. Hence, the material prepared by reacting HMS with $\text{Cr}_4(\text{CH}_2\text{Si}(\text{CH}_3)_3)_8$ at a doping level of 0.2 molar equivalents of Cr relative to Si retained its XRD pattern with a drop in the BET surface area to $946 \text{ m}^2/\text{g}$ from $1284 \text{ m}^2/\text{g}$. A schematic representation of this reaction is shown in **Scheme 4.3**. The adsorption capacity of this sample reaches 2.12 wt% at 77 K and 85 atm (Fig. 9), which equates 2.20 H_2 per Cr center on the basis of 6.43% Cr as determined by ICP-AAS. At 298 K this value drops to 0.36 wt % at 85 atm. This sample possesses 4.30% C as compared to 0.24% in the pristine HMS, which corresponds to a 1:2.6 Cr:C ratio, which in turn equates to 0.65 alkyl ligands per Cr center, suggesting a mixture on the surface of the alkyl siloxy Cr (II) species with the bis(siloxy) Cr (II). The adsorption capacity of this sample at 77 K and 85 atm increases to 2.26 wt% as a result of hydrogenation at $170 \text{ }^\circ\text{C}$ at 85 atm for 2 hours as shown in **Fig. 4.13**. This amount equates to 3.5 H_2 per Cr center, almost double that of the sample before hydrogen treatment.

Scheme 4.3 - Schematic representation of the grafting of mesoporous silica by treatment with bis[(trimethylsilyl)methyl] chromium leading to the formation of Cr (II) sites favorable for H_2 binding. $\text{Si}' = \text{Si}(\text{CH}_3)_3$.

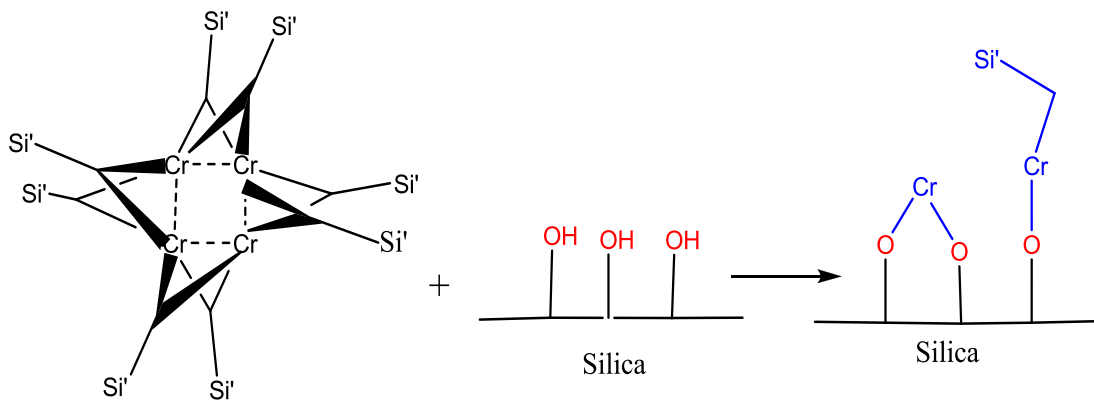


Figure 4.11 - XPS spectrum with simulation for HMS silica treated with tris[bis(trimethylsilyl)methyl] chromium showing the Cr 2p_{1/2}, and 3/2 emissions.

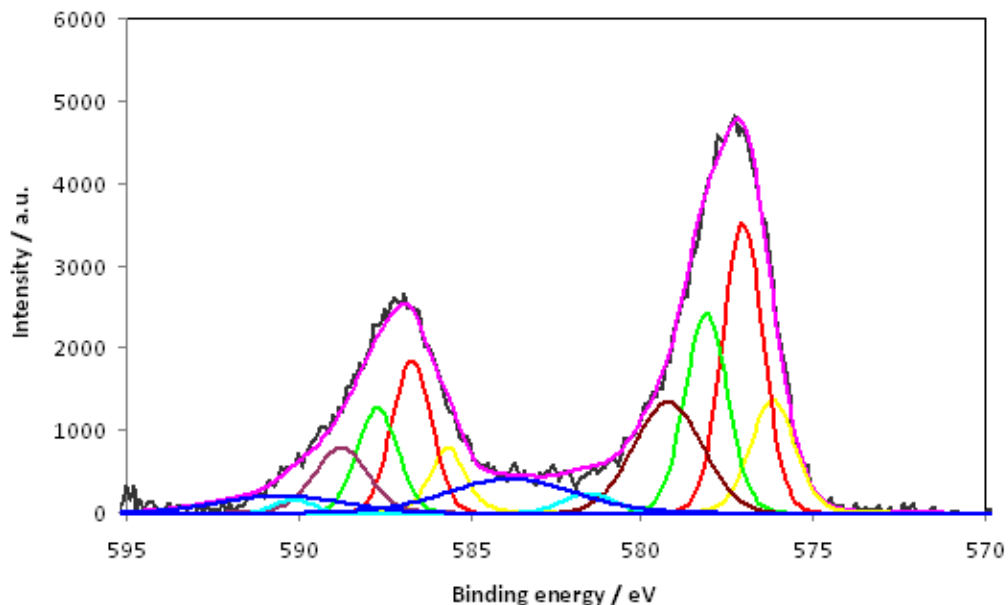
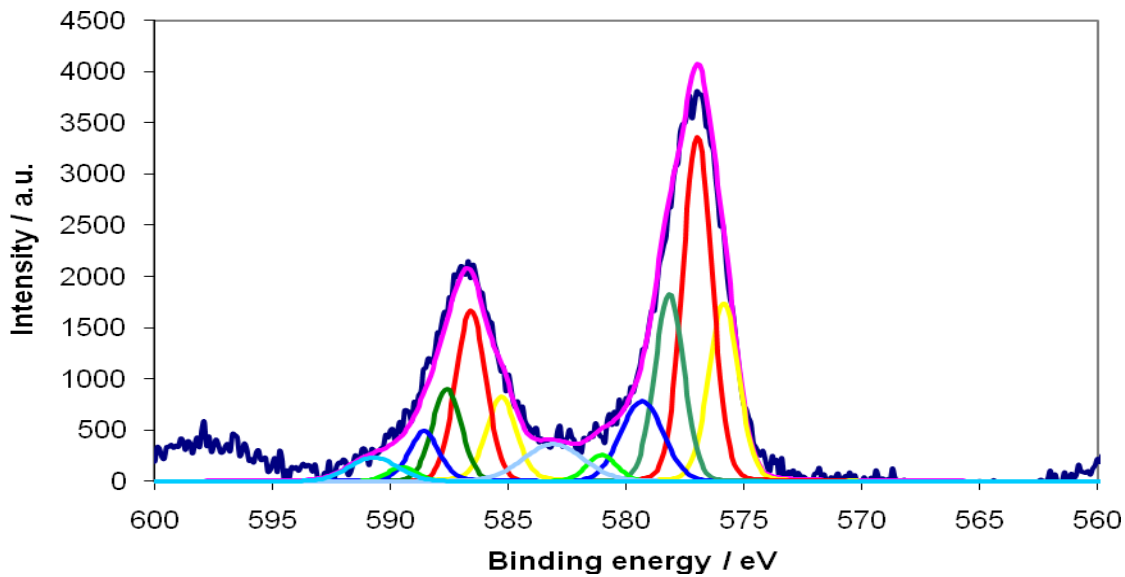


Figure 4.12 - XPS spectrum with simulations for HMS silica treated with tris[bis(trimethylsilyl)methyl] chromium after hydrogenation showing the Cr 2p_{1/2}, and 3/2 emissions.



The %C decreases as a result of hydrogenation to 1.54%, which equates to an average of only 0.21 ligands per Cr center, suggesting that the sigma bond metathesis reaction in this system is more effective than it is for the Cr (III) and V(III) systems, possibly because of the greater kinetic lability of the primary alkyl ligand with respect to the secondary alkyl ligands. At 298 K the hydrogen adsorption for the hydrogenated sample drops to 0.55 wt %. This is also reflected in the increase in % Cr from 6.43% to 6.75%, which increases the available hydrogen binding sites per mass unit. The binding enthalpy of the hydrogenated sample increases to a value of 13.6 kJ/mol compared to 11.4 kJ/mol for the non-hydrogenated sample (**Fig. 4.14**). This slightly higher binding enthalpy may be due to the more effective binding of M-H units to Kubas type H₂ ligands than M-R groups and is may also be reflected in the superior performance of the hydrogenated sample at 77 K (2.2 H₂/Cr vs. 3.5 H₂/Cr) and its greater retention at room temperature (0.36 % vs. 0.55 wt%). Since this increase in enthalpy is not dramatic, other factors such as greater steric accessibility to the metal center on replacement of a bulky alkyl with a hydride may be at play.

The XPS spectrum complete with simulations of the non-hydrogenated bis[(trimethylsilyl)methyl] chromium (II) sample (**Fig. 4.15**) shows 2 major emissions in the Cr 2p 3/2,1/2 region at 576.4 eV and 585.6 eV attributed to Cr (II)^[35] and at 577.5 eV and 586.7 eV, which be assigned to Cr (III) species by direct comparison with the spectrum of Cr₂O₃ which displays an emission at 578.4 eV and 587.6 eV.^[32] The two other emissions that appear at higher binding energies can be attributed to higher oxidation states of Cr.^[39] The appearance of Cr in higher oxidation states than (II) in

materials prepared by reacting Cp_2Cr with silica are well documented and are attributed to oxidation by surface protons.^[40]

Figure 4.13 - Adsorption isotherms of HMS silica treated with bis[(trimethylsilyl)methyl]chromium before and after hydrogenation as compared to that of plain silica. Desorption isotherms omitted for clarity.

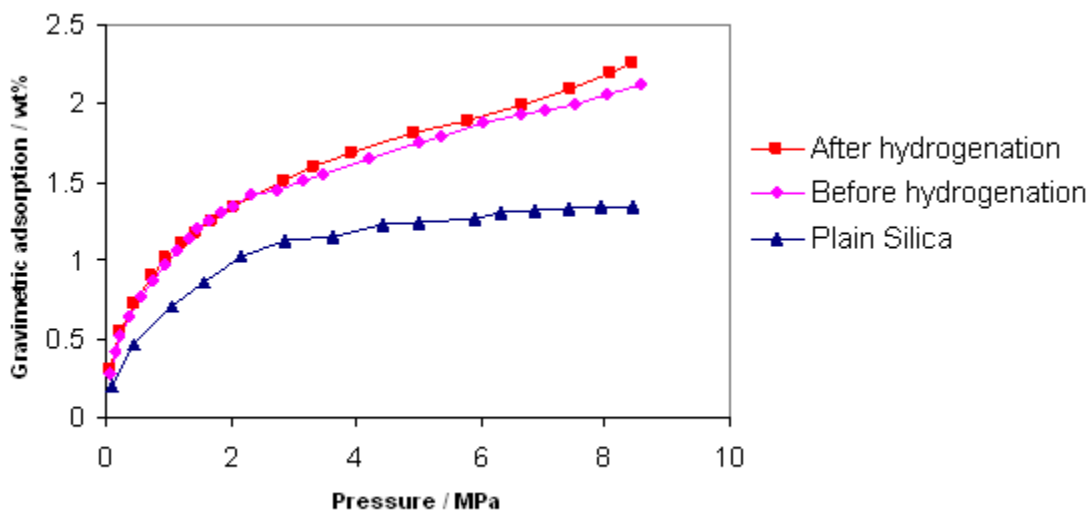
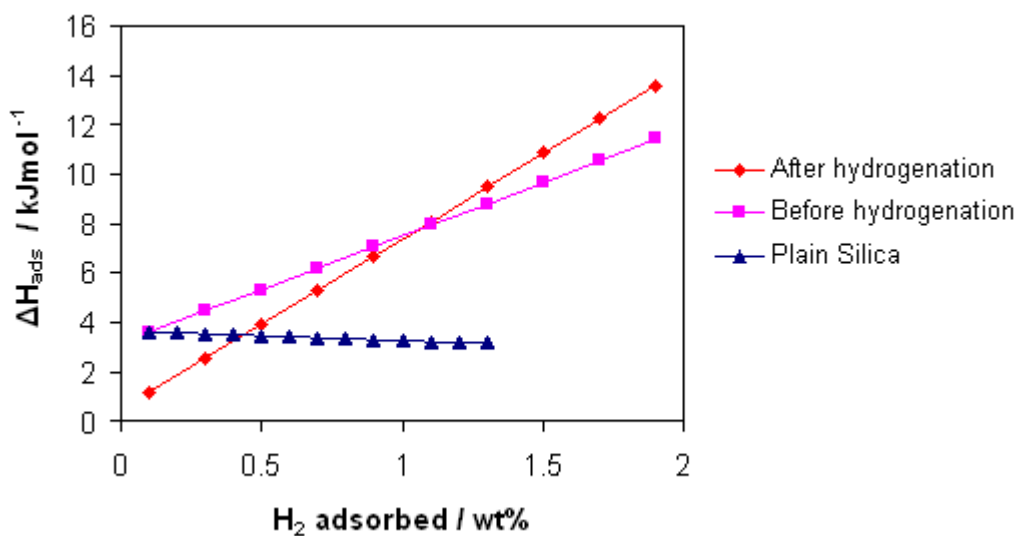


Figure 4.14 - Hydrogen binding enthalpies of HMS silica treated with bis[(trimethylsilyl)methyl]chromium before and after hydrogenation compared to that of plain HMS silica.



The simulated XPS spectrum of the hydrogenated bis[(trimethylsilyl)methyl] chromium sample (**Fig. 4.16**) shows 3 major emissions in the Cr 2p 3/2,1/2 region at 576.4 eV and 585.6 eV, which can be assigned to the same Cr (II) species as in the non-hydrogenated sample by comparison with the spectral lines at this binding energy level, and at 574.7 eV and 584.6 eV, which can be assigned to new Cr (II) species formed on hydrogenation, and at 577.6 eV and 586.8 eV, which can be attributed Cr (III) as in the non-hydrogenated sample.^[32, 39] Another small emission occurs at 579.3 eV and 588.7 eV and can be attributed to Cr (IV).^[41] The new Cr (II) species formed on hydrogenation may possibly be the Cr (II) hydride predicted and likely accounts for the increase in hydrogen storage capacity of this sample, as both the presence of hydrides and lower oxidation states are known to enhance Kubas binding of hydrogen to metals.

Figure 4.15 - XPS spectrum of HMS silica treated with bis[(trimethylsilyl)methyl]chromium before hydrogenation showing the Cr 2p1/2, and 3/2 emissions.

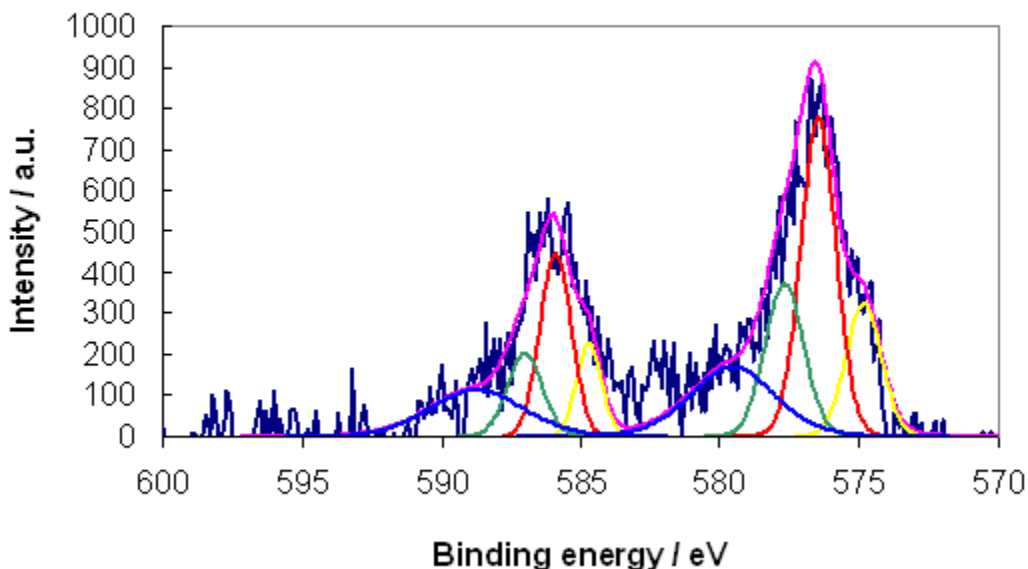
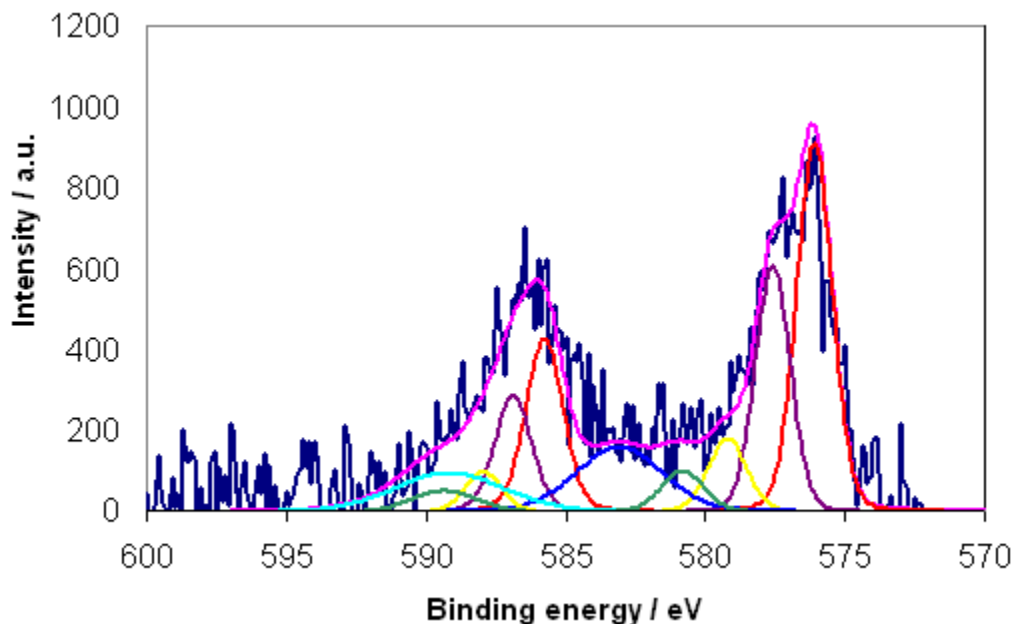


Figure 4.16 - XPS spectrum of HMS silica treated with bis[(trimethylsilyl)methyl]chromium after hydrogenation showing the Cr 2p_{1/2}, and 3/2 emissions.



This paper constitutes the final study in a three-part series from our group on surface-grafted silicas in hydrogen storage. While the low level of metal doping limits the performance and therefore practical applications of these materials, this research was undertaken to establish which organometallic fragments in which ligand environments were the most effective at Kubas-type binding under reasonable pressures for hydrogen storage operating conditions, as very little is known about the interaction of extremely low coordinate transition metal fragments with hydrogen at elevated pressures and whether the number of H₂ ligands predicted by the 18-electron rule for these fragments is actually accessible. The role of binding enthalpy was also explored in this study in an effort to relate storage capacity at 77 K and 298 K to the strength of the M-H₂ interaction. Thus, high surface area HMS silica was treated with various early transition metal organometallic species (M = Cr, V, Ti) in order to establish the influence of metal type, metal oxidation state, and hydrogenation to replace the alkyl groups with hydrides

at the metal center. While an ideal study may have used the same alkyl ligand for all metal precursors in order to eliminate the variation of steric and electronic profiles of the different ligands used, this was not possible due to the relative availabilities and stabilities of early transition metal alkyls in the (II) and (III) oxidation states explored. Even so, we were able to elucidate some clear trends in hydrogen storage properties by normalizing the hydrogen absorbed per metal center at the surface and comparing across the series studied. The highest adsorption values were observed for Ti followed by V and Cr, in that order, regardless of the oxidation state. This can be attributed to the increase in effective nuclear charge with increasing atomic number, which draws the d-electrons closer to the core and makes them less available for π -bonding to the H_2 ligands. This clearly overrides the effect of increasing the number of d-electrons in a metal. The effect of oxidation state for the same metal is hard to gauge in the case of Ti as there are no Ti(II) monohapto alkyls that can be used to compare directly to the grafted benzyl Ti (III) units, and the bis(trimethylsilylmethyl) ligand is sterically more demanding than the trimethylsilylmethyl ligand, thus potentially magnifying any electronic differences between the Cr (II) and Cr (III) systems. The Ti(III) system performed slightly better both at 77 K and 298 K than did the Ti (II) system, which was unexpected on the basis of increased electron density at the metal center (i.e., lower oxidation state) leading to improved Kubas-type binding. Another surprising feature of the Ti (II) system was that the enthalpy was substantially lower than in the Ti (III) system, and in fact much greater than the small difference in excess storage between these two systems would suggest. This goes against what is known about the effect of increased electron density on the strength of Kubas-type hydrogen binding and the role

of isosteric heats of adsorption in hydrogen storage. However this lower enthalpy may be exactly offset by the increase in binding sites offered by the lower level of ligation in the Ti (II) system as compared to the Ti (III) system. To make matters more complicated, the XPS showed that the Ti (II) material was actually a mixture of several oxidation states, including a substantial amount of Ti (IV), which is inactive in Kubas-type hydrogen binding. This makes it difficult to compare the Ti(II) and Ti(III) materials directly, especially when the Ti in the Ti(II) material clearly exists as unligated surface species and/or clusters as opposed to discrete rational units on the pore walls. While structure-property relationships are difficult to establish between these two Ti oxidation states, the case is clearer for Cr. Thus, the Cr (II) material clearly outperforms the Cr(III) material, which was expected on the basis of the lower oxidation state more effectively π -back-donating to the H-H antibonding orbital, as well as the larger steric profile of the bis-trimethylsilylmethyl ligand over the trimethylsilylmethyl ligand. The enthalpies of the Cr (II) and Cr(III) species fall in a similar range, which could be expected on the basis of the presence of Cr (III) in the Cr (II) material (by oxidation) and Cr (II) in the Cr (III) material (by disproportionation), but this does not explain the differences in excess storage between Cr (III) and Cr(II). However, since the enthalpies in this study likely represent a mixture of all the different sites (including physisorption on the silica surface) these numbers can only be used as a suggestive indication of what degree of hydrogen storage might be expected, and clearly cannot yet be used to quantitatively predict the hydrogen storage performance, as too many factors are involved to make direct relations possible. Hydrogenation had only a small effect in the V(III) system and Cr (III) systems, but a much larger effect in the Cr (II) system,

possibly because the primary alkyl ligand was kinetically more labile than the other ligands in this study. The previously reported decomposition on heating of the benzyl titanium system precluded the inclusion of hydrogenated Ti(III) in this study. Hydrogenation has less of an effect for V because of the difficulty in removing the secondary arene group and the η^3 benzyl. The increase in hydrogen storage in the Cr (II) and Cr(III) systems on hydrogenation can be attributed to three factors. The first is the decrease in weight and the opening up of the steric profile of the metal by replacing a bulky alkyl group with a hydride. The second is the superior electronic factors involved in Kubas binding of hydrogen to an M-H over an M-R unit.^[20] The third is the reduction of a metal center on hydrogenation to a lower oxidation state, more able to effectively bind to hydrogen.

4.4 Conclusions

A series of organometallic V, Cr, and Ti grafted silicas were prepared and tested for hydrogen storage with the goal in mind of establishing trends in metal, metal oxidation state, and ligand environment that may be used in designing a practical material for hydrogen storage based on Kubas-type binding. The general performance trends were Ti > V > Cr, M(II) > M(III), and M-H > M-R. Although there were several anomalies, which often made direct comparisons difficult, these could be attributed to inconsistencies in ligand environment necessitated by the availability and stability of metal alkyl complexes for these metals and/or oxidation states and/or the presence of multiple oxidation states at the surface. The best material was based on the previously studied benzyl Ti system and absorbed up to 4.85 H₂/Ti at 77 K and 85 atm, while the most dramatic effect observed was in the hydrogenation of the supported Cr(II) alkyl

species, which led to an almost doubling of the storage capacity at 77 K and 85 atm. While these materials do not achieve practical levels of performance, the results of this study may be valuable in the design and synthesis of new hydrogen storage materials based exclusively on Kubas-binding to hydrogen with little or no physisorption component.

4.5 References

1. Schlapbach, L., Züttel, A., *Nature*, **2001**, 414, 353-358.
2. http://www.hydrogen.energy.gov/annual_review06_plenary.html
3. Yartys, V.A., Harris, I.R., Panasyuk, V.V., *Mater. Sci.*, **2001**, 37, 219.
4. Seayad, A.M., Antonelli, D.M., *Adv. Mater.*, **2004**, 16, 765.
5. Hoang, T.K.A., Antonelli, D.M., *Adv. Mater.*, **2009**, 21, 1787-1800.
6. Rowsell, J.L.C., Milward, A.R., Park, K.S., Yaghi, O.M., *J. Am. Chem. Soc.* **2004**, 126, 5666.
7. Dincă, M., Long, J.R., *Angew. Chem. Int. Ed.*, **2008**, 47, 6766-6779.
8. Murray, L.J., Dincă, M., Long, J.R., *Chem. Soc. Rev.*, **2009**, 38, 1294-1314.
9. Kaye, S.S., Long, J.R., *J. Am. Chem. Soc.*, **2005**, 127, 6506.
10. Dillon, A.C., Jones, K.M., Bekkedahl, T.A., Kiang, C.H., Bethune, D.S., Heben, M.J., *Nature*, **1997**, 386, 377.
11. Germain, J.; Frechet, J.M., Svec, F., *Small*, **2009**, 5, 1098-1111.
12. Durgun, E., Ciraci, S., Yildirim, T., *Phys. Rev. B.*, **2008**, 77, 085405.
13. Yildirim, T., Ciraci, S., *Phys. Rev. Lett.* **2005**, 94, 4948.

14. Georgiev, P.A., Albinati, A., Mojet, B.L., Ollivier, J., Eckert, J., *J. Am. Chem. Soc.*, **2007**, 129, 8086–8087.
15. Turnes Palomino, G., Llop Carayol, M.R., Otero Arean, C., *J. Mater. Chem.*, **2006**, 16, 2884-2885.
16. Zhao, Y., Kim, Y.-H., Dillon, A.C., Heben, M.J., Zhang, S.B., *Phys. Rev. Lett.*, **2005**, 94, 155504/1-155504/4.
17. Bahatia, S.K., Myers, A.L., *Langmuir*, **2005**, 22, 1688.
18. Hamaed, A., Trudeau, M., Antonelli, D.M., *J. Am. Chem. Soc.*, **2008**, 130, 6992-6999.
19. Kubas, G.J., Ryan, R.R., Swanson, B.I., Vergamini, P.I., Wasserman, H.J., *J. Am. Chem. Soc.*, **1984**, 108, 7000.
20. Kubas, G.J., *Chem. Rev.*, **2007**, 107, 4152-4205.
21. Hamaed, A., Hoang, T.K.A., Trudeau, M., Antonelli, D.M., *J. Organomet. Chem.*, **2009**, 694, 2793-2800.
22. Tanev, P.T., Pinnavaia, T.J., *Science*, **1995**, 267 865.
23. Ellis, J.E., Blackburn, D.W., Yuen, P., Jang, M., *J. Am. Chem. Soc.*, **1993**, 115, 11616-11617.
24. Siedel, V.W., Kreisel, Z., *Z. Anorg. Allg. Chem.*, **1977**, 435, 146-152.
25. Barker, G.K., Lappert, M.F., Howard, J.A.K., *J. C. S. Dalton*, **1977**, 734-740.

26. Schulzke, C., Enright, D., Sugiyama, H., LeBlank, G., Gambarotta, S., Yap, L.K., Thomson, G.P.A., Wilson, D.R., and Duchateau, R., *Organometallics*, **2002**, 21, 3810-3816.
27. Roquerol, F., Roquerol, J., Sing, K., *Adsorption by powders and Solids: Principles, Methodology, and Applications*, Academic Press, London, **1999**.
28. Galuska A.A., Uht, J.C., Marquez, N., *J. Vac. Sci. Technol. A*, **1988**, 6, 110.
29. Saied S.O., Sullivan, J.L., Choudhury, T., Pearsce, C.G., *Vacuum*, **1988**, 38, 917.
30. Werfet, F., Brummer, O., *Phys. Scripta*, **1983**, 28, 92.
31. Gonbeau, D., Guimon, C., Pfister-Guillouzo, G., Levasseur A., Meunier, G., Dormoy, R., *Surf. Sci.*, **1991**, 254, 81.
32. Maksimov, N.G., Nesterov, G.A., Zakharov, V.A., Stchastnev, P.V., Anufrienko, V.F., Yermakov, Y.I., *J.Mol. Catal.*, **1977**, 4, 167.
33. Hu, X., Skadtchenko, B.O., Trudeau, M., Antonelli, D.M., *J. Am. Chem. Soc.*, **2006**, 128, 11740-11741.
34. Kubas, G. J., *J. Organomet. Chem.*, **2001**, 635, 37-68.
35. Groenenboom, C.J., Sawatzky, G., Meijer, H.J.D., Jellinek, F., *J.Organomet. Chem.*, **1974**, 76, C4.
36. He, X., Trudeau, M., Antonelli, D.M., *Adv. Mater.*, **2000**, 12, 1036.

37. Hovarth, B., Strutz, J., Geyer-Lippamann, J., Hovarth, E.G., *Z. Anorg. Allg. Chem.*, **1981**, 483, 181.
38. Nag, N.K., Massoth, F.E., *J. Catal.*, **1990**, 124, 127.
39. NIST X-ray Photoelectron Spectroscopy (XPS) Database, Version 3.5.
<http://srdata.nist.gov/xps/Default.aspx> (Accessed December 27, 2009).
40. Hoang, T.K.A., Hamaed, A., Trudeau, M., Antonelli, D.M., *J. Phys. Chem. C*, **2009**, 113 (39) 17240–17246.
41. Ozin, G.A., Gil, C., *Chem. Rev.*, **1989**, 89, 1749.

Chapter 5 – Computational Studies on Silica Supported Transition Metal Fragments for Kubas-Type Hydrogen Storage

5.1 Introduction:

With steadily increasing greenhouse gas emissions and rapidly diminishing reserves of fossil fuels^[1] the search for alternative energy sources is more important than ever. Concurrent with this demand for renewable and environmentally benign energy is the need to find more efficient ways to store and transport energy. Hydrogen is the ideal energy storage medium because it is lightweight, abundant, and water is its only combustion product. However, achieving practical levels of energy density is still a major hurdle.^[2] The 2015 target set by the U. S. Department of Energy (DOE) is 5.5 wt.% and 1.3 kWh/L (0.040 kg hydrogen/L) for a fully reversible system operating near room temperature.^[3] While compressed gas and liquid hydrogen have been used in on-board automotive applications, the cost of compression and/or cooling and the low storage densities of these methods remains a problem. For this reason, chemical carriers such as alloys^[4] and metal hydrides,^[5] or adsorbents such as amorphous carbons,^[6] zeolites,^[7] and metal-organic frameworks^[8] have been employed as hydrogen storage media. While metal hydrides encounter difficulties with heat management issues and slow kinetics, physisorption materials typically maintain only 10-15% of their performance at ambient temperature due to low heats of adsorption (typically 5 – 10 kJ/mol).^[9] To achieve the DOE target under ambient conditions, the ideal H₂ binding energy is predicted to be in the range of 20 – 30 kJ/mol H₂.^[10] Numerous experimental

^[11] and theoretical^[12] investigations focus on the engineering of adsorption sites on porous solids for improved binding enthalpies. Recent advances in our group indicate that coordinatively unsaturated low-valent transition metal centers supported on mesoporous silica can function as ideal σ - π H₂ (Kubas-type)^[13] binding sites with enthalpies as high as 23 kJ/mol.^[14] These composites demonstrate up to 40% relative retention of storage capacity per metal site at room temperature, and have demonstrated coordination of up to 4 H₂ ligands per metal at 77 K and 80 bar.^[14] This is greater than the maximum of two Kubas type H₂ ligands per metal that has been observed in any organometallic compound, so for this reason this research has obvious impact outside of the field of hydrogen storage.^[15] Since these silica supported systems contain less than 10 wt% metal and far too much void space due to the mesoporous structure, they fall far short of the DOE performance targets. However, the ideal binding enthalpies and high density of H₂ ligands per metal suggest that practical systems that meet the DOE targets may one day be developed that use low-coordinate transition metals as principle binding sites. Currently our group has used hydrazine as a linker to create extended solids with a high number of low-coordinate, low-valent metal centers per unit volume. These materials display 49 % retention of performance on going from 77 K to room temperature, the highest ever recorded for a material possess linear isotherms, and enthalpies that rise from 20-40 kJ/mol. For this reason a deeper understanding of the factors at play that determine strength of H₂ binding and maximum number of H₂ units per metal center in the coordination sphere of low-coordinate transition metal fragments such as those observed in the silica-supported Ti system, is necessary. Computational methods are particularly powerful for exploring the dynamics of high energy transition

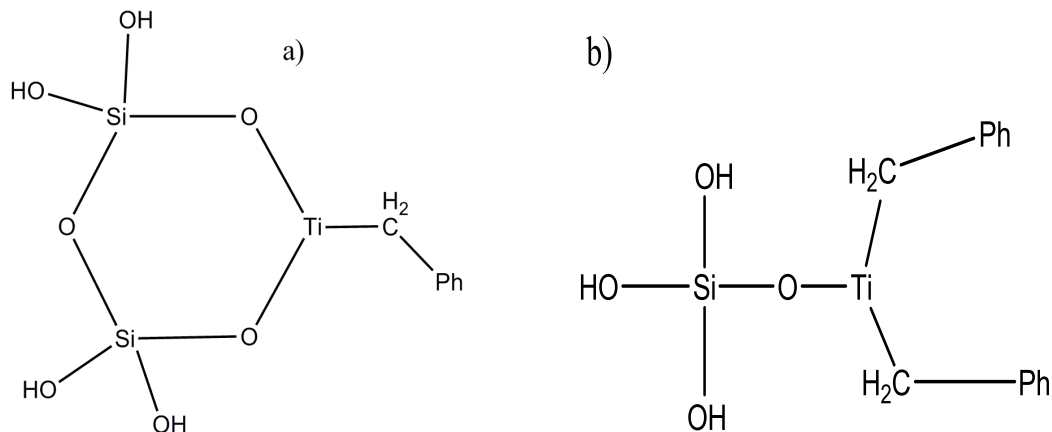
metal fragments and have already been used to predict some possible inorganic structures that use Kubas binding to attain hydrogen storage values that meet or surpass the DOE goals.^[16,17] However, there are currently no papers in the literature that have systematically explored the effect of ligand type and coordination number and geometry about the transition metal center on the strength of Kubas binding in these silica-supported systems. Of particular interest is the prediction of the ideal ligand environment for optimal room temperature storage, while also the rationalization of the unusual rising trend of binding enthalpies with surface coverage observed in these and related materials.^[14] Rising enthalpies have been calculated by Yilidrim^[16] and Heben^[17] in hypothetical molecules using the Kubas interaction for hydrogen storage, but this is the first time that computations and experimental observations are being directly compared in Kubas type systems for hydrogen storage.

5.2 Computational Details

The molecular modules which are believed to replicate the 2 types of binding site of the experimental system are shown in Figure 5.1. A small size module was selected and hydrogen atoms were used to terminate the bulk silica. The molecular module geometries were optimized and then the bond lengths and bond angles from the silicon atoms onwards, moving away from the titanium, were fixed to represent the inflexibility of the silica surface. Hydrogen molecules were then bound to the metals of these binding site representations and the unfixed parts of the molecules were optimized. The metal and/or ancillary ligand was varied to study the effect of these variations on metal-to-H₂ (M-H₂) bonding. The molecular module geometry was then fully optimized

with the changed metal and/or ligand, then bond lengths and bond angles were fixed as before, H₂ units were bound and the unfixed parts of the molecules were optimized.

Figure 5.1 - Schematic representations of the molecular modules employed a) benzyl disiloxy Ti (III) (molecule 1) and b) dibenzyl siloxy Ti (III) (molecule 2).



The calculations obtained by using small basis set were improved by moving to a higher level of theory. Initially, the ADF code,^[18] the Perdew-Burke-Ernzerhof (PBE)^[19] functional and a Slater Type Orbital (STO) DZP/TZP basis set (core double zeta, valence triple zeta, polarized) basis set on the metal, and DZP elsewhere (double zeta, polarized basis set)^[20] were used. Initial lower level calculations using the Gaussian code,^[21] PBE^[19] and SDDALL^[22] (Stuttgart potentials for $Z > 2$) or 6-31G^[23] basis sets did not seem promising as fewer H₂ units could be bound than when using ADF and the results were basis set dependent. The calculations were improved by using the Gaussian code and PBE but with a much larger 6-311++G** basis set^[24] on all of the atoms. A similar increase of basis set size in ADF to TZ2P (core double zeta, valence triple zeta, doubly polarized) bases^[20] on all atoms was investigated and did

show some accuracy improvement but to a lesser extent than when using Gaussian such that the ADF calculations were not adopted.

The Ziegler-Rauk^[25] energy breakdown implemented in the ADF code was employed on the optimized Gaussian geometries to calculate the Ti-H₂ bond energies within these molecules. A TZ2P basis set^[20] was adopted on all atoms for the single point calculations involved. The Ti-H₂ bond energies calculated using the Ziegler-Rauk energy breakdown was corrected for basis set superposition error (BSSE) using the counterpoise method.^[26] In the fragment breakdown the molecule was split into 2 fragments, one containing all of the bound H₂ units and the other the rest of the molecule. The calculated interaction energy between these fragments was divided by the number of H₂ units bound to find the average Ti-H₂ bond energy. The Ziegler-Rauk energy breakdown is usually not designed for systems with unpaired spins and therefore became progressively harder to use moving from Ti to V and Cr and consequently the results became less reliable. Therefore, to compare the M-H₂ bond energy as the metal changes, the same fragments as those used for the Ziegler-Rauk energy breakdown are to be optimized spin unrestricted and the energy of the average M-H₂ bond energy taken as the difference between the fragment energies and the spin unrestricted energy of the whole molecule is to be divided by the number of H₂ units bound.

The computed enthalpies were obtained from the Gaussian calculations as the difference between the sum of the electronic and thermal enthalpies of the products and those of the reactants. This includes the zero point correction and the correction to standard temperature.

Partial charge may be quantified using several different scales. Herein the Mulliken, Voronoi and Hirshfeld scales were employed. All of the partial charges were obtained using the ADF program but the Mulliken values were obtained using Gaussian.

5.3 Results and Discussion

5.3.1 Comparison to the experimental study

With the model of the experimental system, up to 3 H₂ units could be bound to molecule 1, which represents the binding site where the titanium fragment is bound to the silica surface through 2 proximal silanol groups (Fig. 5.2 A). Whereas, up to 4 H₂ units could be bound to molecule 2 which represents the binding site where the titanium fragment is bound to the silica surface through the interaction with only one silanol group (Fig. 5.2 B). This agrees well with the experimental average of 2.7 H₂ units per Ti rising to 3.98 H₂ units per Ti when the experimental system was optimized.^[14]

Figure 5.2 - A) molecule 1 with 3 H₂ units bound, B) molecule 2 with 4 H₂ units bound

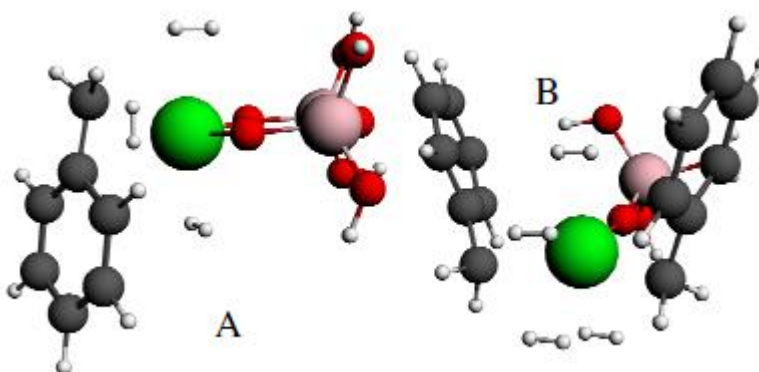
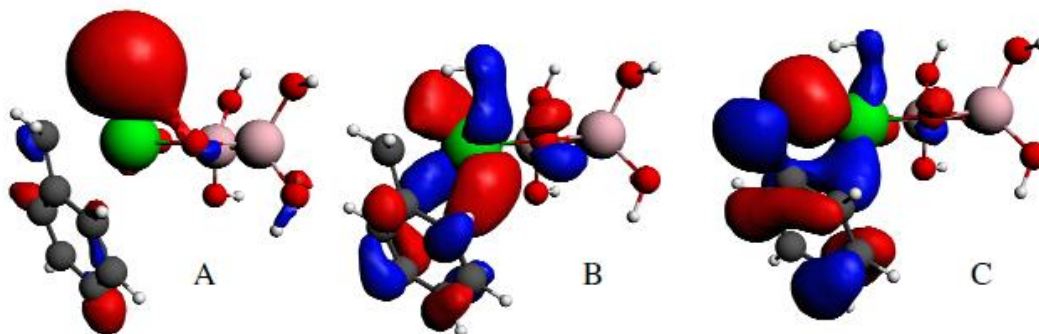


Figure 5.3 - Orbital representations for molecule 1 with 1 H₂ unit bound. A) The HOMO showing σ -bonding from the H₂ unit to the metal. In B) and C) the HOMO and HOMO-1 respectively shows π -back-bonding from the metal to the H₂ unit.



A Kubas model may be invoked to explain the H₂-to-M binding mechanism. This includes orbitals representing the σ -donation from the H₂-to-M (Fig. 5.3A) and orbitals representing π -back-donation from the M-to-H₂ (Fig. 5.3 B and C). In general, the partial charge on the titanium decreases as the number of H₂ molecules binding to the metal center increases. Fig. 5.4 shows that the titanium metal center gains electron density from the interactions, suggesting that the M-H₂ unit interaction is dominated by the H₂→M σ -donation.

Figure 5.4 - The partial charge on the titanium metal center of molecule 1 with a benzyl ligand, as a function of the number of H₂ units bound.

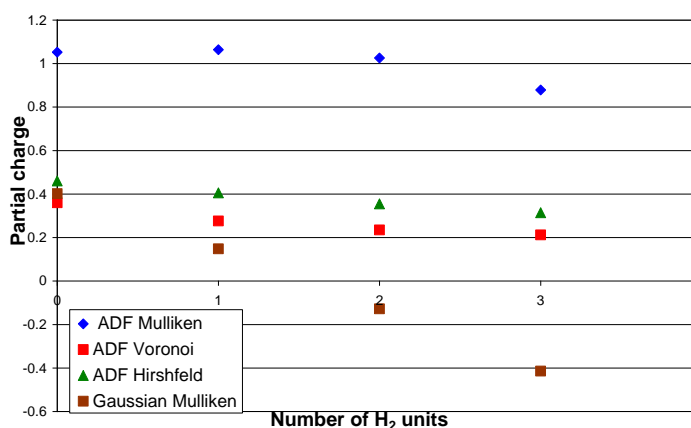
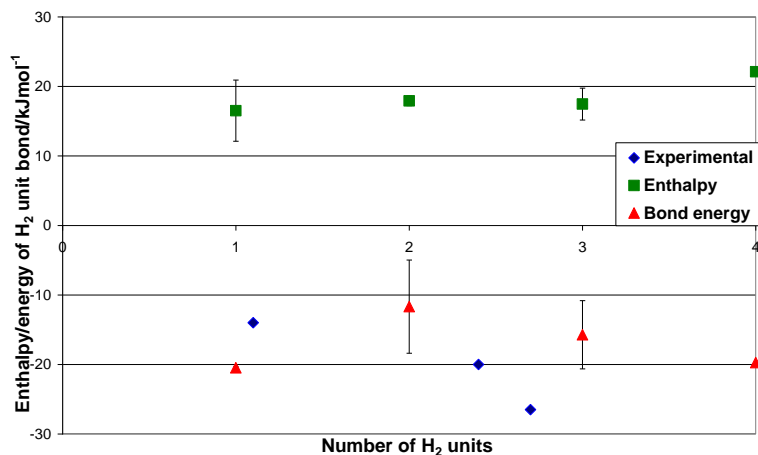


Figure 5.5 - Comparison of the experimental hydrogen binding enthalpies calculated by Hamaed et al.^[14] the computed enthalpies, and Ti-H₂ bond energies of the experimental model. The computational values are a 50:50 average of molecules 1 and 2 and the error bars show the range of these values



The comparison of the experimental enthalpies with the computational ones was not favorable (Fig. 5.5). The computational enthalpies are positive and become slightly more positive as more hydrogen molecules are bound, which is the opposite of the experimental results. This finding is due to destabilization of the molecule representing the binding site of the experimental system upon hydrogen binding. This destabilization is not compensated by the stabilization due to the Ti-H₂ interaction.

The hydrogen molecule was also destabilized upon binding to the metal center, but its slight destabilization was more than compensated by the stabilization due to the Ti-H₂ interaction. Alternatively, the experimental enthalpies were compared to the Ti-H₂ bond energies, and it was found that the calculated Ti-H₂ bond energies were similar to the experimental enthalpies as shown in Fig. 5.5. The computational Ti-H₂ bond energies show a more favorable comparison to the experimental enthalpies. Therefore, the Ti-H₂ bond energies were used to track the effect the metal center and the ancillary ligand on the M-H₂ bond energy of the molecular modules representing the binding sites.

5.3.2 The effect of the ancillary ligand

By changing the ancillary ligand from benzyl to methyl, allyl or hydride, whilst keeping the titanium metal unvaried, it can be clearly noticed that when only 1 H₂ molecule is bound to the metal center, the strength of the Ti-H₂ bond decreases in the order hydride>methyl>benzyl>allyl, as the Figures 5.6 and 5.7 show.

Figure 5.6 - The average Ti-H₂ bond energy calculated for molecule 2 with various ancillary ligands.

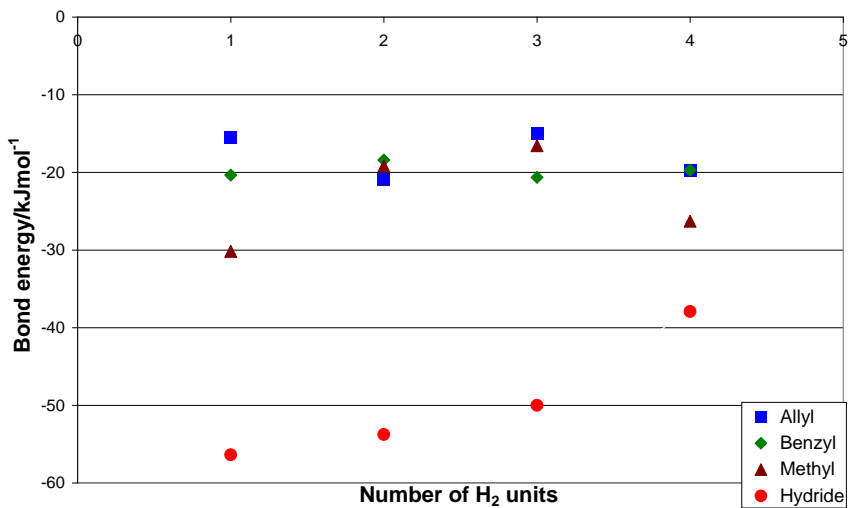
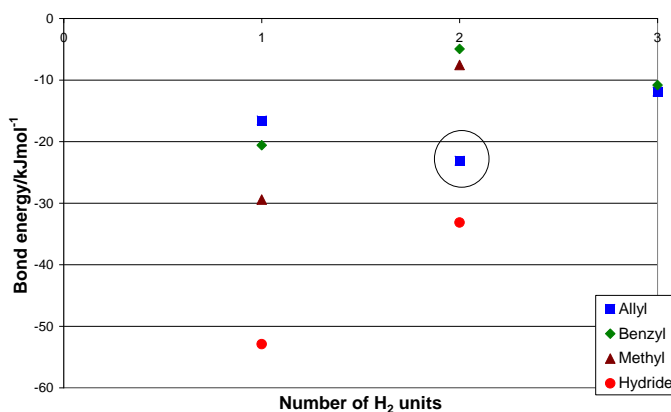


Figure 5.7 - The average Ti-H₂ bond energy calculated for molecule 1 with various ancillary ligands. The high average bond energy when 2 H₂ units are bound to the titanium with an allyl ancillary ligand has been circled.



The Ti-H₂ bond strength decreases as the π -acceptor ability of the ancillary ligand increases hydride<methyl<benzyl<allyl. The more the electron density that the Ti metal center π -back-donates to the ancillary ligand the less will be available to π -back-donate to the H₂ ligand. The Ti-H₂ bond strength should also decrease as the overlap between the HOMOs and LUMOs of the H₂ ligand and the binding site decreases. The more sterically hindered the ancillary ligand is, the less probable it is for the H₂ molecule to approach the metal center in a manner that leads to an optimum HOMO and LUMO overlap and therefore this will lead to a weaker Ti-H₂ bond. The steric hindrance around the Ti metal center should increase in the order hydride<methyl<allyl<benzyl. The hydride ancillary ligand produces by far the strongest Ti-H₂ bond presumably because it has no orbitals to take part in π -back-donation from the Ti and as it possesses very little steric hindrance.

Deviations from the above trend in Ti-H₂ bond energies occur when more than 1 H₂ unit is bound to the Ti center. This may be explained by different ligand coordination

geometries about the Ti, and the subsequent effects on the d-based orbitals. These Ti d-based orbitals form the HOMO and LUMO orbitals where the subsequent H₂ orbitals will interact, and with stronger π -acceptor ligands will lead to a greater splitting of these d-based orbitals. Therefore, to achieve the best overlap with the LUMO (0.717 eV) and HOMO (-10.357 eV) of the H₂ unit, the Ti binding site requires a high HOMO/LUMO energy gap.

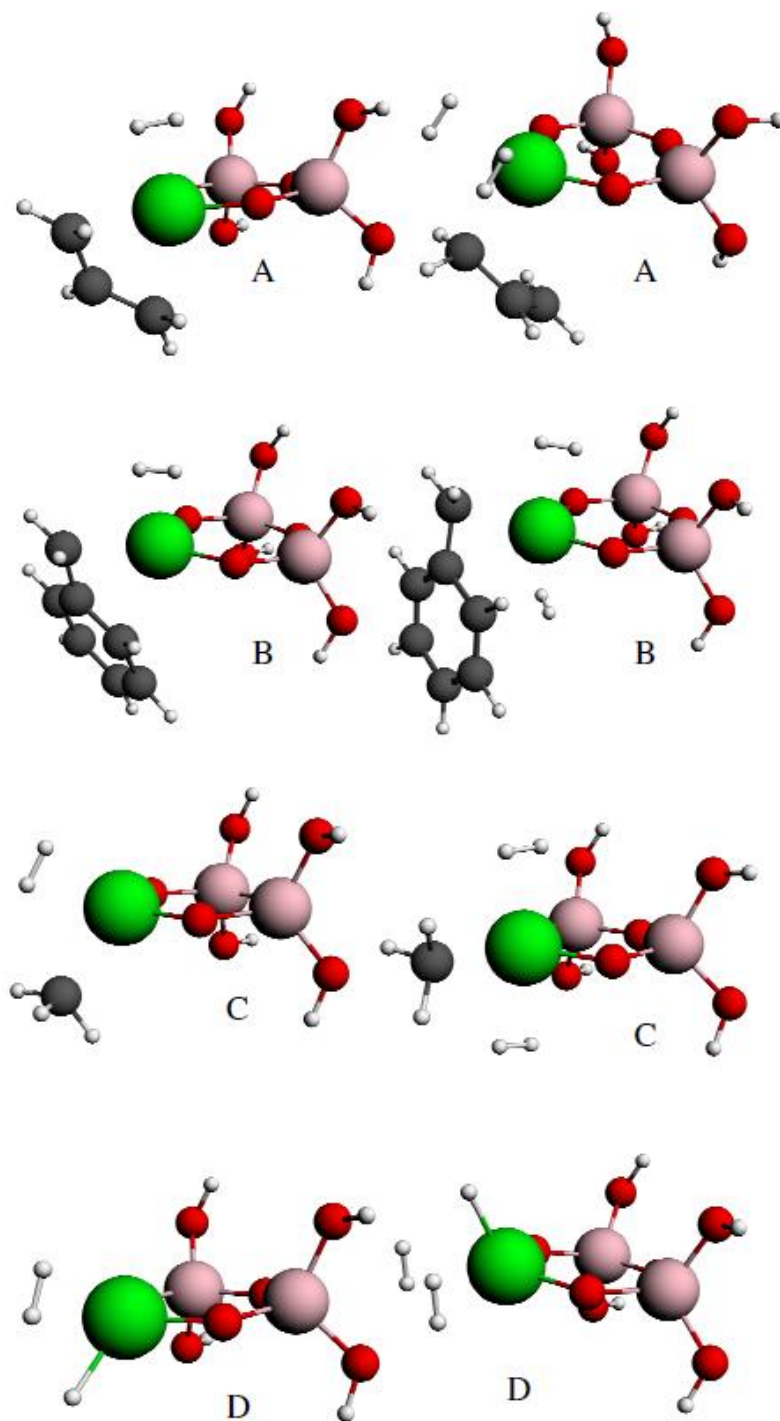
Figure 5.7 shows that, for 2 H₂ bound, the Ti-H₂ bond energy is stronger than expected when allyl is the ancillary ligand. This may be due to the changes in the ligand coordination geometry about the metal center between the cases when only 1 H₂ is bound to the cases when 2 H₂ units are bound. For hydride and allyl the minimum energy geometries found change from tetrahedral-like to capped square planar, for methyl the geometry changes from tetrahedral-like to trigonal bipyramidal and for benzyl it changes from capped trigonal planar-like to bent trigonal bipyramidal (Fig. 5.8). These variations in ligand coordination geometries caused the d-orbitals to split in different manners, which lead to different HOMO/LUMO energy gap each time the coordination geometry changes. This means that new HOMO and LUMO levels interact in each case with the 2nd H₂ unit to form the molecule with 2 H₂ units bound. The energies of these HOMOs and LUMOs are shown in table 5.1. These energy levels suggest that the molecule with a benzyl ancillary ligand would have the strongest bond to an H₂ unit, as it has the optimal HOMO/LUMO levels. However, this may not be the case, presumably, because the benzyl ligand causes steric hindrance around the metal center so that the H₂ molecule is less likely to bind in a manner that can achieve optimum overlap with the HOMO and LUMO of the binding site. On the other hand, the

LUMO of the metal binding site with the allyl ligand bound, was found to be lower in energy than that of benzyl ligand, this low LUMO level may help in explaining explain why the allyl ligand gives a stronger H₂-Ti bond than expected.

Table 5.1 - The HOMO and LUMO levels of molecule 1 with 1 H₂ unit bound and titanium as the metal center with various ligands, which are subsequently involved in bonding to the 2nd H₂. When more than 1 LUMO interacted with the H₂ an average was taken and the ± value shows the range of the LUMO energies.

	Hydride	Methyl	Benzyl	Allyl	Hydrogen molecule
HOMO involved in bonding/eV	-3.779	-3.399	-3.028	-3.299	-10.357
LUMO involved in bonding/eV	-2.126	-2.0±0.3	-2.164	-2.473	0.717

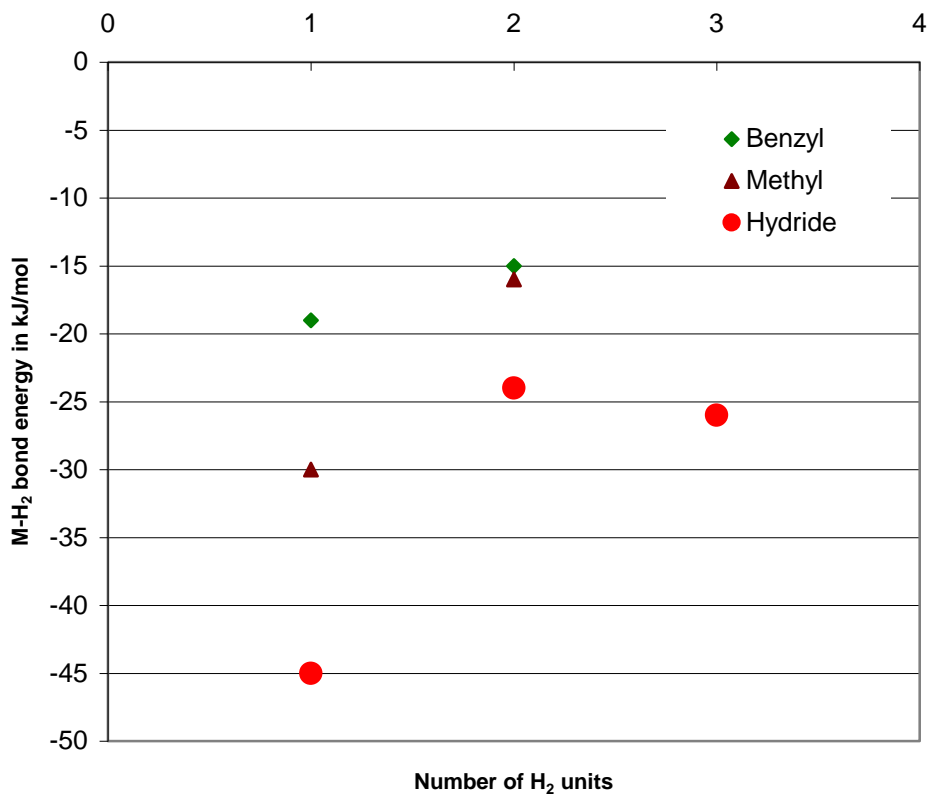
Figure 5.8 - Molecule 1 with titanium as the metal and with 1 or 2 H₂ units bound with A allyl, B benzyl, C methyl and D hydride ancillary ligand.



The variation in the V-H₂ bond energy as a function of the ancillary ligand is shown in Figure 5.9. The average V-H₂ bond energy decreases in the order

hydride>methyl>benzyl. This is the same order as that of titanium, i.e. the trends in the H₂ unit bonding observed upon changing the ancillary ligand bound to the metal appear to be independent of the metal center.

Figure 5.9 - The average V-H₂ bond energy for molecule 1 with vanadium as the metal center and with various ancillary ligands.

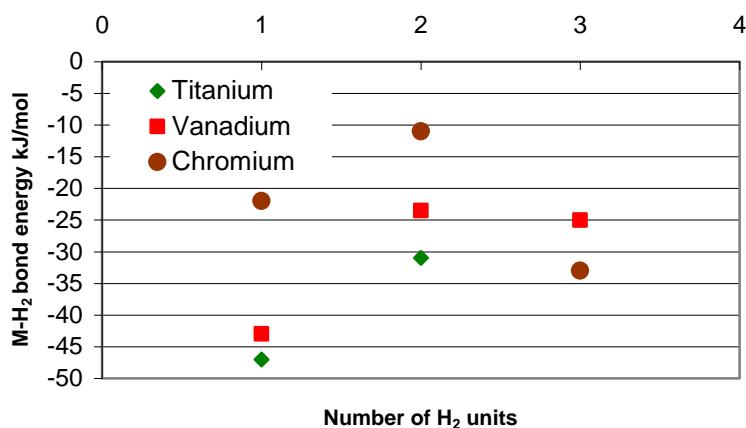


The trends observed when the ancillary ligand is varied have not changed from those found from the initial calculations. The only difference to note is that with the less accurate model fewer H₂ units could be bound to the Ti center and it was thought that the ancillary ligand had an effect on the maximum coordination number of the metal center. With the current, more accurate, model a similar number of H₂ units can be bound to the titanium whichever ancillary ligand is present suggesting that the ligand plays a minor role than previously thought.

5.3.3 The effect of the metal center

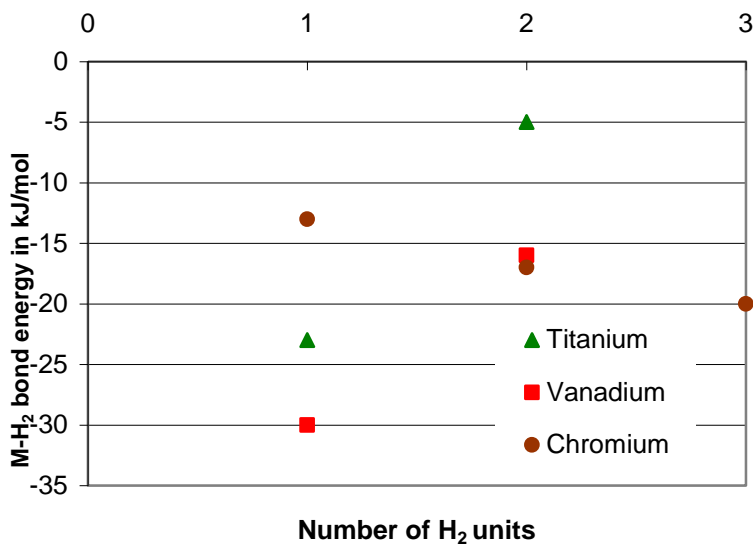
The change in M-H₂ bond energy as the metal is varied is shown in Figures 5.10 and 5.11 for molecule 1 with a hydride or methyl ancillary ligand respectively. These graphs show that the variation in the M-H₂ bond strength is not independent of the ancillary ligand and must be explained on a case by case basis rather than with a general trend.

Figure 5.10 - The average M-H₂ bond energy as a function of the number of H₂ units bound for molecule 1 with a hydride ancillary ligand and various metal centers.



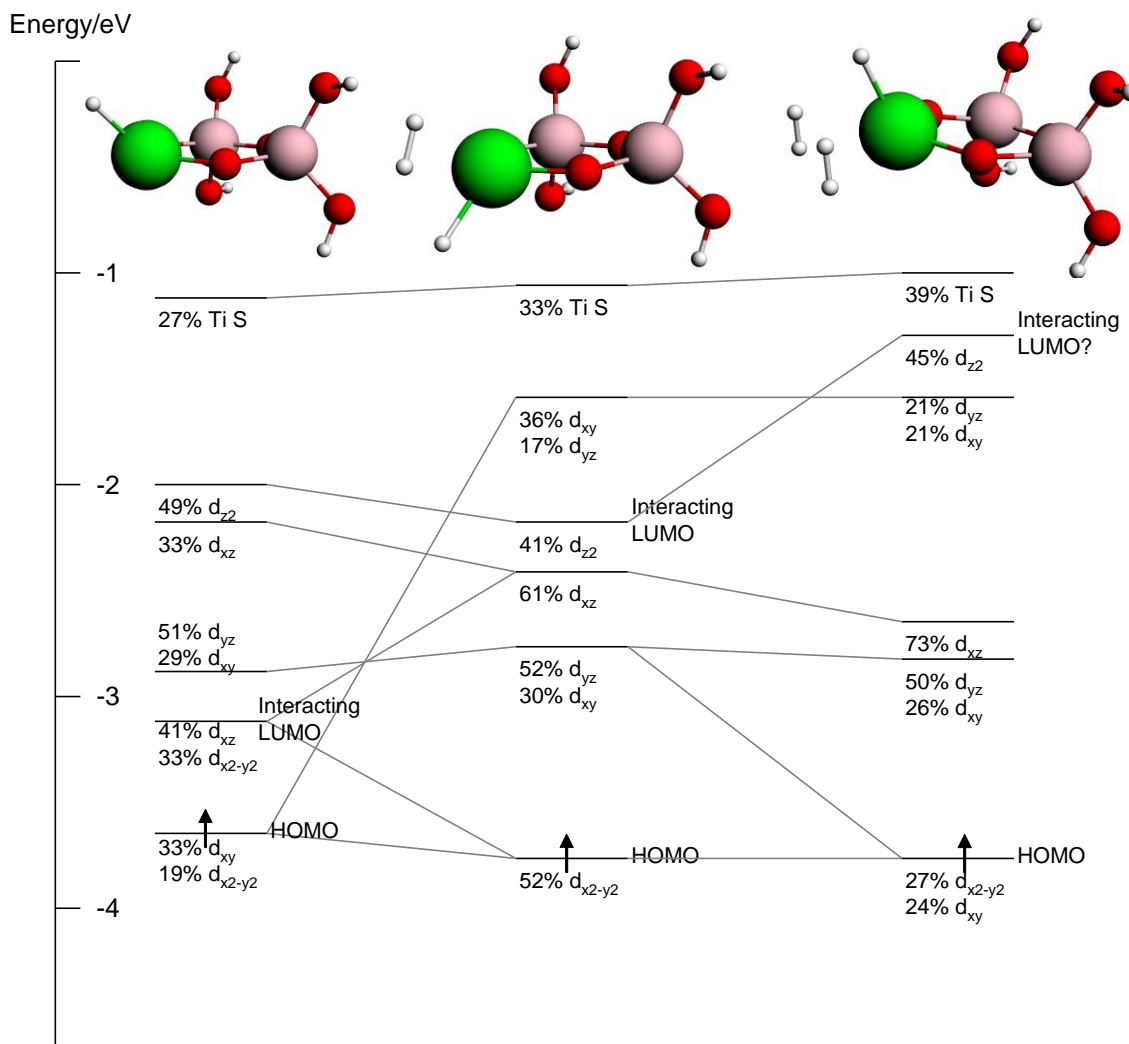
For a given ancillary ligand, the M-H₂ bond energies follow closely the HOMO and LUMO involved in bonding to the next H₂ unit, with a high HOMO and a low LUMO giving the strongest M-H₂ bond. The energy of the metal-based d orbitals from which the HOMO and LUMO are derived varies as the metal changed due to (i) the increase in the number of filled d orbitals, (ii) the decrease in the energy levels of the d orbitals as we go from Ti to Cr and (iii) to the effect of the minimum energy ligand coordination geometries about the metal centers on the splitting of the d orbitals.

Figure 5.11 - The graph of the average M-H₂ bond energy against the number of H₂ units bound for molecule 1 with methyl ancillary ligands and various metal centers.



Consider molecule 1 with a hydride ancillary ligand and Ti as the metal center, as an example. Fig. 5.10 shows that Ti-H₂ bond energy decreases as the number of H₂ units bound increases. This trend may be explained by the molecular orbital diagram shown in Fig. 5.12, where the HOMO (-3.673 eV) and LUMO (-3.151 eV) of the binding site with no H₂ units bound are more favorable in energy to the incoming H₂ unit (higher and lower respectively) than the HOMO (-3.779 eV) and LUMO (-2.126 eV) of the molecule with 1 H₂ unit. Perhaps the Ti does not bind 3 H₂ units in this case as the LUMO (-1.272 eV) of the molecule with 2 H₂ units bound, which would probably interact with the 3rd H₂ unit, is destabilized by the 2nd H₂ binding to become high in energy and so would have poor overlap with the HOMO of the 3rd H₂ unit.

Figure 5.12 - Molecular orbital diagram of molecule 1 with a Ti metal atom and a hydride ancillary ligand with 0, 1 and 2 H₂ units bound.



The trends in M-H₂ bond energy, shown in Figure 5.10, as the metal is changed may be explained by examining the energies of the HOMOs and LUMOs involved in bonding to the next H₂ unit. When 1 H₂ unit binds, the bonds weaken in the order Ti-H₂>V-H₂>Cr-H₂. This may be explained by the energies of the HOMOs and LUMOs of the binding sites with no H₂ units bound which subsequently interact with the H₂ unit

(Table 5.2). The HOMO becomes less favorable in energy for bonding as it decreases in the order Ti>V>Cr. The LUMO energies become less negative in the order Cr>Ti>V, such that the V LUMO is the most favorable in energy for bonding to the H₂ unit. Although the LUMO energies do not follow the order of the bond energies, the level of the V HOMO is 0.421 eV below that of the Ti HOMO, whereas the V LUMO is only 0.390 eV below that of the Ti LUMO. Therefore, overall the V HOMO and LUMO levels are less favorable for overlapping with the 1st H₂ unit than those of the Ti HOMO and LUMO.

Table 5.2 - The HOMO and LUMO energy levels for molecule 1 with no H₂ units bound and with hydride as the ancillary ligand with various metal centers, which are subsequently involved in bonding to the 1st H₂.

	Titanium molecule	Vanadium molecule	Chromium molecule	Hydrogen molecule
HOMO involved in bonding/eV	-3.673	-4.094	-4.548	-10.357
LUMO involved in bonding/eV	-3.151	-3.541	-2.916	0.717

When 2 H₂ units are bound, the M-H₂ bonds are weaker than that of 1 H₂ unit bound, but remain in the order Ti-H₂>V-H₂>Cr-H₂ (Fig. 5.10). This may be explained by noting that the HOMOs and LUMOs of the binding site with 1 H₂ unit bound, which subsequently bind to the 2nd H₂ unit, are less favorable in energy for interacting with an incoming H₂ unit than the analogous HOMOs and LUMOs of the molecule with no H₂ units bound (Table 5.3 as compared to Table 5.2). The energies of both the HOMOs and LUMOs of the binding sites with 1 H₂ bound decrease in the order Ti >V>Cr. The

decreasing energy of the HOMOs is consistent with the trend in the M-H₂ bond energies, while the LUMOs become more favorable in energy for overlapping with the 2nd H₂ unit in the order Ti, V, Cr. While contrary to the trend in M-H₂ bond energy, the change in the HOMO energy is greater than the lowering of the LUMOs, and so, taken together, the HOMO and LUMO energies are most favorable for Ti, then V and then Cr for binding the 2nd H₂ unit.

Table 5.3 - The energies of the HOMOs and LUMOs of molecule 1 with 1 H₂ unit bound and a hydride ancillary ligand with various metal centers, which are subsequently involved in bonding to the 2nd H₂. When more than 1 LUMO interacted with the H₂ an average was taken and the ± value shows the range of the LUMO energies.

	Titanium molecule	Vanadium molecule	Chromium molecule	Hydrogen molecule
HOMO involved in bonding/eV	-3.779	-4.326	-4.643	-10.357
LUMO involved in bonding/eV	-2.126	-2.7±0.4	-2.8±0.3	0.717

Figure 5.10 shows that, when 3 H₂ units bind to Cr and V the M-H₂ bond energies strengthen from the case when 2 H₂ units bind and the M-H₂ bond energies are in the following order Cr-H₂>V-H₂. The M-H₂ bond energy is stronger when 3 H₂ units are bound as the HOMOs and LUMOs of the binding sites with 2 H₂ units bound, which subsequently interact with the 3rd H₂ unit, are more favorable in energy for interacting with the incoming H₂ than the analogous HOMOs and LUMOs of the binding sites with 1 H₂ unit bound (Table 5.4 as compared with Table 5.3). The raised HOMOs follow the

order Cr>V and the fallen LUMOs follow the order V>Cr, both of which agree with the order of the M-H₂ bond energies.

Table 5.4 - The energies of the HOMOs and LUMOs of molecule 1 with 2 H₂ units bound and hydride as the ancillary ligand with various metal centers, which are/would be subsequently involved in bonding to the 3rd H₂. When more than 1 LUMO interacted with the H₂ an average was taken and the ± value shows the range of the LUMO energies.

	Titanium molecule	Vanadium molecule	Chromium molecule	Hydrogen molecule
HOMO involved in bonding/eV	-3.741	-3.977	-3.577	-10.357
LUMO involved in bonding/eV	-1.272	-2.7±0.1	-3.0±0.2	0.717

In general, the trends in the M-H₂ bond energy when hydride, methyl, allyl or benzyl is the ancillary ligand, may be explained using similar graphs, diagrams, tables and arguments as for the case above. The increase in the M-H₂ bond energy as the number of bound H₂ molecules increases thus appears to be a function of the ligand coordination geometry around the metal center, and the resulting d orbital splitting patterns, which alter the HOMO and LUMO energy levels and their overlap with the subsequent H₂ units. This may explain the experimental results where hydrogen adsorption enthalpy is observed to increase as the number of H₂ units bound increases.

5.4 Conclusion

In summary, a computational study was carried out to investigate the hydrogen adsorption capacity and hydrogen binding energy to silica surface grafted with early

transition metal fragments. It was found that up to 4 H₂ units can be bound per Ti metal center which agrees with the experimental result of 3.98 H₂/Ti.^[14] The interaction between H₂ and the metal center is believed to be of the Kubas-type, based on the binding energy values obtained. A stronger M-H₂ bond is formed when the ancillary ligand is a poor π -withdrawing group and the one that causes the least steric hindrance around the metal centre. The allyl and benzyl ligands change from η^3 to η^1 binding mode to accommodate more hydrogen.

The order of the M-H₂ bond energies when the metal is changed from Ti to V or Cr is not independent of the ancillary ligand bound to the metal and needs to be explained on a case by case basis. The changes in the M-H₂ bond energies when the ancillary ligand stays the same may be explained/ predicted by how close in energy are the HOMOs and LUMOs of the binding sites to those of the incoming H₂. The closer they are in energy, the better the overlap and the stronger the M-H₂ bond.

The experimentally observed increasing trend in the binding enthalpies with the hydrogen loading level, and the computationally calculated values for Ti-H₂ bond energy as a function of the H₂ loading level may help in explaining the facts behind this increasing trend. The different coordination geometries about the metal centre as more H₂ units bind alter the splitting of the d orbitals so that the HOMO and LUMO formed from them, which subsequently interact with the next H₂ unit, become energetically favorable.

5.5 References

1. Schlapbach, L., Züttel, A., *Nature* **2001**, *414*, 353; Cohen, R.L., Wernick, J.H., *Science*, **1981**, *214*: 1081-1087.
2. Züttel, A., Borgaschulte, A., Schlapbach, L., *Hydrogen as a Future Energy Carrier*, WILEY-VCH Verlag GmbH & Co. KGaA, Weinheim, **2008**.
3. http://www1.eere.energy.gov/hydrogenandfuelcells/storage/current_technology.html, US Department of Energy website.
4. Seayad, A.M., Antonelli, D.M., *Adv. Mater.*, **2004**, *16*, 765;
5. a) Wiswall, R.H. Jr., Reilily, J.J., *Science*, **1974**, *186*, 1158; b) Orimo, S., Nakamori, Y., Eliseo, J.R., Züttel, A., Jensen, C.M., *Chem. Rev.* **2007**, *107*, 4111-4132; c) Heung, L.K., *On-board Hydrogen Storage System Using Metal Hydride*, HYPOTHESIS II, **1997**, 1.
6. Yang, R.T., Wang, Y., *J. Am. Chem. Soc.*, **2009**, *131* (12), 4224–4226.
7. Pacuła, A., Mokaya, R., *J. Phys. Chem. C*, **2008**, *112* (7), 2764–2769.
8. a) Thomas, M.K., *Dalton trans.*, **2009**, 1487-1505; b) Kaye, S.S., Dailly, A., Yaghi, O.M., Long, J.R., *J. Am. Chem. Soc.*, **2007**, *129* (46), 14176–14177. c) Rosi, N.L., Eddaoudi, M., Vodak, D.T., Kim, J., O'Keeffe, M., and Yaghi, O. M., *Science*, **2003**, *300*, 1127-1129.
9. a) Dailly, A.; Vajo, J.J., Ahn, C.C., *J. Phys. Chem. B*, **2006**, *110*, 1099; b) Rowsell, J.L.C., Yaghi, O.M., *Angew. Chem., Int. Ed.*, **2005**, *44*, 4670.
10. Lochan, R. C.; Head-Gordon, M. *Phys. Chem. Chem. Phys.*, **2006**, *8*, 1357.
11. a) Eberle, U., Felderhoff, M., Schüth, F., *Angew. Chem. Int. Ed.* **2009**, *48*, 2-25; b) Li, Y., Yang, R.T., *J. Am. Chem. Soc.*, **2006**, *128* (3), 726–727; c) Dincă, M.,

- Long, J.R., *Angew. Chem. Int. Ed.* **2008**, 47, 6766 – 6779.
12. a) Han, S.S., Mendoza-Cortés, J.L., Goddard III, W.A., *Chem. Soc. Rev.*, **2009**, 38, 1460 – 1476; b) Sillar, K., Hofmann, A., Sauer, J., *J. Am. Chem. Soc.*, **2009**, 131 (11), 4143-4150.
13. a) Kubas, G.J., *Metal dihydrogen and σ -Bond complexes*, Kluwer Academic Publishers, **2001**; b) Heinekey, D.M., Oldham, W.J., *Chem. Rev.*, **1993**, 93 (3), 913-926.
14. a) Hamaed, A., Trudeau, M., and Antonelli, D.M., *J. Am. Chem. Soc.*, **2008**, 130 (22), 6992–6999. b) Hamaed, A., Hoang, T.K.A., Trudeau, M., Antonelli, D.M., *J. Organomet. Chem.*, **2009**, 694(17), 2793-2800. c) Hamaed, A., Van Mai, H., Hoang, T. K.A., Trudeau, M., Antonelli, D.M., *J. Phys. Chem C*, **2010**, 114(18), 8651-8660. d) Hoang, T.K.A., Hamaed, A., Trudeau, M., Antonelli, D.M., *J. Phys. Chem. C*, **2009**, 113(39), 17240-17246. e) Hoang, T.K.A., Antonelli, D.M., *Adv. Mater.* **2009**, 21, 1787–1800.
15. Morris, R.H., *Coord. Chem. Rev.*, **2008**, 252, 2381-2394.
16. Yilidrim, T.; Cirati, S., *Phys Rev Lett*, **2005**, 94, 1755501.
17. Zhao, Y., Kim, Y.-H., Dillon, A.C., Heben, M.J., Zhang, S.B., *Phys Rev Lett*, **2005**, 94, 155504.
18. a) Velde, G. te, Bickelhaupt, F.M., Van Gisbergen, S.J.A., Fonseca Guerra, C., Baerends, E.J., Snijders, J.G., and Ziegler, T., *J. Comput. Chem.*, **2001**, 22, 931
b) Fonseca Guerra, C., Snijders, J.G., Velde G. te, and Baerends, E.J., *Theor. Chem. Acc.*, **1998**, 99, 391 c) ADF2009.01, SCM, Theoretical Chemistry, Vrije Universiteit, Amsterdam, The Netherlands, <http://www.scm.com>
19. a) Perdew, J.P., Burke, K., and Ernzerhof, M., *Phys. Rev. Lett.*, **1996**, **77**, 3865 b)

- Perdew, J.P., Burke, K., and Ernzerhof, M., *Phys. Rev. Lett.*, **1997**, 78, 1396.
20. a) Raffenetti, R.C., *J. Chem. Phys.*, **1973**, 59, 5936 b) Chong, D.P., *Can. J. Chem.*, **1995**, 73, 79 c) Zeiss, G.D., Scott, W.R., Suzuki, N., Chong D.P., and Langhoff, S.R., *Mol. Phys.*, **1979**, 37, 1543 d) Van Lenthe, E., and Baerends, E. J., *J. Comput. Chem.*, **2003**, 24, 1142 e) Chong, D.P., Van Lenthe, E., Van Gisbergen, S.J.A., and Baerends, E.J., *J. Comp. Chem.*, **2004**, 25, 1030.
21. Gaussian 03, Revision E.01, Frisch, M.J., Trucks, G.W., Schlegel, H.B., Scuseria, G.E., Robb, M.A., Cheeseman, J.R., Montgomery, J.A. Jr., Vreven, T., Kudin, K.N., Burant, J.C., Millam, J.M., Iyengar, S.S., Tomasi, J., Barone, V., Mennucci, B., Cossi, M., Scalmani, G., Rega, N., Petersson, G. A., Nakatsuji, H.; Hada, M.; Ehara, M.; Toyota, K.; Fukuda, R.; Hasegawa, J.; Ishida, M.; Nakajima, T., Honda, Y., Kitao, O., Nakai, H., Klene, M., Li, X., Knox, J.E., Hratchian, H.P., Cross, J.B., Bakken, V., Adamo, C., Jaramillo, J., Gomperts, R., Stratmann, R.E., Yazyev, O.; Austin, A.J., Cammi, R., Pomelli, C., Ochterski, J. W., Ayala, P.Y., Morokuma, K., Voth, G.A., Salvador, P., Dannenberg, J.J., Zakrzewski, V.G., Dapprich, S., Daniels, A.D., Strain, M.C., Farkas, O., Malick, D.K., Rabuck, A.D., Raghavachari, K., Foresman, J.B., Ortiz, J.V., Cui, Q., Baboul, A.G., Clifford, S., Cioslowski, J., Stefanov, B.B., Liu, G., Liashenko, A., Piskorz, P., Komaromi, I., Martin, R.L., Fox, D.J., Keith, T., Al-Laham, M. A., Peng, C.Y., Nanayakkara, A., Challacombe, M., Gill, P.M.W., Johnson, B., Chen, W., Wong, M.W., Gonzalez, C., and Pople, J.A., Gaussian, Inc., Wallingford CT, **2004**.
22. a) Dunning, T.H. Jr., and Hay, P.J., Schaefer III, H.F. (Ed), *Modern Theoretical*

Chemistry, Vol. 3, 1-28, Plenum, New York, **1976** b) Fuentealba, P., Preuss, H., Stoll, H., and Szentpaly, L.V., *Chem. Phys. Lett.*, **1989**, 89, 418 c) Szentpaly, L.V., Fuentealba, P., Preuss, H., and Stoll, H., *Chem. Phys. Lett.*, **1982**, 93, 555 d) Fuentealba, P., Stoll, H., Szentpaly, L.V., Schwerdtfeger, P., and Preuss, H., *J. Phys. B*, **1983**, 16, 1323 e) Stoll, H., Fuentealba, P., Schwerdtfeger, P., Flad, J., Szentpaly, L.V., and Preuss, H. *J. Chem. Phys.*, **1984**, 81, 2732 f) Fuentealba, P., Szentpaly, L.V., Preuss, H., and Stoll, H., *J. Phys. B*, **1985**, 18, 1287 g) Wedig, U., Dolg, M., Stoll, H., and Preuss, H., *Quantum Chemistry: The Challenge of Transition Metals and Coordination Chemistry*, Veillard, Reidel, and Dordrecht (Eds), **1986**, 79 h) Dolg, M., Wedig, U., Stoll, H., and Preuss, H., *J. Chem. Phys.*, **1987**, 86, 866 i) Igel-Mann, G., Stoll, H., and Preuss, H., *Mol. Phys.*, **1988**, 65, 1321 j) Dolg, M., Stoll, H., and Preuss, H., *J. Chem. Phys.*, **1989**, 90, 1730 k) Schwerdtfeger, P., Dolg, M., Schwarz, W.H.E., Bowmaker, G.A., and Boyd, P.D.W., *J. Chem. Phys.*, **1989**, 91, 1762 l) Dolg, M., Stoll, H., Savin, A., and Preuss, H., *Theor. Chim. Acta*, **1989**, 75, 173 m) Andrae, D., Haeussermann, U., Dolg, M., Stoll, H., and Preuss, H., *Theor. Chim. Acta*, **1990**, **77**, 123 n) Kaupp, M., Schleyer, P.V.R., Stoll, H., and Preuss, H., *J. Chem. Phys.*, **1991**, 94, 1360 o) Kuechle, W., Dolg, M., Stoll, H., and Preuss, H., *Mol. Phys.*, **1991**, 74, 1245 p) Dolg, M., Fulde, P., Kuechle, W., Neumann, C.-S., and Stoll, H., *J. Chem. Phys.*, **1991**, 94, 3011 q) Dolg, M., Stoll, H., Flad, H.-J., and Preuss, H., *J. Chem. Phys.*, **1992**, 97, 1162 r) Bergner, A., Dolg, M., Kuechle, W., Stoll, H., and Preuss, H., *Mol. Phys.*, **1993**, 80, 1431 s) Dolg, M., Stoll, H., and Preuss, H., *Theor. Chim. Acta*, **1993**, 85, 441 t) Dolg, M., Stoll, H., Preuss,

- H., and Pitzer, R.M., *J. Phys. Chem.*, **1993**, 97, 5852 u) Haeussermann, U., Dolg, M., Stoll, H., and Preuss, H., *Mol. Phys.*, **1993**, 78, 1211 v) Kuechle, W., Dolg, M., Stoll, H., and Preuss, H., *J. Chem. Phys.*, **1994**, 100, 7535 w) Nicklass, A., Dolg, M., Stoll, H., and Preuss, H., *J. Chem. Phys.*, **1995**, 102, 8942 x) Leininger, T., Nicklass, A., Stoll, H., Dolg, M., and Schwerdtfeger, P., *J. Chem. Phys.*, **1996**, 105, 1052 y) Cao, X.Y., and Dolg, M. *J. Chem. Phys.*, **2001**, 115, 7348 z) Cao X.Y., and Dolg, M., *J. Mol. Struct. (Theochem)*, **2002**, 581, 139
23. a) Ditchfield, R., Hehre, W.J., and Pople, J.A., *J. Chem. Phys.*, **1971**, 54, 724 b) Hehre, W. J., Ditchfield, R., and Pople, J.A., *J. Chem. Phys.*, **1972**, 56, 2257 c) Hariharan, P.C., and Pople, J.A., *Mol. Phys.*, **1974**, 27, 209 d) Gordon, M.S., *Chem. Phys. Lett.*, 1980, **76**, 163 e) Hariharan P.C., and Pople, J.A., *Theo. Chim. Acta*, **1973**, 28, 213 f) Blaudeau, J.-P., McGrath, M.P., Curtiss, L.A., and Radom, L., *J. Chem. Phys.*, **1997**, 107, 5016 g) Francl, M.M., Pietro, W.J., Hehre, W.J., Binkley, J.S., DeFrees, D.J., Pople, J.A., and Gordon, M.S., *J. Chem. Phys.*, **1982**, 77, 3654 h) Binning, R.C. Jr., and Curtiss, L.A., *J. Comp. Chem.*, **1990**, 11, 1206 i) Rassolov, V.A., Pople, J.A., Ratner, M.A., and Windus, T.L., *J. Chem. Phys.*, **1998**, 109, 1223 j) Rassolov, V.A., Ratner, M.A., Pople, J.A., Redfern, P.C., and Curtiss, L.A., *J. Comp. Chem.*, **2001**, 22, 976
24. a) McLean A.D., and Chandler, G.S., *J. Chem. Phys.*, **1980**, 72, 5639 b) Krishnan, R., Binkley, J.S., Seeger, R., and Pople, J.A., *J. Chem. Phys.*, **1980**, 72, 650 c) Wachters, A.J.H., *J. Chem. Phys.*, **1970**, 52, 1033 d) Hay, P.J., *J. Chem. Phys.*, **1977**, 66, 4377 e) Raghavachari, K., and Trucks, G.W. *J. Chem. Phys.*, **1989**, 91, 1062 f) Clark, T., Chandrasekhar, J., Spitznagel, G.W., and

Schleyer, P.V.R., *J. Comp. Chem.*, **1983**, 4, 294 g) Frisch, M.J., Pople, J.A., and Binkley, J.S., *J. Chem. Phys.*, **1984**, 80, 3265.

25. Ziegler T., and Rauk, A., *Theor. Chim. Acta*, 1977, 46, 1.

26. Boys, S.F., Bernardi, F., *Mol. Phys.*, **1970**, 19, 553.

Chapter 6 – Hydride-induced Amplification of Performance and Binding Enthalpies in Alkylchromium (II) Hydrazide Gels for Kubas-type Hydrogen Storage

6.1 Introduction

Steadily increasing oil prices and the tremendous pressure on the international community to control greenhouse gas emissions, make the demand for cleaner, renewable and sustainable energy sources greater than it has ever been.^[1] Dihydrogen is an ideal energy carrier because it contains more energy per gram than any other chemical substance.^[2] However, it has major drawbacks that limit its applicability as a future energy provider. Among these drawbacks are its very low density and the difficulty and energy cost to compress it.^[3,4] For this reason a number of approaches have been developed using chemical substances as carriers. In these materials hydrogen can be bound in the form of an M-H bond (metal hydride),^[5,6] nested in interstitial sites in a metal alloy, or physisorbed to a surface.^[7] However, each of these methods has certain drawbacks. Metal hydrides often have slow kinetics of uptake and release,^[8] alloys are expensive and possess low gravimetric capacities, and physisorption materials must be cooled to 77 K to be effective, making them impractical for on-board application.^[9] To date none of these approaches have reached the 2015 DOE targets of 5.5 wt% and 40 kg/m³.^[10] An often overlooked feature of a hydrogen storage material is the enthalpy of binding. If this value is too high, as in metal hydrides which possess enthalpies generally greater than 70 kJ/mol, large quantities of heat are released on charging and heat is required to drive the hydrogen off when it is required by the engine.^[11] If this value is too low, as in physisorption materials which generally possess

enthalpies lower than 10 kJ/mol, the hydrogen does not adhere strongly enough to the material and energy-consuming cryogenic temperatures are required.^[12] Recent calculations by several groups predicted that Kubas type binding of hydrogen to a transition metal center should possess enthalpies of 20-30 kJ/mol, predicted to be ideal for room temperature applications.^[13] This was confirmed in our group by measurements on mesoporous silica materials with Ti(III) benzyl fragments on the surface.^[14] These materials possessed enthalpies which rise on surface coverage to 22 kJ/mol. This rising behavior is highly unusual and has been observed in our group on all materials in which Kubas type binding is proposed. The Ti (III) units on the surface were able to improve the hydrogen adsorption capacity of the material from 1.2 wt% at 65 atm and 77 K to 2.4 wt% under the same conditions. This corresponded to an average of 3.2 H₂ per Ti. At room temperature these fragments retained 40 % of their activity, demonstrating that the higher enthalpies of binding improved room temperature performance as anticipated. The major drawback of these materials is that performance drops off with surface coverage higher than 0.6 Ti/nm² due to cluster formation. This means that the majority of hydrogen storage in these systems is still traditional physisorption. Also low coordinate Ti metal complexes are very unstable and difficult to handle due to their high sensitivity to O₂, moisture and light.^[15] For this reason materials which have much higher percentages of the crucial transition metal must be synthesized. These materials must possess metals in low oxidation states for effective Kubas binding, the metal must be in a low coordinate environment to allow maximum hydrogen binding, and they should be moderately stable. The metal and support structure must also be light, so as not to affect gravimetric performance. In 2010,^[16] we

reported silica grafted with Cr(II) material that shows a major increase of its adsorption capacity and binding enthalpy as a result of hydrogenation at 170 °C and 85 atm. We also reported a new cyclopentadienyl Cr hydrazide gel, which uses hydrazine as a linker to incorporate a high concentration of low coordinate Cr sites useful for Kubas binding. These materials possess linear isotherms, enthalpies that rise on surface coverage to 45 kJ/mol, and retain 49% of their adsorption at room temperature as opposed to 77 K (1.8 wt%). For this reason they must be considered a new class of hydrogen storage materials distinct from hydrides and physisorption materials. The main drawback of these materials was that one cyclopentadienyl group per Cr was retained, thus blocking coordination sites that could be used for hydrogen. For this reason precursors containing more readily cleaved primary alkyl ligands in place of cyclopentadienyl groups may lead to final products with a higher concentration of free coordination sites per unit volume. In this paper we present novel Cr(II) hydrazide gels in which the multiply bridging hydrazide ligand supports a vast network of low valent, low coordinate Cr units for Kubas binding.

6.2 Experimental

Chemicals were purchased from Aldrich and used as is. Solvents for handling air-sensitive materials were also used.

6.2.1 Preparation of bis[(trimethylsilyl) methyl]chromium(II) or



To a stirred suspension of CrCl₂ (4.8 mmol) in hexane, was added a solution of (CH₃)₃Si CH₂Li (18.1 mmol) also in hexane. The color of the slurry changed to dark purple after a few hours. The mixture was stirred at RT for 2 days, and then filtered, and the

residue was washed with three portions of hexane (10 ml each). The solution was concentrated to 50 ml and allowed to stand at -34 °C for 12 h. The color of the solution slowly turned brown upon standing at that temperature. The product was isolated by cold filtration, washed twice with pre-cooled hexane and dried *in vacuo*.

6.2.2 Preparation of anhydrous hydrazine: Pure hydrazine was prepared from hydrazine monohydrate by azeotropic distillation with toluene to remove water and avoid possible explosion. 100 ml of hydrazine monohydrate and 250 ml of toluene were added to a 500 ml one neck round bottom flask, equipped with a thermometer to measure the gas temperature. **Hydrazine is toxic, corrosive and flammable; it should be handled with extreme care.**^[18] A water condenser was connected and followed by 2 flashes to collect the waste liquid and dry hydrazine. After distillation and removal of water 35 g of NaOH was added to the hydrazine-toluene flask and the hydrazine was distilled under nitrogen.^[18]

6.2.3 Preparation of 1:1 chromium hydrazide gel (Cr-MHZ (1.0)): In a typical synthesis, the Cr-MHZ (1.0) sample was synthesized as follows: bis[(trimethylsilyl)methyl]chromium (6.50 g, 31.64 mmol) was dissolved in 150 ml of dry toluene at room temperature in a Schlenk tube. 1.014 ml of hydrazine (1.014 ml, 31.64 mmol) was then added by syringe with vigorous stirring. The stirring was continued for 24 hours. The solution was then heated to 50 °C for 24 hours, to 80 °C for 24 hours and to 100 °C for another 24 hours with stirring. After this, the solution was filtered and a black solid was obtained. This solid was washed with hexane and was then transferred to an air-free tube and divided into 3 aliquots. One aliquot was dried at room temperature under

vacuum for 4h, the other two aliquots were dried by heating at 100 °C for a period of 8 hours for one of them and at 150 °C for 8 h for the other one.

6.2.4 Preparation of Cr-MHZ (0.5), Cr-MHZ (1.5), Cr-MHZ (2.0): The same procedure was followed as with the Cr-MHZ (1.0) for the preparations of Cr-MHZ (0.5), Cr-MHZ (1.5), Cr-MHZ (2.0), but with 0.507, 1.521, and 2.028 ml of hydrazine respectively.

6.2.5 Hydrogenation of Cr-MHZ: The hydrogenation of all chromium hydrazide samples was conducted by treating the sample loaded onto the sample chamber of a gas reaction controller (GRC) with pure hydrogen for 4 hours at 85 atm and 180 °C. This optimal hydrogenation condition was obtained by running a series of hydrogenation reactions at 100 °C and 85 atm for 2 hours; at 100 °C and 85 atm for 24 hours; at 150 °C and 85 atm for 4 hours; at 180 °C and 85 atm for 4 hours; and at 200 °C and 85 atm for 4 hours. The reaction was monitored by IR. The C-H stretch peak at $< 3000 \text{ cm}^{-1}$ decreases and a new peak assigned to Cr-H appears at $1700\text{-}2300 \text{ cm}^{-1}$. The hydrogenation reaction is considered complete when the intensity of the C-H stretch peak approaches zero.

6.2.6 Infra-red Spectroscopy: The infrared spectroscopy was conducted on a Bruker Vector 22 instrument. In a typical experiment, 7 mg of sample was mixed with 600 mg of dry KBr and the pellet was made in a dry box. The pellet was then transferred to the IR instrument in a capped vial and the measurement was conducted immediately.

Nitrogen adsorption and desorption data were collected on a Micromeritics ASAP 2010.

6.2.7 Hydrogen adsorption measurements

Hydrogen adsorption isotherms were obtained by using a computer controlled commercial Gas Reaction Controller manufactured by Advanced Materials Corporation, Pittsburgh, PA. High purity hydrogen (99.9995% purity) was used as the adsorbent. Hydrogen storage measurements on a standard AX-21 sample (4.5 wt. %) were performed to ensure proper calibration and functioning of the instrumentation. Leak testing was also performed during each measurement by checking for soap bubbles at potential leak points. These measurements are necessary to ensure the veracity of the isotherms. In the H₂ adsorption-desorption experiments complete reversibility was observed for all samples across the whole range of pressures. Samples were run at liquid nitrogen temperature (77K), liquid argon temperature (87K), and room temperature (298K) to 85 bar. Isotherms were always measured first at room temperature and then at 77 K or 87 K and the temperature is kept constant by keeping the sample chamber in liquid N₂, liquid Ar, or water. The skeletal density was measured using a Quantachrome Ultrapycnometer. When the skeletal density is used for the gravimetric hydrogen uptake measurement, the compressed hydrogen within the pores is treated as part of the sample chamber volume and hence subtracted. Therefore only the hydrogen contained on or beneath the walls of the structure will be recorded by the PCI instrument. This gravimetric value is termed the adsorption or excess storage. When the bulk density is used the hydrogen in the pores of the sample is automatically included in the calculation without any further correction factors and the final value is termed the total storage^[19] or absolute storage,^[20] which represents all hydrogen contained in the sample including the compressed gas in the voids and the hydrogen adsorbed on or beneath the walls of the structure. Gravimetric densities are recorded as read from the isotherms while

volumetric densities are calculated from the adsorption data and the skeletal or bulk density, depending on the desired value. The excess volumetric storage is typically calculated from the excess storage and the bulk density and gives a measure of the gas adsorbed on or in the solid phase of the material scaled across the entire volume occupied by the sample including the void space. In materials such as MOFs that possess a well-defined and constant ratio between mass and void space this value is often quoted. For compressible materials that may have variable ratios of solid mass and void space it can often help to scale the volumetric density to the solid phase alone as the void space will vary on sample preparation. For this purpose, we define the true volumetric adsorption as the amount of hydrogen adsorbed on or in the solid portion of the sample. This is calculated from the excess storage data and the skeletal density. This value neglects the void space and is useful in comparing volumetric densities of ball-milled powders and gels to pure solid phase materials such as metal hydrides. Since the materials in this study are between hydrides and physisorption materials in their mechanism of storage, this value is important. It also allows us to compare volumetric adsorption values of the solid phase alone from one sample to another without having to subtract out the void space. The absolute volumetric adsorption has also been defined^[20] and is a representation of the sum of the excess volumetric storage plus the compressed gas in the void space. This can be calculated from the volumetric storage as measured from the instrument and the bulk density, or by taking the volumetric adsorption and adding on the amount in the void space calculated from the pore volume and the ideal gas law.^[20] The first method is only possible when using the Advanced Materials instrument. In this paper we have chosen not to calculate this value (or the total

gravimetric storage) because the differences between the skeletal densities and bulk densities are much smaller than in MOFs and hence the void space contribution is negligible and will vary due to sample preparation.

Enthalpies of adsorption were calculated using a variant of the Clapeyron – Clausius I equation taking both 77 K and 87 K hydrogen excess storage data.^[21]

$$\ln\left(\frac{P_2}{P_1}\right) = -\Delta H_{\text{adsorption}} \frac{T_2 - T_1}{R \cdot T_2 \cdot T_1} \quad (1)$$

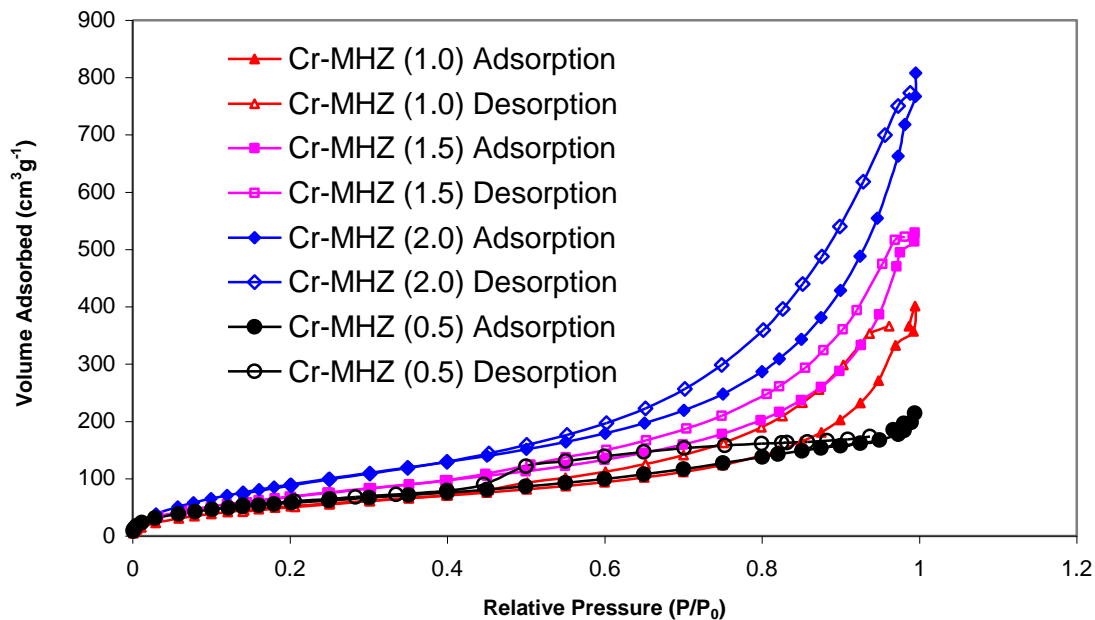
Where P_n = pressure for isotherm n , T_n = temperature for isotherm n , R : gas constant. Pressure as a function of the amount adsorbed was determined by using exponential fit for each isotherm; the first 10 – 11 points of the isotherms were picked up and fit to the exponential equation. This exponential equation gives an accurate fit over the pressure up to 1 MPa with the goodness of fit (R^2) above 0.99. The corresponding P_1 and P_2 values at a certain amount of H_2 adsorbed at both temperatures can be obtained by the simulated exponential equation. Inputting these numbers into equation 1, we then calculate the adsorption enthalpies.

6.3 Results and Discussion

Bis[(trimethylsilyl) methyl] chromium (II), obtained from the reaction of $CrCl_2$ and (trimethylsilyl) methyl Li, was mixed with anhydrous hydrazine in dry toluene. The molar ratio of bis[(trimethylsilyl) methyl]chromium(II) to hydrazine was varied according to the ratios 2: 1, 1:1, 1:1.5 and 1:2 and the as-synthesized Cr- hydrazide samples given the following annotations: Cr-MHZ (0.5), Cr-MHZ (1.0), Cr-MHZ (1.5) and Cr-MHZ (2.0) corresponding to Cr-to hydrazine in molar ratios of 2: 1, 1:1, 1:1.5 and 1:2 respectively.

After mixing the Bis[(trimethylsilyl) methyl]chromium(II) with the appropriate amount of hydrazine in dry toluene, the mixture was stirred at room temperature for 24 hours then it was heated to 50 °C for 24 hours, followed by another heating at 80 °C for 24 hrs and finally it was heated at 100 °C for 24 hours too. The reaction mixture was then filtered under inert atmosphere, and the dark solid obtained was split into 3 aliquots. The first aliquot was dried at room temperature under vacuum for 4 hours. The second one was dried at 100 °C, under vacuum for 8 hours and the third aliquot was dried under vacuum at 150 °C, for 8 hours. The skeletal density of each sample was then determined and then the excess hydrogen storage capacity was measured. From the 4 sets of results, it was obvious that the drying condition at 100 °C, for 8 hrs under vacuum was optimal. For example, for Cr-MHZ (2.0) the excess storage was 2.01 wt% and 3.47 wt% and 2.79 wt% for room temperature, 100 °C, and 150 °C respectively at 77 K and 80 bar. The room temperature drying conditions were clearly not enough to drive all of the hydrocarbon by protonolysis. On the other hand, a temperature as high as 150 °C, led to structure collapse as confirmed by BET surface area measurements. For instance, the BET surface area of the Cr-MHZ (2.0) decreases from 374 m²/g to 279 m²/g as the drying temperature increases from 100 °C to 150 °C. Nitrogen adsorption isotherms recorded at 77K are shown in Figure 6.1 and 6.2 for the as-synthesized and the hydrogenated samples respectively. These isotherms show a small amount of microporosity comprising ca. 20% the total volume adsorbed, with additional mesoporosity and textural porosity accounting for the remaining adsorption in roughly equal proportions as evidenced by the slow rise between 0.2 and 0.8 P/P₀ and the sharp incline above 0.8 P/P₀, respectively.

Figure 6.1 – Nitrogen adsorption/desorption isotherms of the as-synthesized Cr-MHZ materials.



A proposed structure for the chromium hydrazide gel, product of the reaction of bis[(trimethylsilyl) methyl] chromium(II) with hydrazine, is shown in the Scheme 6.1.

Scheme 6.1 – Proposed structure of Cr-MHZ (before hydrogenation).

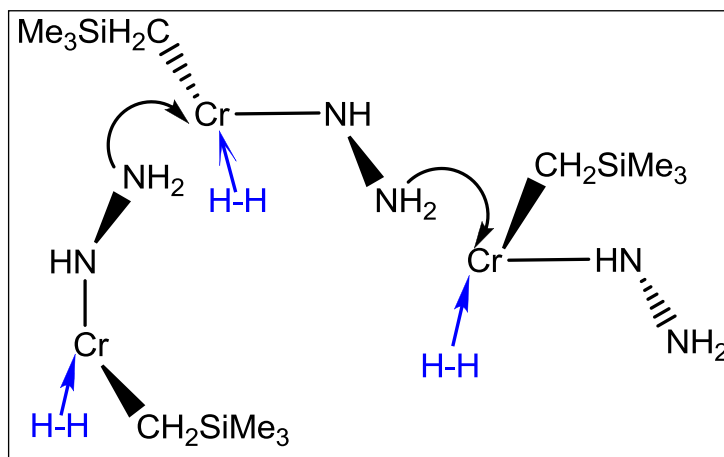
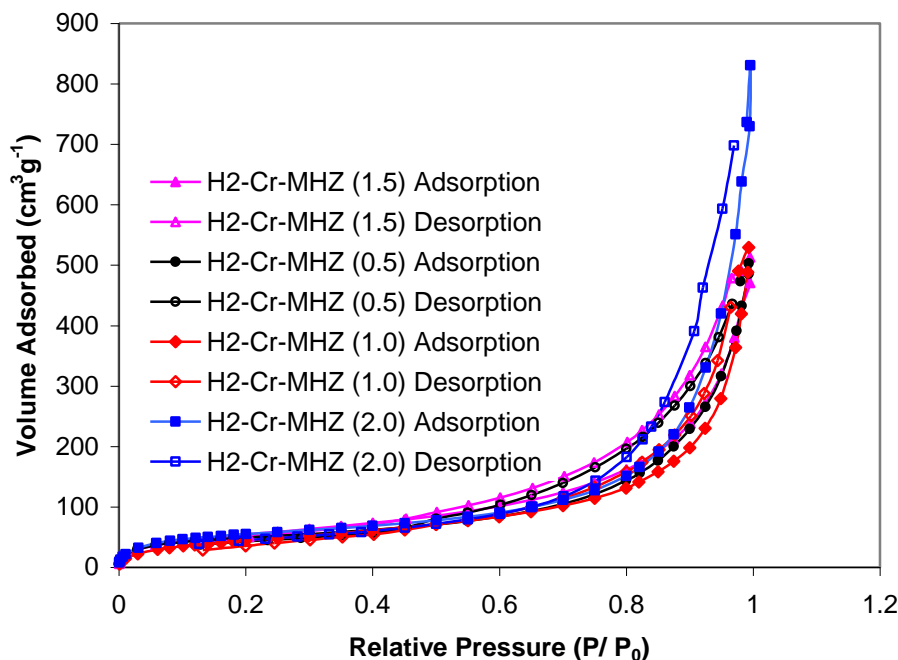
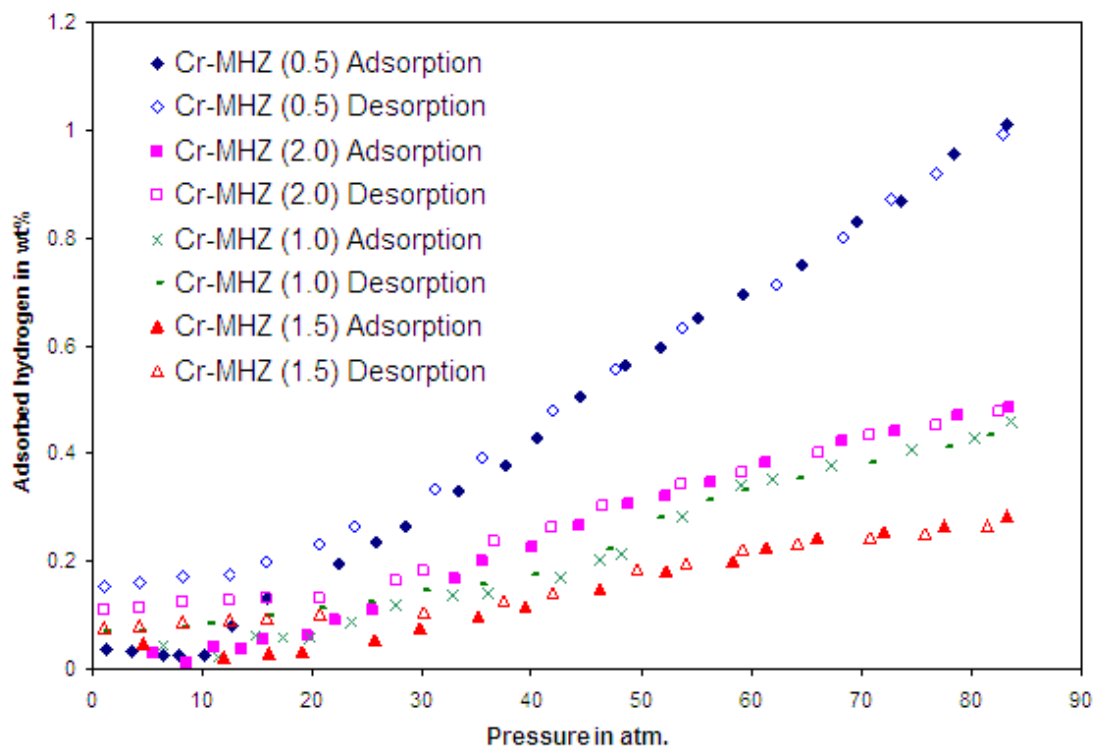


Figure 6.2 – Nitrogen adsorption/desorption isotherms of the hydrogenated Cr-MHZ materials. Samples were measured on ASAP-2010 instrument at 77K.



The room temperature excess storage isotherms of the Cr-MHZ samples prepared in various Cr-to-hydrazine molar ratios are shown in **Figure 6.3**. These room temperature isotherms show very little increase for the H₂ excess storage with pressure up to about 25 bar. After 25 bar the H₂ uptake increases more sharply with pressure and in a linear fashion. The excess storage reached 1.01 wt% for the Cr-MHZ (0.5) at 85 atm, and 0.42 wt%, 0.26 wt%, 0.48wt%, and for the Cr-MHZ (1.0), Cr-MHZ (1.5), and Cr-MHZ (2.0) respectively (Table 1). The BET surface areas for these materials range from 374 m²/g for the Cr-MHZ (2.0) to 210 m²/g for Cr-MHZ (1.0). The isotherms returned on desorption to zero with a slight hysteresis.

Figure 6.3 – Excess storage isotherms at 298K for the as-synthesized Cr-hydrazide samples prepared with various ratios (samples were dried at 100 °C).

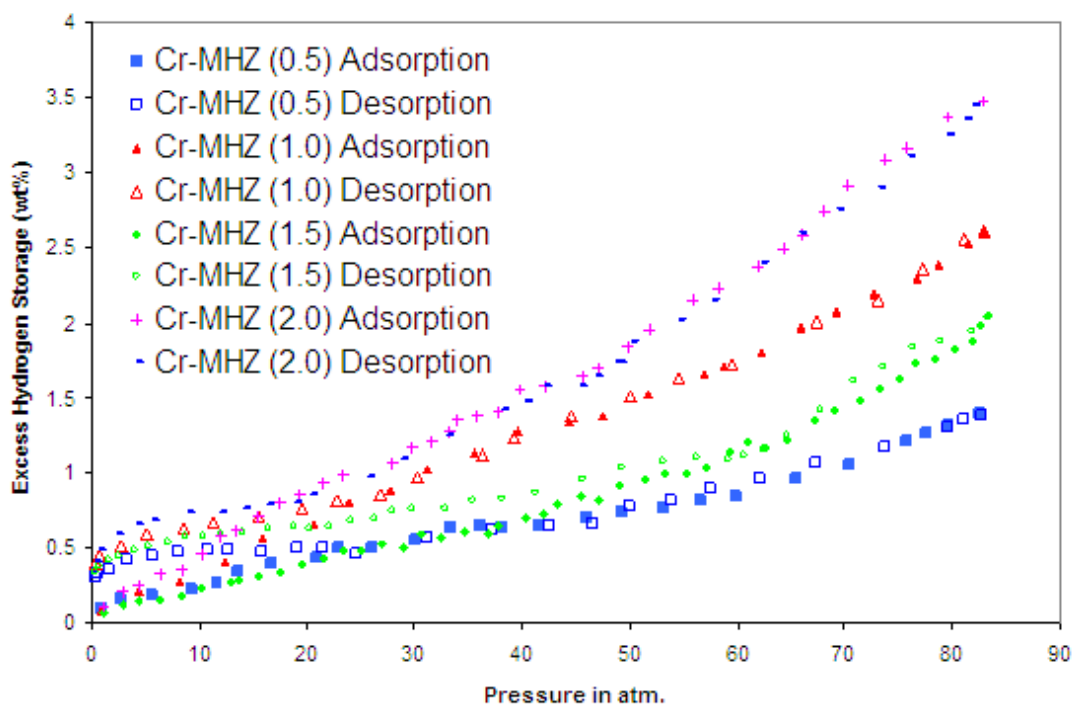


The excess hydrogen storage at 77K for the as-synthesized materials ranges from 3.47 wt% for the Cr-MHZ (2.0) to 1.39 wt% for Cr-MHZ (0.5) as shown in **Figure 6.4**. Therefore, the room temperature storage retention of these materials reaches up to 72.66% in the case of Cr-MHZ (0.5). The skeletal densities of these materials are in the range 1.64-1.32 g/cc. A summary of all data related to the as-synthesized and after hydrogenation chromium hydrazide samples is shown in table 6.1.

Table 6.1 – Summary of excess storage results on chromium hydrazide materials before and after hydrogenation (data are taken at 85 bar, and the samples were dried at the optimal drying temperature of 100 °C).

Material	BET Surface Area (m ² /g)	Skeletal Density (g/cm ³)	Gravimetric Adsorption (wt. %)	Volumetric Adsorption (kg/m ³)	Retention (%)
Cr-MHZ (0.5)	221	1.32	1.39 (at 77K) 1.01 (at 298K)	18.35 (at 77K) 13.33 (at 298K)	73
H ₂ -Cr-MHZ (0.5)	181	1.86	2.28 (at 77K) 1.41 (at 298K)	42.41 (at 77K) 26.23 (at 298K)	62
Cr-MHZ (1.0)	210	1.47	2.02 (at 77K) 0.42 (at 298K)	29.69 (at 77K) 6.17 (at 298K)	21
H ₂ -Cr-MHZ (1.0)	171	1.47	2.05 (at 77K) 1.65 (at 298K)	30.13 (at 77K) 24.25 (at 298K)	80
Cr-MHZ (1.5)	276	1.64	2.05 (at 77K) 0.26 (at 298K)	33.62 (at 77K) 4.264 (at 298K)	13
H ₂ -Cr-MHZ (1.5)	208	1.93	1.87(at 77K) 1.55 (at 298K)	36.09 (at 77K) 29.92 (at 298K)	83
Cr-MHZ (2.0)	374	1.41	3.47 (at 77K) 0.48 (at 298K)	48.93 (at 77K) 6.77 (at 298K)	14
H ₂ -Cr-MHZ (2.0)	203	1.65	1.23 (at 77K) 1.41 (at 298K)	20.29 (at 77K) 23.26 (at 298K)	100

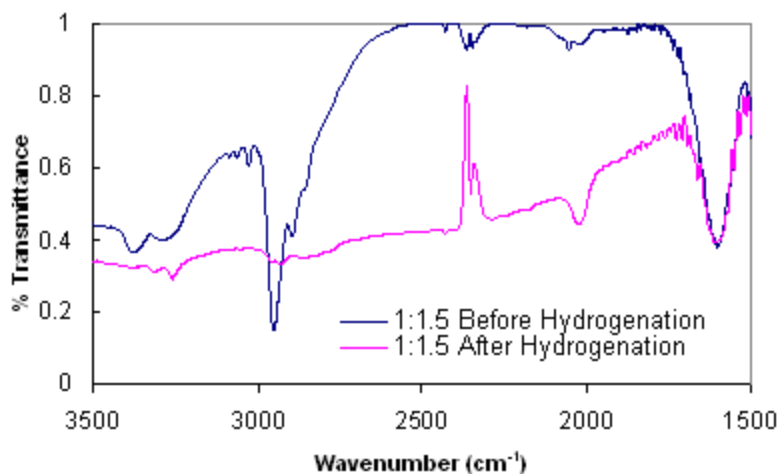
Figure 6.4 – Excess storage isotherms at 77K for the as-synthesized Cr-hydrazide samples prepared with various ratios.



Computational studies,^[22] and experimental investigations^[16] on metal-fragments grafted silica show that M-H moieties are more effective at hydrogen binding than M-R, where R is a bulky ligand. In this work, different hydrogenation conditions were applied to the Cr-MHZ (1.5) aliquots in order to arrive at the right condition for the substitution of the (trimethylsilyl) methyl ligand with a hydride, and the reaction was monitored by IR spectroscopy. The IR spectra were obtained on each sample before and after hydrogen treatment. The Cr-MHZ (1.5) was loaded into the Gas Reaction Controller (GRC), the sample was soaked with H₂ at an initial pressure of 5 atm, then the temperature was set to 100 °C and the pressure was gradually increased to 85 atm. The sample was left at 85 atm and 100 °C for 2 hours, then the IR spectra of the hydrogenated sample was measured. It was found that there was a small decrease in the C-H stretch peak intensity. Another aliquot of the Cr-MHZ (1.5) sample was treated

with hydrogen at the same temperature and pressure as those of the previous aliquot, but was left under these conditions for 24 hours. The IR spectra was measured, and it was found that lengthening the duration of reaction while keeping other factors unchanged does not lead to a substantial decrease in the C-H stretch peak intensity. Therefore, a reaction temperature higher than 100 °C is recommended in order to drive the (trimethylsilyl)methyl ligand out of the Cr coordination sphere. It was found that the 4 hours hydrogenation at 180 °C condition was the optimal hydrogenolysis condition as confirmed by a large decrease in the C-H stretch peak intensity accompanied by the appearance of a peak at about 2000 cm^{-1} , which is assigned to Cr-H stretch as shown in **Figure 6.5** below.

Figure 6.5 – Infra-red spectra of Cr-MHZ (1.5) before (BLUE) and after (PINK) hydrogenation at 180 °C and 85 atm for 4 hours.



The optimal hydrogenation conditions were applied to the other Cr-MHZ synthesized with various Cr to hydrazine molar ratios and the hydrogenation reaction was monitored by running the IR before and after reaction as shown in **Figures 6.6, 6.7 and 6.8**. The IR spectra of the hydrogenated samples exhibit a decrease and sometimes

a total disappearance of the C-H stretch band at 2850-2950 cm^{-1} and the appearance of a new band at 1900-2100 cm^{-1} assigned to a Cr-H stretch.

Figure 6.6 – Infra-red spectra of Cr-MHZ (1.0) before (BLUE) and after (PINK) hydrogenation at 180 °C and 85 atm for 4 hours.

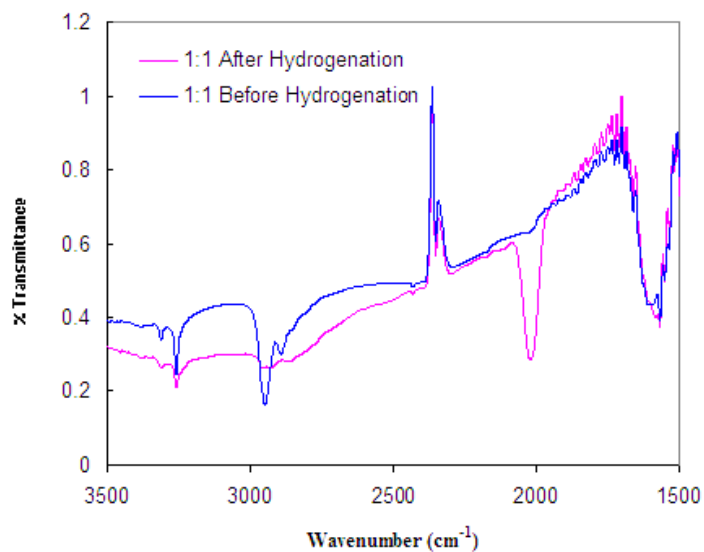


Figure 6.7: Infra-red spectra of Cr-MHZ (2.0) before (BLUE) and after (PINK) hydrogenation at 180 °C and 85 atm for 4 hours.

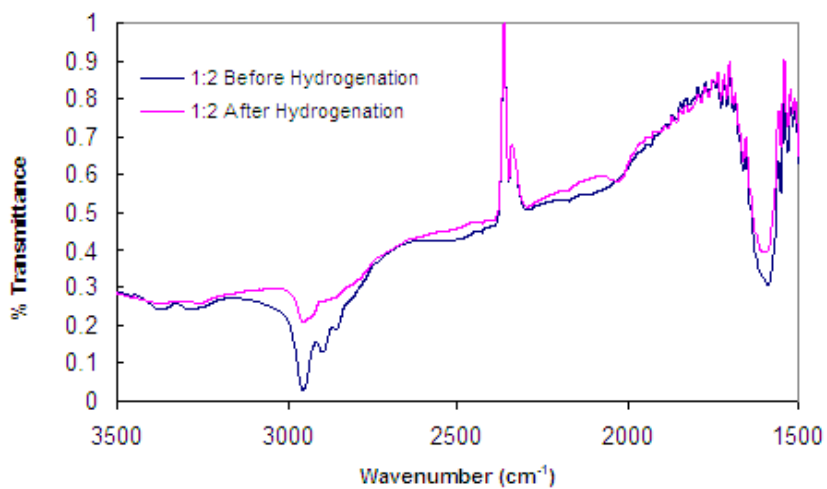
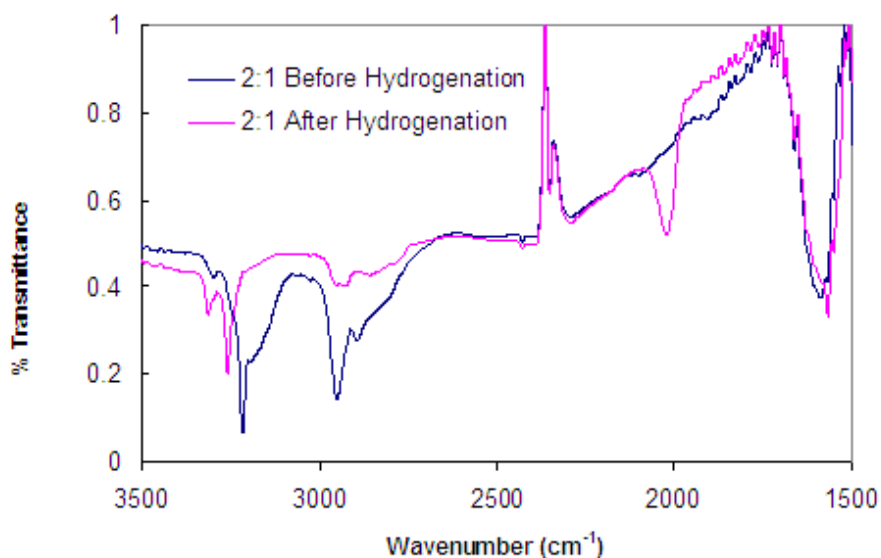
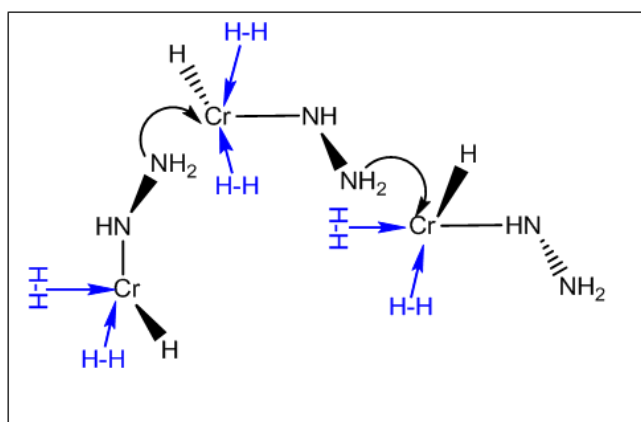


Figure 6.8 – Infra-red spectra of Cr-MHZ (0.5) before (BLUE) and after (PINK) hydrogenation at 180 °C and 85 atm for 4 hours.



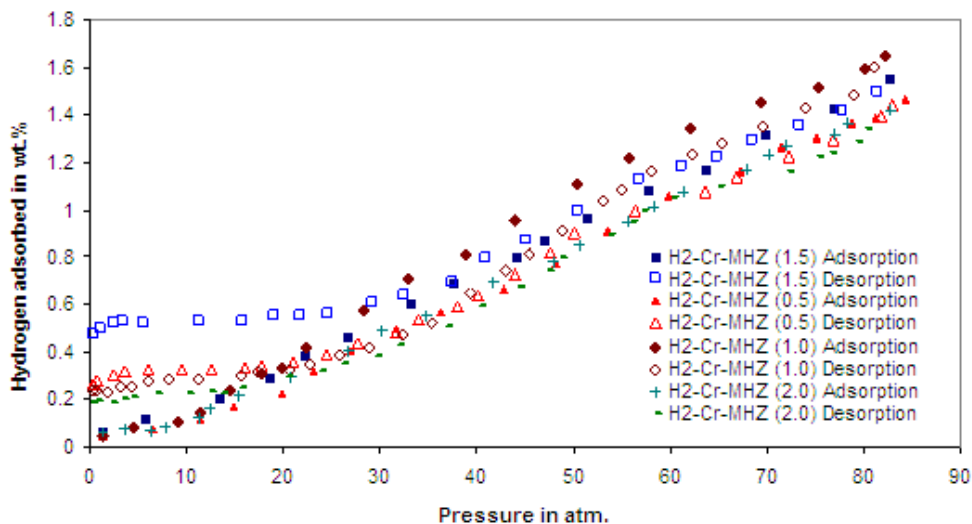
Scheme 6.2 illustrates a proposed structure of the chromium hydrazide gels after complete hydrogenation. The Cr-H moieties are considered as much more favorable at binding hydrogen than any other Cr-ligand moiety according to experiment and computation. The BET surface areas of the hydrogenated samples were in the range 171-208 m²/g and they were always lower than their non-hydrogenated counterparts.

Scheme 6.2 – Proposed structure of Cr-MHZ (after hydrogenation).



The room temperature performance of the hydrogenated chromium hydrazides reached as high as 1.65 wt% at 298 K and 85 bar for the H₂-Cr-MHZ (1.0), which equates to 24.27 kg/m³ of true volumetric density. Whereas, H₂-Cr-MHZ (1.5) uptakes 1.55 wt% under the same conditions, which translates to a true volumetric density of 29.92 kg/m³, since this sample has a slightly higher density than that of the H₂-Cr-MHZ (1.0). To our knowledge these results are the highest room temperature hydrogen excess storage ever. It is also of great importance the amplification in the adsorption capacity as a result of a simple hydrogenolysis reaction. For example, hydrogenation of Cr-MHZ (1.5) pushes its hydrogen excess storage to 1.55 wt%, which is about 6 fold its hydrogen capacity value before hydrogenation. The excess room temperature storage isotherms for the hydrogenated chromium metal hydrazides (H₂-Cr-MHZ) in various ratios are shown in Figure 6.9 below.

Figure 6.9 – Room temperature excess storage isotherms of Cr-hydrazides prepared with various ratios after hydrogenation at 180 °C and 85 atm for 4 hours.



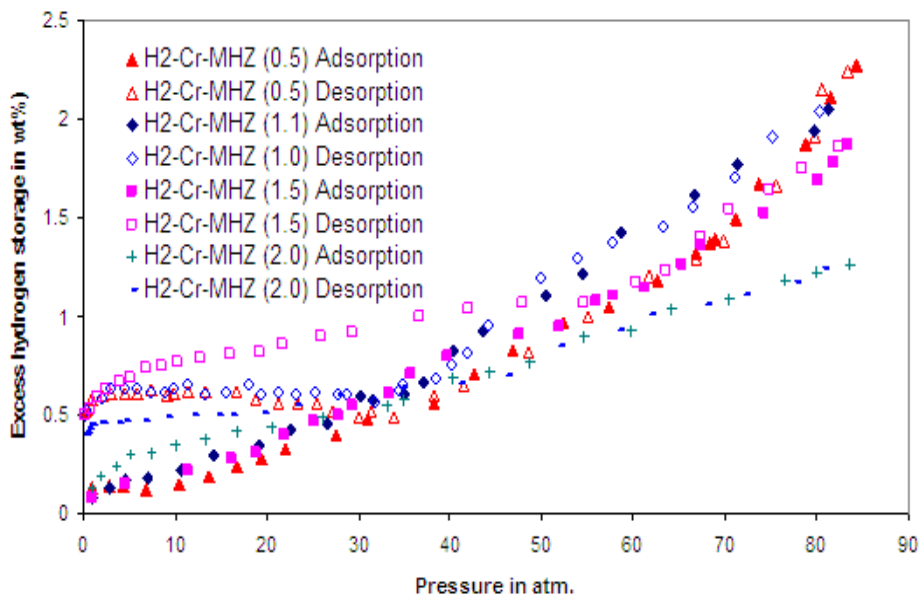
The fact that these isotherms are linear and do not saturate indicate that excess storage values will be higher at higher pressures. 200 bar defines the upper limit of safe

storage for transportation, and it is conceivable that these materials may possess excess storage values as high as 2.5 times their values at 80 bar under these conditions. If this is so, these materials would become attractive as practical solutions to hydrogen storage.

A pellet was made by compressing the H₂-Cr-MHZ (1.5) sample at 2500 psi, and the apparent density and total storage were measured. With an apparent density value of 1.275 g/cc, the pellet absorbs 1.45 wt% at room temperature and 2.07 wt% at 77K. This translates into 70% hydrogen retention at room temperature. The absolute room temperature volumetric density of the pellet is therefore 18.49 kg/m³, compared to 10.92 kg/m³ for the MOF-177 at the same conditions.^[23] The pellet absolute volumetric density at 77K is 26.39 kg/m³ which is comparable to that of compressed gas at the conditions (28.05 kg/m³ at 85 atm), without the disadvantage of the energy loss during the compression procedure.^[24] The relatively small difference of apparent density and the skeletal density of this sample is consistent with a low surface area material with a large degree of textural porosity created by spaces between the particles with only a small amount of microporosity.

The improvement in the room temperature excess storage performance is attributed to the amplification in the binding enthalpies values as the bulky (trimethylsilyl) methyl ligand was substituted with a hydride. Hydride has the advantage of being a weak electron withdrawing group, with the least steric hindrance around the metal center thanks its small size. The excess storage isotherms of the hydrogenated samples at 77 K do not show any improvement over those of the nonhydrogenated ones at the same temperature (**Figure 6.10**).

Figure 6.10 – Excess storage isotherms of Cr-hydrazides prepared with various ratios at 77K after hydrogenation.

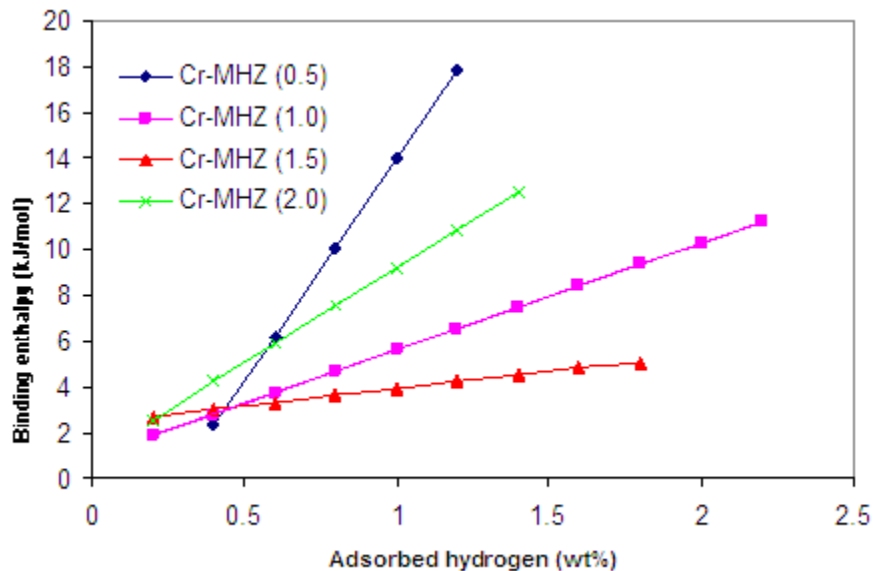


This is likely because hydrogenation does not affect the overall number of vacant coordination sites, but only the binding enthalpy of these coordination sites. At 77 K hydrogen can bind effectively to a surface with enthalpies of lower than 5 kJ/mol, while enthalpies of at least 15-20 kJ/mol are required for substantial room temperature binding. Thus hydrogenation has a much greater impact on room temperature performance than it does at 77 K. We have seen this trend in previous work involving low valent, low coordinate transition metal fragments on silica surfaces.

The hydrogen binding enthalpies of the as-synthesized Cr-MHZ samples (Figure 6.11) rise with the hydrogen loading level up to 17.86 as in the case of H₂-Cr-MHZ (0.5). This relatively high binding enthalpy is manifested by the 1.01 wt% hydrogen retention at room temperature. The other nonhydrogenated Cr-MHZ have binding enthalpies in the ranges 2.55-12.54 kJ/mol, 1.87-11.22 kJ/mol and 2.55-5.03 kJ/mol for

Cr-MHZ (2.0), Cr-MHZ (1.0), and Cr-MHZ (1.5) respectively. The higher is the upper range of the binding enthalpy, the higher is the excess storage capacity at 298 K.

Figure 6.11 – Binding enthalpies for the as-synthesized chromium hydrazide samples prepared in various ratios.



For the hydrogenated samples the binding energies increase much steeper with H₂ loading than those of the unhydrogenated samples and reached 22.9 kJ/mol, and 22.1 kJ/mol for H₂-Cr-MHZ (2.0), H₂-Cr-MHZ (1.5), respectively, and rises to 50.24 kJ/mol and 51.58 kJ/mol as for H₂-Cr-MHZ (1.0) and H₂-Cr-MHZ (0.5), respectively, as shown in Figure 6.12. These binding enthalpy values in the optimal range for ambient temperature hydrogen storage are the reason behind the promising room temperature excess storage of the hydrogenated chromium hydrazides.

A 20 cycle run of adsorption and desorption at 298 K and with pressure up to 85 atm was carried out on the Cr-MHZ (1.5) sample as shown in Figure 6.13. There was no excess storage loss between the first and the last run. The adsorption results from all the

runs were in the range 1.49-1.59 wt%, which corresponds to the excess storage capacity \pm the instrumental error.

Figure 6.12 – Binding enthalpies of chromium hydrazides prepared in various ratios after hydrogenation

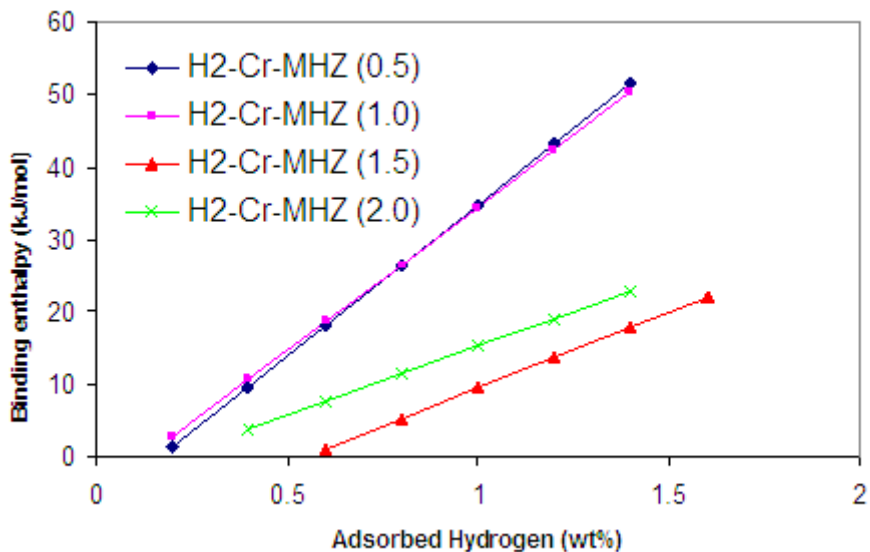
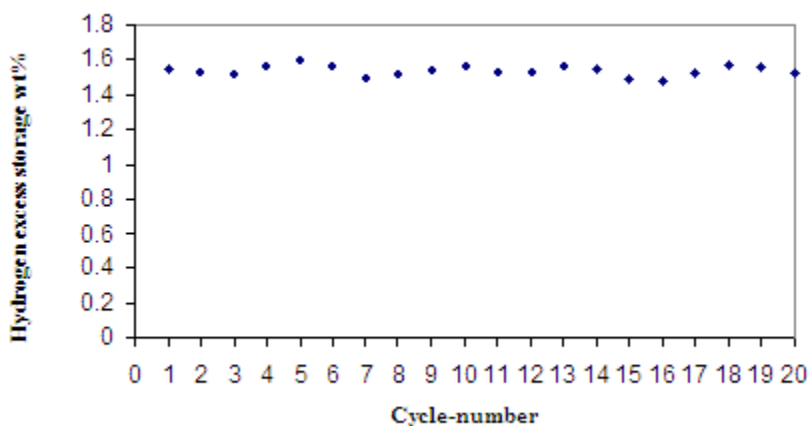


Figure 6.13 - Hydrogen excess storage at 298 K in a 20 cycle test of H₂-Cr-MHZ (1.5).



6.4 Conclusions

New materials containing an extended network of low coordinate chromium metal centers for Kubas-type hydrogen storage were obtained by treating

bis[(trimethylsilyl) methyl]chromium(II) with hydrazine followed by thermal treatment and then hydrogenation. After hydrogenation, there was 3 to 6 fold increase in the adsorption capacity at 298 K, which is attributed to an increase in the binding enthalpies of the Cr center as a result of the substitution of the Cr-[(trimethylsilyl) methyl] moieties with Cr-H moieties. The hydride ligand with its low steric profile and weak electron-withdrawing capability constitutes an optimal ligand in the coordination sphere of the H₂ binding sites. This fact was confirmed by both computational and experimental investigations. Further processing of these materials, in order to get rid of all hydrocarbons from the Cr coordination sphere and the application of higher pressure may lead to materials that meet or surpass the DOE 2015 targets.

6.5 References

1. Murray, L.J., Dincă, M., Long, J.R., *Chem. Soc. Rev.*, **2009**, 38, 1294-1314.
2. Thomas, K.M., *Dalton Trans.*, **2009**, 1487-1505.
3. Rowsell, J.L.C., Yaghi, O., *Angew. Chem. Int. Ed.*, **2005**, 44, 4670-4679.
4. Schlapbach, L., Züttel, A., *Nature*, **2001**, 414, 353-358.
5. Seayad, A.M., Antonelli, D.M., *Adv. Mater.*, **2004**, 16, 765.
6. Hoang, T.K.A., Antonelli, D.M., *Adv. Mater.*, **2009**, 21, 1787-1800.
7. Dincă, M., Long, J.R., *Angew. Chem. Int. Ed.*, **2008**, 47, 6766-6779.
8. Hamilton, C.W., Baker, R.T., Staubiltz, A., Manners, I., *Chem. Soc. Rev.*, **2009**,

38, 279-293.

9. Germain, J.; Frechet, J.M., Svec, F., *Small*, **2009**, 5 (10), 1098-1111.
10. http://www1.eere.energy.gov/hydrogenandfuelcells/storage/pdfs/targets_onboard_hydro_storage.pdf.
11. Lochan, R.C., Head-Gordon, M., *PhysChemChemPhys*, **2006**, 8, 1357.
12. Bhatia, S.K., Myers, A.L., *Langmuir*, **2006**, 22, 1688-1700.
13. Zhao, Y., Kim, Y.-H., Dillon, A.C., Heben, M.J., Zhang, S.B., *Phys. Rev. Lett.*, **2005**, 94(15), 155504/1-155504/4.
14. Hamaed, A., Trudeau, M., Antonelli, D.M., *J. Am. Chem. Soc.*, **2008**, 130 (22) 6992-6999.
15. a) Hamaed, A., Hoang, T.K.A., Trudeau, M., Antonelli, D.M., *J. Organomet. Chem.*, **2009**, 694(17) 2793-2800. b) Hoang, T.K.A., Hamaed, A., Trudeau, M., and Antonelli, D.M., *J. Phys. Chem. C*, **2009**, 113 (39), 17240-17246.
16. Hamaed, A., Mai, H.V., Hoang, T.K.A., Trudeau, M., and Antonelli, D.M., *J. Phys. Chem. C*, **2010**, 114, 8651-8660.
17. Schulzke, C., Enright, D., Sugiyama, H., LeBlank, G., Gambarotta, S., Yap, L.K., Thomson, G.P.A., Wilson, D.R., and Duchateau, R., *Organometallics*, **2002**, 21(18), 3810-3816.
18. a) Schmidt, E.W., *Hydrazine and its Derivatives: Preparation, Properties, Application*, John Wiley & Sons, New York, **2001**, p.99. b) Mai, H.V., Hoang, T.K.A., Hamaed, A., Trudeau, M., and Antonelli, D.M., *Chem. Comm.*, **2010**,

- 46, 3206-3208.
19. Hu, X., Skadtchenko, B.O., Trudeau M., and Antonelli, D.M., *J. Am. Chem. Soc.*, **2006**, 128 (36), 11740-11741.
 20. Furukawa, H., Miller, M.A., Yaghi, O.M., *J. Mater. Chem.*, **2007**, 17 (30), 3197-3204.
 21. Roquerol, F., Roquerol, J., Sing, K., *Adsorption by powders and Solids: Principles, Methodology, and Applications*, Academic Press, London, **1999**.
 22. Skipper, C., Kaltsoyannis, N., *Hydrogen Storage Materials: The Binding of Hydrogen to Transition Metals*, Masters Thesis, **2010**.
 23. Li, Y., Yang, R.T., *Langmuir*, **2007**, 23, 12937-12944.
 24. Züttel, A., Borgschulte, A., Schlapbach, L. (Eds.), *Hydrogen as a Future Energy Carrier*, Wiley-VCH, Weinheim, **2008**.

Chapter 7 – Dissertation Summary and Future Outlook

7.1 Summary

Driven by the rising standards of living and the economic growth in the developing nations, the increasing trend in petroleum fuel demand and consumption that we encountered in the last 8 decades will be more pronounced in the near future.^[1] Hydrogen has been considered as an alternative fuel and the energy currency of the future for many reasons, but its problem of low energy content per unit volume has to be solved.^[2]

Extensive research into the area of hydrogen storage has been going on for decades. However, the relatively cheap oil prices and the little concerns about reserves depletion and the environmental problems caused by oil burning put the search for alternative energy sources at the bottom of the international community's priority list back in the sixties, which is definitely not the case today. However, the 1973 energy crisis led to greater interest in alternative, renewable energy and spurred the hydrogen storage research. In the early 1980's, a major breakthrough by Kubas and co-workers^[3] in the field of H₂ coordination chemistry initiated the beginning of a new era in coordination chemistry research and later on hydrogen storage research.

Metal organic frameworks materials^[4] have attracted lots of attention in the last two decades as potential candidates for hydrogen storage, but their application at only cryogenic temperature limits their use as hydrogen storage materials for practical application. In order to improve their usefulness as hydrogen storage materials, MOFs H₂ binding enthalpies are to be in the optimal range for adsorption and desorption at

ambient conditions. But this criterion is still far from being realistic for MOF due to the fact that they employ weak dispersive forces for interacting H₂ molecules with the binding sites. Many attempts have been made to improve the binding enthalpies in MOF materials, for instance, via frameworks interpenetration and catenation or by introduction of high concentrations of exposed metal ions within the surfaces of the structure, however these modifications were not enough to meet practical demands.^[5]

In this thesis, a strategy for designing hydrogen storage materials by looking at model systems with the ideal enthalpy for room temperature storage has been devised. On the basis of the metal-fragments grafted silicas results,^[6-8] extended solids with binding sites of the same characteristics as those of silica framework materials but with a higher percentage of metal in order to maximize uptake were synthesized.^[9,10] These novel metal hydrazide gels use low-coordinate early transition metal centers interconnected via hydrazine bridges. The newly devised and synthesized materials have excess hydrogen storage of up to 1.65 wt% with a true volumetric density up to 29.9 kg/m³ at 85 atmosphere, and ambient temperature, with a negligible contribution from physisorption. The excess gravimetric storage at 298 K of our best material (1.65 wt%, at 85 atm) is more than triple that of the best MOF (MOF-177, 0.52 wt%, at 85atm),^[11] with a true volumetric density of about 2 kg/m³ over that of compressed gas at the same conditions (28.05 kg/m³ at 85 atm) .^[12]

Our initial work in this area focused on grafting Ti-benzyl fragments on hexagonally-packed mesoporous silica (HMS).^[6] The grafting was achieved by treating HMS with tetrabenzyl or tribenzyl Ti in toluene. The obtained materials, with only ca. 5% Ti by weight, have double the hydrogen uptake as compared to plain silica at 77 K.

with 0.42 wt.% greater hydrogen uptake at room temperature with binding enthalpies of up to 22 kJ/mol (Chapter 2 and 3).

Yildirim^[13] and Heben^[14] had conducted computational studies on transition metals grafted on single-walled nanotubes. They found that single Ti atom coated on a single-walled nanotube (SWNT) may bind up to four hydrogen molecules. In our turn, we tried to further optimize the surface area, pore size and pore volume of the silica framework materials and then maximize the Ti loading level by employing various Ti precursors with ligands of different steric and electronic profiles (methyl, allyl, and benzyl). This optimization led to materials with hydrogen capacity of up to 3.98 H₂/Ti center.^[7] This result is the highest number of Kubas ligands per metal ever observed and was confirmed by computational chemistry calculations (Chapter 5).

To study the effect of metal type, metal oxidation state and ligand environment on the hydrogen storage capacity and binding enthalpy of organometallic-fragments grafted on silica, a series of V, Cr, and Ti metal-fragments supported on HMS silica were prepared and tested for hydrogen storage.^[8] This systematic study showed that the general performance trends were Ti > V > Cr, M(II) > M(III), and M-H > M-R. But the most intriguing result observed was that of the hydrogenation of the supported Cr(II) alkyl species which led to almost doubling the storage capacity at 77K and 85 atm (Chapter 4).

Computational chemistry was employed to investigate the effect of the metal type, metal oxidation state and ancillary ligand on the H₂ adsorption and H₂ binding enthalpy of organometallic grafted on silica.^[15] This study showed that Ti atom can bind up to 4 H₂/atom, and that the binding is of Kubas type, and that to form a strong M-

H₂ bond the ancillary ligand must be a weak π -acceptor, and of low steric profile. This study also proved that a strong correlation exists between the HOMO and LUMO energy levels of the binding site and those of the incoming H₂ molecule. The closer their energy levels are to each other, the stronger is the interaction (Chapter 5).

The valuable results and conclusions drawn from Chapter 2, 3, 4, and 5 were very crucial in the design and synthesis of the chromium-metal hydrazine material which features a higher concentration of Cr metal than those of silica-supported materials and with hydrogen capacity of up to 1.65 wt% at room temperature with very negligible contribution from physisorption, and with binding enthalpy in the optimal range of those of Kubas-interaction.^[16]

Finally, a deep understanding of the types of bonding involved in hydrogen storage as well as the location of the binding sites and the strategies to strengthen, or sometimes to weaken, these bonding interactions are prerequisites to gain insights into the mechanisms of the H₂ interactions and to design hydrogen storage materials that function at ambient temperature.^[17]

7.2 Future Outlook

This research project aims at achieving a promising hydrogen storage technology to the point where driving a hydrogen-fueled car is not only feasible but totally warranted. Once the materials have been optimized to store about 5 kg of hydrogen at room temperature for a driving range of about 500 km, in a volume comparable to that of a gasoline fuel tank, then the only barrier to use these materials in a system will be developing a tank to house the solid. Further materials processing will include metal optimization as well as bulk studies on heat release over pressure in order to gauge

suitability in a tank. One must also consider cost of metals (V is expensive, Cr is moderate, Mn and Ti are cheap). Currents tanks for chemical hydrogen systems are cumbersome and require either complex heat exchanging lines, or dramatic cooling measures to be used in a vehicle. These restrictions are serious and have kept existing technologies from being implemented. Since our materials, with few tunings, are able to make it up to many of the DOE goals and the low enthalpy characteristics of these materials and fast kinetics allow use in 200 bar containers that are conformable to an auto design. We anticipate that a commercially viable solution to hydrogen vehicles may now be only 5 years away. The success of this research will enrich the Canadian economy through sales of high technology products which will be accompanied by a global improvement in environment and health issues associated with toxic emissions and it will eventually lead to greater energy security.

7.3 References

1. Liu, C., Li, F., Lai-Peng, M., Hui-Ming, C., *Adv. Mater.*, **2010**, 22, E28-E62.
2. Fichtner, M., *Adv. Eng. Mater.*, **2005**, 7, 6, 443-455.
3. Kubas, G.J., Ryan, R.R., Swanson, B.I., Vergamini, P.J., Wasserman, H.J., *J. Am. Chem. Soc.*, **1984**, 106, 451.
4. a) Rowsell, J.L.C., Yaghi, O., *Angew. Chem. Int. Ed.*, **2005**, 44, 4670-4679. b) Dincă, M., Long, J.R., *Angew. Chem. Int. Ed.*, **2008**, 47, 6766-6779.
5. Murray, L.J., Dincă, M., Long, J.R., *Chem. Soc. Rev.*, **2009**, 38, 1294-1314.

6. Hamaed, A., Trudeau, M., Antonelli, D.M., *J. Am. Chem. Soc.*, **2008**, 130 (22) 6992-6999.
7. Hamaed, A., Hoang, T.K.A., Trudeau, M., Antonelli, D.M., *J. Organomet. Chem.*, **2009**, 694(17) 2793-2800.
8. Hamaed, A., Mai, H.V., Hoang, T.K.A., Trudeau, M., and Antonelli, D.M., *J. Phys. Chem. C*, **2010**, 114, 8651-8660.
9. Mai, H.V., Hoang, T.K.A., Hamaed, A., Trudeau, M., and Antonelli, D.M., *Chem. Comm.*, **2010**, 46, 3206-3208.
10. Hoang, T.K.A., Webb, M.I., Mai, H.V., Hamaed, A., Trudeau, M., Walsby, C., and Antonelli, D.M., *J. Am. Chem. Soc.*, **2010** (Submitted)
11. Li, Y., Yang, R.T., *Langmuir*, **2007**, 23, 12937-12944.
12. Züttel, A., Borgschutle, A., Schlapbach, L. (Eds.), *Hydrogen as a Future Energy Carrier*, Wiley-VCH, Weinheim, **2008**.
13. Yilidrim, T.; Cirati, S., *Phys Rev Lett*, **2005**, 94, 1755501.
14. Zhao, Y., Kim, Y.-H., Dillon, A.C., Heben, M.J., Zhang, S.B., *Phys. Rev. Lett.*, **2005**, 94(15), 155504/1-155504/4.
15. Skipper, C., Hamaed, A., Kaltsoyannis, N., Antonelli, D., Computational Studies on Silica Supported Transition Metal Fragments for Kubas-Type Hydrogen Storage, *J. Am. Chem. Soc.*, **2010**. (Submitted)
16. Hamaed, A., Hoang, T.K.A., Trudeau, M., Antonelli, D. Hydride-induced

Amplification of Performance and Binding Enthalpies in Alkylchromium (II)
Hydrazide Gels for Kubas- type Hydrogen Storage, (Manuscript in Preparation)

17. Kubas, G.J., *Chem. Rev.*, **2007**, 107, 4152-4205

Appendices

Appendix A – Supplementary Tables for Chapter 6

Table A. 6.1 - Summary of excess storage results on the as-synthesized chromium hydrazide materials for the samples dried at room T (data are taken at 85 bar).

Material	BET Surface Area (m ² /g)	Skeletal Density (g/cm ³)	Gravimetric Adsorption (wt. %)	Volumetric Adsorption (kg/m ³)	Retention (%)
Cr-MHZ (0.5)	575	1.26	1.07 (at 77 K) 0.52 (at 298 K)	13.48(at 77 K) 6.55 (at 298 K)	48.6
Cr-MHZ (1.0)	251	1.38	2.43 (at 77 K) 0.45 (at 298 K)	33.53(at 77 K) 6.21 (at 298 K)	18.5
Cr-MHZ (1.5)	278	1.73	1.81 (at 77 K) 0.37 (at 298 K)	31.31(at 77 K) 6.40 (at 298 K)	20.44
Cr-MHZ (2.0)	332	1.60	2.01 (at 77 K) 0.32 (at 298 K)	32.16(at 77 K) 5.12 (at 298 K)	15.92

Table A. 6.2 - Summary of excess storage results on the as-synthesized chromium hydrazide materials for the samples dried at 150 °C (data are taken at 85bar).

Material	BET Surface Area (m ² /g)	Skeletal Density (g/cm ³)	Gravimetric Adsorption (wt. %)	Volumetric Adsorption (kg/m ³)	Retention (%)
Cr-MHZ (0.5)	171	1.76	0.77 (at 77 K) 0.62 (at 298 K)	13.55 (at 77 K) 10.91 (at 298 K)	80.53
Cr-MHZ (1.0)	170	1.75	0.75 (at 77 K) 0.22 (at 298 K)	13.12(at 77 K) 3.85 (at 298 K)	29.34
Cr-MHZ (1.5)	269	1.76	1.40 (at 77 K) 0.15 (at 298 K)	24.64 (at 77 K) 2.64 (at 298 K)	10.71
Cr-MHZ (2.0)	279	1.83	2.79 (at 77 K) 0.51 (at 298 K)	51.06(at 77 K) 9.33 (at 298 K)	18.27

Appendix B – Supplementary Figures for Chapter 4

Figure B. 4.1 - Hydrogen adsorption and desorption isotherms at 77 K and at 298 K for plain silica (HMS).

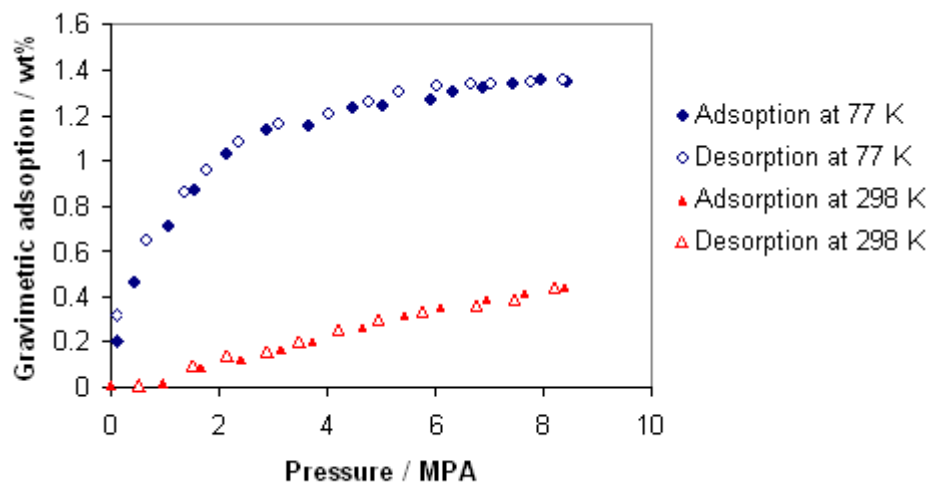


Figure A. 4.2 - Hydrogen adsorption and desorption isotherms at 77 K and at 298 K for tetra(benzyl)Ti-HMS.

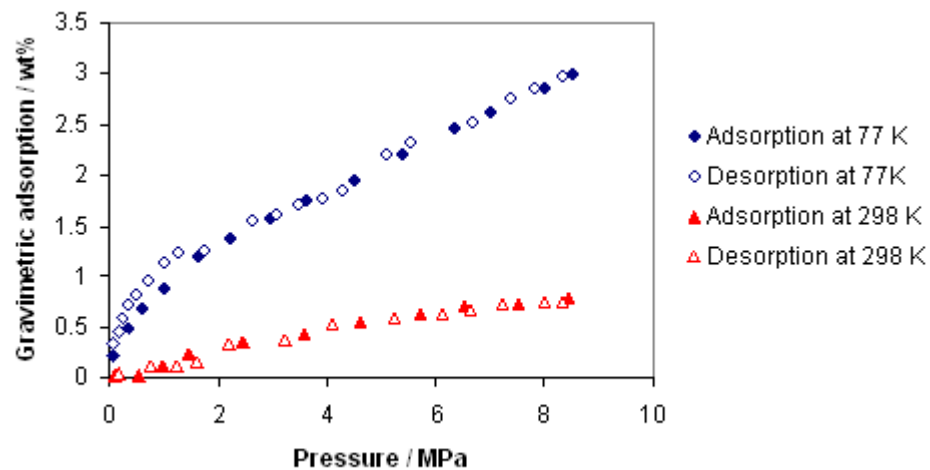


Figure B. 4.3 - Hydrogen adsorption and desorption isotherms at 77 K and at 298 K for bis(naphthalene)Ti-HMS.

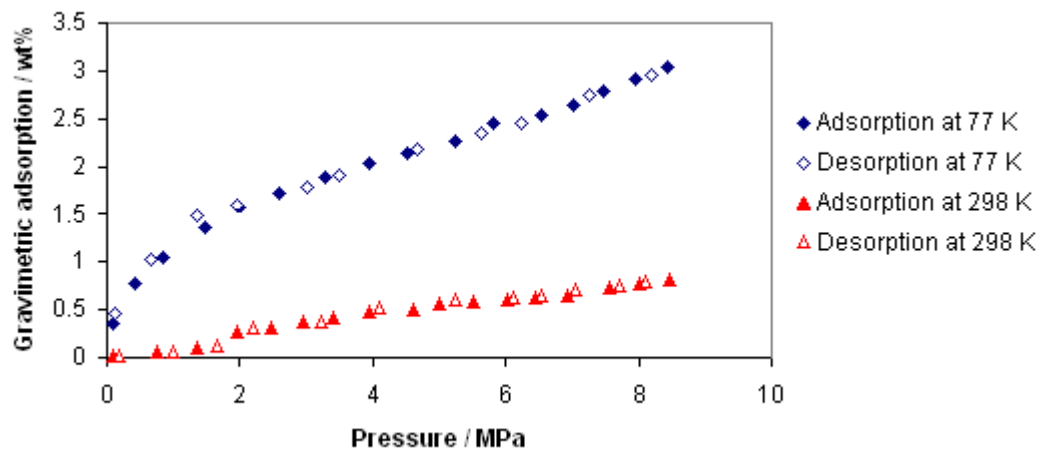


Figure B. 4.4 - Hydrogen adsorption and desorption isotherms at 77 K and at 298 K for tris(mesityl)V-HMS before hydrogenation.

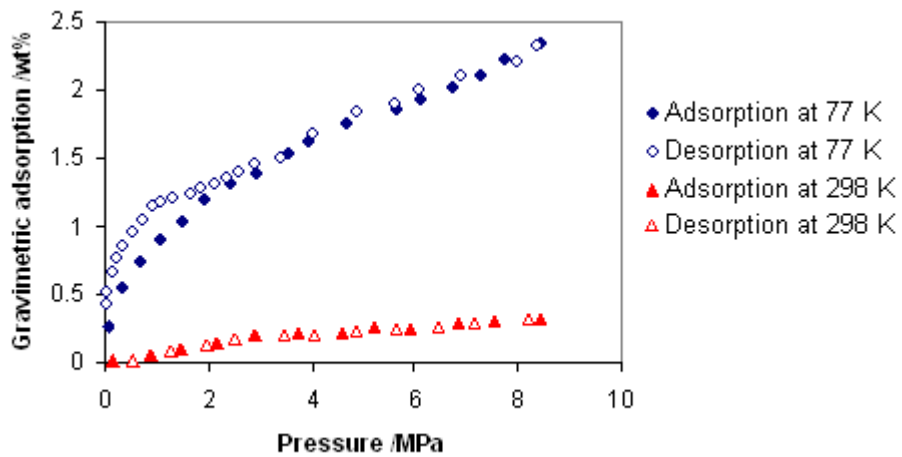


Figure B. 4.5 - Hydrogen adsorption and desorption isotherms at 77 K and at 298 K for tris(mesityl)V-HMS after hydrogenation.

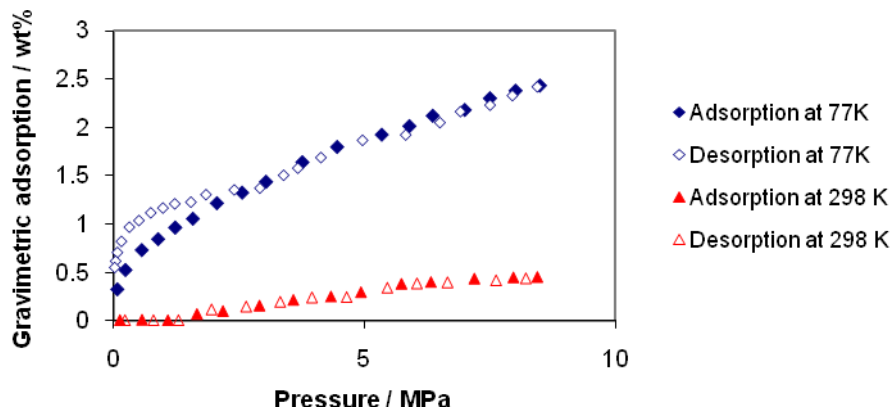


Figure B. 4.6 - Hydrogen adsorption and desorption isotherms at 77 K and at 298 K for tris[bis(trimethylsilyl)methyl]Cr-HMS before hydrogenation.

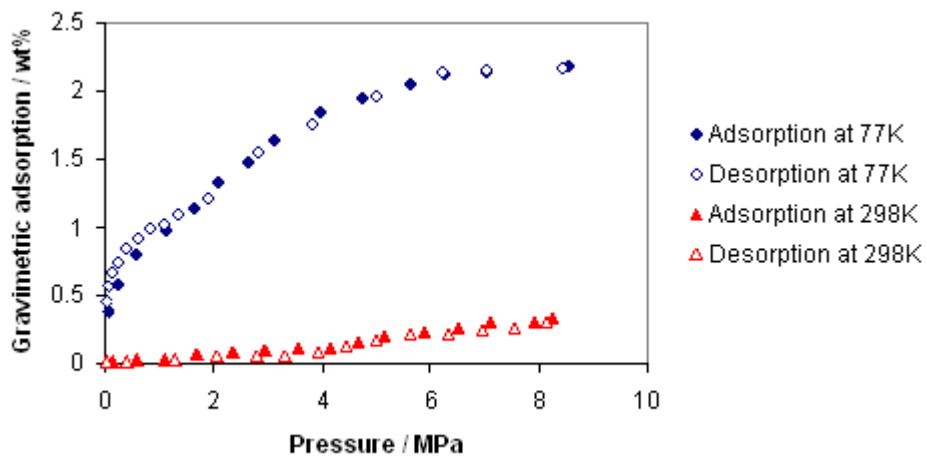


Figure B. 4.7 - Hydrogen adsorption and desorption isotherms at 77 K and at 298 K for tris[bis(trimethylsilyl)methyl]Cr-HMS after hydrogenation.

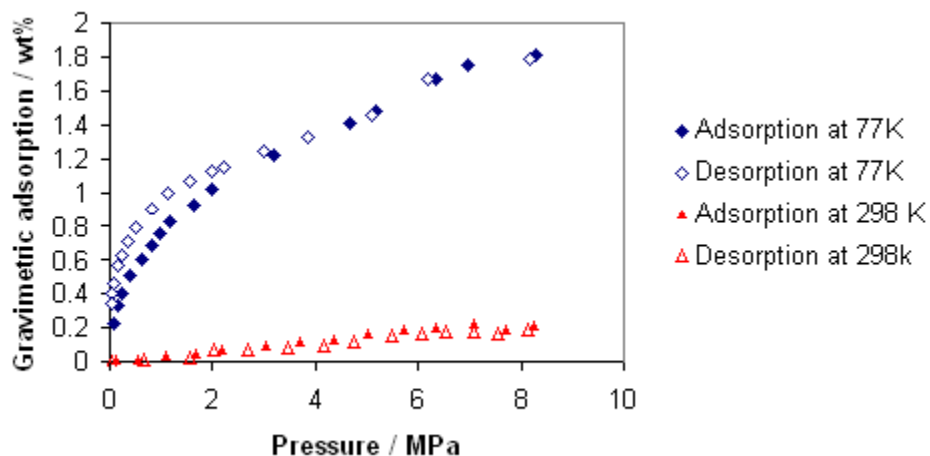


Figure B. 4.8 - Hydrogen adsorption and desorption isotherms at 77 K and at 298 K for bis[(trimethylsilyl)methyl]Cr-HMS before hydrogenation.

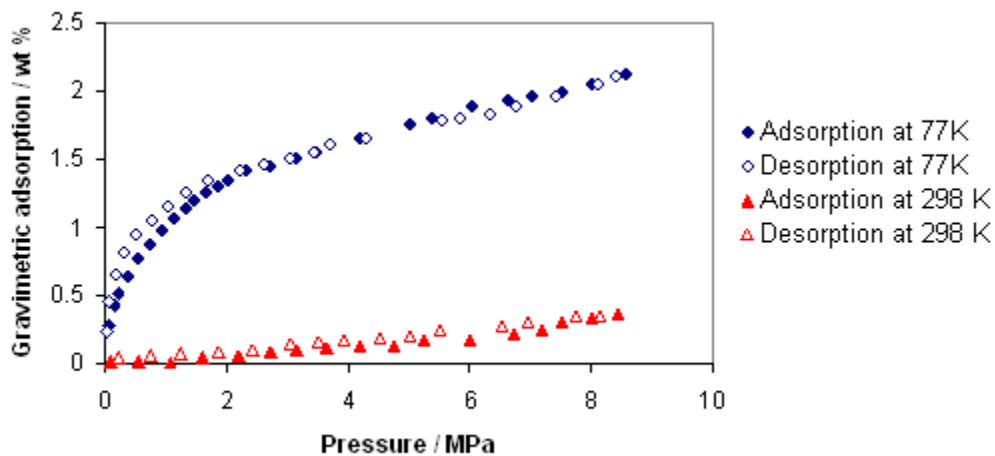
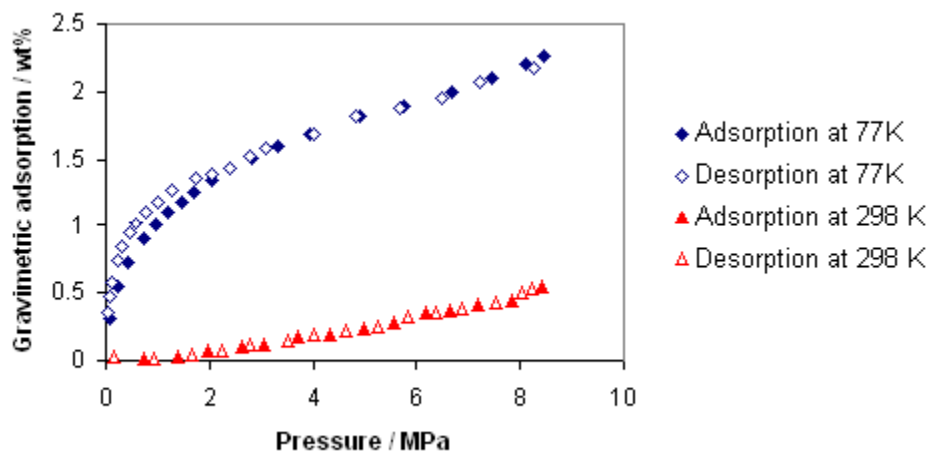


Figure B. 4.9 - Hydrogen adsorption and desorption isotherms at 77 K and at 298 K for bis[(trimethylsilyl)methyl]Cr-HMS after hydrogenation.



Appendix C – Copyright Release Forms

C.1- Permission to include my Journal of the American Chemical Society paper in this thesis

American Chemical Society's Policy on Theses and Dissertations

If your university requires a signed copy of this letter see contact information below.

Thank you for your request for permission to include **your** paper(s) or portions of text from **your** paper(s) in your thesis. Permission is now automatically granted; please pay special attention to the implications paragraph below. The Copyright Subcommittee of the Joint Board/Council Committees on Publications approved the following:

Copyright permission for published and submitted material from theses and dissertations

ACS extends blanket permission to students to include in their theses and dissertations their own articles, or portions thereof, that have been published in ACS journals or submitted to ACS journals for publication, provided that the ACS copyright credit line is noted on the appropriate page(s).

Publishing implications of electronic publication of theses and dissertation material

Students and their mentors should be aware that posting of theses and dissertation material on the Web prior to submission of material from that thesis or dissertation to an ACS journal may affect publication in that journal. Whether Web posting is considered prior publication may be evaluated on a case-by-case basis by the journal's editor. If an ACS journal editor considers Web posting to be "prior publication", the paper will not be accepted for publication in that journal. If you intend to submit your unpublished paper to ACS for publication, check with the appropriate editor prior to posting your manuscript electronically.

If your paper has not yet been published by ACS, we have no objection to your including the text or portions of the text in your thesis/dissertation in **print and microfilm formats**; please note, however, that electronic distribution or Web posting of the unpublished paper as part of your thesis in electronic formats might jeopardize publication of your paper by ACS. Please print the following credit line on the first page of your article: "Reproduced (or 'Reproduced in part') with permission from [JOURNAL NAME], in press (or 'submitted for publication'). Unpublished work copyright [CURRENT YEAR] American Chemical Society." Include appropriate information.

If your paper has already been published by ACS and you want to include the text or portions of the text in your thesis/dissertation in **print or microfilm formats**, please print the ACS copyright credit line on the first page of your article: "Reproduced (or 'Reproduced in part') with permission from [FULL REFERENCE CITATION.] Copyright [YEAR] American Chemical Society." Include appropriate information.

Submission to a Dissertation Distributor: If you plan to submit your thesis to UMI or to another dissertation distributor, you should not include the unpublished ACS paper in your thesis if the thesis will be disseminated electronically, until ACS has published your paper. After publication of the paper by ACS, you may release the entire thesis (**not the individual ACS article by itself**) for electronic dissemination through the distributor; ACS's copyright credit line should be printed on the first page of the ACS paper.

Use on an Intranet: The inclusion of your ACS unpublished or published manuscript is permitted in your thesis in print and microfilm formats. If ACS has published your paper you may include the manuscript in your thesis on an intranet that is not publicly available. Your ACS article cannot be posted electronically on a publicly available medium (i.e. one that is not password protected), such as but not limited to, electronic archives, Internet, library server, etc. The only material from your paper that can be posted on a public electronic medium is the article abstract, figures, and tables, and you may link to the article's DOI or post the article's author-directed URL link provided by ACS. This paragraph does not pertain to the dissertation distributor paragraph above.

Questions? Call +1 202/872-4368/4367. Send e-mail to copyright@acs.org or fax to +1 202-776-8112. 10/10/03, 01/15/04, 06/07/06

C.2 - Permission to include my Journal of the Organometallic Chemistry paper in this thesis (Chapter 3).

ELSEVIER LICENSE
TERMS AND CONDITIONS

Jun 18, 2010

This is a License Agreement between Ahmad Hamaed ("You") and Elsevier ("Elsevier") provided by Copyright Clearance Center ("CCC"). The license consists of your order details, the terms and conditions provided by Elsevier, and the payment terms and conditions.

Supplier	Elsevier Limited The Boulevard, Langford Lane Kidlington, Oxford, OX5 1GB, UK
Registered Company Number	1982084
Customer name	Ahmad Hamaed
Customer address	401 Sunset Ave Windsor, ON N9B 3P4
License Number	2451990736569
License date	Jun 18, 2010
Licensed content publisher	Elsevier
Licensed content publication	Journal of Organometallic Chemistry
Licensed content title	Optimization of hydrogen storage capacity in silica-supported low valent Ti systems exploiting Kubas binding of hydrogen
Licensed content author	Ahmad Hamaed, Tuan K.A. Hoang, Michel Trudeau, David M. Antonelli
Licensed content date	1 August 2009
Volume number	
Issue number	
Pages	0
Type of Use	Thesis / Dissertation
Portion	Full article
Format	Both print and electronic
You are an author of the Elsevier article	Yes
Are you translating?	No
Order Reference Number	
Expected publication date	Jul 2010
Elsevier VAT number	GB 494 6272 12
Permissions price	0.00 USD
Value added tax 0.0%	0.00 USD
Total	0.00 USD

C.3 - Permission to include the Figure 1.1 in this thesis

ELSEVIER LICENSE TERMS AND CONDITIONS

Jul 03, 2010

This is a License Agreement between Ahmad Hamaed ("You") and Elsevier ("Elsevier") provided by Copyright Clearance Center ("CCC"). The license consists of your order details, the terms and conditions provided by Elsevier, and the payment terms and conditions.

Supplier	Elsevier Limited The Boulevard, Langford Lane Kidlington, Oxford, OX5 1GB, UK
Registered Company Number	1982084
Customer name	Ahmad Hamaed
Customer address	401 Sunset Ave Windsor, ON N9B 3P4
License number	2461560859221
License date	Jul 03, 2010
Licensed content publisher	Elsevier
Licensed content publication	Physics Letters A
Licensed content title	Primitive phase diagram for hydrogen
Licensed content author	W. B. Leung, N. H. March, H. Motz
Licensed content date	3 May 1976
Licensed content volume number	56
Licensed content issue number	6
Number of pages	2
Type of Use	reuse in a thesis/dissertation
Requestor type	Not specified
Intended publisher of new work	n/a
Portion	figures/tables/illustrations
Number of figures/tables/illustrations	
Format	both print and electronic
No	
No	
Order reference number	
Title of your thesis/dissertation	Hydrogen storage in metal fragments grafted silicas and Chromium hydrazide gels
Expected completion date	Jul 2010
Estimated size (number of pages)	200
Elsevier VAT number	GB 494 6272 12
Terms and Conditions	

C.4 - Permission to include Figure 1.4 in this thesis

ELSEVIER LICENSE TERMS AND CONDITIONS

Jul 03, 2010

This is a License Agreement between Ahmad Hamaed ("You") and Elsevier ("Elsevier") provided by Copyright Clearance Center ("CCC"). The license consists of your order details, the terms and conditions provided by Elsevier, and the payment terms and conditions.

Supplier	Elsevier Limited The Boulevard, Langford Lane Kidlington, Oxford, OX5 1GB, UK
Registered Company Number	1982084
Customer name	Ahmad Hamaed
Customer address	401 Sunset Ave Windsor, ON N9B 3P4
License number	2461561466205
License date	Jul 03, 2010
Licensed content publisher	Elsevier
Licensed content publication	Chemical Physics Letters
Licensed content title	Raman spectra of hydrogen and deuterium adsorbed on a metal-organic framework
Licensed content author	Andrea Centrone, Diana Y. Siberio-Pérez, Andrew R. Millward, Omar M. Yaghi, Adam J. Matzger, Giuseppe Zerbi
Licensed content date	15 August 2005
Licensed content volume number	411
Licensed content issue number	4-6
Number of pages	4
Type of Use	reuse in a thesis/dissertation
Requestor type	Not specified
Intended publisher of new work	other
Portion	figures/tables/illustrations
Number of figures/tables/illustrations	
Format	both print and electronic
No	
No	
Order reference number	
Title of your thesis/dissertation	Hydrogen storage in metal fragments grafted silicas and Chromium hydrazide gels
Expected completion date	Jul 2010
Estimated size (number of pages)	200
Elsevier VAT number	GB 494 6272 12
Terms and Conditions	

C.5 - Permission to include Figure 1.5 in this thesis

ELSEVIER LICENSE TERMS AND CONDITIONS

Jul 03, 2010

This is a License Agreement between Ahmad Hamaed ("You") and Elsevier ("Elsevier") provided by Copyright Clearance Center ("CCC"). The license consists of your order details, the terms and conditions provided by Elsevier, and the payment terms and conditions.

Supplier	Elsevier Limited The Boulevard, Langford Lane Kidlington, Oxford, OX5 1GB, UK
Registered Company Number	1982084
Customer name	Ahmad Hamaed
Customer address	401 Sunset Ave Windsor, ON N9B 3P4
License number	2461570945283
License date	Jul 03, 2010
Licensed content publisher	Elsevier
Licensed content publication	Journal of Alloys and Compounds
Licensed content title	Inelastic neutron scattering of H ₂ adsorbed in HKUST-1
Licensed content author	Y. Liu, C.M. Brown, D.A. Neumann, V.K. Peterson, C.J. Kepert
Licensed content date	31 October 2007
Licensed content volume number	446-447
Licensed content issue number	
Number of pages	4
Type of Use	reuse in a thesis/dissertation
Requestor type	Not specified
Intended publisher of new work	other
Portion	figures/tables/illustrations
Number of figures/tables/illustrations	
Format	both print and electronic
No	
No	
Order reference number	
Title of your thesis/dissertation	Hydrogen storage in metal fragments grafted silicas and Chromium hydrazide gels
Expected completion date	Jul 2010
Estimated size (number of pages)	200
Elsevier VAT number	GB 494 6272 12

C.6: Permission to include the computational calculations in this thesis.

From: Claire C V J Skipper <claire.skipper.09@ucl.ac.uk>
Sent: Thu, 27 May 2010 14:02:30 +0000
Subject: RE: Computational Studies
To: Ahmad Hamaed <hamaed1@uwindsor.ca>

Dear Ahmad,

I would be happy for you to include my calculations in your thesis as long as you reference me appropriately. I will forward you an email with my report as a pdf.

I have already started calculations on hydrazine based materials.

Kind regards,

Claire Skipper

From: Ahmad Hamaed [hamaed1@uwindsor.ca]
Sent: 27 May 2010 12:41
To: Claire C V J Skipper
Subject: Computational Studies

Dear Claire:

This is Ahmad Hamaed, from Dr. Antonelli Group in Windsor, Canada.

Thank you for your excellent computational studies on Silica supported transition metal fragments. I need your permission to include these calculations in my thesis, this will add another perspective to the thesis, and I will really appreciate that.

I know it is a large file, but I am used to sharing large files with Dr Antonelli back and forth. The easiest way is by uploading it to google documents, if it is too big you may split it into 2 documents and just send me the link.

Thank you once again for your efforts

I will appreciate your time

Thanks

Note: We already designed new materials based on transition metals linked with hydrazine these are the best ever as hydrogen storage materials, and no body did any computational studies on those so far. I think Dr Antonelli will introduce these materials to your advisor and this can lead to a great paper in a prestigious journal.

Ahmad

Ahmad M. Hamaed

Ph.D Candidate, University of Windsor

Department of Chemistry&Biochemistry

This e-mail may be privileged and/or confidential, and the sender does not waive any related rights and obligations. Any distribution, use or copying of this e-mail or the information it contains by other than an intended recipient is unauthorized. If you received this e-mail in error, please advise me (by return e-mail or otherwise) immediately.

VITA AUCTORIS

Name: Ahmad Hamaed

Place of Birth: Bint Jbeil, Lebanon

Year of Birth: 1977

Education: University of Windsor, Windsor, Ontario, Canada
2005-2010, Ph.D. (Chemistry)

University of Windsor, Windsor, Ontario, Canada
2001-2005, B.Sc. Honours (Chemistry)